Molecular-Thermodynamic Theories of Micellization of Multicomponent Surfactant Mixtures and of pH-Sensitive Surfactants

by

Arthur Clayton Goldsipe

B.S., Tennessee Technological University (1997)
M.S., Tennessee Technological University (1999)

Submitted to the Department of Chemical Engineering
in partial fulfillment of the requirements for the degree of

Doctor of Philosophy in Chemical Engineering

at the

MASSACHUSETTS INSTITUTE OF TECHNOLOGY

May 2006

Author .....
Department of Chemical Engineering
May 15, 2006

Certified by .....
Daniel Blankschtein
Professor of Chemical Engineering
Thesis Supervisor

Accepted by .....
William Deen
Professor of Chemical Engineering
Chairman, Committee for Graduate Students

Molecular-Thermodynamic Theories of Micellization of Multicomponent Surfactant Mixtures and of pH-Sensitive Surfactants

by

Arthur Clayton Goldsipe

Submitted to the Department of Chemical Engineering
on May 15, 2006, in partial fulfillment of the
requirements for the degree of
Doctor of Philosophy in Chemical Engineering

Abstract

This thesis focuses on two research areas that are particularly relevant to the practical application of surfactant science: (1) the micellization of multicomponent surfactant mixtures, and (2) the micellization of pH-sensitive (or amphoteric) surfactants. Surfactant formulations of practical utility typically consist of many surfactant components. In many practical applications, pH-sensitive surfactants are added as a secondary surfactant because they enhance performance properties, including solubility, foaming, and mildness to the skin or to the eyes. In addition, pH-sensitive surfactants may be used effectively in novel applications where pH variations can be utilized to control self-assembly, including controlled drug release, targeted gene delivery, and the fabrication of nanoscale materials for optics, electronics, and sensors.

First, a molecular-thermodynamic (MT) theory was developed to account for counterion binding to mixed micelles composed of ionic-nonionic and ionic-zwitterionic binary surfactant mixtures. The theory successfully predicted the degree of counterion binding (β) of monovalent and multivalent ions to mixed micelles as a function of the micelle composition (α). The theory was also found to be consistent with the concept of critical counterion binding. An inflection in the β vs. α curve was correlated to a micelle shape transition.

Second, the MT theory was generalized to include pH effects in order to model the micellization of pH-sensitive surfactants. The theory was validated by comparing predictions of critical micelle concentrations (cmc's), micelle aggregation numbers, and micellar titration behavior to experimental data for alkyldimethylamine oxide surfactants, which are cationic in the protonated state (at low pH) and zwitterionic in the deprotonated state (at high pH). The MT theory qualitatively reproduced the minimum in the cmc and the maximum in the micelle aggregation number, which are both observed experimentally at intermediate pH values, resulting from the synergy between the two forms of the pH-sensitive surfactant in the micelle. This self-synergy, which was previously attributed by other researchers to the formation of

surfactant-surfactant hydrogen bonds in the micelle, was rationalized instead in terms of electrostatic interactions operating between surfactants and bound counterions in the micelle. Very good quantitative agreement was obtained for the predicted cmc's in solutions containing no added salt. In particular, the experimentally observed maximum in the cmc, which originated from changes in the solution ionic strength, was reproduced by the MT theory but not by the empirical regular solution theory (RST). Micellar titration data were also examined in terms of the relative values of the micellar deprotonation equilibrium parameter ($\Delta \mathrm{p}K$). The $\Delta \mathrm{p}K$ was related to the derivative of the electrostatic contribution to the free energy of micellization (g_{elec}) with respect to α. The molecular model of g_{elec} predicted $\Delta \mathrm{p}K > 0$ in the limit of micelles composed entirely of the deprotonated form of the pH-sensitive surfactant, consistent with the experimental data.

Third, a theory based on RST was developed to model the titration behavior of micelles containing a pH-sensitive surfactant and an arbitrary number of conventional surfactants. The conventional surfactants were successfully modeled as a single effective surfactant, thus considerably simplifying the theoretical analysis of multicomponent surfactant mixtures. The RST description was validated using experimental micellar titration data for single surfactant systems (obtained from the literature) and for binary surfactant mixtures (measured as part of this thesis). Experimental uncertainties in the micellar titration data were examined, and a new method was introduced to account for these uncertainties by using a weighted regression analysis.

Fourth, a MT theory was developed to model the micellization of mixtures containing an arbitrary number of conventional surfactants. The maximum micelle radius was examined theoretically for a ternary surfactant mixture. Due to the limited availability of experimental data, only the predicted cmc's were compared with the experimental cmc's. Good agreement was obtained for the predicted cmc's, which were comparable to, and sometimes better than, the cmc's determined using RST. The MT theory was also used to model a commercial nonionic surfactant (Genapol UD-079), which was modeled as a mixture of 16 surfactant components. The predicted cmc agreed remarkably well with the experimental cmc. The monomer concentration was predicted to increase significantly above the cmc. In addition, the monomer and the micelle compositions were predicted to vary significantly with surfactant concentration. These composition variations were rationalized in terms of competing steric and entropic effects and a micelle shape transition near the cmc.

Finally, the MT theory was further generalized to model the micellization behavior of mixtures of a pH-sensitive surfactant and an arbitrary number of conventional surfactants. Predicted values of the solution pH of mixtures of a pH-sensitive surfactant and an ionic surfactant, as well as of the cmc's of mixtures of two pH-sensitive surfactants, compared favorably with the experimental values. The MT theory was also validated using micellar titration data for varying compositions of mixed micelles containing dodecyldimethylamine oxide (C_{12}DAO) and a cationic, nonionic, or anionic surfactant. The MT theory accurately modeled the titration behavior of C_{12}DAO mixed with the nonionic surfactant. However, C_{12}DAO appeared to interact more favorably with the anionic and the cationic surfactants than was

predicted by the MT theory.

The MT theories presented in this thesis represent *the first molecular-based models* of the micellization behavior of the following systems: (1) pH-sensitive surfactants, (2) mixtures of three or more conventional surfactants, and (3) mixtures of pH-sensitive surfactants and conventional surfactants. The MT theories resulted in *qualitative* and *quantitative* predictions of the micellization properties for a variety of surfactant systems. A simpler theory based on RST was also developed to model titrations of micelles containing pH-sensitive and conventional surfactants. In addition, this thesis resulted in the first experimental study of the effect of micelle composition on the titration behavior of mixed micelles containing a pH-sensitive surfactant and a conventional surfactant. The resulting MT theories have provided fundamental, physical insight, and they may also decrease the need for the costly and time-consuming process associated with "trial-and-error" surfactant formulation.

Thesis Supervisor: Daniel Blankschtein
Title: Professor of Chemical Engineering

Acknowledgments

Visiting MIT as a prospective graduate student was my first glimpse of Boston. Like many of my future classmates, I was unsure about whether MIT was the right school for me. One of my strongest memories from that weekend was visiting the North End and standing in a narrow little street, surrounded by buildings. Just for a minute, I was overwhelmed by a sense of claustrophobia. Where was the sky? But the feeling passed, and the historic buildings, Italian culture, and Mike's Pastries won me over.

My time at MIT mirrored that first trip to the North End. I felt the weight of courses and research surrounding me on all sides. And many long days in the lab kept me from seeing much of the sky. But I also loved my experience here. Watching from my lab window, I saw the Stata Center slowly rise to a strangely satisfying conclusion. Although living off campus meant being somewhat disconnected from MIT culture, I still felt a sense of community when I'd see a new hack or overhear MIT lingo. Then there are the many mysteries of food. Why does pizza taste so much better when it's free? Why is the Goosebeary's food truck so popular when every dish tastes the same?

However, what makes my time at MIT unforgettable is the people. I never could have completed my thesis without the help of my friends and mentors at MIT. My thesis committee members, Professors Alan Hatton and Bruce Tidor, have been helpful and supportive of my research. Professor Daniel Blankschtein has been a kind and caring advisor. He helped me look through the numbers and equations to find the physical insight they can provide. Although we sometimes disagreed (especially about when and where to use commas), I hold profound respect for him as a teacher and a mentor.

I am sincerely thankful to the past and present members of the Blanschtein group for making the lab a wonderful place to work. At first, it was easier to get to know the extroverts, like Dan Kamei and Peter Moore. (And a very special thanks to Dan, who was also my superb 10.40 TA and my first good friend in the lab.) But I also shared many great moments with that first generation of labmates: Mike Mulqueen, Hua

Tang, Betty Yu, Dave Cochran, Vibha Srinivasan, Henry Lam, and Joe Kushner. I happily pass the torch to another generation of great people: Srinivas Moorkanikkara, Saswata Ghosh, Brian Stephenson, Jon Mendenhall, Amanda Engler, Jennifer Seto, and Baris Polat. There have also been some great visitors to the lab. Isaac Reif, muchas gracias por las grandes discusiones y los consejos. Beijos e abraços para os meus amigos da Faculdade de Ciências Farmacêuticas da Universidade de São Paulo: Adalberto Pessoa Jr., Carlota Yagui, and Priscila Mazzola. And hallo to Dik van Roosmalen in the Netherlands. I thank my UROP, Doris Grillo, for bringing her energy and joy to the lab.

I never would have come this far without the support of my teachers, friends, and family. The love and support of my wife, Mel Goldsipe, carried me through the ups and downs of my PhD. She helps me in countless ways, from editing my writing, to being a lifeline to the local music scene. Most important, she is my best friend. Her wonderful family–parents Jeff and Jo Ellen, brother Danny, and grandparents–have given me a second home. How can I ever put into words my thanks to my Mom (Edna), Dad (Clayton), and step-mom (Jane)? They never had the opportunity to go to college, but their intelligence, curiosity, and dedication were the best educational tools I could have. In addition, my grandparents always will hold a special place in my heart. Only one of them was able to attend high school, but the lessons they taught me are invaluable. I was fortunate enough to grow up with a wonderful extended family of aunts, uncles, and cousins in Tennessee and beyond. My Tennessee "family" also includes my lifelong friends and teachers from Meadowbrook and Unity, and from Forest Hill, Montvale, and Heritage public schools.

Finally, I thank the Fannie and John Hertz Foundation for providing me with the fellowship that gave me the confidence and the financial means to come to MIT. My annual meetings with the Foundation and their recent National Symposium offered valuable guidance and a broader scientific perspective. It is an honor and a privilege to be part of such a great community of scientists.

Contents

1 Introduction **21**

1.1 Surfactant Behavior 21

1.2 Multicomponent Surfactant Mixtures 23

1.2.1 Motivation 23

1.2.2 Theoretical Approaches 25

1.3 pH-Sensitive Surfactants 27

1.3.1 Motivation 27

1.3.2 Theoretical Approaches 29

1.4 Thesis Overview 30

2 Modeling Counterion Binding in Ionic-Nonionic and Ionic-Zwitterionic Binary Surfactant Mixtures **33**

2.1 Introduction 33

2.2 Thermodynamic Framework 37

2.3 Molecular Model for the Free Energy of Mixed Micellization 40

2.3.1 Modeling the Hydrophobic Micelle Core 41

2.3.1.1 Transfer Free-Energy Contribution 41

2.3.1.2 Interfacial Free-Energy Contribution 42

2.3.1.3 Packing Free-Energy Contribution 43

2.3.2 Modeling the Micelle Interfacial Shell 44

2.3.2.1 Steric Free-Energy Contribution 44

2.3.2.2 Electrostatic Free-Energy Contribution 45

2.3.2.3 Entropic Free-Energy Contribution 45

2.3.3 Evaluation of the Electrostatic Free-Energy Contribution . . . 47
2.3.3.1 Discharge Free-Energy Contribution 49
2.3.3.2 Charging Free-Energy Contribution 50
2.4 Determination of Useful Micellar Solution Properties 53
2.4.1 Determination of the Micelle Size Distribution 53
2.4.2 Determination of the Critical Micelle Concentration 56
2.4.3 Determination of Average Micelle Aggregation Numbers 57
2.5 Model Validation 58
2.5.1 Prediction of the Degree of Counterion Binding 59
2.5.1.1 Cationic-Nonionic Binary Surfactant Mixture 59
2.5.1.2 Anionic-Nonionic Binary Surfactant Mixture 66
2.5.1.3 Cationic-Zwitterionic Binary Surfactant Mixture . . 68
2.5.1.4 Divalent Anionic-Nonionic Binary Surfactant Mixture 68
2.5.2 Prediction of the Critical Micelle Concentration 72
2.5.3 Prediction of the Weight-Average Micelle Aggregation Number 77
2.6 Conclusions 79

3 Molecular-Thermodynamic Theory of Micellization of pH-Sensitive Surfactants 81

3.1 Introduction 81
3.2 Theory 84
3.2.1 Thermodynamic Framework 86
3.2.2 Molecular Model for the Free Energy of Micellization 90
3.3 Determination of Useful Micellar Solution Properties 92
3.3.1 Calculating the Critical Micelle Concentration and Average Micelle Aggregation Numbers 93
3.3.2 Calculating the Micellar Deprotonation Parameter, pK_m . . . 95
3.4 Results and Discussion 98
3.4.1 Selection of Model System 98
3.4.2 Prediction of the Critical Micelle Concentration 100

3.4.3 Prediction of Critical Micelle Concentrations without Added Salt: A Comparison with Regular Solution Theory 103
3.4.4 Prediction of Micelle Sizes 105
3.4.5 Prediction of the Titration Behavior 110
3.4.5.1 Prediction of the Salt Dependence of the ΔpK . . . 110
3.4.5.2 Prediction of the Effect of the Surfactant Tail Length on the ΔpK 113
3.5 Conclusions 115

4 Titration of Mixed Micelles Containing a pH-Sensitive Surfactant and Conventional Surfactants: A Regular Solution Theory Modeling Approach 117

4.1 Introduction 117
4.2 Materials and Experimental Methods 120
4.3 Theory 123
4.3.1 Notation 123
4.3.2 Implications of the RST to Analyze Micellar Titrations 124
4.3.2.1 Single pH-Sensitive Surfactant Systems 125
4.3.2.2 Mixtures of a pH-Sensitive Surfactant and Conventional Surfactants 127
4.4 Analysis of the Experimental Titration of Micelles Containing a pH-Sensitive Surfactant 130
4.4.1 Uncertainty in the Analysis of the Experimental Micellar Titration Data 130
4.4.2 Single pH-Sensitive Surfactant Systems 131
4.4.2.1 Effect of the Surfactant Tail Length 133
4.4.2.2 Effect of the Surfactant Head 137
4.4.3 Mixed Surfactant Systems 140
4.5 Conclusions 144

5 Molecular-Thermodynamic Theory of Micellization of Ternary and Multicomponent Surfactant Mixtures 147

5.1 Introduction . . . 147

5.2 Theory . . . 149

5.2.1 Thermodynamic Framework . . . 150

5.2.2 Molecular Model for the Free Energy of Micellization . . . 152

5.3 Determination of Useful Micellar Solution Properties . . . 153

5.3.1 Calculating the Critical Micelle Concentration and Average Micelle Aggregation Numbers . . . 154

5.3.2 Theoretical Model for the Maximum Micelle Radius . . . 155

5.4 Results and Discussion . . . 158

5.4.1 Comparison of $r_{\max}$ Values Predicted Using Eqs 5.14 and 5.15 and Explicit g_{pack} Calculations . . . 158

5.4.2 Prediction of cmc's of Ternary Surfactant Mixtures . . . 162

5.4.2.1 The cmc's of a Homologous Series of Cationic Surfactants . . . 162

5.4.2.2 The cmc's of a Cationic/Anionic/Nonionic Ternary Surfactant Mixture . . . 164

5.4.3 Prediction of Various Micellization Properties of a Commercial Nonionic Surfactant . . . 168

5.4.3.1 Prediction of the Monomer and the Micelle Concentrations . . . 169

5.4.3.2 Prediction of the Monomer and the Micelle Compositions . . . 169

5.5 Conclusions . . . 178

6 Molecular-Thermodynamic Theory of Micellization of Mixtures of pH-Sensitive and Conventional Surfactants 181

6.1 Introduction . . . 181

6.2 Materials and Experimental Methods . . . 183

6.3 Theory . . . 184
6.3.1 Notation . . . 185
6.3.2 Thermodynamic Framework . . . 186
6.3.3 Molecular Model for the Free Energy of Micellization . . . 188
6.4 Determination of Useful Micellar Solution Properties . . . 189
6.5 Results and Discussion . . . 190
6.5.1 Prediction of the Solution pH and of the Degree of Counterion Binding . . . 190
6.5.2 Prediction of the cmc of a pH-Sensitive Surfactant Mixture . . . 196
6.5.3 Prediction of the Micellar Titration Behavior . . . 199
6.5.3.1 Mixtures of C_{12}DAO and the Nonionic Surfactant $C_{12}E_8$ . . . 200
6.5.3.2 Mixtures of C_{12}DAO and the Cationic Surfactant C_{12}TAB . . . 202
6.5.3.3 Mixtures of C_{12}DAO and the Anionic Surfactant SDS . . . 204
6.6 Conclusions . . . 206

7 Conclusions and Future Work **209**
7.1 Thesis Summary . . . 209
7.2 Future Research Directions . . . 213
7.2.1 Future Research Directions on Counterion Binding . . . 214
7.2.2 Future Research Directions on Multicomponent Surfactant Mixtures . . . 215
7.2.3 Future Research Directions on pH-Sensitive Surfactants . . . 217
7.2.4 Future Research Directions on Self-Assembly . . . 221
7.3 Concluding Remarks . . . 224

A Diffuse-Layer Contribution to the Mole Balances **225**

B Key Equations of the g_{mic} Model for pH-Sensitive Surfactants **229**

C Evaluation of $\frac{\partial g_{\mathrm{m}}}{\partial \alpha}$ **235**

D Derivation of eqs 4.10 and 4.14 in the Context of RST **237**

E Generalization of the g_{mic} Model to Multicomponent Surfactant Mixtures **243**

F Diffuse-Layer Contribution to the Mole Balances at High Micelle Concentrations and at Low Ionic Strengths **247**

List of Figures

2-1 Determination of the charge per surfactant molecule on the surface of an anionic-zwitterionic mixed micelle 46

2-2 Comparison between the predicted and the experimental degrees of Br^+ binding to $C_{16}TAB$-$C_{12}E_6$ mixed micelles 61

2-3 The predicted weight-average micelle aggregation number of $C_{16}TAB$-$C_{12}E_6$ mixed micelles, $\langle n \rangle_w$ 63

2-4 The micelle composition at which $\beta_{cyl} = \beta_{sph}$ as a function of the concentration of added [NaBr], for $C_{16}TAB$-$C_{12}E_6$ micelles 65

2-5 Comparison between the predicted and the experimental degrees of Na^+ binding to STS-$C_{12}E_6$ mixed micelles 67

2-6 Comparison between the predicted and the experimental degrees of Cl^- binding to $C_{18}TAC$-$C_{12}PO$ mixed micelles 69

2-7 Comparison between the predicted and the experimental degrees of Cu^{2+} binding to CuDS-$C_{12}E_{23}$ mixed micelles 71

2-8 Comparison between the predicted and the experimental cmc's of SDS-OG at varying NaCl concentrations 74

2-9 Comparison between the predicted and the experimental Corrin-Harkins slope for SDS-OG mixtures 76

2-10 Comparison between the predicted weight-average and the experimental quencher-average aggregation numbers of SDS-$C_{12}E_4$ mixed micelles 78

3-1 Comparison between the predicted and the experimental cmc's of C_iDAO in 0.1 M NaCl 101

3-2 Comparison between the predicted and the experimental cmc's of C_{12}DAO without added salt 104
3-3 Comparison between the predicted and the experimental weight-average micelle aggregation number of C_{12}DAO in 0.1 M NaCl 106
3-4 Comparison between the predicted and the experimental weight-average micelle aggregation number of C_{12}DAO in 0.2 M NaCl 107
3-5 Comparison between the predicted and the experimental ΔpK's of 50 mM C_{12}DAO solutions at varying NaCl concentrations 111
3-6 Comparison between the predicted and the experimental ΔpK's of solutions of C_iDAO with no added salt 114

4-1 Error analysis of the pK_m as a function of x_{mic} for C_{12}DAO micelles . 132
4-2 Comparison of the RST predictions and the experimental ΔpK for C_iDAO ($i = 10$, 12, and 14) in 0.1 M NaCl 134
4-3 Comparison of the RST predictions and the experimental ΔpK for C_{12}DAO, C_{12}DHEAO, and $C_{12}C_6$Bet in 0.1 M NaCl 138
4-4 Comparison of the RST predictions and the experimental ΔpK for mixtures of C_{12}DAO/C_{12}TAB 141
4-5 Comparison of the RST predictions and the experimental ΔpK for mixtures of C_{12}DAO/$C_{12}E_8$ 142

5-1 Comparison of $r_{max}^{(theory)}$ and $r_{max}^{(g_{pack})}$ of Micelles Containing C_7, C_{11}, and C_{15} Tails 161
5-2 Comparison between the predicted and the experimental cmc's of C_iTAB homologues ($i = 8$, 10, 12, 14, and 16) 163
5-3 Comparison between the predicted and the experimental cmc's of representative equimolar ternary mixtures of C_iTAB homologues ($i =$ 8, 10, 12, 14, and 16) 165
5-4 Comparison between the predicted and the experimental cmc's of single component and ternary mixtures of the anionic surfactant $NaC_{10}S$, the cationic surfactant C_{10}TAB, and the nonionic surfactant C_8E_4 167

5-5 Predicted monomer and micelle concentrations of the commercial surfactant Genapol UD-079 170
5-6 Predicted monomer composition of the commercial surfactant Genapol UD-079 172
5-7 Predicted micelle composition of the commercial surfactant Genapol UD-079 173
5-8 Predicted compositions of spherical micelles, infinite cylindrical micelles, and the number-average micelle composition of the commercial surfactant Genapol UD-079 176

6-1 Comparison between the predicted and the experimental solution pH's of 80 mM mixtures of C_{12}DAO/SDS 191
6-2 Comparison between the predicted and the experimental degree of sodium binding to C_{12}DAO/SDS micelles 194
6-3 Comparison between the predicted and the experimental solution pH's of 56 mM equimolar mixtures of C_{12}DAO/SDS 195
6-4 Comparison between the predicted and the experimental cmc's of C_{14}DAO/C_{16}Bet mixtures 198
6-5 Comparison between the predicted and the experimental $\Delta \mathrm{p}K_{\mathrm{m}}$'s of C_{12}DAO/$C_{12}E_8$ micelles 201
6-6 Comparison between the predicted and the experimental $\Delta \mathrm{p}K_{\mathrm{m}}$'s of C_{12}DAO/C_{12}TAB micelles 203
6-7 Comparison between the predicted and the experimental $\Delta \mathrm{p}K_{\mathrm{m}}$'s of C_{12}DAO/SDS micelles 205

List of Tables

2.1 Molecular characteristics of ionic surfactants 42

2.2 Molecular characteristics of the zwitterionic surfactant dodecyldimethylphosphine oxide, $C_{12}PO$ 42

2.3 Molecular characteristics of nonionic surfactants 43

3.1 Molecular parameters of C_iDAOH^+ and C_iDAO 99

4.1 RST analysis of the experimental micellar titration data for single pH-sensitive surfactant systems 135

4.2 RST analysis of the experimental micellar titration data for mixtures of a pH-sensitive and a conventional surfactant 143

5.1 Compositions of ternary mixtures of $NaC_{10}S$, $C_{10}TAB$, and C_8E_4 . . . 166

6.1 Compositions of mixtures of $C_{14}DAO$ and $C_{16}Bet$ 199

Chapter 1

Introduction

1.1. Surfactant Behavior

Surfactants are an interesting class of chemicals consisting of two chemical moieties that interact very differently with a solvent. One moiety, the surfactant "head", is lyophilic, indicating that it interacts favorably with a solvent.[1–3] The other moiety, the surfactant "tail", is lyophobic, indicating that it interacts unfavorably with a solvent.[1–3] When the solvent is water (the solvent of interest in this thesis), the hydrophobic tail is typically a hydrocarbon or a fluorocarbon, and the hydrophilic head is an ionic or a polar (nonionic or zwitterionic) moiety.[1–3]

This dual chemical nature of surfactants leads to two particularly interesting and practically useful phenomena in aqueous media: (1) their preferential adsorption at surfaces (for example, air/water) and at interfaces (for example, oil/water), and (2) their ability to spontaneously self-assemble in water into a variety of structures.[1–3] (In fact, the name "surfactant" is a contraction of surface-active agent.) When the total concentration of surfactant in the aqueous solution exceeds the critical micelle concentration (cmc), the surfactant molecules begin to spontaneously self-assemble into structures known as micelles.[1–3] Micelles form in a variety of shapes (including spheres, cylinders, and disks), and always in a manner that reduces the contacts of the hydrophobic tails with water, while maintaining the favorable contacts of the hydrophilic heads with water. The surfactant molecules that remain in the singly

dispersed state are typically referred to as the surfactant monomers (or simply as the monomers). The cmc and other properties of the monomers and the micelles, including their composition (in the case of mixed surfactant systems) or concentration, are of practical interest. For example, the behavior of the cmc has been correlated with various predicted measures of cleaning efficiency.[4]

Surfactants have found a wide range of application in both academia and industry, as illustrated, for example, by the publication of more than 130 books in the Surfactant Science Series published by Marcel Dekker and Taylor & Francis. Although, historically, the largest application of surfactants has been in the formulation of detergents and personal care products,[5] the versatile surfactant has been utilized as much more than a cleaning agent. Modern uses of surfactants include the micellar solubilization or encapsulation of drugs[6,7] and nucleic acids[8–13] for therapeutic applications, the formation of proto-cells to study the origin of life,[14] and the pH-controlled fabrication of nanoscale materials with potential applications in electronics, optics, and sensing.[15]

Unfortunately, surfactant "science" often consists of a trial-and-error approach. Such an approach can be assisted by statistical design principles, as demonstrated in a recent study aimed at designing improved detergent formulations.[16] Even more powerful is the guidance that the development of new physical models would bring to surfactant formulation. However, theory has typically lagged behind the experimental advances made in surfactant science. One popular modeling approach has made use of "toy models" of surfactants to gain general insights into micellization.[17–25] However, the development of more realistic models that explicitly incorporate the actual surfactant chemical structure as well as the molecular details of micellization could help bridge the gap between theory and applications.

With the above in mind, this thesis focuses on two research areas that are particularly relevant to the practical application of surfactant science: (1) the micellization of multicomponent surfactant mixtures, and (2) the micellization of pH-sensitive (or amphoteric) surfactants. Multicomponent surfactant mixtures are of relevance because commercial surfactants and surfactant formulations are typically

polydisperse. In addition, pH-sensitive surfactants are often added to formulations in order to enhance their performance. Additional motivation for investigating these two research areas, including a survey of available theories, is provided next in sections 1.2 and 1.3.

1.2. Multicomponent Surfactant Mixtures

1.2.1. Motivation

Surfactant formulations of practical utility typically consist of multicomponent surfactant mixtures. These mixtures may result from a design constraint, due to the difficulty and expense associated with synthesizing or purifying monodisperse surfactants. The polydispersity of a commercial surfactant can result from the polydispersity in the hydrocarbon raw materials used, and from the reaction kinetics associated with the synthesis step, such as the Poisson distribution of head lengths in the case of alkyl poly(ethylene oxide) nonionic surfactants. In addition, pH-sensitive surfactants, like dodecyldimethylamine oxide (C_{12}DAO), can exist as binary mixtures of the protonated and the deprotonated forms (see also section 1.3).[26] To illustrate the benefit of utilizing surfactant mixtures, we consider three topics of relevance to detergent formulations: (1) hard water tolerance, (2) surfactant-induced skin irritation, and (3) cleaning performance.

Hard water is characterized by a high concentration of multivalent metal ions. In hard water, anionic surfactants readily precipitate to form soap scum, an insoluble complex of the metal ion and the anionic surfactant.[27,28] Since the major surfactant component of most common detergents is an anionic surfactant,[29–31] hard water tolerance is a practical concern in many areas. Thermodynamically, the precipitation of soap scum is governed by the activities of the multivalent ion and the anionic surfactant, through a solubility product. Although the activity of the multivalent ion is related to its concentration (and therefore to the "hardness" of the water), the activity of the anionic surfactant is related to its *monomer concentration*.

Consequently, greater hard water tolerance can be achieved by decreasing the monomer concentration of an anionic surfactant. Since each distinct surfactant species is governed by its own solubility product, a mixture of two anionic surfactants can have the same *total* monomer concentration as a solution of a single anionic surfactant, yet a solution consisting of the binary surfactant mixture will tolerate hard water better than the single surfactant solution, since the monomer concentration of each species of anionic surfactant will be lower. In that case, the use of a polydisperse surfactant mixture is preferable to the use of a "pure" surfactant. An even more effective strategy for improving hard water tolerance is to add a small amount of nonionic surfactant to the anionic surfactant.[27,28] The addition of a nonionic surfactant results in a monomer concentration of the anionic surfactant that is lower than what would result from the addition of an equivalent amount of anionic surfactant.

An additional property of interest in detergent formulation is the surfactant-induced skin irritation that may result from skin exposure to the detergent aqueous solutions. Recently, it was demonstrated that adding a nonionic surfactant to an aqueous solution containing an ionic surfactant resulted in a reduction in skin irritation, even though the *total* surfactant concentration was increased.[32] This somewhat surprising result was rationalized by considering which micellization properties are responsible for surfactant-induced skin irritation. Historically, only the surfactant monomers were assumed to induce skin irritation because of their ability to readily penetrate into the skin due to their small size. However, micelles have recently been shown to contribute to skin irritation as well, by penetrating through aqueous pores that exist in the skin, if the micelles are smaller than the aqueous pores.[33] The addition of a nonionic surfactant to an aqueous solution containing an anionic surfactant was shown to reduce the irritation potential of both the monomers and the micelles: (1) by reducing the monomer concentration, and (2) by increasing the size of the micelles, thus reducing their ability to penetrate into the skin.[33]

Recently, the cleaning performance of several multicomponent surfactant mixtures was optimized by varying the surfactant composition.[16] In all cases, the cleaning performance of the multicomponent surfactant mixtures was found to exceed that of

any of the single surfactant components. Although detergency is a relatively complex phenomenon, the cleaning performance of surfactant mixtures has been correlated with the cmc behavior.[4] In particular, the number of plates washed and the amount of soil removed were maximized when Δcmc (defined below) was maximized. As an illustration, for a binary surfactant mixture, Δcmc is defined[4] as the difference between the ideal cmc of the mixture[34,35] ($\mathrm{cmc_{ideal}}$) and the actual cmc of the mixture ($\mathrm{cmc_{mix}}$) (that is, $\Delta\mathrm{cmc} = \mathrm{cmc_{ideal}} - \mathrm{cmc_{mix}}$), where

$$\frac{1}{\mathrm{cmc_{ideal}}} = \frac{\alpha_1}{\mathrm{cmc_A}} + \frac{(1-\alpha_1)}{\mathrm{cmc_B}} \tag{1.1}$$

where α_1 is the monomer composition of surfactant A, and $\mathrm{cmc_A}$ and $\mathrm{cmc_B}$ are the cmc's of the single surfactants A and B.

1.2.2. Theoretical Approaches

Theoretical approaches to model surfactant mixtures were recently reviewed by Hines.[36] The most commonly utilized model to quantify the micellization of surfactant mixtures is regular solution theory (RST) in the context of the pseudophase approximation.[35] The RST is a thermodynamic model that characterizes the specific interaction (or synergy) between two surfactants with a single quantity known as the β parameter. If the β parameter and the individual cmc's of a pair of surfactants are known, then the RST can be utilized to predict the cmc of any mixture of the two surfactants. However, the β parameter is usually determined empirically by fitting the RST to the experimentally determined cmc of one, or more, surfactant mixtures. Although RST was extended to model mixtures containing an arbitrary number of surfactants,[37] most studies have been limited to binary surfactant mixtures. Despite its widespread use, RST suffers from several limitations. Several studies cited in ref 36 have identified systems for which cmc data is not well modeled by RST. These limitations have been interpreted as resulting from β parameters that vary with surfactant composition or concentration. In addition, the use of the pseudophase approximation implies that details of the micelle structure (shape and

size, in particular) are not accounted for, since the micelles are approximated as an infinitely large phase. Lastly, applying RST to multicomponent surfactant mixtures requires β parameters *for each surfactant pair*. Consequently, in systems containing a large number of surfactants, the required number of cmc measurements required to obtain the needed β parameters can become prohibitively large.[38]

More recently, molecular-thermodynamic (MT) theories, which overcome many of the limitations of RST, have been developed to model the micellization of surfactant mixtures.[36] The MT theories were inspired by the phenomenological approach of Tanford[1] and by the molecular-geometric approach of Israelachvili.[3] The MT theories combine a thermodynamic description of the equilibrium constraints governing micellization with a molecular model of the free-energy change associated with transferring the surfactant molecules from the bulk aqueous solution to the micelles. Unlike RST, however, the MT theories predict the shape and the size of micelles and are predictive at the molecular level. In fact, the MT approach solely requires knowledge of the molecular structures of the surfactants and of the solution conditions (such as the total surfactant concentration, the temperature, and the type and concentration of any added salt). In our group, a MT theory was first developed to model the micellization of a single nonionic surfactant,[39] and later was extended to model the micellization of binary mixtures of nonionic surfactants.[40,41] Subsequent developments focused on electrostatic interactions, which were first studied in binary surfactant mixtures containing charged surfactants.[4] Explicit counterion binding was then incorporated into the theory, which resulted in more accurate predictions for ionic surfactants.[42,43]

At present, the MT theories introduced by our group and by others have been developed to model the micellization of mixtures containing at most two surfactant components.[4,40,41,44] Even so, these MT theories can assist in the modeling of multicomponent surfactant mixtures. In particular, the MT theories have been coupled with RST to reduce, or eliminate altogether, the need for experimental inputs. For example, the β parameters,[45] or both the single-surfactant cmc's and the β parameters,[38,46] have been predicted using MT theories. Nevertheless, the

development of a MT theory to model the micellization of mixtures containing an arbitrary number of surfactants would eliminate the need to rely on the pseudophase approximation and on the β parameters associated with RST.

1.3. pH-Sensitive Surfactants

1.3.1. Motivation

Many types of surfactants are pH-sensitive, including some ionic, zwitterionic, and "semipolar" surfactants. Soap, which is the deprotonated form of a fatty acid, is a pH-sensitive ionic surfactant. Zwitterionic surfactants carry no net charge but contain two functional groups that are oppositely charged. For typical zwitterionic surfactants, one or both charged groups are pH-sensitive. For example, carboxybetaines (or simply betaines) are zwitterionic surfactants containing a pH-sensitive carboxylate group. Semipolar surfactants are similar to zwitterionic surfactants but have a smaller reduced dipole moment, which essentially means that they do not have a full formal charge on any of their functional groups.[47] The pH-sensitive surfactants studied in this thesis include several amine oxides, which are semipolar, and a zwitterionic betaine.

A typically small, yet very important, fraction of many surfactant formulations consists of pH-sensitive, amphoteric surfactants. Their unique chemistry increases their synergy with other surfactants, by improving solubility, by reducing skin or eye irritation, and by improving foaming properties. These benefits have led to the incorporation of pH-sensitive surfactants in personal care formulations, disinfectants, and anti-corrosion coatings.[48] Accordingly, it is not surprising that in recent years amphoteric surfactants have shown stronger market growth than other classes of surfactants.[5,48]

A pH-sensitive surfactant behaves effectively like a binary mixture of its protonated and deprotonated forms, where the composition of the surfactant is controlled by the solution pH. In particular, the protonation equilibrium of the

surfactant monomers can be characterized by an equilibrium deprotonation constant (pK_1). As a result, pH-sensitive surfactants allow experimental access to properties that are often difficult to measure in "conventional" binary surfactant mixtures. For example, titrating solutions of pH-sensitive surfactants (that is, measuring the solution pH as a function of the amount of added acid or base) can allow experimental access to the monomer and the micelle compositions.[49,50] Titration experiments have also been used to determine the electrostatic potential at the micelle interface.[51]

Furthermore, recent studies indicate that pH-sensitive surfactants may also be useful in novel applications, such as drug release, targeted gene delivery, and the fabrication of nanoscale materials for optics, electronics, and sensors.[6,8–13,52–60] A common goal for the controlled release of drugs or nucleic acids (for gene delivery) is to find a suitable pH-sensitive surfactant (or mixture of surfactants) that will release the active material upon a change in local pH.[6,8–13,58–60] Ideally, the delivery and release process is as follows: (1) at physiological pH ($\sim$7.4), the surfactants assemble into vesicles or liposomes that encapsulate the active material, (2) the vesicles enter cells, for example, by endocytosis, (3) upon localization in an endosomal compartment, which has a lower pH (4–6), the vesicles can fuse with the endosomal membrane, and (4) in response to the pH change, the pH-sensitive surfactants disrupt the endosome, triggering the release of the active material.[10–12,58]

Another promising class of pH-sensitive surfactants replace the hydrophobic and/or the hydrophilic moieties with an oligomer of pH-sensitive amino acids. Consequently, these novel surfactants are known as peptide amphiphiles. Because of extensive technological advances in the synthesis of peptides, utilizing robotic synthesizers and bioengineered organisms, peptide amphiphiles may be more cost effective than surfactants.[61] In addition, peptide amphiphiles have been observed to self-assemble into a wide array of structures, including micelles, vesicles, nanotubes, fibrils, sheets, bundles, and tubules.[61–63] The particular structure formed can usually be controlled reversibly via changes in solution pH or temperature. The nanostructures can serve as templates, or be further derivatized, for use as nanowires or photonics devices.[61] Although the rational design of peptide amphiphiles is highly

desirable, this goal is complicated by the fact that a small change in the molecular structure of a peptide amphiphile often leads to a large change in the macromolecular structure that it forms.[62]

1.3.2. Theoretical Approaches

Unfortunately, few of the available micellization models explicitly incorporate the effects of the solution pH. A few thermodynamic approaches have recently been developed to study the micellization of a single pH-sensitive surfactant. Rathman and Scamehorn developed a method for determining surfactant activities from micellar titration data, but only for the case of a swamping electrolyte.[49] Zimmerman and Schnaare extended the approach to the case of a non-swamping electrolyte.[50]

Micellar titration behavior has been modeled by several methods. For example, micellar titration behavior has been analyzed in terms of electrostatic interactions.[64,65] Mille, who, along with Vanderkooi, initially modeled vesicles of pH-sensitive surfactants,[66] subsequently modeled micellar titration by accounting for the nearest-neighbor interactions, but found that electrostatic interactions were insufficient to explain the observed titration behavior of C_{12}DAO.[64] Maeda utilized a form of the Gibbs-Duhem equation to obtain a thermodynamic model for micellar titrations.[67] Like Mille, he found that electrostatic interactions were insufficient to explain the titration behavior of C_{12}DAO. Maeda also examined the implications of his thermodynamic model when the micelles are modeled using RST. In this case, the titration curve was found to be linear with a slope related to the β parameter.[67] More recently, Lair et al. developed a thermodynamic relationship relating the cmc to the degree of protonation of the pH-sensitive micelles.[68] By using a linear regression analysis of the experimental micellar titration curves, they successfully predicted the pH-dependence of the cmc of C_{12}DAO.

Very few studies have attempted to model surfactant *mixtures* containing a pH-sensitive surfactant, with the exception of one study which utilized RST to predict the pH-dependence of the cmc of mixtures of two pH-sensitive surfactants, tetradecyldimethylamine oxide (C_{14}DAO) and hexadecyldimethyl betaine (C_{16}Bet).[69]

In this study, Zimmerman and Schnaare examined solution pH's at which C_{16}Bet was only present in its deprotonated, zwitterionic form, while C_{14}DAO was present in both its protonated, cationic form and in its deprotonated, zwitterionic form. They found that RST yielded reasonable predictions of the cmc's of what were effectively ternary surfactant mixtures. However, extensive cmc measurements of single and binary surfactant mixtures were required to obtain the parameters required by the RST.

In addition, the titration behavior of micelles containing a small fraction of a pH-sensitive surfactant was recently predicted theoretically by using Poisson-Boltzmann calculations and Monte Carlo simulations.[70] The pH-sensitive surfactant, lauric acid, was added to cationic, anionic, and nonionic micelles. The titration behavior of the micellized lauric acid was found to be significantly different in each type of micelle considered. The results of these studies suggested that the titration behavior could be explained by electrostatic interactions. However, it was found that the predicted titration behavior was very sensitive to the choice of dielectric constant near the surface of the micelle.

Although, undoubtedly, each of the models discussed above has advanced our fundamental understanding of pH-dependent micellization, to date, no comprehensive *molecular-level theory* of the micellization behavior of pH-sensitive surfactants has been formulated. In addition, no studies have examined the relationship between micelle composition and micellar titration behavior in micelles containing both pH-sensitive and conventional surfactants. Clearly, both experimental studies and theoretical models of such systems are of interest for both fundamental and practical reasons.

1.4. Thesis Overview

The primary goal of this thesis was to model the micellization of pH-sensitive surfactants, with a particular emphasis on developing *molecular* theories. However, this goal closely overlaps with the goal of understanding multicomponent surfactant

mixtures, since pH-sensitive surfactants behave as binary mixtures of the protonated and the deprotonated forms. Therefore, the first two chapters focus on systems that can be modeled as binary surfactant mixtures. Chapter 2 presents a MT theory for binary mixtures of conventional surfactants that explicitly accounts for counterion binding. This theory is extended in Chapter 3 to include pH effects in order to model the micellization of a pH-sensitive surfactant. The remaining chapters focus on mixtures containing an arbitrary number of conventional surfactants. Chapter 4 presents an RST approach to model the micellar titration behavior of mixtures of a pH-sensitive surfactant and conventional surfactants. In Chapter 5, a MT theory is developed to model the micellization of an arbitrary number of conventional surfactants. Chapter 6 extends this theory by incorporating pH effects in order to model mixtures of pH-sensitive and conventional surfactants. Finally, concluding remarks and future research directions are presented in Chapter 7.

Chapter 2

Modeling Counterion Binding in Ionic-Nonionic and Ionic-Zwitterionic Binary Surfactant Mixtures

2.1. Introduction

The type and concentration of ions can have a pronounced effect on micellar solution properties of ionic surfactants in aqueous solutions.[42,43] Understanding the interactions between ions and charged micelles is relevant to both fundamental research and industrial applications involving ionic surfactants. Furthermore, ionic surfactants are often key components of surfactant mixtures, which may arise as a byproduct of synthesis or from the use of commercial-grade materials. In addition, pH-sensitive surfactants, like dodecyldimethylamine oxide, can exist as binary mixtures of charged and uncharged species (see also Chapter 3).[26] Perhaps more importantly, surfactant mixtures are intentionally used because they can exhibit improved performance properties when compared to formulations that utilize a single surfactant component.[71] For example, mixing nonionic surfactants with ionic surfactants has been shown to improve hard-water tolerance[27] and to reduce surfactant-induced skin irritation.[32] In this paper, we focus on the effect of counterion

binding on the micellization behavior of binary mixtures of *ionic and nonionic (or zwitterionic)* surfactants.

Ions can have a *non-specific effect* on charged micelles due to their effect on the solution ionic strength. For example, increasing the solution ionic strength (by changing the valence or the concentration of added salt) can induce the growth of micelles composed of ionic surfactants, from spherical micelles to long, cylindrical micelles.[1,3] Co-ions, or ions with the same sign charge as the surfactant ion, primarily affect micellar properties through their effect on the solution ionic strength. On the other hand, counterions, or ions with charge having the opposite sign to that of the surfactant ion, are known to have an additional *specific effect*. For example, sodium bromide was found to induce the growth of micelles of the cationic surfactant cetyl pyridinium bromide, while sodium chloride did not.[72] In addition, the valence of counterions can have a pronounced effect on micelles containing ionic surfactants. For example, Alargova et al. measured the micelle aggregation number of solutions of the anionic surfactant sodium dodecyl sulfate (SDS), with added sodium chloride, and either calcium chloride or aluminum chloride salts.[73,74] Bucci and Fagotti obtained similar results in binary mixtures of SDS and the nonionic surfactant β-dodecyl maltoside.[75]

In this chapter, we present a model that accounts for the effect of ions on the micellization behavior of binary mixtures of ionic-nonionic (or ionic-zwitterionic) surfactants in aqueous solutions. This model also serves as the basis for our ongoing work aimed at modeling the micellization behavior of *pH-sensitive surfactants*, which are effectively binary surfactant mixtures of protonated and deprotonated species.

We focus primarily on predicting the degree of counterion binding to a charged *mixed micelle*, which can be used to determine the effective micelle charge (an important property in interpreting experimental results or in designing surfactant formulations). The degree of counterion binding can be estimated using various experimental techniques, each yielding a slightly different value, because the specific details of the technique determine which counterions are considered to be bound. For example, spectroscopic techniques[76,77] (such as NMR) and micellar

catalysis[78] measure as being bound only those counterions that are located within a few Angstroms of the charged micelle surface. Techniques that probe transport properties[79–81] (such as diffusion or conductivity measurements) measure as being bound only those counterions that are transported along with the charged micelle. Gunnarsson et al. have shown how knowledge of the distribution of ions around a charged micelle can be used to estimate the different degrees of counterion binding that are measured using various experimental techniques.[82]

Attempts have been made in the past[83–88] to model counterion binding to single-component ionic surfactant micelles. These previous models have been reviewed and contrasted with a recently proposed model of counterion binding to *single-component ionic surfactant micelles*.[42] The few theoretical studies that have focused on the degree of counterion binding to *binary mixed micelles* are discussed below.

An empirical relationship to describe the variation of the degree of counterion binding with micelle composition was first proposed by Hall et al., who studied the degree of counterion binding to several mixed micellar systems.[89,90] Maeda recently presented a theoretical justification of this relationship based on a charged-plate cell model of micelles at the Poisson-Boltzmann level.[91] The resulting equation, which relates the degree of counterion binding to the ionic composition of the mixed micelle, was successfully applied to several binary surfactant mixtures. Although, in principle, the theory may be used to predict the degree of counterion binding over the entire micelle composition range, in practice, good quantitative agreement was only obtained when the degree of counterion binding to the pure ionic surfactant micelles was treated as an adjustable parameter. Because of the inherent simplicity of this model, many details of the micellization process were not captured. In particular, the dependence of the degree of counterion binding on micelle shape was ignored, since curvature effects were not accounted for. The model also predicts the same degree of counterion binding regardless of the identity of the nonionic surfactant, contrary to experimental observations.[92–94] Furthermore, the model does not predict the existence of a composition range over which negligible counterion binding occurs,

contrary to the findings by Treiner et al.[93,95,96] These limitations are largely due to the fact that the model does not incorporate a molecular-level description of the micellization process, and as such it can only capture general trends arising solely from the electrostatic interactions.

Rathman and Scamehorn modeled counterion binding in binary mixed micelles, using either a localized adsorption model or a mobile adsorption model.[94,97] Their results show good quantitative agreement for several binary surfactant mixtures. However, their approach assumes that the shape and size of micelles are known and do not vary with micelle composition, and it also requires a fitted parameter which describes counterion adsorption. This parameter may be obtained by fitting the degree of counterion binding to the pure ionic surfactant micelle.

To date, no molecular-level model of mixed micellization has been developed that predicts the detailed micelle structure, including the shape, size, composition, *and the degree of counterion binding*. In this chapter, we present a molecular-thermodynamic theory that combines a recently developed model of counterion binding to single-component ionic surfactant micelles[42,43] with a general theoretical framework developed earlier to model mixed micellization in binary surfactant mixtures.[4,39–41,44] The theory requires knowledge of the basic chemical structures of the surfactants and the counterions, and solution conditions (the temperature and the concentrations of added surfactant and salt). Using this theory, we predict the degree of counterion binding to charged mixed micelles, the critical micelle concentration (cmc), and the micelle aggregation number. In addition, the theory can be used to predict other micellar solution properties, including the monomer and micelle concentrations, the monomer and micelle compositions, and the micelle shape and size.[4] The resulting theoretical framework also facilitates the study of the dependence of counterion binding (and other micelle properties) on surfactant structure and solution conditions.

The remainder of this chapter is organized as follows. The thermodynamic framework is presented in section 2.2. The molecular model for the free energy of mixed micellization is presented in section 2.3. section 2.4 briefly describes how the micelle size distribution and related micelle properties are calculated. In section 2.5,

the theory is applied to several binary surfactant mixtures for which experimental data is available in the literature. Concluding remarks are presented in section 2.6.

2.2. Thermodynamic Framework

As discussed, we extend a theoretical framework to model the micellization behavior of binary surfactant mixtures[4,40,41] by incorporating a recently developed model for counterion binding to single-component ionic surfactant micelles.[42] In this section, we briefly review this theory with particular emphasis on its new aspects. For simplicity, the theoretical framework is developed for a binary mixture of an ionic surfactant (component A) mixed with a nonionic, or zwitterionic, surfactant (component B). Quantities related to the counterion of the ionic surfactant are denoted by the subscript C. To simplify our development, we assume that any added salt consists of the same ion C (the counterion) and any ion X (the co-ion). All the surfactant ions are assumed to be monovalent (with a valence $z_A = \pm 1$), while the surfactant counterions can be monovalent (with a valence $z_C = \pm 1$) or multivalent (with $|z_C| > 1$).

First, we consider a micelle consisting of $n\alpha$ surfactant ions, $n(1-\alpha)$ nonionic surfactant molecules, and $n\hat{\beta}$ bound counterions, where n is the aggregation number of the micelle, α is the ionic micelle composition, and $\hat{\beta}$ is the number of bound counterions *per surfactant molecule in the micelle*. This definition of the degree of counterion binding simplifies the theoretical developments that follow and highlights the similarities between the micellization treatment of surfactants and counterions. However, for convenience and comparison with the experimental results, we also define the more traditional degree of counterion binding β as the number of bound counterions *per ionic surfactant molecule in the micelle*. The two definitions are related by the following equation:

$$\beta = \hat{\beta}/\alpha \tag{2.1}$$

In other words, the micelle valence is given by: $z_{mic} = n(z_A\alpha + z_C\hat{\beta}) = nz_A\alpha(1-|z_C|\,\beta)$,

and a micelle with $\beta = 1/|z_C|$ (or $\hat{\beta} = \alpha/|z_C|$) would carry no net charge because the ionic surfactant molecules in the micelle would be completely neutralized by the bound counterions. Note that $\hat{\beta} = \beta$ when the system is composed of a single ionic surfactant component (that is, when $\alpha = 1$).

The thermodynamic equilibrium condition for micelle formation can be expressed in terms of the chemical potentials of the singly dispersed surfactants A and B (μ_A and μ_B), of the singly dispersed counterions C (μ_C), and of the mixed micelles of aggregation number n, composition α, and degree of counterion binding $\hat{\beta}$ ($\mu_{n\alpha\hat{\beta}}$) as follows:

$$n\alpha\mu_A + n(1-\alpha)\mu_B + n\hat{\beta}\mu_C = \mu_{n\alpha\hat{\beta}} \tag{2.2}$$

The chemical potentials in eq 2.2 can be expressed as functions of the species mole fractions, where X_{1i} denotes the mole fraction of species i (A, B, and C) in monomeric form, and $X_{n\alpha\hat{\beta}}$ denotes the mole fraction of micelles of type $n\alpha\hat{\beta}$. By substituting appropriate expressions for the chemical potentials μ_A, μ_B, μ_C, and $\mu_{n\alpha\hat{\beta}}$[4,40,41] in eq 2.2, the following expression is obtained for $X_{n\alpha\hat{\beta}}$:

$$X_{n\alpha\hat{\beta}} = \frac{1}{e} X_{1A}^{n\alpha} X_{1B}^{n(1-\alpha)} X_{1C}^{n\hat{\beta}} \exp\left[-\frac{n}{k_B T} g_{mic}\left(S, l_c, \alpha, \hat{\beta}\right)\right] \tag{2.3}$$

where g_{mic} is defined as follows:

$$g_{mic} = \frac{1}{n}\mu^0_{n\alpha\hat{\beta}} - \left[\alpha\mu^0_A + (1-\alpha)\mu^0_B + \hat{\beta}\mu^0_C\right] - k_B T\left(1+\hat{\beta}\right) \tag{2.4}$$

In eq 2.4, μ_i^0 is the standard-state chemical potential of species i (A, B, C, and $n\alpha\hat{\beta}$), k_B is the Boltzmann constant, and T is the absolute temperature. The quantity g_{mic} is the free energy of mixed micellization, which is the free-energy gain per surfactant molecule associated with transferring the $n\alpha$ surfactant A monomers, the $n(1-\alpha)$ surfactant B monomers, and the $n\hat{\beta}$ counterions from the bulk aqueous solution to the micelle (the $n\alpha\hat{\beta}$-mer). Note that g_{mic} is a function of the following micelle characteristics: the shape parameter, S, the core minor radius, l_c, the ionic composition, α, and the degree of counterion binding, $\hat{\beta}$. The quantity S is 3 for

spherical micelles, 2 for cylindrical micelles, and 1 for planar or discoidal micelles. Note that l_c refers to the radius of the hydrophobic core of spherical or cylindrical micelles, or to the half-width of the hydrophobic core of planar micelles.

We next introduce the modified free energy of mixed micellization, g_m, originally introduced for binary surfactant mixtures in the absence of counterion binding,[4,41] as follows:

$$g_m = g_{mic} - k_B T \left[\alpha \ln \alpha_1 + (1-\alpha) \ln (1-\alpha_1) + \hat{\beta} \ln X_{1C} \right] \tag{2.5}$$

where $\alpha_1 = X_{1A}/X_1$ is the ionic composition of the free surfactant monomers, and $X_1 = X_{1A} + X_{1B}$ is the total mole fraction of surfactant monomers. The last term in eq 2.5, $-k_B T \hat{\beta} \ln X_{1C}$, quantifies the translational entropy loss of the bound counterions. Equation 2.3 can be rewritten in a form that is easier to solve numerically, by replacing X_{1A} and X_{1B} by $\alpha_1 X_1$ and $(1-\alpha_1) X_1$, respectively. After algebraic simplification, one obtains the following expression for $X_{n\alpha\hat{\beta}}$:

$$X_{n\alpha\hat{\beta}} = \frac{1}{e} X_1^n \exp \left[-\frac{n}{k_B T} g_m \right] \tag{2.6}$$

Each species of surfactant and ion in solution can be: (1) part of a micelle, (2) part of the diffuse ion cloud surrounding a micelle, or (3) part of the bulk solution. Due to the net charge of a micelle, the concentration of counterions in the diffuse ion cloud surrounding a micelle will be enhanced by electrostatic attractions, relative to the concentration of the counterions in the bulk solution. Likewise, co-ions and ionic surfactant monomers will be depleted in the diffuse ion cloud. Mole balances on the various species can therefore be expressed as follows:

$$\begin{aligned} X_A &= X_{1A} + \sum_{\{S,n,\alpha,\hat{\beta}\}} n\alpha X_{n\alpha\hat{\beta}} + E_{dl,A} \\ X_B &= X_{1B} + \sum_{\{S,n,\alpha,\hat{\beta}\}} n(1-\alpha) X_{n\alpha\hat{\beta}} \\ X_C &= X_{1C} + \sum_{\{S,n,\alpha,\hat{\beta}\}} n\hat{\beta} X_{n\alpha\hat{\beta}} + E_{dl,C} \end{aligned} \tag{2.7}$$

where X_i refers to the *total* mole fraction of species i (i = A, B, or C) in solution, the summations in eq 2.7 account for micelles of different types (that is, having different values of S, α, n, and $\hat{\beta}$), and $E_{\mathrm{dl},i}$ (i = A or C) is a term accounting for the enhancement or the depletion of ions of species i in the diffuse layer (dl), relative to their concentrations in the bulk. Since component B (nonionic or zwitterionic surfactant) carries no net charge, its monomer concentration is assumed to be uniform throughout both the bulk solution and the diffuse ion clouds surrounding the charged micelles (that is, $E_{\mathrm{dl,B}} = 0$). Details of the derivation of the diffuse layer contribution to the mole balances, including the evaluation of $E_{\mathrm{dl},i}$ (i = A or C), are presented in Appendix A. If an appropriate model for g_{mic} is available, the properties of the micellar solution can be predicted by simultaneously solving Eqs. 2.6 and 2.7, as described in section 2.4.

2.3. Molecular Model for the Free Energy of Mixed Micellization

We use a conceptual thought process to model the free energy of mixed micellization, g_{mic}, as the sum of several contributions that model the essential physics underlying the micellization process. Specifically, we model g_{mic} as follows:

$$g_{\mathrm{mic}} = g_{\mathrm{tr}} + g_{\mathrm{int}} + g_{\mathrm{pack}} + g_{\mathrm{st}} + g_{\mathrm{elec}} + g_{\mathrm{ent}} \tag{2.8}$$

The first three terms of the sum are associated with the surfactant tails and the formation of the micelle core: g_{tr} is the transfer contribution, g_{int} is the interfacial contribution, and g_{pack} is the packing contribution. The final three terms of the sum are associated with the surfactant heads and the bound counterions that form the micelle interfacial shell: g_{st} is the steric contribution, g_{elec} is the electrostatic contribution, and g_{ent} is the entropic contribution. In the following subsections, we briefly present the key equations for the various free-energy contributions in eq 2.8, while highlighting the key differences from previous models. Complete details are

provided in earlier publications.[4,39,42,43]

In section 2.3.1, we discuss the free-energy contributions associated with the core of a mixed micelle. In section 2.3.2, we discuss the free-energy contributions associated with the interfacial shell of a mixed micelle. Finally, section 2.3.3 provides more details about the electrostatic model.

2.3.1. Modeling the Hydrophobic Micelle Core

The first free-energy contributions that will be described are those related to the formation of the hydrophobic micelle core. These contributions therefore depend on the structure of the surfactant tails, as well as on the micelle composition, α, and on the micelle core minor radius, l_c. Since all the surfactants considered in this chapter are composed of a linear alkane tail, each surfactant tail can be specified by the number of carbon atoms in the hydrophobic portion of its tail, n_t. This quantity may be less than the total number of carbon atoms in the tail, because some carbon atoms may acquire a hydrophilic character if they are adjacent to other strongly hydrophilic functional groups. To determine which atoms are hydrophobic, we have used the chemistry software Molecular Modeling Pro[98] to estimate the hydrophilic/hydrophobic character of the atoms in several classes of surfactant molecules. (The software uses a proprietary group-contribution method to estimate the hydrophilicity/hydrophobicity of each atom.[99]) In general, we observed that the atoms in an alkane tail are hydrophobic in nature, unless they are adjacent to a charged group. Based on these calculations, for all the ionic and zwitterionic surfactants discussed in this chapter, $n_t = n_c - 1$, where n_c is the number of carbon atoms in the alkane tail, and for the nonionic surfactants, $n_t = n_c$ (see Tables 2.1-2.3).

2.3.1.1. Transfer Free-Energy Contribution

The transfer free-energy contribution, g_{tr}, accounts for the hydrophobicity of the surfactant tails, and is the driving force for micellization in aqueous media. Specifically, g_{tr} is the average free-energy change per surfactant molecule associated

Table 2.1: Molecular characteristics of ionic surfactants (for unabbreviated names and notation, see the text).

Ionic Surfactant	n_{tA}	a_{hA} [Å^2]	l_{hA} [Å]	d_{zA} [Å]	z_{A}	z_{C}	r_{C} [Å]
C_{16}TAB	15	32.0	5.76	2.5	+1	–1	2.10
C_{18}TAC	17	32.0	5.76	2.5	+1	–1	2.13
SDS	11	25.0	6.27	3.7	–1	+1	2.18
CuDS	11	25.0	6.27	3.7	–1	+2	2.97
STS	13	25.0	6.27	3.7	–1	+1	2.18

Table 2.2: Molecular characteristics of the zwitterionic surfactant dodecyldimethylphosphine oxide, C_{12}PO (for notation, see the text).

Zwitterionic Surfactant	n_{tB}	a_{hB} [Å^2]	d_{zB} [Å]	d_{sepB} [Å]	z_{innerB}
C_{12}PO	11	28.0	2.6	1.13	+1

with transferring the surfactant tails from the aqueous phase to a bulk oil phase. This contribution is modeled as $\alpha g_{\mathrm{trA}} + (1-\alpha)\, g_{\mathrm{trB}}$, where $g_{\mathrm{tr}i}$ is the transfer contribution of surfactant tail i (A or B). The individual contributions can be calculated as a function of n_{t} and of temperature using a correlation based on experimental solubility data for linear alkanes in water.[1,41] We have also allowed for the dependence of g_{tr} on added salt type and concentration using a model for the effect of added salt on the solubility of alkanes in water.[100]

2.3.1.2. Interfacial Free-Energy Contribution

The interfacial free-energy contribution, g_{int}, accounts for the free-energy penalty associated with the formation of the interface between the hydrophobic micelle core and the aqueous phase, and is modeled using the following expression:

$$g_{\mathrm{int}} = (a - a_0)\left[\alpha\sigma_{\mathrm{A}} + (1-\alpha)\,\sigma_{\mathrm{B}}\right] \tag{2.9}$$

Table 2.3: Molecular characteristics of nonionic surfactants (for unabbreviated names and notation, see the text).

Nonionic Surfactant	n_{tB}	a_{hB} [Å^2]
OG	8	40.0
$C_{12}E_4$ (25°C)	12	30.6
$C_{12}E_6$ (30°C)	12	40.9
$C_{12}E_6$ (50°C)	12	35.3
$C_{12}E_{23}$ (25°C)	12	53.3

where a is the area per surfactant molecule at the micelle core-water interface, a_0 is the interfacial area that is screened by a surfactant head (estimated as 21 Å^2 for a single-tailed hydrocarbon surfactant), and σ_i is the curvature-dependent interfacial tension between water and an oil phase of surfactant tails of type i (A or B), estimated as described in ref 39. The area a is calculated using the following expression:

$$a = \frac{S\,\overline{v}_{\mathrm{t}}}{l_{\mathrm{c}}} \tag{2.10}$$

where $\overline{v}_{\mathrm{t}} = \alpha v_{\mathrm{tA}} + (1-\alpha) v_{\mathrm{tB}}$ is the average tail volume ($v_{\mathrm{t}i}$ is the hydrophobic tail volume of surfactant i (in Å^3), calculated from the tail length $n_{\mathrm{t}i}$).[1] The addition of salt is known to have a small but measurable effect on the oil-water interfacial tension, and we have included a salt-dependent correction as suggested in ref 100.

2.3.1.3. Packing Free-Energy Contribution

The packing free-energy contribution, g_{pack}, accounts for the fact that the hydrophobic core of the micelle has more internal constraints than a droplet of bulk hydrocarbon. In particular, one end of each surfactant tail must be anchored at the micelle core-water interface, resulting in an increase in the free energy of micellization (that is, $g_{\mathrm{pack}} > 0$). The packing free energy is modeled by generalizing a single-chain mean-field model pioneered by Ben-Shaul, Szleifer, and Gelbart.[101–103]

This approach involves sampling the conformations and orientations of the surfactant tail, and ensuring that the micelle core is at a uniform density. Because this step is computationally intensive, we generated packing free energies once for the various surfactant tails of interest, for all relevant micelle shapes, sizes, and compositions. These data were then fit to polynomial functions of α and l_c, as described previously.[4,104] For a particular set of surfactant tails $\{n_{tA}, n_{tB}\}$, one polynomial was obtained for each micelle shape (spherical, cylindrical, and planar).

2.3.2. Modeling the Micelle Interfacial Shell

The following free-energy contributions are associated with the interactions in the hydrophilic region of the micelle, located at the micelle core-water interface. Because these contributions depend on the structure of the hydrophilic surfactant heads as well as on the structure of the bound counterions, we present here a generalized interfacial model that combines two of our previous interfacial models, one developed for binary mixed micelles containing an ionic surfactant,[4] and the other for single-component ionic surfactant micelles and their bound counterions.[42] Each of these free-energy contributions includes an explicit dependence on the degree of counterion binding.

2.3.2.1. Steric Free-Energy Contribution

The steric free-energy contribution, g_{st}, accounts for the penalty associated with steric interactions between surfactant heads and bound counterions. We use the test-particle approach,[41] which models the various components as being part of an ideal monolayer, to obtain the following expression:

$$g_{st} = -k_B T \left(1 + \hat{\beta}\right) \ln \left[1 - \frac{\alpha a_{hA} + (1-\alpha)\, a_{hB} + \hat{\beta} a_{hC}}{a}\right] \tag{2.11}$$

where a_{hi} is the cross-sectional area of the head of surfactant i (A or B) or of counterion C. Equation 2.11 reveals, as expected, that g_{st} increases with an increase in the cross-sectional areas of the surfactants, a_{hA} or a_{hB}, or the counterion, a_{hC}; with an increase in the degree of counterion binding, $\hat{\beta}$; or with a decrease in the micelle surface

area per surfactant molecule, a. The factor $(1+\hat{\beta})$ appears because g_{st} increases with the *total number of molecules* in the micelle, $n(1+\hat{\beta})$, but g_{st} is normalized by dividing the total steric free-energy contribution for a micelle by the *total number of surfactant molecules* in the micelle, n.

The head cross-sectional area a_{h} is estimated from the molecular structure of the head. In particular, in the case of poly(ethylene oxide) nonionic surfactant heads, the following temperature-dependent correlation for the cross-sectional area has been developed:[39]

$$a_{\mathrm{h}}(n_{\mathrm{EO}}, T) = a_{\mathrm{h0}} \left[1 - H\left(T - T_0\right)\right] \left(\frac{n_{\mathrm{EO}}}{6}\right)^z \tag{2.12}$$

where n_{EO} denotes the number of ethylene oxide units, T_0 is 273 K, $a_{\mathrm{h0}} = 49.4$ Å^2 denotes the cross-sectional area of a hexa(ethylene oxide) head ($n_{\mathrm{EO}} = 6$) at T_0, $H = 0.0057$ K^{-1} models the temperature dependence of the head area due to hydration effects, and $z = 0.8$ models the scaling of the head cross-sectional area with n_{EO}.

2.3.2.2. Electrostatic Free-Energy Contribution

The electrostatic free-energy contribution, g_{elec}, accounts for the interactions associated with assembling the charges in the micelle interfacial region. These charges arise from the ionic surfactants, the bound counterions, and any zwitterionic surfactants in the micelle (see Figure 2-1). Because this contribution to g_{mic} is relatively complex and is the driving force for counterion binding, it is described separately in section 2.3.3.

2.3.2.3. Entropic Free-Energy Contribution

A favorable contribution to g_{mic} arises from the entropy gain associated with mixing the two surfactant components (A and B) and the counterions (C), g_{ent}, which is calculated using a model for ideal mixing of three components randomly arranged on the micelle surface. On a surfactant-molecule basis, the entropic contribution is given

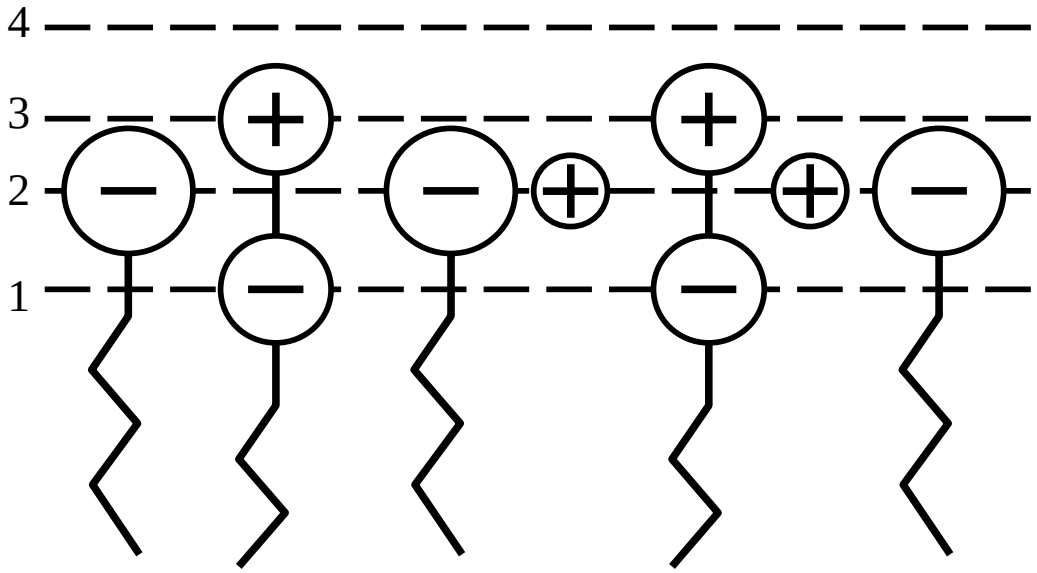

$$q_{3\mathrm{f}} = z_{\mathrm{outerB}}(1-\alpha) = +(1-\alpha)$$

$$q_{2\mathrm{f}} = z_{\mathrm{A}}\alpha + z_{\mathrm{C}}\hat{\beta} = -\alpha(1-\beta)$$

$$q_{1\mathrm{f}} = z_{\mathrm{innerB}}(1-\alpha) = -(1-\alpha)$$

Figure 2-1: Determination of $q_{i\mathrm{f}}$, the final charge per surfactant molecule on surface i, for an anionic-zwitterionic mixed micelle with bound counterions. The three surfaces of charge are numbered 1, 2, and 3 from the interior outwards. The Stern surface is numbered 4. In this example, all the positively charged counterions are assumed to bind to the negatively charged surface 2.

by:

$$g_{\text{ent}} = k_{\text{B}}T\left[\alpha \ln\left(\frac{\alpha}{1+\hat{\beta}}\right) + (1-\alpha)\ln\left(\frac{1-\alpha}{1+\hat{\beta}}\right) + \hat{\beta}\ln\left(\frac{\hat{\beta}}{1+\hat{\beta}}\right)\right] \tag{2.13}$$

or, equivalently, by:

$$g_{\text{ent}} = k_{\text{B}}T\left[\alpha \ln \alpha + (1-\alpha)\ln(1-\alpha) + \hat{\beta}\ln\hat{\beta} - \left(1+\hat{\beta}\right)\ln\left(1+\hat{\beta}\right)\right] \tag{2.14}$$

The factor $(1+\hat{\beta})$ appearing in Eqs. 2.13 and 2.14 is used to convert from compositions defined on a surfactant basis to micelle mole fractions, which are defined on the basis of the total number of molecules (surfactants and counterions) that are in the micelle, since g_{ent} depends on the mole fraction of each component in the micelle. In the limit of no counterion binding ($\hat{\beta} = 0$), we recover the expression for g_{ent} developed for mixed micelles in refs 41 and 4. When only a single ionic surfactant component is present ($\alpha = 1$), we recover the expression for g_{ent} presented in ref 42 for a single-component ionic surfactant micelle with bound counterions.

2.3.3. Evaluation of the Electrostatic Free-Energy Contribution

The electrostatic free-energy contribution, g_{elec}, is modeled by assuming that the micelle interfacial region consists of up to three concentric surfaces of charge (see below). The exact locations of these surfaces are determined by the chemical structures of surfactants A (ionic) and B (zwitterionic), and more specifically by the locations of the charges within each chemical structure. We also assume that bound counterions are located exclusively on these surfaces. Because the surfaces are modeled as having a uniform charge per unit area, the micelle surface potential is calculated using the Poisson-Boltzmann equation. The limitations inherent to this approximation have been discussed previously.[42]

The electrostatic free-energy contribution depends on several molecular characteristics of the surfactants and the counterions. For the ionic surfactant

(component A), these characteristics include the valence of the ionic surfactant, z_{A}, and the distance from the tail (as measured from the first hydrophobic carbon atom) to the location of the charge in the head, d_{zA}. For the zwitterionic surfactant (component B), these characteristics include the valences of the two constituent dipole charges, z_{innerB} and $z_{\mathrm{outerB}} = -z_{\mathrm{innerB}}$, (where z_{innerB} is the valence of the "inner" charge, closer to the tail, and z_{outerB} is the valence of the "outer" charge), the dipole length (the distance between the two charges), d_{sepB}, and the distance from the tail (as measured from the first hydrophobic carbon atom) to the inner charge group, d_{zB}. Counterions are characterized by their valence, z_{C}, and their hydrated radius, r_{C}.

When a zwitterionic surfactant is mixed with an ionic surfactant, three charged surfaces are generated, two associated with the zwitterionic surfactant and one associated with the ionic surfactant. The surfaces of charge corresponding to an example anionic-zwitterionic surfactant mixture are shown in Figure 2-1. Counterions will not bind to a similarly charged surface (anions will not bind to negatively charged surfaces, and cations will not bind to positively charged surfaces), since in our model electrostatics is the driving force responsible for counterion binding. As a result, only two charged surfaces need to be considered for counterion binding in the case of ionic-zwitterionic surfactant mixtures. Although we have implemented the theory to allow for counterions to bind simultaneously to all the charged surfaces, for the ionic-zwitterionic surfactant mixture discussed in this chapter, all the bound counterions are located on a single charged surface, as illustrated in Figure 2-1.

We model the finite size of the ions in the diffuse layer through the use of a Stern layer, which is a volume around the charged micelle where unbound counterions cannot penetrate.[105,106] Note that numerous other micellization models have included a Stern layer.[82–87,94,97,105–110] Specifically, if ions are not bound, we consider them to be in a diffuse region that begins at a distance R_{Stern} from the micelle center, which we refer to as the Stern surface.

We assume that the position of the Stern surface depends on the size of the ionic surfactant head, l_{hA}, and on the hydrated radius of the counterion, r_{C}. More specifically, we assume that $R_{\mathrm{Stern}} = l_{\mathrm{c}} + l_{\mathrm{hA}} + r_{\mathrm{C}}$. The Stern model implies

that unbound counterions do not interact significantly with the nonionic, or the zwitterionic, surfactants in the micelle. Since we neglect any additional shielding that long polymeric, nonionic surfactant heads may provide, this model is expected to be most appropriate when surfactant B has a rigid head (as in the case of glucoside surfactants), or for relatively short-chained polymeric, nonionic surfactant heads. In the ionic-zwitterionic surfactant system considered in this chapter, both surfactant heads are of similar size, and, therefore, we expect that using a Stern layer of constant thickness over the entire range of micelle compositions represents a reasonable approximation.

In our conceptual thought process of forming the micelle, ions are discharged in the bulk solution before they are transferred to the micelle interfacial region. After assembling the uncharged entities, the charges are brought back to the micelle interfacial region using a charging process. As a result, the electrostatic free-energy contribution, g_{elec}, is the sum of the self-energy of the ions that is released when they are discharged in the bulk solution, g_{disch}, and the work of charging the micelles, g_{charge}. In other words,

$$g_{\text{elec}} = g_{\text{disch}} + g_{\text{charge}} \tag{2.15}$$

2.3.3.1. Discharge Free-Energy Contribution

The discharge free-energy contribution, g_{disch}, is given by:

$$g_{\text{disch}} = \alpha g_{\text{dischA}} + (1-\alpha)\, g_{\text{dischB}} + \hat{\beta} g_{\text{dischC}} \tag{2.16}$$

where $g_{\text{disch}i}$ is the discharge free-energy contribution of component i (A, B, or C). If component B is nonionic, this contribution is zero. However, if it is zwitterionic, it is modeled using the Onsager model for the self energy of a dipole:[111,112]

$$g_{\text{dischB}} = -\frac{d_{\text{sepB}}^2 e_0^2}{4\pi\epsilon_0 (2\eta_{\text{w}} + 1)\, r_{\text{hB}}^3} \tag{2.17}$$

where e_0 is the charge of a proton, ϵ_0 is the dielectric permittivity of vacuum, η_w is the dielectric constant of bulk water, and r_{hB} is the hydrated radius of the head of surfactant B (the same radius used to calculate the head cross-sectional area, a_{hB}). We use the following temperature-dependent correlation for η_w derived from the data tabulated in ref 113:

$$\eta_w = 78.38 \exp\left[-0.00460\,(T - 298.15)\right] \tag{2.18}$$

where T is the temperature in degrees Kelvin. The dielectric constant of water has been shown to decrease linearly with the concentration of added salt, up to concentrations of approximately 2 molal in the case of NaCl.[114] For the systems considered in this chapter, we estimate that the maximum effect of added salt on ϵ_w is a 4% decrease in its value. For completeness, we have included a correction for the effect of salt on ϵ_w, using the data in ref 114.

The discharge free-energy contribution associated with the ionic surfactants and counterions is modeled using the Debye-Hückel expression for the self energy on an ion:[42,106]

$$g_{\mathrm{disch}i} = -\frac{z_i^2 e_0^2}{2\epsilon_b r_{hi}\,(1 + \kappa r_{hi})} \tag{2.19}$$

where z_i is the valence of component i (A or C), $\epsilon_b = 4\pi\epsilon_0\eta_w$, and r_{hi} is the hydrated radius of component i (A or C). The inverse Debye-Hückel screening length is given by $\kappa = (8\pi e_0^2 I/\epsilon_b k_B T)^{1/2}$, where $I = \left(\sum_i z_i^2 C_i\right)/2$ is the solution ionic strength. The summation in the definition of I is over *all* the ionic components, including co-ions, where C_i is the bulk concentration of species i, (A, C, or X).

2.3.3.2. Charging Free-Energy Contribution

The charging free-energy contribution, or the reversible work of charging, g_{charge}, is calculated via a Guntelberg charging process,[105] which in the case of an ionic surfactant mixed with a nonionic surfactant is given by:[4]

$$g_{\text{charge}} = \int_0^{q_{\text{f}}} \psi_0 \left(q\right) \, \mathrm{d}q \tag{2.20}$$

where ψ_0 is the electrostatic potential at the surface of charge of the micelle as a function of q, the average charge per surfactant molecule in a micelle at an arbitrary step along the charging process, and q_{f} is the final average charge per surfactant molecule in the micelle being considered. Note that counterion binding reduces g_{charge} by decreasing q_{f} in eq 2.20. The Laplace equation applies in the Stern layer and can be solved to relate ψ_0 to ψ_{s}, the electrostatic potential at the Stern surface.[42]

In the case of a binary mixture containing an ionic and a zwitterionic surfactant, three charged surfaces exist, and by extension of eq 2.20, the charging contribution is given by:[115]

$$g_{\text{charge}} = \sum_{i=1}^{3} \int_0^{q_{i\text{f}}} \psi_i(q_i) \, \mathrm{d}q_i \tag{2.21}$$

where the subscript i denotes the particular charged surface, ψ_i denotes the electrostatic potential on surface i, q_i denotes the average charge on surface i per surfactant molecule in a micelle at an arbitrary step along the charging process, and $q_{i\text{f}}$ denotes the final charge on surface i per surfactant molecule. For example, Figure 2-1 illustrates how $q_{i\text{f}}$ is determined for an ionic-zwitterionic mixed micelle with the bound counterions located on charged surface 2. The electrostatic potential at each charged surface can be determined by solving the Laplace equation in each region.[115] The resulting expression for the work of charging is given by:[116]

$$g_{\text{charge}} = \sum_{i=1}^{3} \frac{2\pi}{4\pi\epsilon_0\eta_{\text{int}}a_i} \left(\sum_{j=1}^{i} q_{j\text{f}} \right)^2 \mathcal{F}\left(S, d_i, R_i\right) + \int_0^{q_{\text{f}}} \psi_{\text{s}} \left(q\right) \, \mathrm{d}q \tag{2.22}$$

where η_{int} denotes the dielectric constant in the micelle interfacial region (which we define as the region from the micelle core-water interface to the Stern surface), a_i denotes the area per surfactant molecule at surface i, R_i is the distance from the micelle center to surface i, and d_i is the distance between surface i and surface $(i+1)$, with the surfaces numbered as in Figure 2-1. Note that $R_4 = R_{\text{Stern}}$ refers to the position of the Stern surface, and, therefore, $d_3 = R_{\text{Stern}} - R_3$.) We chose η_{int} to be

half the value in bulk water, η_{w} (see eq 2.18), to be consistent with the recent model of counterion binding for single-component ionic surfactant micelles.[42] The summation term in eq 2.22 can be interpreted as the work of charging associated with forming a series of capacitors. The function $\mathcal{F}$ captures the dependence of the capacitor's energy on its geometry, and is defined as follows:

$$\mathcal{F}\left(S, d_i, R_i\right) = \begin{cases} d_i, & \text{for } S = 1 \text{ (planar micelles)} \\ R_i \ln\left(1 + d_i/R_i\right), & \text{for } S = 2 \text{ (cylindrical micelles)} \\ d_i/\left(1 + d_i/R_i\right), & \text{for } S = 3 \text{ (spherical micelles)} \end{cases} \tag{2.23}$$

To calculate the potential at the Stern surface, we use approximate analytical solutions to the Poisson-Boltzmann equation. In the case of a monovalent counterion, we use the following expression derived by Oshima, Healy, and White (OHW):[117]

$$s = 2\sinh(y_0/2) + \frac{2\left(S-1\right)}{x_0}\tanh(y_0/4) \tag{2.24}$$

where $s = (4\pi e_0/\epsilon_{\mathrm{w}} k_{\mathrm{B}} T \kappa) q/a_{\mathrm{s}}$ is the dimensionless surface charge density (a_{s} is the area per surfactant molecule at the Stern surface), $y_0 = e_0\psi/k_{\mathrm{B}}T$ is the dimensionless surface potential, and $x_0 = \kappa R_{\mathrm{Stern}}$ is the dimensionless location of the Stern surface.

Rather than using the integral in eq 2.22 to solve directly for g_{charge}, which involves using a numerical technique (for example, the Newton-Raphson method) to solve for y_0 at each step of a numerical integration, we use the following identity, obtained by application of the chain rule:

$$\int_0^{q_{\mathrm{f}}} \psi_{\mathrm{s}}\left(q\right)\, \mathrm{d}q = \psi_{\mathrm{s}}\left(q_{\mathrm{f}}\right) q_{\mathrm{f}} - \int_0^{\psi_{\mathrm{s}}(q_{\mathrm{f}})} q\, \mathrm{d}\psi_{\mathrm{s}} \tag{2.25}$$

Rewriting the integral in eq 2.25, and the dimensionless surface potential of the micelle, $y_{\mathrm{f}} = y_0(\psi_{\mathrm{s}}) = e_0\psi_{\mathrm{s}}/k_{\mathrm{B}}T$, one obtains:

$$\int_0^{q_{\mathrm{f}}} \psi_{\mathrm{s}}\left(q\right)\, \mathrm{d}q = \left(\frac{k_{\mathrm{B}}T}{e_0}\right) q_{\mathrm{f}} \left[y_{\mathrm{f}} - \frac{1}{s_{\mathrm{f}}}\int_0^{y_{\mathrm{f}}} s\left(y\right)\, \mathrm{d}y\right] \tag{2.26}$$

Combining eq 2.26 with eq 2.24, the following analytical result is obtained for the integral in eq 2.22:

$$\int_0^{q_\mathrm{f}} \psi_\mathrm{s}(q)\ \mathrm{d}q = \left(\frac{k_\mathrm{B}T}{e_0}\right) q_\mathrm{f} \left[y_\mathrm{f} - \frac{1}{s_\mathrm{f}} \left(4\cosh(y_\mathrm{f}/2) - 4 + \frac{8\,(S-1)}{x_0} \log\left(\cosh(y_\mathrm{f}/4)\right) \right) \right] \tag{2.27}$$

Using this approach, no numerical integration is required to evaluate g_charge in eq 2.22, and eq 2.24 is solved only once in order to obtain y_f.

When multivalent counterions are present, we use approximate analytical solutions to the Poisson-Boltzmann equation that were derived by Alargova et al.[73,74]

2.4. Determination of Useful Micellar Solution Properties

This section provides an overview of how the model equations (Eqs. 2.5, 2.6, and 2.7), along with a description of g_mic (see section 2.3), are used to obtain various useful micellar solution properties. In section 2.4.1, we first discuss our assumptions to determine the micelle size distribution, including the models that we use to describe spherical and finite-size cylindrical micelles. In section 2.4.2, we discuss the determination of the critical micelle concentration (cmc). In section 2.4.3, we discuss the determination of the various average micelle aggregation numbers and the bulk concentrations of the surfactants and the counterions present in the solution.

2.4.1. Determination of the Micelle Size Distribution

The summations in eq 2.7 account for the entire distribution of micelles, summing over every possible combination of aggregation number n, composition α, degree of counterion binding $\hat{\beta}$, and micelle shape S. We have found that for a particular micelle aggregation number, only micelles with the optimal composition α^* and degree of counterion binding $\hat{\beta}^*$ are present at a significant concentration. With this in mind, to facilitate the numerical solution of eq 2.7, the summations are only carried out

over n. More specifically, for each n, the corresponding micelle shape $S^*(n)$, core minor radius $l_c^*(n)$, composition $\alpha^*(n)$, and degree of counterion binding $\hat{\beta}^*(n)$, are the *optimal values* which minimize g_m as defined in eq 2.5 (or, equivalently, which maximize $X_{n\alpha\hat{\beta}}$ as defined in eq 2.6). This approximation is reasonable because small deviations from the minimum value of g_m lead to a sharp decrease in $X_{n\alpha\hat{\beta}}$, due to the exponential dependence on the quantity $(-ng_m)$, combined with $n \gg 1$ (see eq 2.6). Note that this approximation is similar in spirit to the approximations made previously for the micelle composition in ref 4 and for the degree of counterion binding in ref 42.

The minimization of g_m is performed for each of the "regular" micelle shapes (spheres, infinite cylinders, and infinite planar bilayers), because our electrostatics model can only be implemented for these regular shapes. Since planar or discoidal micelles are not observed experimentally in the binary surfactant systems considered in this chapter, their modeling is not pursued any further. The micelle shape with the lowest g_m value corresponds to the optimal shape for the given experimental conditions. If the optimal micelle shape is spherical, then the micelle size distribution is approximated as being monodisperse. Using eq 2.6, we then find that for spherical micelles the micelle mole fraction is given by:

$$X_{n^*_{sph}\alpha^*_{sph}\hat{\beta}^*_{sph}} = \frac{1}{e} X_1^{n^*_{sph}} \exp\left[-\frac{n^*_{sph}}{k_B T} g^*_m \left(S = 3, l^*_{c,sph}, \alpha^*_{sph}, \hat{\beta}^*_{sph}, \alpha_1, X_{1C}\right)\right] \qquad (2.28)$$

where the subscript "sph" in eq 2.28 denotes the *optimal characteristics of spherical micelles*. Note that g^*_m depends on the optimal micelle characteristics ($l^*_{c,sph}$, α^*_{sph}, and $\hat{\beta}^*_{sph}$), and also on the monomer composition α_1 and the bulk counterion mole fraction X_{1C} (see eq 2.5). The aggregation number of the optimal spherical micelle n^*_{sph} can be determined from an expression that equates the total volume occupied by the surfactant tails in the micelle core ($n^*_{sph}\overline{v}_t$) to the volume of the micelle core $\left(\frac{4}{3}\pi(l^*_{c,sph})^3\right)$, that is, from:[3]

$$n^*_{sph} = \left(\frac{4}{3}\pi(l^*_{c,sph})^3\right)/\overline{v}_t \qquad (2.29)$$

where $\overline{v}_t$ is the average surfactant tail volume (see eq 2.10).

When the optimal micelle shape is cylindrical, it is necessary to model *finite* cylindrical micelles. Several models of varying complexity have been proposed to describe finite cylindrical micelles.[83,107,118–120] After examining several of these models, we have found that, in spite of their increased complexity, they have a relatively minor impact on counterion binding in the binary surfactant systems that we have considered. Since these models introduce complexity to the theory developed here but do not provide significant insight into counterion binding, we will use instead a simplified model to describe finite cylindrical micelles, which we discuss below.

To calculate the free energy of mixed micellization for finite cylindrical micelles, we interpolate between the free energies of micellization corresponding to spherical and to infinite cylindrical micelles, which results in the well-known ladder model of micelle growth.[4,39–41] The resulting interpolation equation can be conveniently expressed in terms of the growth parameter, $\Delta\mu$, which models the free-energy difference between spherical and cylindrical micelles, and is given by:[43]

$$\Delta\mu = g^*_{\mathrm{m,sph}} - g^*_{\mathrm{m,cyl}} \tag{2.30}$$

where $g^*_{\mathrm{m,sph}}$ and $g^*_{\mathrm{m,cyl}}$ are the optimal modified free energies of micellization (see eq 2.5) for spheres and for infinite cylinders, respectively. Note that a positive value of $\Delta\mu$ implies that cylindrical micelles are more favorable. However, if $\Delta\mu$ has a relatively small value, or if the surfactant concentration is near the cmc, then the average micelle may not be significantly larger than a spherical micelle.

In the context of this model of micelle growth, the modified free energy of mixed micellization of a finite cylindrical micelle of aggregation number n (where $n > n_{\mathrm{sph}}$), denoted by $g^*_{\mathrm{m}}(n)$, is given by:[41]

$$g^*_{\mathrm{m}}(n) = g^*_{\mathrm{m,cyl}} + \left(n^*_{\mathrm{sph}}/n\right)\Delta\mu. \tag{2.31}$$

where n^*_{sph} is the aggregation number of an optimal spherical micelle. The degree of counterion binding and the composition of finite cylindrical micelles can be

determined using analogous formulas.[40,42] This interpolation procedure results in the smallest micelles having the properties of the optimal spherical micelles, while the larger micelles asymptotically approach the properties of the optimal infinite cylindrical micelles.

As noted previously,[39] the interpolated free energy in eq 2.31 is expected to deviate most significantly from the actual free energy when the micelles are "globular" (namely, ellipsoidal in shape with an aggregation number which is not much larger than that of spherical micelles). We anticipate that in cases where globular micelles are the true preferred shape, our model will predict: (1) spherical micelles as the preferred shape, and (2) a larger free energy of micellization than that corresponding to globular micelles. The overestimation of the free energy of micellization will result in an overestimation of the predicted cmc and in an underestimation of the predicted micelle aggregation number.

2.4.2. Determination of the Critical Micelle Concentration

The critical micelle concentration (cmc) can be estimated using the expression $\exp(g_{\rm m}^*/k_{\rm B}T)$, where $g_{\rm m}^*$ is the optimal modified free energy of mixed micellization of the preferred micelle shape at the given solution conditions.[39,42] By examining eq 2.6, we see that, if $X_1 \ll \exp(g_{\rm m}^*/k_{\rm B}T)$, then the concentration of micelles will be negligible, and micelles will begin to form as X_1 approaches $\exp(g_{\rm m}^*/k_{\rm B}T)$. Accordingly, $\exp(g_{\rm m}^*/k_{\rm B}T)$ provides a reasonable estimate of the cmc.

However, in the case of binary surfactant mixtures, $g_{\rm m}^*$ can vary significantly with surfactant concentration (due to changes in the ionic strength or in the composition of the surfactant monomers present in the bulk solution). In order to select a value of $g_{\rm m}^*$ that yields a reasonable estimate of the cmc, we must also ensure that, at the given solution conditions, the *total concentration of surfactant* in mole fraction units ($X_{\rm S}$), rather than the mole fraction of surfactant monomers (X_1), is equal to our cmc estimate. In other words, we determine the cmc by solving $X_{\rm S} = \exp(g_{\rm m}^*(X_{\rm S})/k_{\rm B}T)$, where we have explicitly indicated that $g_{\rm m}^*$ can vary with $X_{\rm S}$.

We have also compared our estimate of the cmc as $\exp(g_{\rm m}^*/k_{\rm B}T)$ to the cmc

estimated as the total surfactant concentration at which 95% of the surfactant is present in monomeric form and 5% is present in micellar form.[41] We found that the second definition yields very similar (but slightly lower) cmc values for the surfactant systems considered in this chapter.

2.4.3. Determination of Average Micelle Aggregation Numbers

To calculate several commonly encountered average micelle aggregation numbers, we use the following relations:[121]

$$\begin{aligned} \langle n \rangle_n &= \frac{M_1}{M_0} \\ \langle n \rangle_w &= \frac{M_2}{M_1} \\ \langle n \rangle_z &= \frac{M_3}{M_2} \end{aligned} \tag{2.32}$$

where $\langle n \rangle_n$, $\langle n \rangle_w$, and $\langle n \rangle_z$ are the number-, the weight-, and the z-average micelle aggregation numbers, respectively, and M_k is the kth moment of the micelle size distribution, defined as follows:[121]

$$M_k = \sum_{n \geq n^*_{\text{sph}}} n^k X_{n\alpha^*\hat{\beta}^*} \tag{2.33}$$

where $X_{n\alpha^*\hat{\beta}^*}$ is the mole fraction of micelles of aggregation number n, optimal composition $\alpha^*(n)$, and optimal degree of counterion binding $\hat{\beta}^*(n)$. Note that the summation in eq 2.33 begins at $n = n^*_{\text{sph}}$, indicating that the monomers are excluded from the evaluation of the moments in order to avoid any bias from their contribution. Recall that when the micelle shape with the minimum g^*_{m} is spherical, we model the micelle size distribution as being monodisperse. In this case, $\langle n \rangle_n = \langle n \rangle_w = \langle n \rangle_z = n^*_{\text{sph}}$, where n^*_{sph} is determined from $\overline{v}_{\text{t}}$ and $l^*_{\text{c,sph}}$ by eq 2.29. When infinite cylindrical micelles have the minimum free energy, the summation in eq 2.33 is carried out over $n^*_{\text{sph}} \leq n < \infty$, since our model of micelle growth assumes

that micelles with $n < n^*_{\text{sph}}$ do not form.

The concentrations of the two surfactant components (A and B) and the counterions C in the bulk solution are determined by simultaneously solving the mole balances (eq 2.7) and the expression for the monomer-micelle equilibrium (eq 2.6). The ionic strength, which affects the free energy of micellization, is calculated from the bulk concentrations of the ionic species: the monomeric ionic surfactants, the bulk (unbound) counterions, and co-ions from any added salt. To actually solve the resulting system of equations (Eqs. 2.5 and 2.7), we make an initial guess of the bulk concentration of each component, and iteratively solve the system of equations until a self-consistent solution is obtained. Although the exact values of the initial guesses are relatively unimportant, we typically use the following procedure:

1. Choose any reasonable estimate of the concentration of the surfactant monomers (from 0.01 to 10 mM for the surfactants considered in this chapter).

2. Assume that the surfactant monomer composition is equal to the overall surfactant composition.

3. Assume that the bulk concentration of counterions is equal to the concentration of added salt plus the concentration of ionic surfactant monomers.

4. Assume that the bulk concentration of co-ions is equal to the concentration of added salt.

2.5. Model Validation

In this section, the molecular-thermodynamic theory presented in sections 2.2, 2.3, and 2.4 is validated for several binary surfactant mixtures using experimental data available in the literature. Estimated values of the molecular characteristics of the ionic surfactants and the counterions modeled are listed in Table 2.1. Estimated values of the molecular characteristics of the zwitterionic surfactant and the nonionic surfactants modeled are listed in Tables 2.2 and 2.3, respectively.

In section 2.5.1, we present predictions of the degree of counterion binding. In section 2.5.2, we present predictions of the critical micelle concentration. In section 2.5.3, we present predictions of the weight-average micelle aggregation number. In each section, we also compare the predictions with the available experimental data.

2.5.1. Prediction of the Degree of Counterion Binding

In this section, we compare our theoretical predictions of the dependence of the degree of counterion binding, β, on the micelle ionic composition, α, with experimental data available in the literature. Recall that the degree of counterion binding per micellized surfactant molecule, $\hat{\beta}$, is predicted by minimizing the free energy of micellization with respect to $\hat{\beta}$, as described in section 2.4, and eq 2.1 is then used to obtain β from $\hat{\beta}$.

As indicated in section 2.1, the experimentally determined degree of counterion binding can vary with the experimental technique used. We expect that the β values predicted in our model are a lower bound for the experimental values, corresponding most closely to experimental values obtained via spectroscopic measurements (such as NMR) or via micellar catalysis techniques, since these techniques consider as bound only those counterions within a few Angstroms of the micelle surface. The majority of the experiments discussed in the literature, including those presented in this chapter, measure counterion binding via thermodynamic measurements (primarily using ion-selective electrodes), which yield the largest estimates of counterion binding.[82] Nevertheless, we expect the same qualitative trends in counterion binding to hold in both predictions and experiments, regardless of the experimental technique used. Below, we consider several binary surfactant mixtures.

2.5.1.1. Cationic-Nonionic Binary Surfactant Mixture

We first consider the binary surfactant mixture of the cationic surfactant hexadecyltrimethylammonium bromide (C_{16}TAB) and the nonionic surfactant dodecyl hexa(ethylene oxide) ($C_{12}E_6$). Hall and Price determined the degree

of bromide binding to the C_{16}TAB-$C_{12}E_6$ micelles via ion-selective electrode measurements of the mean ionic activity.[89] The experiments were conducted at a temperature of 30°C with added sodium bromide (NaBr) at a concentration of 0.01 molal. The concentration of C_{16}TAB remained fixed at 0.05 molal, while the concentration of $C_{12}E_6$ was varied. At all the conditions studied, nearly all of the surfactant was present in micellar form, since the cmc of any C_{16}TAB-$C_{12}E_6$ mixture should be less than 0.1 mmolal, which corresponds to the cmc of pure C_{16}TAB in water.[2] Therefore, the micelle composition in this case is essentially equal to the overall surfactant composition, as required to satisfy the mass balances.[4,122]

Figure 2-2 shows the predicted (solid line) and the experimental (circles) degrees of binding of bromide, β_{Br}, for the C_{16}TAB-$C_{12}E_6$ binary mixture as a function of the micelle C_{16}TAB composition, $\alpha_{C_{16}\mathrm{TAB}}$. The reported accuracy in the measured degrees of counterion binding was 0.003, smaller than the plotted symbols. The experimental data were also fitted using a smoothing spline (the dashed-dotted line) to help guide the eye. The experimentally deduced β_{Br} is always larger than the predicted β_{Br}, which is consistent with our assertion that our model provides a lower bound for β. In addition, the observed qualitative trends in theory and experiments are quite similar. Specifically, at low $\alpha_{C_{16}\mathrm{TAB}}$, β_{Br} is very small but increases rather sharply with increasing $\alpha_{C_{16}\mathrm{TAB}}$. At higher ionic compositions ($\alpha_{C_{16}\mathrm{TAB}} \gtrsim 0.4$), β_{Br} increases more slowly with increasing $\alpha_{C_{16}\mathrm{TAB}}$. This general behavior is expected based on electrostatic considerations and is also predicted by the models developed by Rathman and Scamehorn,[94,97] as well as by Maeda.[91] However, we are able to make several more specific observations, because our model predicts a variation in the micelle shape and size with concomitant changes in the degree of counterion binding.

For example, we expect a micelle shape transition to occur at some intermediate $\alpha_{C_{16}\mathrm{TAB}}$ composition, since experimental evidence indicates that pure $C_{12}E_6$ micelles are cylindrical[116] while pure C_{16}TAB micelles are spherical.[123] Since the experimental uncertainty is relatively small, we believe that this micelle shape transition may also be indicated by a change in the behavior of the experimentally measured β_{Br} as a function of $\alpha_{C_{16}\mathrm{TAB}}$. Indeed, although β_{Br} varies smoothly with $\alpha_{C_{16}\mathrm{TAB}}$ at most

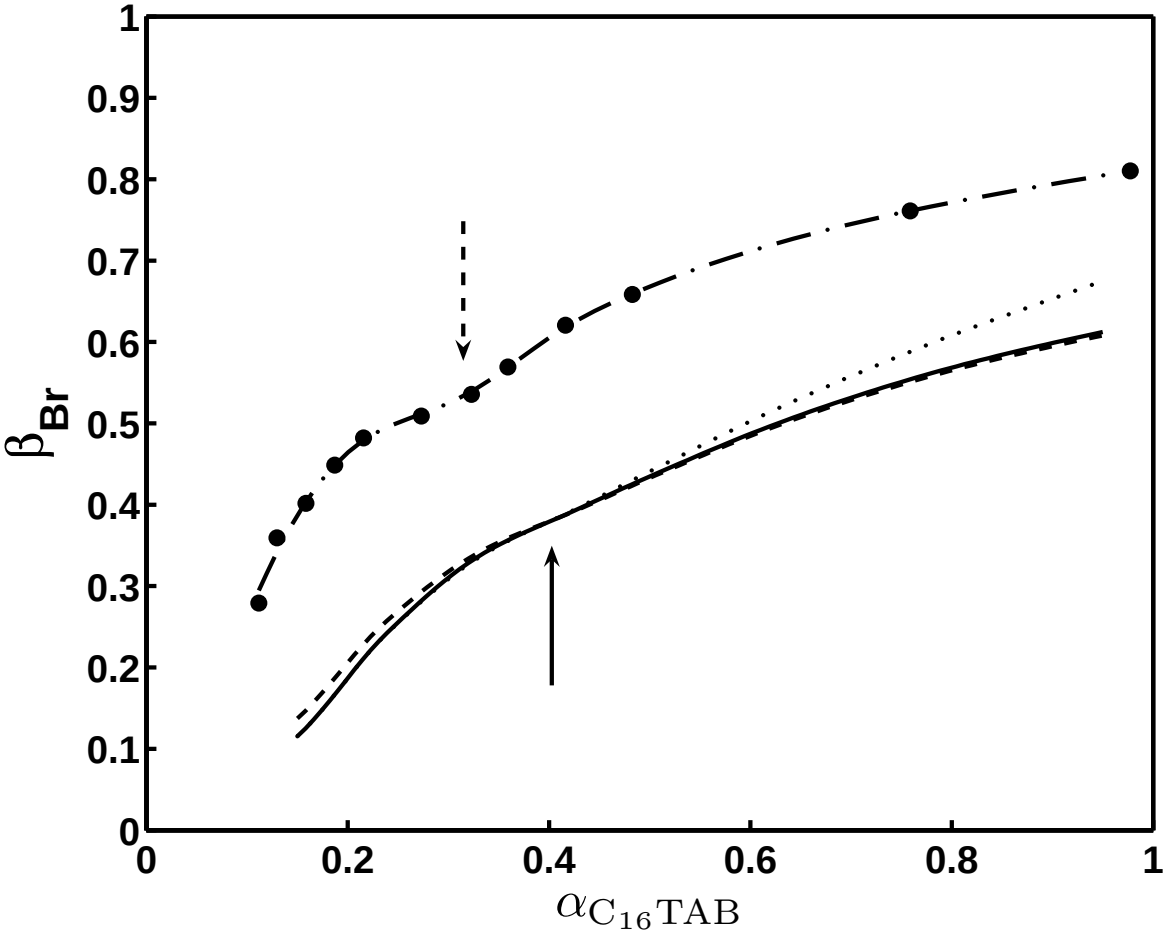

Figure 2-2: Comparison between the predicted (solid line) and the experimental (circles) degrees of Br^+ binding to C_{16}TAB-$C_{12}E_6$ mixed micelles, β_{Br}, as a function of the micelle C_{16}TAB composition, $\alpha_{C_{16}TAB}$. The experimental data were collected by Hall and Price[89] (as reported by Maeda[91]), and were fitted using a smoothing spline (dashed-dotted line) to help guide the eye. The solid line corresponds to the predicted average degree of Br^+ binding. The dashed line corresponds to β_{sph}, the predicted degree of Br^+ binding to spherical micelles. The dotted line corresponds to β_{cyl}, the predicted degree of Br^+ binding to infinite cylindrical micelles. The solid arrow denotes the location of the predicted cylinder-to-sphere micelle shape transition as $\alpha_{C_{16}TAB}$ increases, while the dashed arrow denotes the micelle shape transition, as inferred from the experimental variation of β_{Br} with $\alpha_{C_{16}TAB}$.

compositions, there is an inflection at $\alpha_{C_{16}TAB} \approx 0.3$ (indicated by the dashed arrow in Figure 2-2). We also verified the presence of an inflection by examining the slope and the curvature of the smoothing spline fitted to the data. This change in curvature can be rationalized by a micelle shape transition, which, as stated above, is likely to occur over this C_{16}TAB composition range.

To further justify the above observation, we first examine the predicted weight-average micelle aggregation numbers, $\langle n \rangle_w$, which are shown as a function of $\alpha_{C_{16}TAB}$ in Figure 2-3. Our predictions reveal a transition in micelle shape from long cylindrical micelles with aggregation numbers well above 100 (as predicted for $\alpha_{C_{16}TAB} < 0.4$), to short cylindrical micelles with aggregation numbers around 100 (as predicted for $\alpha_{C_{16}TAB} \approx 0.4$, indicated in Figure 2-3 by the solid arrow), to spherical micelles with aggregation numbers around 70 at $\alpha_{C_{16}TAB} \gtrsim 0.5$. Although micelle aggregation numbers were not measured for this particular system, another similar surfactant mixture, sodium dodecyl sulfate (SDS)-$C_{12}E_6$, exhibits a similar micelle shape transition over a comparable SDS composition range.[116]

The theory also has the ability to predict the degree of counterion binding onto micelles of various shapes and sizes. As an illustration, in Figure 2-2, we superimpose the predicted degree of bromide binding to spherical micelles, β_{sph} (the dashed line), and to infinitely long cylindrical micelles, β_{cyl} (the dotted line). For $\alpha_{C_{16}TAB} \gtrsim 0.4$, the predicted average β_{Br} corresponds to β_{sph}, as shown by the extremely close overlap of the solid and the dashed lines. For $\alpha_{C_{16}TAB} \lesssim 0.4$, the predicted average β_{Br} corresponds to β_{cyl}, as shown by the complete overlap of the solid and the dotted lines. This finding is, of course, consistent with the prediction that there is a micelle shape transition from long, cylindrical micelles to spherical micelles at $\alpha_{C_{16}TAB} \approx 0.4$ (indicated by the solid arrow in Figure 2-2).

Furthermore, in Figure 2-2, β_{cyl} is larger than β_{sph} for $\alpha_{C_{16}TAB} \gtrsim 0.4$, while β_{sph} is slightly larger for $\alpha_{C_{16}TAB} \lesssim 0.4$. In order to rationalize these predicted trends, we examined the various contributions to the free energy of micellization (see eq 2.8) and found that the predicted inflection in the β_{Br} vs. $\alpha_{C_{16}TAB}$ curve is due primarily to the variation of g_{elec} with $\alpha_{C_{16}TAB}$. More specifically, when the ionic content of the mixed

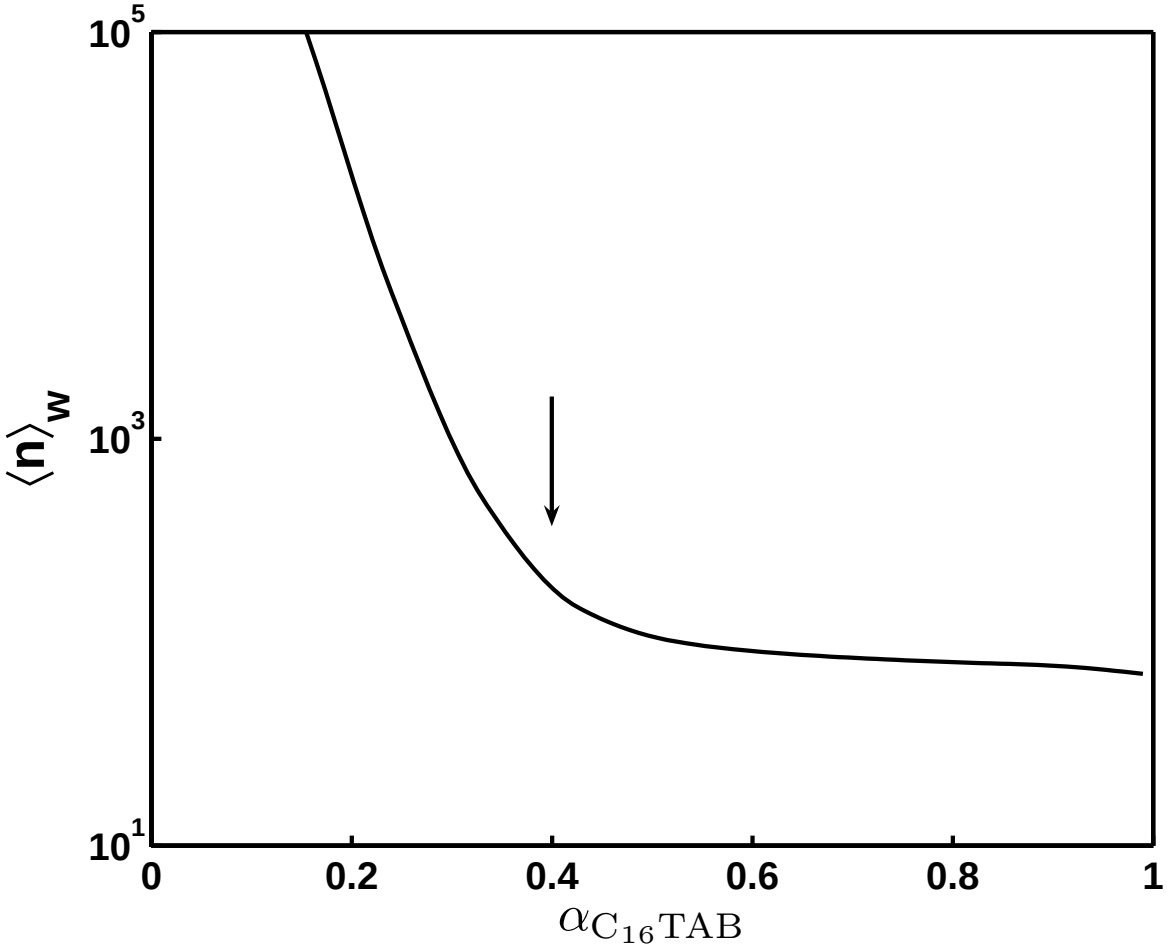

Figure 2-3: The predicted weight-average micelle aggregation number of C_{16}TAB-$C_{12}E_6$ mixed micelles, $\langle n \rangle_w$, as a function of $\alpha_{C_{16}TAB}$. The solid arrow denotes the location of the predicted cylinder-to-sphere micelle shape transition as $\alpha_{C_{16}TAB}$ increases.

micelle is high, β is controlled by the relatively large value of g_{elec}, which is reduced by counterion binding. Due to the differing curvatures, g_{elec} is generally larger for cylindrical micelles than for spherical micelles. At high $\alpha_{C_{16}TAB}$ values, larger values of g_{elec} lead to more counterion binding, which leads to $\beta_{\text{cyl}} > \beta_{\text{sph}}$. However, when the ionic content is lower, the magnitude of g_{elec} is relatively low, and other contributions to g_{mic} (see eq 2.8) become important. In particular, the steric penalty associated with binding (modeled in g_{st}) is larger for cylindrical micelles than for spherical micelles, because cylindrical micelles have a smaller curvature, which is reflected by a smaller area per surfactant molecule (see eq 2.10). Since counterion binding increases g_{st}, β_{cyl} becomes smaller than β_{sph} as g_{st} becomes increasingly important. Furthermore, at low ionic content, when g_{elec} becomes less important, the quantitative variation of β with $\alpha_{C_{16}TAB}$ can be affected by all the other contributions to g_{mic} (see eq 2.8). This behavior is different than that observed in pure ionic micelles, where β_{cyl} is always observed to be greater than β_{sph},[42,124,125] since it is controlled primarily by g_{elec}. Although the effect of the changes in the steric and the electrostatic penalties on β can be rationalized qualitatively without a molecular model, the quantitative determination of the combined effect of g_{st} and g_{elec} on the degree of counterion binding, including establishing a relation with the various micelle shapes, requires the development of a molecular model of micellization of the type presented in this chapter.

Because the shape-dependence of β depends primarily on the interplay between g_{st} and g_{elec}, we expect that the concentration of added salt should play a significant role. In particular, we examine the salt dependence of α_c, the composition at which $\beta_{\text{sph}} = \beta_{\text{cyl}}$. For example, in the C_{16}TAB-$C_{12}E_6$ surfactant mixture at a sodium bromide concentration, [NaBr], of 0.01 molal, we predict $\alpha_c = 0.4$ (see Figure 2-2). Also note that $\beta_{\text{sph}} > \beta_{\text{cyl}}$ for $\alpha_{C_{16}TAB} < \alpha_c$, and $\beta_{\text{sph}} < \beta_{\text{cyl}}$ for $\alpha_{C_{16}TAB} > \alpha_c$. In Figure 2-4, we plot α_c as a function of [NaBr] for the C_{16}TAB-$C_{12}E_6$ surfactant mixture. The main effect of increasing [NaBr] is to decrease g_{elec}.

As a result, α_c increase sharply from 0.35 to approximately 0.6 as [NaBr] increases to 0.1 molal. At these conditions, the composition window where $\beta_{\text{cyl}} < \beta_{\text{sph}}$ increases

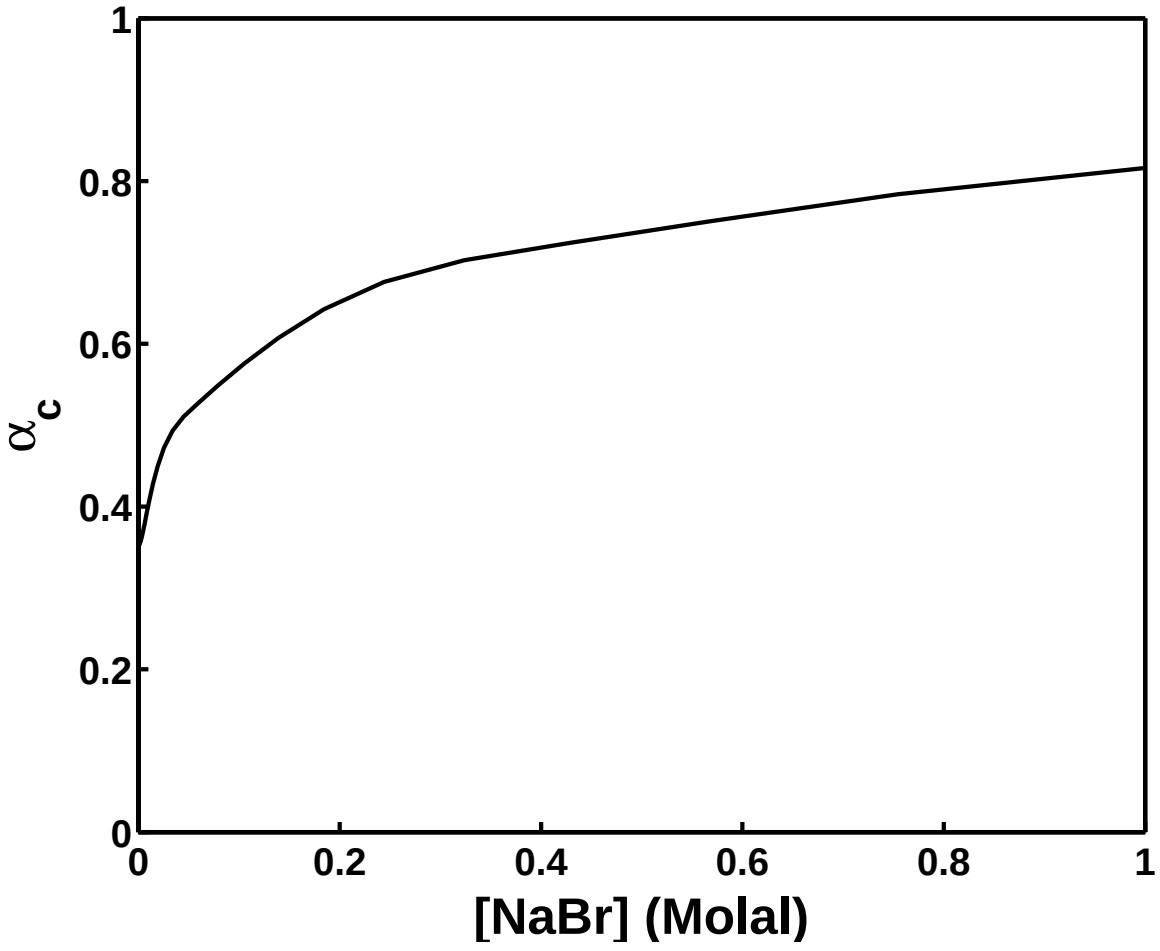

Figure 2-4: The predicted variation of α_c, the micelle composition at which $\beta_{cyl} = \beta_{sph}$, with the concentration of added sodium bromide, [NaBr], for the C_{16}TAB-$C_{12}E_6$ surfactant mixture.

rapidly with increasing [NaBr]. At greater [NaBr], g_{elec} becomes less sensitive to the ionic strength, and α_{c} increases slowly to 0.8. At high [NaBr], although $\beta_{\text{cyl}} < \beta_{\text{sph}}$ for most micelle compositions, pure ionic micelles incur a sufficiently strong electrostatic penalty that cylindrical micelles continue to bind more counterions than do spherical micelles.

2.5.1.2. Anionic-Nonionic Binary Surfactant Mixture

We next examine the binary surfactant mixture of the anionic surfactant sodium tetradecyl sulfate (STS) and the nonionic surfactant $C_{12}E_6$, also studied by Hall and Price via mean ionic activity measurements using ion-specific electrodes.[89] The experiments on the STS-$C_{12}E_6$ mixture were conducted at a temperature of 50°C with added NaCl at a concentration of 0.01 molal. The concentration of STS was fixed at 0.05 molal, while the concentration of $C_{12}E_6$ was varied.

In Figure 2-5, we present a comparison between the predicted (solid line) and the experimental (circles) degrees of sodium binding, β_{Na}, as a function of the micelle STS composition, α_{STS}, for the STS-$C_{12}E_6$ surfactant mixture. The experimental data were also fitted using a smoothing spline (dashed line) to help guide the eye. Similar to the C_{16}TAB-$C_{12}E_6$ case, we also observe an inflection in the β_{Na} vs. α_{STS} curve, at an experimental $\alpha_{\text{STS}} \approx 0.5$ (dashed arrow) and at a predicted $\alpha_{\text{STS}} \approx 0.6$ (solid arrow).

Although the specific quantitative trends depend on the particular surfactant structures, the following qualitative trends are generally observed: (1) a transition in the shape of mixed micelles with the ionic composition can be correlated to an observed change in the behavior of β with the ionic composition, (2) when the ionic surfactant content is sufficiently high, electrostatic effects cause β_{cyl} to be larger than β_{sph} (which is consistent with the observations in the case of single ionic surfactant micelles), (3) when the ionic surfactant content is sufficiently low, β_{cyl} should be smaller than β_{sph}, primarily due to the different dependence of g_{st} on micelle shape.

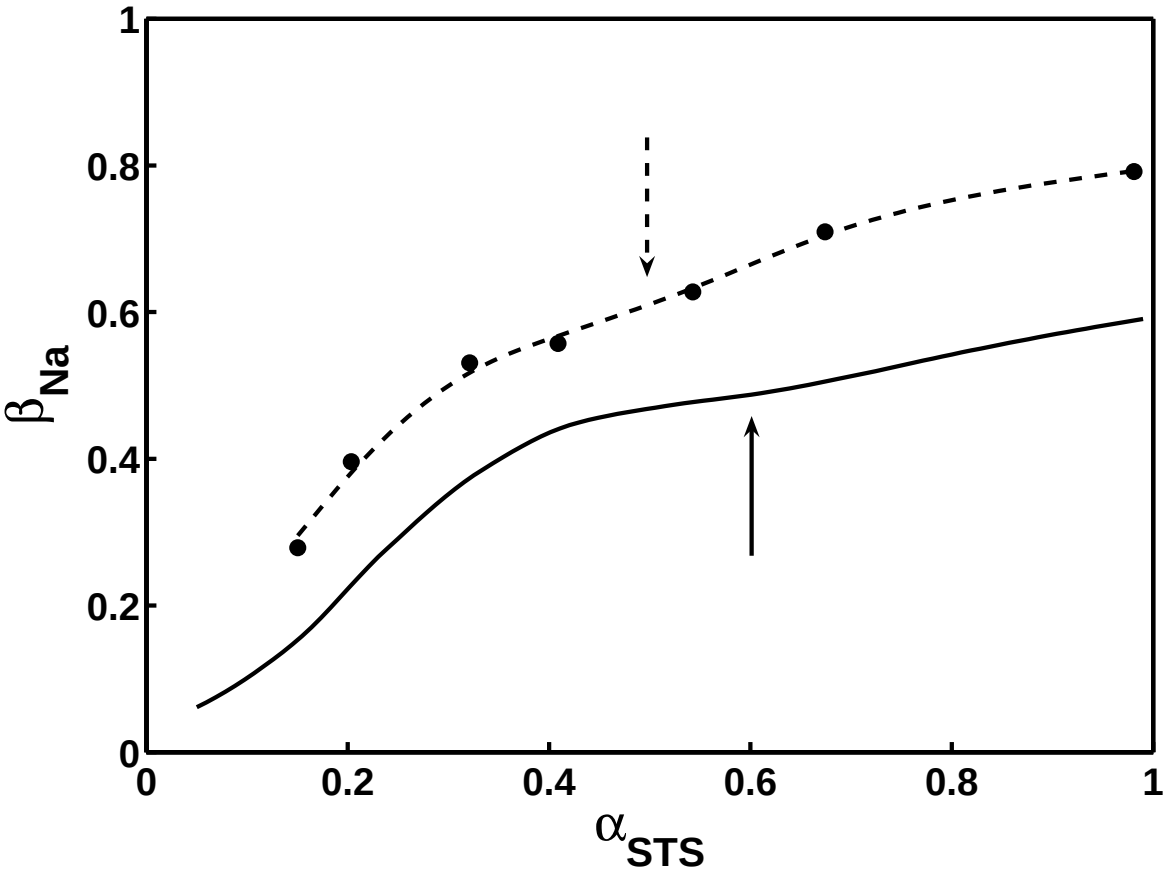

Figure 2-5: Comparison between the predicted (solid line) and the experimental (circles) degrees of Na^+ binding to STS-$C_{12}E_6$ mixed micelles, β_{Na}, as a function of the micelle SDS composition, α_{SDS}. The experimental data were collected by Hall and Price[89] (as reported by Maeda[91]), and were fitted using a smoothing spline (dashed line) to help guide the eye. The solid arrow denotes the location of the predicted cylinder-to-sphere micelle shape transition, while the dashed arrow denotes the micelle shape transition, as inferred from the experimental variation of β_{Na} with α_{STS}.

2.5.1.3. Cationic-Zwitterionic Binary Surfactant Mixture

The model was also tested on the binary surfactant mixture of the cationic surfactant octadecyltrimethylammonium chloride (C_{18}TAC) and the zwitterionic surfactant dodecyldimethylphosphine oxide (C_{12}PO). The degree of chloride binding, β_{Cl}, was measured by Akisada[126] via conductivity measurements. The experiments were conducted at a temperature of 30°C at a constant total surfactant concentration of 0.1 molal. The predicted (solid line) and the experimental (circles) β_{Cl} values as a function of the micelle C_{18}TAC composition, α_{C18TAC}, are shown in Figure 2-6. The experimental data were also fitted using a smoothing spline (dashed line) to help guide the eye. The predictions are slightly smaller than the experimental β_{Cl} values, as expected when comparing our predictions to a transport measurement like conductivity. Furthermore, we predict that chloride binding is essentially negligible when $\alpha_{C_{18}TAC} < 0.10$. As stressed earlier, the degree of counterion binding at low ionic compositions is extremely sensitive to all the contributions to g_{mic} (see eq 2.8). These predictions are indicative of the phenomenon of "critical ion condensation," which asserts that counterion binding should only occur above a critical charge density (which is analogous to the so-called Manning parameter in the case of linear polyelectrolytes[127]). In micellar systems, this parameter corresponds to a critical ionic composition. Experimental β_{Cl} values were not measured at $\alpha_{C_{18}TAC} < 0.10$, and, therefore, we could not verify our prediction of the existence of critical ion condensation in the C_{18}TAC-C_{12}PO binary surfactant mixture.

2.5.1.4. Divalent Anionic-Nonionic Binary Surfactant Mixture

In order to verify the phenomenon of critical ion condensation experimentally, use of an experimental technique which is sensitive at low values of α and β is required. To this end, Treiner et al.[95] constructed an electrode which is extremely sensitive to copper in order to analyze the anionic-nonionic surfactant mixture copper dodecyl sulfate (CuDS)-Brij-35. The nonionic surfactant Brij-35 ($C_{12}E_{23}$) is a commercial-grade dodecyl poly(ethylene oxide) surfactant with an average degree

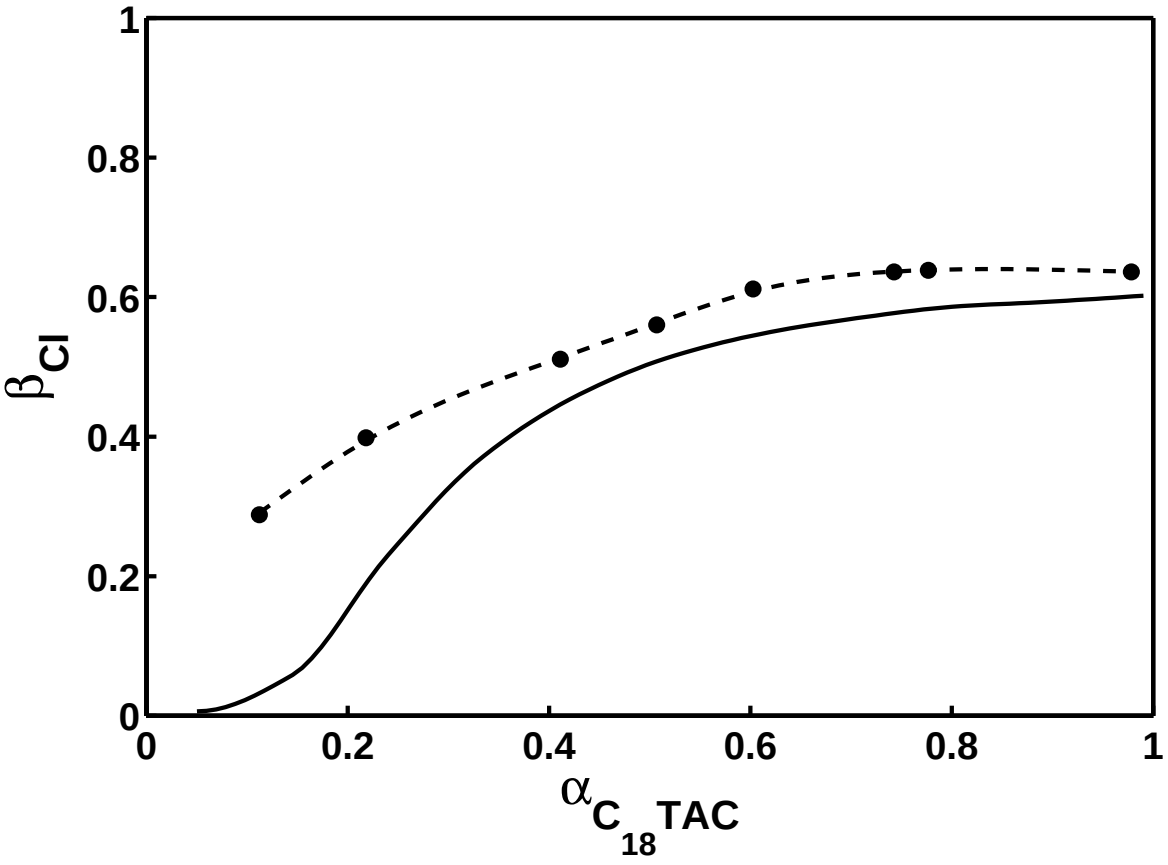

Figure 2-6: Comparison between the predicted (solid line) and the experimental (circles) degrees of Cl^- binding to C_{18}TAC-C_{12}PO mixed micelles, β_{Cl}, as a function of the micelle C_{18}TAC composition, $\alpha_{C_{18}TAC}$. The experimental data were measured by Akisada[126] (as reported by Maeda[91]), and were fitted using a smoothing spline (dashed line) to help guide the eye.

of ethoxylation of 23. Although the nonionic surfactant is, in reality, a complex mixture of surfactants with different degrees of ethoxylation, we modeled it as a monodisperse surfactant with an effective head area, which was recently shown to be a good approximation for cmc predictions in commercial C_iE_j nonionic surfactants obeying the Poisson distribution in the degree of ethoxylation.[38] We expect this approximation to be reasonable for predicting the degree of counterion binding, although the method used to select the effective head cross-sectional area should affect the quantitative predictions at low ionic compositions, where the steric interactions become more important than the electrostatic ones. We believe that, for large poly(ethylene oxide, EO) heads ($n_{EO} > 10$), eq 2.12 severely overestimates the value of g_{st} in eq 2.8, because our hard-disk model for the steric interactions does not account for the fact that the polymeric heads can actually interpenetrate. In fact, using eq 2.12 yields an excessively large head cross-sectional area of 124 $Å^2$. To obtain a more reasonable estimate, we exploited the fact that the cmc's of Brij-35 and monodisperse $C_{12}E_8$ (as determined by dye solubilization) are quite similar, 0.068 mM and 0.070 mM, respectively,[128] suggesting that the steric contribution of a polydisperse E_{23} head can be approximated in terms of that corresponding to a monodisperse E_8 head. Accordingly, we estimated the effective head cross-sectional area of Brij-35 using eq 2.12, which yields a head area of 53.3 $Å^2$. Although this approximation is rather simplistic, we believe that it is appropriate to capture the underlying physics associated with the steric contribution to counterion binding in this surfactant mixture.

The predicted and the experimental degrees of copper binding, β_{Cu}, as a function of the micelle CuDS composition, α_{CuDS}, are shown in Figure 2-7. The experimental data were collected using two different techniques: (1) for $\alpha_{CuDS} > 0.5$, β_{Cu} was obtained for a particular α_{CuDS} from measurements at several total surfactant concentrations, and (2) for $\alpha_{CuDS} < 0.5$, the $C_{12}E_{23}$ concentration was held constant, and each β_{Cu} value was measured at one CuDS concentration. The first technique can provide additional information (such as the cmc), but the second procedure requires less time. For the predicted results for $\alpha_{CuDS} > 0.5$, we predicted β_{Cu} at a single total

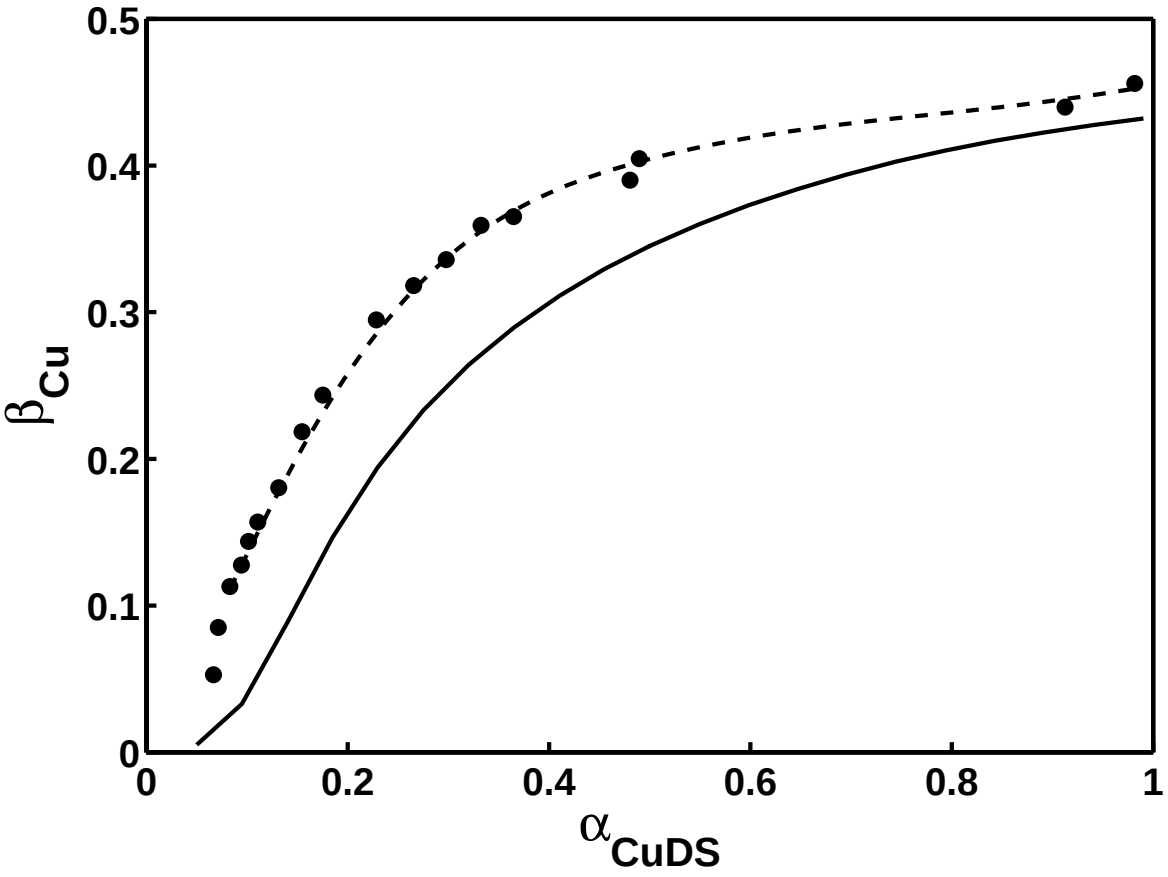

Figure 2-7: Comparison between the predicted (solid line) and the experimental (circles) degrees of Cu^{2+} binding to CuDS-$C_{12}E_{23}$ mixed micelles, β_{Cu}, as a function of the micelle CuDS composition, α_{CuDS}. The experimental data were measured by Treiner et al.,[95] and were fitted using a smoothing spline (dashed line) to help guide the eye.

surfactant concentration of 100 mM, rather than averaging the predicted β_{Cu} values at several total surfactant concentrations, since the specific concentration ranges used by Treiner et al. were not reported. For the predicted results for $\alpha_{\mathrm{CuDS}} < 0.5$, we followed the same method as Treiner et al., although we estimated the $C_{12}E_{23}$ concentration to be 50 mM since it was not reported by the authors. The predictions and the experimental results correspond to 25°C. The experimental data were also fitted using a smoothing spline (dashed line) to help guide the eye.

As Figure 2-7 shows, both the experimental (solid line) and the predicted (circles) β_{Cu} values appear to approach zero when $\alpha_{\mathrm{CuDS}} \lesssim 0.05$. Treiner et al. explain this effect in terms of Bjerrum's classical model for ion condensation, which compares the magnitude of the electrostatic interactions to the thermal energy.[129] However, our molecular model offers another possible explanation. By examining the various contributions to g_{mic} (see eq 2.8), the ion condensation effect can also be rationalized in terms of the competition between g_{elec} and g_{st}. When $\alpha_{\mathrm{CuDS}} < 0.05$, the surface charge density of the micelle is low, and most of the surfactant heads in the micelle have a large cross-sectional area. At these conditions, counterion binding is unfavorable because it would result in a net increase in g_{mic}, due to only a small decrease in g_{elec} but a larger increase in g_{st}.

2.5.2. Prediction of the Critical Micelle Concentration

The degree of counterion binding is often inferred by examining the dependence of the cmc of an ionic surfactant on the counterion concentration. This relationship, known as the Corrin-Harkins relation,[130] is expressed as follows:

$$\log_{10} \mathrm{CMC} = \hat{\beta}_{\mathrm{app}} \log_{10} C_{\mathrm{counterion}} + B \tag{2.34}$$

where $C_{\mathrm{counterion}}$ is the concentration of counterions in the solution and B is the intercept, which corresponds to the $\log_{10}$CMC of the surfactant when the counterion concentration is 1 in the selected concentration units. Since the slope of this curve is often taken as a measure of the degree of counterion binding (per

micellized surfactant), in eq 2.34 we refer to it as the apparent degree of counterion binding, $\hat{\beta}_{\mathrm{app}}$.[131] Maeda recently provided an expanded theoretical discussion of the Corrin-Harkins relationship.[132] Akisada analyzed the apparent degree of counterion binding in mixed micelles using the Gibbs-Duhem relation, and has further examined its relationship to the real degree of counterion binding.[126] The difference between the apparent and the real degrees of counterion binding in the case of a single ionic surfactant component (note that, in this case, $\hat{\beta}_{\mathrm{app}} = \beta_{\mathrm{app}}$, see eq 2.1) was also addressed recently.[42]

Kameyama et al. inferred the degree of sodium binding to mixed micelles of SDS and the nonionic surfactant octyl glucoside (OG) using this approach.[133] In Figure 2-8, the predicted (various lines) and the experimentally measured (various symbols) cmc's as a function of $\alpha_{\mathrm{tot,SDS}}$, the fraction of the total added surfactant that is SDS, are shown for various concentrations of sodium chloride: 20 mM NaCl (solid line and circles), 75 mM NaCl (dashed line and squares), and 150 mM NaCl (dotted line and diamonds). As can be seen, very good agreement is obtained, capturing trends both as a function of $\alpha_{\mathrm{tot,SDS}}$ and as a function of NaCl concentration. At a given value of $\alpha_{\mathrm{tot,SDS}}$, both the predicted and the experimental cmc's decrease as the NaCl concentration increases. For nonionic micelles, this effect is attributed to the "salting out" of the surfactant tails. Our predictions for pure OG micelles ($\alpha_{\mathrm{tot,SDS}} = 0$) underestimate the effect. In particular, we predict that the cmc decreases by approximately 1 mM between each of the considered NaCl concentrations, while the experimental change is approximately 3 mM. These deviations may occur because the salt concentrations are so low, since our model for the effect of added salt uses experimental data obtained at salt concentrations in the 1 M range.[100] In fact, the experimentally measured change in the cmc of OG with added NaCl is smaller and more consistent with our predictions when the NaCl concentrations are in the 1 M range.[134] For mixtures containing an ionic surfactant, the observed decrease in the cmc with increasing salt concentration is largely due to electrostatic effects, and the salting-out phenomenon is overshadowed.

To further test our model, we fitted the predicted and the experimental cmc's

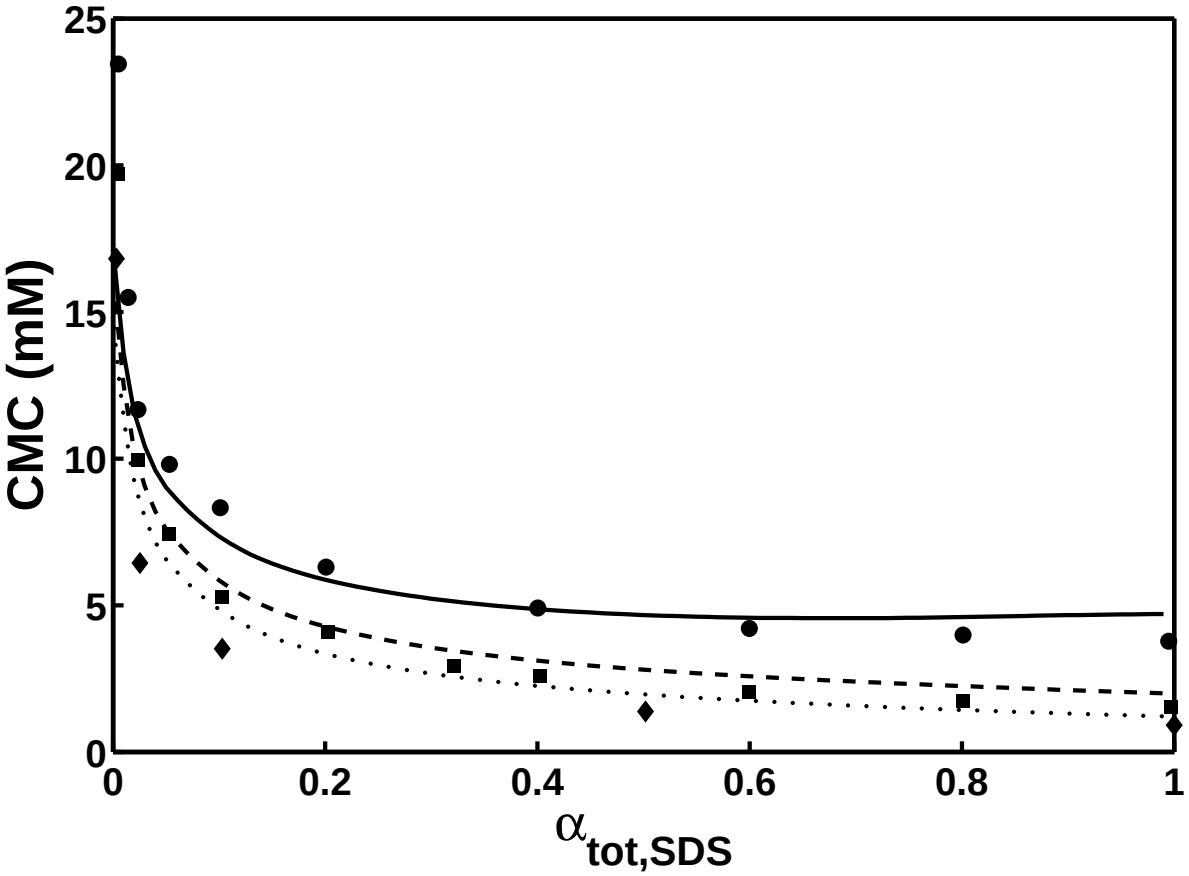

Figure 2-8: Comparison between the predicted (various lines) and the experimental (various symbols) cmc's of SDS-OG binary mixtures as a function of the fraction of the total added surfactant that is SDS, $\alpha_{\mathrm{tot,SDS}}$, at varying NaCl concentrations: 20 mM NaCl (solid line and circles), 75 mM NaCl (dashed line and squares), and 150 mM NaCl (dotted line and diamonds). The experimental data were reported by Kameyama et al.[133]

to eq 2.34 and compared the deduced values of $\hat{\beta}_{\rm app}$. In Figure 2-9, the predicted (solid line) and the experimental (circles) $\hat{\beta}_{\rm app}$ values as a function of the micelle SDS composition, $\alpha_{\rm SDS}$, are seen to be quite similar. At low ionic content, $\hat{\beta}_{\rm app}$ is small but positive, primarily due to: (1) an increase in $g_{\rm tr}$ with increasing salt concentration, reflecting a decrease in the solubility of the surfactant hydrocarbon tails, and (2) an increase in $g_{\rm int}$ with increasing salt concentration, reflecting an increase in the interfacial tension between the oil-like micelle core and the aqueous solution. (Note that $\hat{\beta}_{\rm app}$ can be negative if $g_{\rm tr}$ or $g_{\rm int}$ decrease with salt concentration.) These effects appear to be underestimated by our model, leading to a slight underestimation of $\hat{\beta}_{\rm app}$ at low values of $\alpha_{\rm SDS}$. When $\alpha_{\rm SDS} \gtrsim 0.5$, $\hat{\beta}_{\rm app}$ is observed to sharply increase with $\alpha_{\rm SDS}$ at a nearly constant rate. This effect is primarily due to the dependence of $g_{\rm elec}$ on salt concentration, as governed by the ionic strength of the solution. A secondary effect arises from changes in the counterion entropy loss associated with binding, as a result of changes in the salt concentration. The reasonable agreement between the predicted and the experimental $\hat{\beta}_{\rm app}$ values suggests that our electrostatic model, which includes counterion binding, is able to predict the effect of added salt on the cmc.

Finally, to test whether the Corrin-Harkins relationship can be used to estimate the degree of counterion binding, we also compared $\hat{\beta}_{\rm app}$ to $\hat{\beta}$ (results not shown). Although $\hat{\beta}$ was observed to increase slightly with increasing salt concentration (due to a corresponding decrease in the entropic penalty associated with counterion binding), $\hat{\beta}_{\rm app}$ was within 0.2 units of $\hat{\beta}$ at all conditions. The primary qualitative difference was that in the nonionic limit ($\alpha \rightarrow 0$), $\hat{\beta}_{\rm app}$ remained positive while counterion binding was negligible ($\hat{\beta} \rightarrow 0$). As stated above, at low α, non-electrostatic effects can contribute significantly to $\hat{\beta}_{\rm app}$. Therefore, we conclude that the Corrin-Harkins slope ($\hat{\beta}_{\rm app}$) should only be used as an estimate of the degree of counterion binding for micelles composed primarily of ionic surfactant.

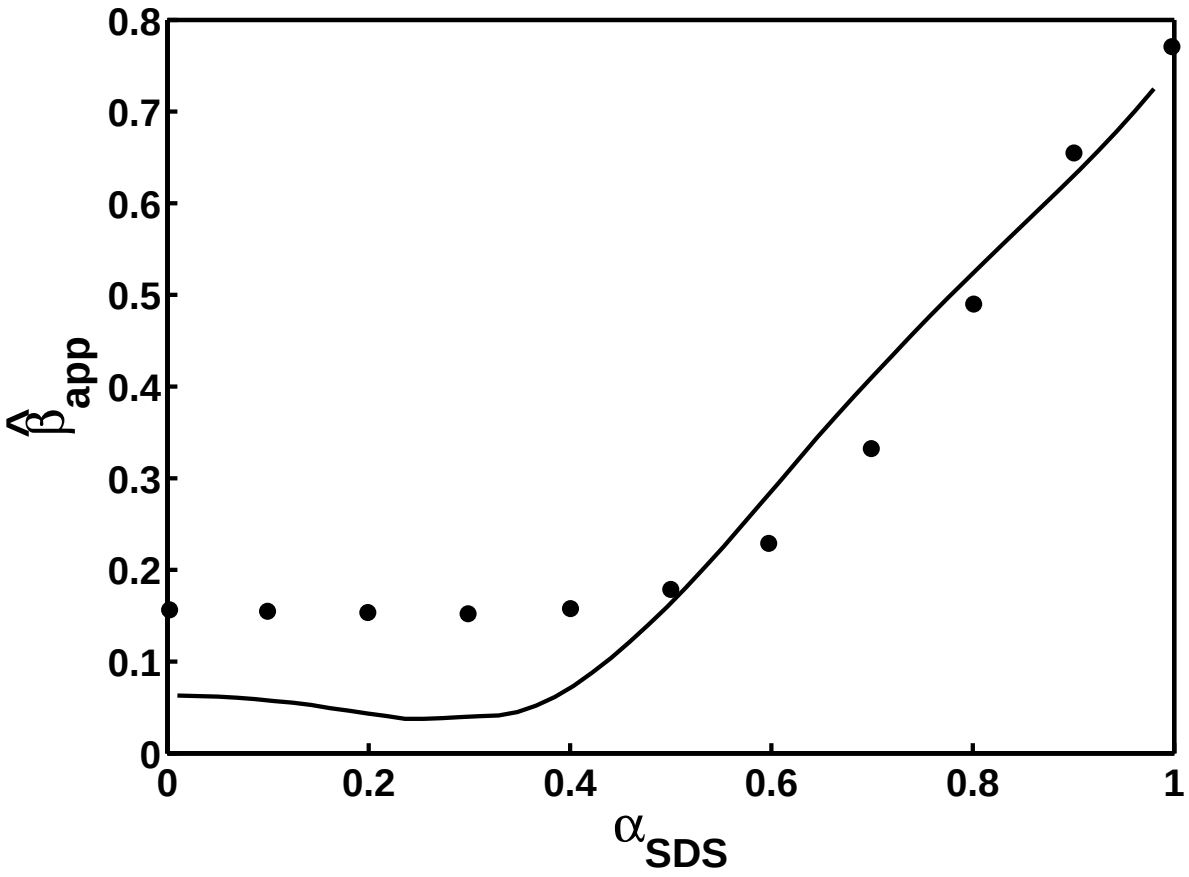

Figure 2-9: Comparison between the predicted (line) and the experimental (circles) Corrin-Harkins slope (the apparent degree of Na^+ binding), $\hat{\beta}_{app}$, for SDS-OG mixtures, as a function of the micelle SDS composition, α_{SDS}. The experimental cmc's used to obtain the Corrin-Harkins slope were obtained by Kameyama et al.[133]

2.5.3. Prediction of the Weight-Average Micelle Aggregation Number

Although experimental aggregation numbers of mixed micelles are less commonly reported in the literature, a mixed surfactant system that was studied experimentally by Moisés de Oliveira and Gehlen consists of a binary mixture of the anionic surfactant SDS and the nonionic surfactant dodecyl tetra(ethylene oxide), $C_{12}E_4$.[135] These authors used time-resolved fluorescence quenching to determine the quencher-average micelle aggregation number, $\langle n \rangle_Q$, of SDS-$C_{12}E_4$ mixtures at 25°C. Note that in the limit of low ratios of quencher to micellized surfactant, $\langle n \rangle_Q$ is equivalent to the weight-average micelle aggregation number, $\langle n \rangle_w$, introduced earlier.[136] All the SDS-$C_{12}E_4$ mixtures examined contained 30 mM SDS, while the concentration of $C_{12}E_4$ varied from 0 to 30 mM. The predicted $\langle n \rangle_w$ (solid line) and the experimental $\langle n \rangle_Q$ values (circles) are shown in Figure 2-10 as a function of the micelle SDS composition, α_{SDS}. For a dodecyl-tailed surfactant, the maximum aggregation number of spherical micelles, n_{sph}^{max} is approximately 55 (see eq 2.29), and larger aggregation numbers suggest the formation of cylindrical micelles. At $\alpha_{SDS} = 0.5$, the predicted and the experimental aggregation numbers are approximately 2 and 3 times n_{sph}^{max}, respectively. However, as α_{SDS} increases and the mixed micelles become progressively more charged, their size decreases until they become nearly spherical at $\alpha_{SDS} = 1$. The experimental aggregation numbers are only slightly larger than n_{sph}^{max}, which suggests that the preferred micelle shape is globular. Since we do not explicitly model such micelle shapes, we expect to underestimate the aggregation numbers of globular micelles (see section 2.4.1). Furthermore, the observed discrepancy between the predicted and the experimental aggregation numbers at other compositions could also be explained by the approximations inherent in our model when dealing with small, cylindrical micelles. As previously observed,[43] because $\langle n \rangle_w$ depends exponentially on $\Delta\mu$, small errors in g_m can lead to large errors in the predicted $\langle n \rangle_w$. We believe that without counterion binding, $\langle n \rangle_w$ will be systematically underestimated in ionic-nonionic surfactant mixtures. For example, we found that the predicted

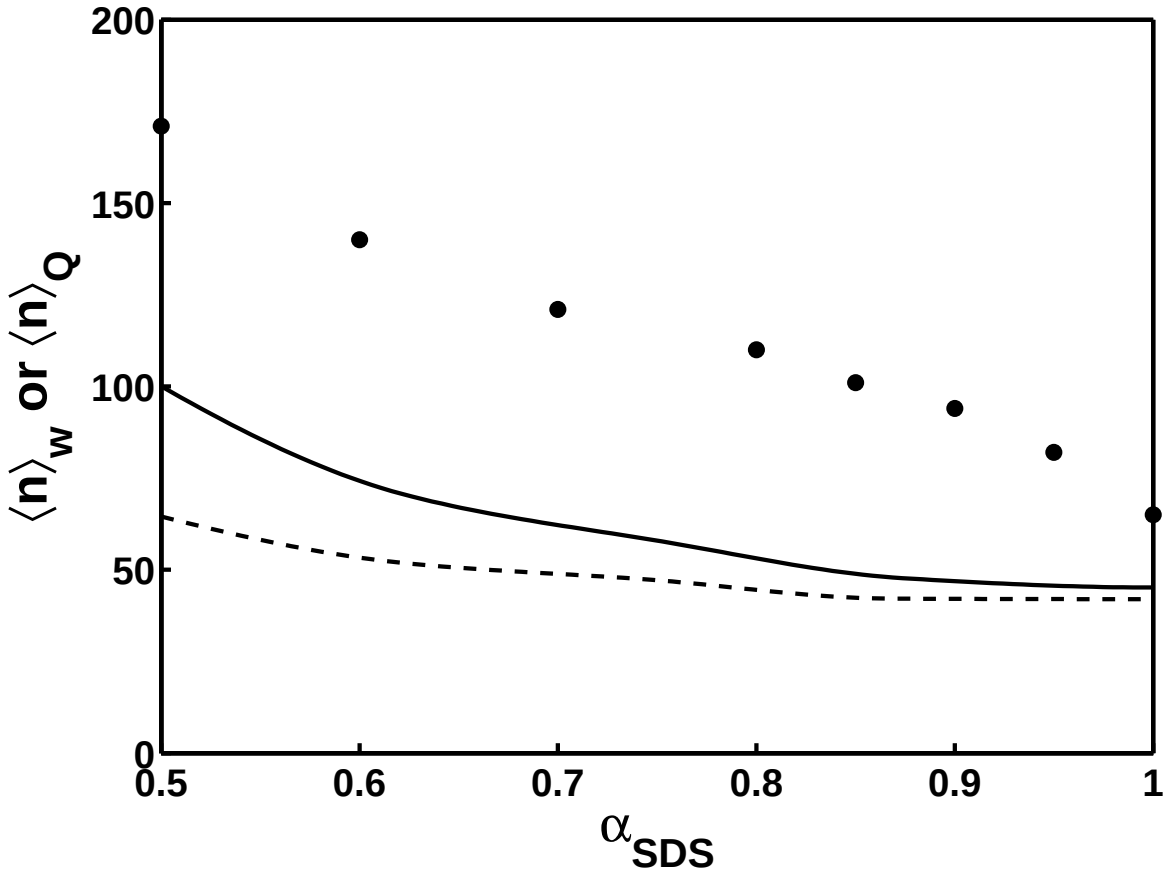

Figure 2-10: Comparison of the predicted weight-average ($\langle n \rangle_{\mathrm{w}}$, solid line) and the experimental quencher-average ($\langle n \rangle_{\mathrm{Q}}$, circles) aggregation numbers of SDS-$C_{12}E_4$ mixed micelles. The predicted $\langle n \rangle_{\mathrm{w}}$ are also shown using our model in the absence of counterion binding (dashed line). The experimental values were reported by Moisés de Oliveira and Gehlen.[135]

aggregation numbers are 42 to 65 for the entire range of $0.5 \leq \alpha_{SDS} \leq 1$ (dashed line in Figure 2-10) when our model is used *without counterion binding*. Since the micelle shape transition in the SDS/$C_{12}E_4$ mixture occurs primarily because g_{elec} decreases significantly as α_{SDS} decreases, *significant micelle growth is predicted only when counterion binding is included in the model.*

2.6. Conclusions

In this chapter, we presented a molecular-thermodynamic model to describe the micellization of binary surfactant mixtures that explicitly accounts for counterion binding. The model was applied to binary surfactant mixtures consisting of an ionic surfactant mixed with a nonionic (or a zwitterionic) surfactant. Under most conditions, the model accurately predicts how the degree of counterion binding varies with the ionic composition of the micelle. We rationalized an experimentally observed inflection in the curve of the degree of counterion binding as a function of the micelle ionic composition as resulting from a transition in micelle shape from spherical to cylindrical. We also observed that the degree of counterion binding at very low micelle ionic compositions is sensitive to all the contributions to the free energy of mixed micellization, which highlights the difficulty associated with making predictions at these ionic compositions. However, this sensitivity also provided insight into the phenomenon of ion condensation as seen by the existence of a micelle ionic composition below which negligible counterion binding occurs. This phenomenon was observed experimentally and predicted by our model in the CuDS-$C_{12}E_{23}$ binary surfactant mixture. The model was also successful at predicting other micellization properties, specifically cmc's and weight-average micelle aggregation numbers.

The theoretical framework presented in this chapter also serves as the basis for modeling more complex surfactant systems. Specifically, in Chapter 3, we extend the theory to model the micellization of pH-sensitive surfactants.

Chapter 3

Molecular-Thermodynamic Theory of Micellization of pH-Sensitive Surfactants

3.1. Introduction

Many surfactants contain functional groups that are pH-sensitive, including some surfactants that are typically considered to be ionic, like soaps (fatty acid salts). Zwitterionic surfactants, which contain both cationic and anionic functional groups, are sometimes referred to as amphoteric, since their ionic groups are often pH-sensitive. The unique properties of amphoteric surfactants (for example, solubility over large pH ranges, low potential for skin or eye irritation, good foaming characteristics) has led to their use in a wide range of products, including personal care formulations, disinfectants, detergents, and anti-corrosion coatings.[48] Another important class of pH-sensitive surfactants, for which Laughlin has suggested the name "semipolar," possess a relatively large dipole moment but do not contain ionized functional groups.[47] Commonly encountered semipolar groups include amine oxides, phosphine oxides, and sulfoxides.

At an appropriate pH, a solution of a pH-sensitive surfactant may behave like

a binary surfactant mixture of the protonated and the deprotonated forms of the surfactant. Even under conditions where the free surfactant monomers exist almost entirely in one form (protonated or deprotonated), micelles may contain significant amounts of both forms of the surfactant. For example, for the semipolar surfactant dodecyldimethylamine oxide (C_{12}DAO) in 0.1 M NaCl at pH 3, approximately 1% of the monomeric surfactant molecules are deprotonated while 10% of the micellized surfactant molecules are deprotonated.[67] It is therefore important to recognize that pH-sensitive surfactants behave effectively like binary surfactant mixtures, where the relative compositions of the monomers and the micelles are controlled primarily by the solution pH.

A particularly interesting characteristic of pH-sensitive surfactants is that they allow experimental access to properties that are often difficult to measure in "conventional" binary surfactant mixtures. For example, the ability to titrate solutions of pH-sensitive surfactants can allow experimental access to the monomer and the micelle compositions.[49,50] Titration experiments have also been used to determine the electrostatic potential at the micelle interface.[51]

In spite of the growing body of experimental data, few models of pH-dependent micellization have been developed. The most common theoretical description of the micellization behavior of pH-sensitive surfactants (and of binary surfactant mixtures in general) is regular solution theory (RST).[37] Use of RST typically requires that the individual surfactant critical micelle concentrations (cmc's) be known. In addition, use of RST for a binary surfactant mixture requires input of an interaction parameter (the β_{RST} parameter), which reflects the interactions between the two surfactant types in the micelle. Note that the β_{RST} parameter is usually determined by fitting to additional measured cmc values. In the context of pH-sensitive surfactants, the implementation of RST requires knowledge of the cmc's of: (1) the protonated form of the surfactant, (2) the deprotonated form of the surfactant, and (3) the surfactant at one or more intermediate degrees of ionization (to determine the β_{RST} parameter). For example, β_{RST} parameters have been estimated for the pH-sensitive surfactants C_{12}DAO and tetradecyldimethylamine oxide (C_{14}DAO) by fitting experimental cmc's

to those predicted by RST.[51] The RST approach was also used to predict cmc's of a mixture of C_{14}DAO and hexadecyldimethylbetaine.[69] In spite of its practical utility, RST has several limitations, including: (1) the time and effort associated with obtaining the required experimental inputs, (2) the inability to accurately capture strong interactions at the micelle level, (3) the lack of a clear physical basis for the β_{RST} parameter, which is often treated as a fitting parameter, and (4) the lack of a detailed description of micelle structure (such as micelle shape and size), since the micelle is assumed to be an infinitely large pseudo-phase.

Another model for pH-dependent micellization was proposed by Mille, who analyzed the difference in the titration behavior of the micellized surfactant relative to that of the surfactant monomers using a model for nearest-neighbor electrostatic interactions at the micelle interface.[64] Electrostatics alone was found to be inadequate to model the observed micellar titration behavior, and the existence of an additional attractive interaction was proposed.[64]

Additional theoretical models have been developed for alkyldimethylamine oxide surfactants, primarily by Maeda and others. For example, a statistical-thermodynamic approach was used to analyze C_{12}DAO titration data and to separate the free energy into electric and non-electric components.[65] Maeda also developed a theoretical approach similar to RST to analyze the cmc of pH-sensitive surfactants.[137] Maeda recently used a thermodynamic model and RST to analyze the titration of pH-sensitive micelles.[67] Lair et al. recently developed a model that relates the variation of the cmc with pH to the degrees of protonation of the micelles and of the surfactant monomers.[68] Although undoubtedly each of these models advances our fundamental understanding of pH-dependent micellization, to date, no comprehensive *molecular-level theory* of the micellization behavior of pH-sensitive surfactants has been formulated.

With the above in mind, in this chapter, we present a molecular-thermodynamic theory of micellization of pH-sensitive surfactants that generalizes the theoretical description presented in ref 138 and Chapter 2 for the micellization of binary surfactant mixtures, in which counterion binding was modeled explicitly. The theory

presented here is completely predictive in that it does not require any prior knowledge of the micellization behavior of the pH-sensitive surfactant. Instead, the theory relies on knowledge of the molecular characteristics of the pH-sensitive surfactant and of the solution conditions (including the temperature and the concentrations of additives). The equilibrium deprotonation constant of the surfactant monomer (pK_1) is used to capture the pH-dependent behavior of both the monomers and the micelles. The theory can then be used to predict various useful surfactant solution properties of practical and fundamental interest, including the cmc, the micelle composition, the degree of counterion binding to micelles, the micelle shape and size, the micelle deprotonation equilibrium parameter (pK_m), and the solution pH. Moreover, the theoretical framework can also be used to gain physical insight into the relationship between the molecular structure of the pH-sensitive surfactant and its micellization behavior. In addition, significant physical insight can be gained by studying any systematic deviations between the theoretical predictions and experiments in order to identify physical interactions that may have been neglected or poorly modeled in the context of the theory.

The remainder of this chapter is organized as follows. In section 3.2, the thermodynamic and the molecular components of the theory are described. The prediction of various micellar solution properties in the context of the molecular-thermodynamic theory is discussed in section 3.3. In section 3.4, the theoretical predictions are compared to available experimental data for several pH-sensitive surfactants. Finally, concluding remarks are presented in section 3.5.

3.2. Theory

A pH-sensitive surfactant behaves effectively like a binary surfactant mixture composed of the protonated and the deprotonated forms, where the mixture composition is controlled by the solution pH. The theoretical framework presented here is based on the theoretical description presented in ref 138 and Chapter 2 for the micellization behavior of binary surfactant mixtures that accounts explicitly for

counterion-binding effects. In the context of this description, counterion binding was previously shown to be necessary to correctly capture the micellization behavior of ionic surfactants.[42,43] In this section, we briefly highlight the novel aspects associated with the pH-sensitivity of the surfactant.

In what follows, we develop a theoretical framework to model an aqueous solution containing a *single* surfactant type having a *single* pH-sensitive functional group, along with added salt and acid (or base). Note that we can further classify such a pH-sensitive surfactant based on whether its protonated form is charged. If the protonated form of the surfactant is uncharged, then the deprotonated form will be anionic. Such a surfactant will effectively form a nonionic-anionic (or zwitterionic-anionic) pair. An example of this type of surfactant is soap, which can exist either as a nonionic fatty acid or as an anionic fatty acid salt.[139] The other class of pH-sensitive surfactant forms a nonionic-cationic (or zwitterionic-cationic) pair. An example of this type of surfactant is an alkylbetaine, which can exist either as a zwitterionic surfactant containing a positively charged (quaternary) ammonium group and a negatively charged carboxylate group, or as a cationic surfactant containing a positively charged (quaternary) ammonium group and a neutral carboxylic acid group.[47,140] The well studied alkyldimethylamine oxides are also members of the zwitterionic-cationic class of pH-sensitive surfactants.[51]

For simplicity, we assume that any added salt consists of a monovalent cation (denoted by M^+) and a monovalent anion (denoted by X^-). Furthermore, we assume that any added acid has the molecular formula HX, and that any added base has the molecular formula MOH. For example, if the added salt is sodium chloride (NaCl), then the corresponding acid and base are hydrochloric acid (HCl) and sodium hydroxide (NaOH), respectively. Finally, we assume that, if the surfactant is added in ionized form, its associated counterion is M^+ (if the surfactant is anionic, as in the case of fatty acid salts) or X^- (if the surfactant is cationic, as in the case of alkyldimethylamine oxide salts).

With the above assumptions in mind, in section 3.2.1, we first present the thermodynamic framework to model the micellar equilibrium, including pH effects.

Subsequently, in section 3.2.2, we briefly discuss the molecular model to compute the free energy of micellization.

3.2.1. Thermodynamic Framework

We model the thermodynamic equilibrium in a solution containing a pH-sensitive surfactant in terms of: (1) the equilibrium between the protonated and the deprotonated forms of the surfactant monomers, and (2) the equilibrium between the micelles and the surfactant monomers. Before we present the formalism describing the equilibrium conditions in (1) and (2), we first discuss our notation.

We denote the deprotonated surfactant species, having valence z_S, as S and to the hydrogen ions as H^+. The protonated form of the surfactant, having valence $(z_S + 1)$, is denoted as HS (to reflect the deprotonation reaction, which can be written as $HS^{z_S+1} \rightarrow H^+ + S^{z_S}$). For quantities referring to the counterion (which can be either M^+ or X^-, see above), the subscript C and valence z_C are used. These counterions may originate from surfactant that is added in the ionized form, or from added salt, acid, or base. We do not consider the possibility of electrostatic binding of H^+ or OH^-, because in most practical cases, including the surfactant systems considered in this chapter, neither H^+ nor OH^- "counterions" are present at sufficient concentrations to yield significant binding. For example, OH^- is in principle a counterion for protonated, cationic alkyldimethylamine oxide surfactants. However, these surfactants are only cationic at low pH, where the OH^- concentration is very low.

We can now write the thermodynamic equilibrium for a micelle consisting of n surfactant molecules, where $n\alpha$ are in the protonated state and $n(1-\alpha)$ are in the deprotonated state, and $n\hat{\beta}_C$ bound counterions, where α denotes the degree of protonation of the micelle (which we subsequently refer to as the *micelle composition*), and $\hat{\beta}_C$ denotes the number of bound counterions per surfactant molecule in the micelle. The more traditional degree of counterion binding β_C, defined as the number of bound counterions per ionic surfactant in the micelle, is then related to $\hat{\beta}_C$ as

follows (see ref 138 and Chapter 2):

$$\beta_{\mathrm{C}} = \begin{cases} \hat{\beta}_{\mathrm{C}}/\alpha, & \text{for nonionic-cationic or zwitterionic-cationic surfactants} \\ \hat{\beta}_{\mathrm{C}}/\left(1-\alpha\right), & \text{for nonionic-anionic or zwitterionic-anionic surfactants} \end{cases} \tag{3.1}$$

The denominators on the right-hand side of eq 3.1 correspond to the ionic fractions of micellized surfactant molecules, given by α for nonionic-cationic or zwitterionic-cationic surfactants, and by $(1-\alpha)$ for nonionic-anionic or zwitterionic-anionic surfactants.

Using this notation, we obtain the following expression characterizing the condition of thermodynamic equilibrium between micelles, protonated and deprotonated surfactant monomers, and free counterions (see ref 138 and Chapter 2):

$$X_{n\alpha\hat{\beta}_{\mathrm{C}}} = \frac{1}{e} X_{1\mathrm{HS}}^{n\alpha} X_{1\mathrm{S}}^{n(1-\alpha)} X_{1\mathrm{C}}^{n\hat{\beta}_{\mathrm{C}}} \exp\left[-\frac{n}{k_{\mathrm{B}}T} g_{\mathrm{mic}}\left(S, l_{\mathrm{c}}, \alpha, \hat{\beta}_{\mathrm{C}}\right)\right] \tag{3.2}$$

where X_{1i} denotes the mole fraction of species i (HS, S, and C) in monomeric form, $X_{n\alpha\hat{\beta}_{\mathrm{C}}}$ denotes the mole fraction of micelles of type $n\alpha\hat{\beta}_{\mathrm{C}}$, k_{B} is the Boltzmann constant, T is the absolute temperature, and g_{mic} is the free energy of micellization. The quantity g_{mic} represents the free-energy gain per surfactant molecule associated with forming a micelle (an $n\alpha\hat{\beta}_{\mathrm{C}}$-mer) from $n\alpha$ protonated surfactant monomers, $n\left(1-\alpha\right)$ deprotonated surfactant monomers, and $n\hat{\beta}_{\mathrm{C}}$ counterions. Note that g_{mic} is a function of the following micelle characteristics: the shape factor, S, the core minor radius, l_{c}, the micelle composition, α, and the degree of counterion binding, $\hat{\beta}_{\mathrm{C}}$. The shape factor S is 3 for spherical micelles, 2 for cylindrical micelles, and 1 for planar or discoidal micelles.[39] Note that l_{c} refers to the radius of the hydrophobic core of spherical or cylindrical micelles, or to the half-width of the hydrophobic core of planar or discoidal micelles.[39]

The micelle equilibrium can also be written in terms of the total concentration of

surfactant monomers, $X_1 = X_{1\mathrm{HS}} + X_{1\mathrm{S}}$, as follows (see ref 138 and Chapter 2):

$$X_{n\alpha\hat{\beta}_\mathrm{C}} = \frac{1}{e} X_1^n \exp\left[-\frac{n}{k_\mathrm{B}T} g_\mathrm{m}\right] \tag{3.3}$$

where g_m is the modified free energy of micellization, defined as[4, 42, 138] (see Chapter 2):

$$g_\mathrm{m} = g_\mathrm{mic} - k_\mathrm{B}T\left[\alpha \ln \alpha_1 + (1-\alpha)\ln(1-\alpha_1) + \hat{\beta}_\mathrm{C} \ln X_{1\mathrm{C}}\right] \tag{3.4}$$

Note that $\alpha_1 = X_{1\mathrm{HS}}/X_1$ is the protonated fraction of the surfactant monomers.

The relationship governing the protonation equilibrium of the surfactant monomers is often written in the form of the Henderson-Hasselbalch equation:[51, 141]

$$\mathrm{pK}_1 = \mathrm{pH} - \log\frac{X_{1\mathrm{S}}}{X_{1\mathrm{HS}}} = \mathrm{pH} + \log\frac{\alpha_1}{1-\alpha_1} \tag{3.5}$$

where $\mathrm{p}K_1 = -\log K_1$, and K_1 is the deprotonation equilibrium constant of the surfactant monomers.

For each species, we also use a mass balance that equates its total mole fraction to its mole fraction in the bulk solution plus its mole fraction in the micelles. The total mole fraction of surfactant, $X_\mathrm{S}^\mathrm{total}$, corresponds to the sum of the surfactant added in the protonated and the deprotonated forms. The total mole fraction of counterions, $X_\mathrm{C}^\mathrm{total}$, corresponds to the sum of counterions originating from the added salt, acid, and base, and from any surfactant added in its ionic form, which must include its counterion in order to maintain electroneutrality. Following the methodology described in ref 138 and Chapter 2 the mass balances are given by the following equations:

$$X_\mathrm{S}^\mathrm{total} = X_1 + \sum_{\{S,n,\alpha,\hat{\beta}_\mathrm{C}\}} n X_{n\alpha\hat{\beta}_\mathrm{C}} + E_\mathrm{dl,S} \tag{3.6}$$

$$X_\mathrm{C}^\mathrm{total} = X_{1\mathrm{C}} + \sum_{\{S,n,\alpha,\hat{\beta}_\mathrm{C}\}} n\hat{\beta}_\mathrm{C} X_{n\alpha\hat{\beta}_\mathrm{C}} + E_\mathrm{dl,C} \tag{3.7}$$

where the summations in eqs 3.6 and 3.7 account for micelles of different types (that

is, having different values of S, α, n, and $\hat{\beta}_{\mathrm{C}}$), and $E_{\mathrm{dl},i}$ (i =S and C) is a term accounting for the depletion of charged surfactant monomers, or for the enhancement of counterions, in the diffuse layer (dl), relative to their concentrations in the bulk solution (see Appendix A for details).

In addition, the pH equilibrium requires mass balances on the hydrogen (H^+) and on the hydroxide (OH^-) ions, which are given, respectively, by

$$X_{\mathrm{H}}^{\mathrm{total}} = X_{\mathrm{H_2O}} + \alpha_1 X_1 + X_{1\mathrm{H}} + \sum_{\{S,n,\alpha,\hat{\beta}_{\mathrm{C}}\}} n\alpha X_{n\alpha\hat{\beta}_{\mathrm{C}}} + E_{\mathrm{dl,H}} \tag{3.8}$$

$$X_{\mathrm{OH}}^{\mathrm{total}} = X_{\mathrm{H_2O}} + X_{1\mathrm{OH}} + E_{\mathrm{dl,OH}} \tag{3.9}$$

where X_i^{total} (i =H^+ and OH^-) is the total concentration of added species i, X_{1i} (i =H^+ and OH^-) is the bulk concentration of species i, and $E_{\mathrm{dl},i}$ (i =H^+ and OH^-) represents the enhancement or the depletion of species i in the diffuse layer (see Appendix A). Note that hydrogen ions may be added to the solution from any added acid, HX, or from surfactant that is added in its protonated form, HS. Typically, hydroxide ions will only be added to the solution from any added base, MOH. The quantity $X_{\mathrm{H_2O}}$, the total mole fraction of water, contributes to the mass balances of both the hydrogen and the hydroxide ions. However, we can eliminate $X_{\mathrm{H_2O}}$ from the mass balances by subtracting eq 3.9 from eq 3.8. This yields

$$\left(X_{\mathrm{H}}^{\mathrm{total}} - X_{\mathrm{OH}}^{\mathrm{total}}\right) = (X_{1\mathrm{H}} - X_{1\mathrm{OH}}) + \alpha_1 X_1 + \sum_{\{S,n,\alpha,\hat{\beta}_{\mathrm{C}}\}} n\alpha X_{n\alpha\hat{\beta}_{\mathrm{C}}} + (E_{\mathrm{dl,H}} - E_{\mathrm{dl,OH}}) \tag{3.10}$$

The equilibrium constant for the dissociation of water (K_{w}, obtained from ref 113) is used to relate $X_{1\mathrm{OH}}$ to $X_{1\mathrm{H}}$, specifically,

$$X_{1\mathrm{H}} X_{1\mathrm{OH}} = K_{\mathrm{w}} \tag{3.11}$$

Note that we have assumed that activity coefficient effects are negligible or that they can be included in terms of effective values of the equilibrium constants. For $\mathrm{p}K_1$ (eq 3.5), this approximation appears to be reasonable, based on experimental titration

data for alkyldimethylamine oxide surfactants.[51] Activity coefficient corrections (estimated using the Davies empirical correction to the Debye-Hückel expression for activity coefficients[142,143]) were found to have minimal impact on eq 3.11.

In summary, the experimentally known quantities (X_i^{total}, i =S, H^+, OH^-, and C) are used, along with eqs. 3.3, 3.5, 3.6, 3.7, 3.10, and 3.11, to solve for the solution conditions (α_1, X_1, $X_{1\text{C}}$, $X_{1\text{H}}$, $X_{1\text{OH}}$, and X_{mic}). Note that eq 3.3 also requires a model for the free energy of micellization, g_{mic}, which we describe next in section 3.2.2.

3.2.2. Molecular Model for the Free Energy of Micellization

The molecular component of the theory is identical to that described in ref 138 and Chapter 2. With that in mind, in this section, we briefly summarize the key results of the g_{mic} model without presenting specific equations. Instead, the key equations of the g_{mic} model as applied to a pH-sensitive surfactant are summarized in Appendix B. These equations, which are referenced below by number (for example, eq B.1), may be useful to more clearly rationalize the results presented in section 3.4.

The free energy of micellization, g_{mic}, is modeled as the sum of six contributions (see ref 138 and Chapter 2):

$$g_{\text{mic}} = g_{\text{tr}} + g_{\text{int}} + g_{\text{pack}} + g_{\text{st}} + g_{\text{elec}} + g_{\text{ent}} \tag{3.12}$$

The first three contributions are associated with the formation of the micelle core: The transfer contribution, g_{tr}, accounts for the transfer of the surfactant hydrophobic tails from an aqueous to an oil-like environment. The interfacial contribution, g_{int}, accounts for the free-energy penalty associated with the formation of an interface between the oil-like micelle core and the surrounding aqueous environment. The packing contribution, g_{pack}, accounts for the additional entropic constraints associated with anchoring one end of each surfactant hydrophobic tail at the micelle core-water interface. The fourth and fifth contributions are associated with the formation of the micelle interfacial region: The steric contribution, g_{st}, accounts for the steric interactions between the surfactant hydrophilic heads and the bound counterions in

the micelle interfacial region. The electrostatic contribution, g_{elec}, accounts for the electrostatic interactions at the micelle interface that operate in the case of ionic and zwitterionic surfactants and bound counterions. The last contribution, g_{ent}, accounts for the entropy of mixing the various components in a micelle. Below, we briefly discuss how the various free-energy contributions depend on the micelle properties and on the surfactant and counterion molecular structures.

The transfer contribution, g_{tr}, is independent of the micelle structure; it depends solely on the composition of the micelle and on the number of carbon atoms in the surfactant hydrophobic tail, n_{t} (see eq B.1). Both g_{int} and g_{pack} depend on the micelle structure via l_{c} and S. The interfacial contribution, g_{int}, is modeled using a curvature-corrected interfacial tension that depends weakly on n_{t}, and is modeled as the product of the interfacial tension and the unshielded interfacial area of the micelle core (see eq B.3). The packing contribution, g_{pack}, is modeled using a mean-field approach that samples the conformations and orientations of the surfactant hydrophobic tails in the micelle core (see eq B.5). Since the protonated and the deprotonated surfactant forms generally have the same hydrophobic tail (that is, have identical n_{t} values), g_{tr}, g_{int}, and g_{pack} are all independent of the micelle composition, α, (see eqs B.2, B.4, and B.6).

The steric contribution, g_{st}, models the interactions of the surfactant hydrophilic heads and the bound counterions due to their physical sizes. Therefore, this contribution depends on the effective cross-sectional area of the surfactant head, a_{h}, and on the effective cross-sectional area of a bound counterion $a_{\mathrm{hC}} = 4\pi r_{\mathrm{C}}^2$, where r_{C} is the radius of a counterion (see eq B.7). This contribution also depends on the available micelle surface area per surfactant molecule, which is determined from S, l_{c}, and the average surfactant tail volume. Since the protonated and the deprotonated forms of the surfactant generally have the same a_{h} values, g_{st} is independent of α (see eq B.8).

The electrostatic contribution, g_{elec}, is modeled as the sum of a discharge contribution, g_{disch}, and a charging contribution, g_{charge}. First, g_{disch} is calculated for the ionic surfactants (see eq B.13), the zwitterionic (or dipolar) surfactants

(see eq B.12), and the counterions (see eq B.13) in their unassembled states. As a result, g_{disch} is independent of the micelle structure but depends on the valence of each ionic surfactant and counterion, z and z_{C}, respectively (see eq B.13), and on the dipole separation of each zwitterionic surfactant, d_{sep}, (see eq B.12). In addition, g_{disch} depends on the size of the surfactant heads and the counterions. The charging contribution, g_{charge}, is modeled by re-assembling the charges onto the micelle surface. The location of the charges are determined by the molecular structure of the surfactant, specifically, by the distance from the beginning of the tail to the charge on an ionic surfactant or to the innermost charge on a zwitterionic surfactant, d_z, and also by d_{sep} (the charge separation distance) for zwitterionic surfactants. Furthermore, the surface charge density depends on the micelle structure through S and l_{c}. The charging contribution also depends strongly on the ionic strength of the bulk solution through the inverse Debye-Hückel screening length, κ (see eqs B.15 and B.18). Note that our electrostatic model also includes a Stern layer, which is a region around the micelle that the unbound counterions cannot penetrate.[105,106] The position of the Stern layer is determined in part by the length of the surfactant head, l_{h}.

The entropic contribution, g_{ent}, is derived from a model for ideal mixing. Therefore, g_{ent} is independent of the molecular structures of the surfactant and the counterion, and is also independent of the micelle structure. In other words, g_{ent} depends solely on the micelle composition through α and $\hat{\beta}_{\text{C}}$ (see eq B.9).

3.3. Determination of Useful Micellar Solution Properties

To determine various useful micellar solution properties, we simultaneously solve the mass balances (eqs 3.6, 3.7, and 3.10) along with the equilibrium conditions for micelle formation (eq 3.3), for the dissociation of water (eq 3.11), and for the protonation of the surfactant monomers (eq 3.5). In these mass balances, the summations are over the mole fractions of micelles of every possible shape (S), aggregation number

(n), composition (α), and degree of counterion binding ($\hat{\beta}_{\mathrm{C}}$). Explicitly carrying out these summations would be computationally challenging, but fortunately that is not necessary. Indeed, as shown previously[4,42,138] (see also Chapter 2), these summations can be approximated reasonably well by summations over the micelle aggregation number, n, where the optimal micelle shape (S^*), optimal composition (α^*), and optimal degree of counterion binding ($\hat{\beta}_{\mathrm{C}}^*$) are determined by minimizing g_{m} (see eq 3.4) for a given aggregation number, n, with respect to S, α, and $\hat{\beta}_{\mathrm{C}}$, respectively. The resulting optimal value of g_{m} is denoted by g_{m}^*. This approximation then allows the calculation of additional micellar solution properties of interest, including the cmc and various average micelle aggregation numbers (see section 3.3.1).

3.3.1. Calculating the Critical Micelle Concentration and Average Micelle Aggregation Numbers

We approximate the cmc (in mole fraction units) as $\exp(g_{\mathrm{m}}^*/k_{\mathrm{B}}T)$, where g_{m}^* is the optimal modified free energy of micellization of the preferred micelle shape (having optimal values S^*, α^*, and $\hat{\beta}_{\mathrm{C}}^*$) at the given solution conditions.[39] Note that we must still self-consistently solve the mass balances (eqs. 3.6, 3.7, and 3.10), where the total concentration of surfactant is equal to the cmc.

In practice, our model for g_{m} is only applicable to "regular" micelle shapes (spherical micelles, infinite cylindrical micelles, and infinite planar bilayers), primarily due to restrictions imposed on our models for g_{pack} and g_{elec}.[4,39,42] The surfactants studied in this chapter are known to form spherical or cylindrical micelles (see section 3.4.1), and therefore, we do not consider finite bilayer (discoidal) micelles. However, we are still able to estimate g_{m} for finite cylindrical micelles by interpolating between the results for the corresponding regular micelle shapes. Specifically, the interpolation equation can be conveniently expressed in terms of the growth parameter, $\Delta\mu$, which models the difference between g_{m} of a spherical micelle and g_{m} of an infinite cylindrical micelle, and is given by[41]

$$\Delta\mu = g_{\mathrm{m,sph}}^* - g_{\mathrm{m,cyl}}^* \tag{3.13}$$

where $g^*_{\mathrm{m,sph}}$ and $g^*_{\mathrm{m,cyl}}$ are the optimal modified free energies of micellization (see eq 3.4) for spheres and for infinite cylinders, respectively. The modified free energy of micellization of a finite cylindrical micelle of aggregation number n (where $n > n_{\mathrm{sph}}$), denoted by $g^*_{\mathrm{m}}(n)$, is then given by[41]

$$g^*_{\mathrm{m}}(n) = g^*_{\mathrm{m,cyl}} + \left(n^*_{\mathrm{sph}}/n\right) \Delta\mu \tag{3.14}$$

where n^*_{sph} is the aggregation number of an optimal spherical micelle. Note that if $\Delta\mu$ is negative, cylindrical micelles are unfavorable. Conversely, if $\Delta\mu$ is positive, finite cylindrical micelles will form. The larger the value of $\Delta\mu$, the larger the average size of the cylindrical micelles.

If the optimal micelle shape is cylindrical, we calculate average micelle aggregation numbers using the following relations:[121]

$$\begin{aligned} \langle n \rangle_{\mathrm{n}} &= \frac{M_1}{M_0} \\ \langle n \rangle_{\mathrm{w}} &= \frac{M_2}{M_1} \end{aligned} \tag{3.15}$$

where $\langle n \rangle_{\mathrm{n}}$ and $\langle n \rangle_{\mathrm{w}}$ are the number-average and the weight-average micelle aggregation numbers, respectively, and M_k is the kth moment of the micelle size distribution, defined as follows:[121]

$$M_k = \sum_{n \geq n^*_{\mathrm{sph}}} n^k X_{n\alpha^*\hat{\beta}^*_{\mathrm{C}}} \tag{3.16}$$

where $X_{n\alpha^*\hat{\beta}^*_{\mathrm{C}}}$ is the mole fraction of micelles of aggregation number n, optimal composition $\alpha^*(n)$, and optimal degree of counterion binding $\hat{\beta}^*_{\mathrm{C}}(n)$. In the limit of extensive cylindrical micelle growth, the average aggregation numbers depend exponentially on $\Delta\mu$:[144]

$$\begin{aligned} \langle n \rangle_{\mathrm{n}} &= n^*_{\mathrm{sph}} + \left[\exp\left(n^*_{\mathrm{sph}}\Delta\mu/k_{\mathrm{B}}T\right)\left(X^{\mathrm{total}}_{\mathrm{S}} - X_{\mathrm{cmc}}\right)\right]^{1/2} \\ \langle n \rangle_{\mathrm{w}} &= n^*_{\mathrm{sph}} + 2\left[\exp\left(n^*_{\mathrm{sph}}\Delta\mu/k_{\mathrm{B}}T\right)\left(X^{\mathrm{total}}_{\mathrm{S}} - X_{\mathrm{cmc}}\right)\right]^{1/2} \end{aligned} \tag{3.17}$$

where $X_{\mathrm{cmc}} = \exp\left(g_{\mathrm{m}}^{*}/k_{\mathrm{B}}T\right)$.

If the optimal micelle shape is spherical, we approximate the micelle size distribution as being monodisperse, and therefore, $\langle n \rangle_{\mathrm{n}} = \langle n \rangle_{\mathrm{w}}$.

3.3.2. Calculating the Micellar Deprotonation Parameter, $\mathrm{p}K_{\mathrm{m}}$

The acid deprotonation equilibrium constant, K_{a}, or, equivalently, the $\mathrm{p}K_{\mathrm{a}} = -\log K_{\mathrm{a}}$, is often used as a measure of the protonation equilibrium of a weak acid.[141] In fact, the $\mathrm{p}K_{\mathrm{a}}$ of the surfactant monomers, denoted by $\mathrm{p}K_1$, is used to calculate the surfactant monomer composition, α_1, as a function of pH (see eq 3.5). In the case of micelles, a similar relationship can be used to define the micellar deprotonation parameter, $\mathrm{p}K_{\mathrm{m}}$, as follows[51]

$$\mathrm{p}K_{\mathrm{m}} = \mathrm{pH} + \log \frac{\alpha}{1-\alpha} \tag{3.18}$$

Although it relates the micelle composition, α, to the solution pH, the $\mathrm{p}K_{\mathrm{m}}$ is fundamentally different from the $\mathrm{p}K_{\mathrm{a}}$ of a simple acid: the $\mathrm{p}K_{\mathrm{m}}$ varies with α, similar to the case in polyelectrolytes.[145] Maeda recently related the $\mathrm{p}K_{\mathrm{m}}$ to the excess free energy of interaction per surfactant molecule in a micelle, g_{ex}.[67] Although Maeda presents his results in a slightly different form, the fundamental result of his analysis can be conveniently expressed as follows:

$$\mathrm{p}K_{\mathrm{m}}(\alpha = 0) - \mathrm{p}K_{\mathrm{m}}(\alpha) = \frac{\log e}{k_{\mathrm{B}}T}\left(\frac{\partial g_{\mathrm{ex}}}{\partial \alpha}\right) \tag{3.19}$$

At many salt concentrations and pH values, the $\mathrm{p}K_{\mathrm{m}}$ of alkyldimethylamine oxides varies linearly with α, which suggests that there is a simple relation between the two. In fact, Maeda recently related the slope of a plot of $\mathrm{p}K_{\mathrm{m}}$ versus α to the interaction parameter β_{RST}.[67] This linearity is consistent with eq 3.19 and with the quadratic dependence of g_{ex} on α in the context of RST.

If g_{ex} is dominated by electrostatic interactions, then the variation of the $\mathrm{p}K_{\mathrm{m}}$

with α can be related to the electrostatic potential at the surface of the micelle, ψ_0, using the following equation:[67]

$$\mathrm{p}K_\mathrm{m} = \mathrm{p}K_\mathrm{m}^0 + (\log e)\,\frac{e_0\psi_0}{k_\mathrm{B}T} \tag{3.20}$$

where $\mathrm{p}K_\mathrm{m}^0$ is the $\mathrm{p}K_\mathrm{m}$ of a neutral micelle (at $\psi_0 = 0$) and e_0 is the charge of a proton. In the case of micelles composed of alkyldimethylamine oxide surfactants, $\mathrm{p}K_\mathrm{m}^0$ corresponds to the $\mathrm{p}K_\mathrm{m}$ of the dipolar micelles (at $\alpha = 0$). According to an analysis by Mille,[64] the experimentally observed difference between $\mathrm{p}K_\mathrm{m}^0$ and $\mathrm{p}K_1$ (the $\mathrm{p}K_\mathrm{a}$ of a surfactant monomer) cannot be explained solely using electrostatic considerations. Therefore, Maeda proposed that this difference is due to the formation of hydrogen bonds at the micelle interface (see section 3.4.1).[51] Hydrogen bonding interactions were also discussed earlier by Imae and Ikeda to explain the phase separation behavior of oleyldimethylamine oxide.[146] Alternatively, we will show that our electrostatic model can lead to a difference between $\mathrm{p}K_\mathrm{m}^0$ and $\mathrm{p}K_1$ without the need of invoking the existence of hydrogen bonds.

The molecular-thermodynamic approach presented here offers another way to understand how the $\mathrm{p}K_\mathrm{m}$ depends on the micelle composition. Although we can relate the $\mathrm{p}K_\mathrm{m}$ to g_mic by relating it to g_ex and then using eq 3.19, we present below an alternate derivation of the relationship between the $\mathrm{p}K_\mathrm{m}$ and g_mic. First, the explicit dependence of the $\mathrm{p}K_\mathrm{m}$ on pH is removed by substituting eq 3.5 in eq 3.18. This yields

$$\Delta\mathrm{p}K = \mathrm{p}K_\mathrm{m} - \mathrm{p}K_1 = \log\frac{\alpha}{1-\alpha} - \log\frac{\alpha_1}{1-\alpha_1} \tag{3.21}$$

The logarithmic terms in eq 3.21 may then be related to g_m (which is related to g_mic, see eq 3.4) by utilizing the fact that α is determined by minimizing g_m (see section 3.3), which implies that

$$\left.\frac{\partial g_\mathrm{m}}{\partial\alpha}\right|_{\alpha^*} = 0 \tag{3.22}$$

Using the definitions of g_m and g_mic (eqs 3.4 and 3.12, respectively), eq 3.22 can be

simplified as follows (see Appendix C):

$$\frac{1}{k_{\mathrm{B}}T}\frac{\partial}{\partial\alpha}\left[g_{\mathrm{mic}}-g_{\mathrm{ent}}\right]\Big|_{\alpha^*}+\ln\frac{\alpha^*}{1-\alpha^*}-\ln\frac{\alpha_1}{1-\alpha_1}=0 \tag{3.23}$$

Substituting eq 3.23 in eq 3.21 then yields the following fundamental relationship between the $\Delta\mathrm{p}K$ and g_{mic}:

$$\Delta\mathrm{p}K=-\frac{\log e}{k_{\mathrm{B}}T}\left(\frac{\partial}{\partial\alpha}\left[g_{\mathrm{mic}}-g_{\mathrm{ent}}\right]\Big|_{\alpha^*}\right) \tag{3.24}$$

For alkyldimethylamine oxide surfactants, we can further simplify eq 3.24 by recognizing that we model the protonated and the deprotonated forms of the surfactant as having the same tails and the same head areas (see sections 3.2.2 and 3.4.1). Therefore, as discussed in Appendix B, g_{tr}, g_{int}, g_{pack}, and g_{st} are independent of α (see eqs B.2, B.4, B.6, and B.8, respectively), and the only term in $(g_{\mathrm{mic}}-g_{\mathrm{ent}})$ that depends explicitly on α is g_{elec} (see eqs B.10-B.18). For alkyldimethylamine oxide surfactants, eq 3.24 then simplifies to

$$\Delta\mathrm{p}K=-\frac{\log e}{k_{\mathrm{B}}T}\left(\left.\frac{\partial g_{\mathrm{elec}}}{\partial\alpha}\right|_{\alpha^*}\right) \tag{3.25}$$

which indicates that the $\Delta\mathrm{p}K$ of alkyldimethylamine oxides depends only on the change of g_{elec} with α (evaluated at the optimal micelle composition, α^*). The main difference between eq 3.25 and Maeda's result[67] (eq 3.19) is that, in eq 3.25, the $\mathrm{p}K_{\mathrm{m}}$ is calculated relative to the $\mathrm{p}K_1$, while in (eq 3.19), it is calculated relative to the $\mathrm{p}K_{\mathrm{m}}(\alpha=0)$. This difference arises from the choice of the reference state in the thermodynamic model.

Note that although in eq 3.25 the $\Delta\mathrm{p}K$ depends explicitly only on g_{elec} and on α, the other contributions to g_{mic} (see eq 3.12) and the other micelle characteristics (the shape factor S, the core minor radius l_{c}, and the degree of counterion binding $\hat{\beta}_{\mathrm{C}}$) all play an indirect role. Indeed, this indirect dependence follows because eq 3.22 is evaluated at $\left\{\alpha^*,\hat{\beta}^*_{\mathrm{C}},l^*_{\mathrm{c}},S^*\right\}$, which are the optimal values that fully minimize g_{m}.

3.4. Results and Discussion

3.4.1. Selection of Model System

To test the validity and range of applicability of the molecular-thermodynamic theory presented in section 3.2, several of the micellization properties discussed in section 3.3 will be predicted and compared with the available experimental data for several alkyldimethylamine oxide surfactants. These surfactants were selected because: (1) they are soluble in water at all pH conditions, (2) they exhibit interesting pH-dependent behavior, and (3) they have been studied extensively in the literature. Solubility in water at all pH conditions allows us to test our micellization theory over the entire range of surfactant compositions, from the completely protonated limit to the completely deprotonated limit. Alkyldimethylamine oxide surfactants also exhibit self-synergy, with many micellization properties displaying a minimum, or a maximum, value at a micelle composition near 0.5.[51] This synergy has been attributed to the formation of hydrogen bonds between the surfactant molecules at the micelle interface, with the protonated surfactant molecules serving as hydrogen bond donors, and both the protonated and the deprotonated surfactant molecules serving as hydrogen bond acceptors.[51]

In order to incorporate hydrogen bonding into the molecular-thermodynamic theory, one must estimate the number of hydrogen bonds and the free-energy change associated with hydrogen bond formation. In general, this free-energy change is a function of both the solution conditions and the micelle structure. Monte Carlo simulations suggest that multiple surfactant molecules may be chained together by hydrogen bonds.[147] Such chains of hydrogen-bonded surfactant molecules may behave effectively like a multi-tailed surfactant, which could alter many of the contributions to the free energy of micellization. Because of these complexities, we have not yet incorporated hydrogen bonding into our theoretical description of micellization. If the free-energy change associated with hydrogen bonds is significant, we anticipate that our theory may underestimate the degree of synergy in solutions of alkyldimethylamine oxide surfactants. Nevertheless, significant synergy may still

Table 3.1: Molecular parameters of C_iDAOH^+ and C_iDAO, where n_t, a_h, l_h, d_z, d_{sep}, z, z_C, and r_C are defined in section 3.2.2.

Surfactant	n_t	a_h [Å^2]	l_h [Å]	d_z [Å]	d_{sep} [Å]	z	z_C	r_C [Å]
C_iDAOH^+	$i-1$	30.0	4.5	2.6	-	+1	–1	2.13
C_iDAO	$i-1$	30.0	4.5	2.6	1.33	-	-	-

arise from the electrostatic interactions that operate between the ionic (protonated) and the dipolar (deprotonated) forms of the surfactant molecules.

Alkyldimethylamine oxides exist as cationic surfactants at low pH (in the protonated state) and as dipolar surfactants at high pH (in the deprotonated state). The dipolar character of a typical zwitterionic surfactant arises from two oppositely charged groups separated by a spacer. On the other hand, the dipolar character of alkyldimethylamine oxides arises from the positive character of the nitrogen atom and the negative character of the oxygen atom, which are bonded directly to each other. Nevertheless, we have chosen to model the dimethylamine oxide head as a zwitterion. This selection is also consistent with the observed behavior of the cmc of the dipolar form of the surfactant, which is comparable to the cmc's of other zwitterionic surfactants of similar tail lengths.[2] The required molecular parameters (as described in section 3.2.2) of the alkyldimethylamine oxide surfactants considered in this chapter are summarized in Table 3.1, where C_iDAOH^+ and C_iDAO refer to the protonated (cationic) and the deprotonated (dipolar or zwitterionic) forms of the surfactant, respectively, and i refers to the number of carbon atoms in the surfactant tail. The molecular structure of the protonated and the deprotonated states of the C_iDAO molecules differ only by a hydrogen ion, and the protonation state does not significantly alter the conformation of the molecule. Consequently, we have modeled both the protonated and the deprotonated forms of the C_iDAO surfactants as having identical molecular parameters, except for the presence or the absence of a positively charged group. As discussed in Chapter 2 and ref 138, we identify the methylene group closest to the dimethylamine oxide group as being part of the hydrophilic head. As

a result, the number of hydrophobic carbon atoms in the surfactant tail of a C_iDAO (or C_iDAOH^+) surfactant is $n_t = i - 1$ (see Table 3.1).

3.4.2. Prediction of the Critical Micelle Concentration

We begin by predicting the cmc's of alkyldimethylamine oxides of various tail lengths as a function of the salt concentration and of the micelle composition, which can also be related to the solution pH. In Figure 3-1, the predicted cmc's (solid lines) of three alkyldimethylamine oxide surfactants are compared with the experimental values (circles) as a function of the micelle composition, α, where figures (a), (b), and (c) correspond to $C_{10}DAO$, $C_{12}DAO$, and $C_{14}DAO$, respectively. The corresponding experimental cmc data were obtained from refs 148, 149, and 150, respectively. The uncertainty in the experimental cmc data for $C_{10}DAO$ was reported to be 0.2 mmol/kg,[148] and experimental uncertainties were not reported for the other two surfactants. Each solution contains 0.1 M NaCl and is at 25°C. Note that the limit $\alpha = 0$ corresponds to the deprotonated, dipolar form of the surfactant, and is typically attained at a solution pH near 10. Conversely, the limit $\alpha = 1$ corresponds to the protonated, cationic form of the surfactant, and is typically attained at a solution pH near 2.

The theory is able to reproduce several of the experimental cmc features. First, the predicted cmc's of $C_{10}DAO$ and $C_{12}DAO$ are all within a factor of three of the experimental cmc values, and the predicted cmc's of $C_{14}DAO$ are within a factor of five of the experimental cmc values. In view of the different cmc values that are obtained using different experimental techniques, as well as using different analyses of the same experimental data,[151] the observed agreement between theory and experiment appears quite reasonable. Another key observation is that both the predicted and the experimental cmc's, for a particular tail length, are of the same order of magnitude throughout the entire range of composition values. Although deprotonated alkyldimethylamine oxides are sometimes referred to as nonionic surfactants, their cmc's are much higher than those of true nonionic surfactants having similar tails. Instead, as indicated in section 3.4.1, deprotonated alkyldimethylamine oxides behave

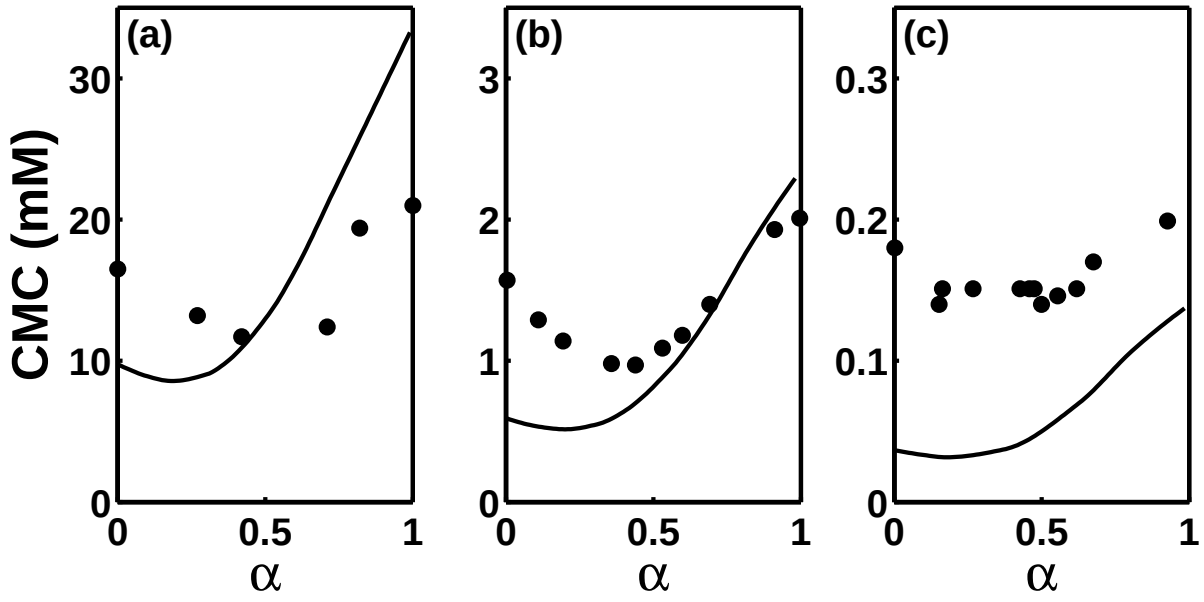

Figure 3-1: Comparison between the predicted (solid lines) and the experimental (circles) cmc's of C_iDAO (i = 10, 12, and 14) in 0.1 M NaCl at 25°C, as a function of the micelle composition, α. The experimental cmc data were taken from refs 148, 149, and 150 for $C_{10}DAO$, $C_{12}DAO$, and $C_{14}DAO$, respectively.

like zwitterionic surfactants. In particular, the cmc of an alkyldimethylamine oxide is larger than that of a nonionic surfactant with the same tail, due to the electrostatic penalty associated with assembling the strongly dipolar dimethylamine oxide heads at the micelle interface, an effect that we capture in g_{elec}.

For the three tail lengths examined, the predicted cmc of the dipolar surfactant (at $\alpha = 0$) is always lower than the experimental cmc. This discrepancy may result from an underestimation of the electrostatic penalty in this limit, as modeled in g_{elec}. In particular, decreasing the estimated value of the dielectric constant in the micelle head-shell region would result in an increase in the predicted cmc of the dipolar form of the surfactant. Although not implemented here, such a modification to the g_{elec} model may be justified if we have underestimated the effect of dielectric saturation due to the polarization of the water molecules around the strongly polar surfactant heads.[106]

Perhaps more importantly, the predicted cmc of both the cationic and the dipolar forms of the surfactant decrease more rapidly with tail length than do the experimental cmc values. For example, as the surfactant tail length increases by two carbon atoms, the experimental cmc's decrease by a factor of approximately 10, while the predicted cmc's decrease by a factor of approximately 15. The predicted cmc is determined primarily by g_{tr}, which decreases by approximately 1.5 $k_{\mathrm{B}}T$ for each additional methylene group in the surfactant tail.[41] However, this model of g_{tr} is derived from solubility data for linear alkanes, and it may slightly overestimate the contribution of a methylene group in a surfactant tail. Although this discrepancy is small, it appears to be systematic, and can be observed in previous cmc predictions for both hydrocarbon-based (see Figure 4 in ref 38) and fluorocarbon-based (see Figure 9 in ref 152) surfactants .

Perhaps the most notable feature observed in the cmc vs. α behavior is the existence of a minimum in the cmc at an intermediate composition for each surfactant. Experimentally, the minimum is located at a micelle composition of approximately 0.5, while the predicted minimum is more shallow and occurs at a micelle composition of approximately 0.2. The predicted minimum occurs because of a minimum in

g_{elec} that results from the balance between the capacitor-like contribution associated with the dipolar surfactant heads and the charging contribution associated with the cationic surfactant heads (see eq B.15). We anticipate that the predicted location of the cmc minimum may be improved by incorporating hydrogen bonding into the theory, if an appropriate model for such a complex directional interaction can be developed (see section 3.4.1).

3.4.3. Prediction of Critical Micelle Concentrations without Added Salt: A Comparison with Regular Solution Theory

As discussed in section 3.1, regular solution theory (RST) is widely used to model the micellization of binary surfactant mixtures.[35] RST is essentially a one-parameter empirical model of binary surfactant micellization. In practice, the implementation of RST in the case of binary surfactant mixtures requires knowledge of three or more experimental cmc values: the cmc's of each of the two surfactant species, and the cmc of at least one of their mixtures. Nonlinear regression can then be used to obtain the value of the RST interaction parameter, β_{RST}, that best describes the experimental cmc data. Although RST has found wide applicability in a variety of surfactant systems,[35] it does not adequately describe strongly interacting surfactant mixtures.[153–156] Maeda has developed a theory for nonionic-ionic mixed micelles which is mathematically equivalent to RST.[137] However, his analysis extracts an additional quantity that accounts for the insertion of an ionic surfactant into a nonionic micelle.[137] In the case of pH-sensitive surfactants, the molecular-thermodynamic approach has advantages over RST, as illustrated below.

The cmc of C_{12}DAO as a function of micelle composition, α, displays surprisingly complex behavior when there is no added salt, as shown in Figure 3-2. The experimental cmc's are shown as circles and were measured by Imaishi et al., with the reported experimental uncertainty varying from 0.01 to 0.20 mM.[157] The molecular-thermodynamic predictions correspond to the solid line. The best-fit results

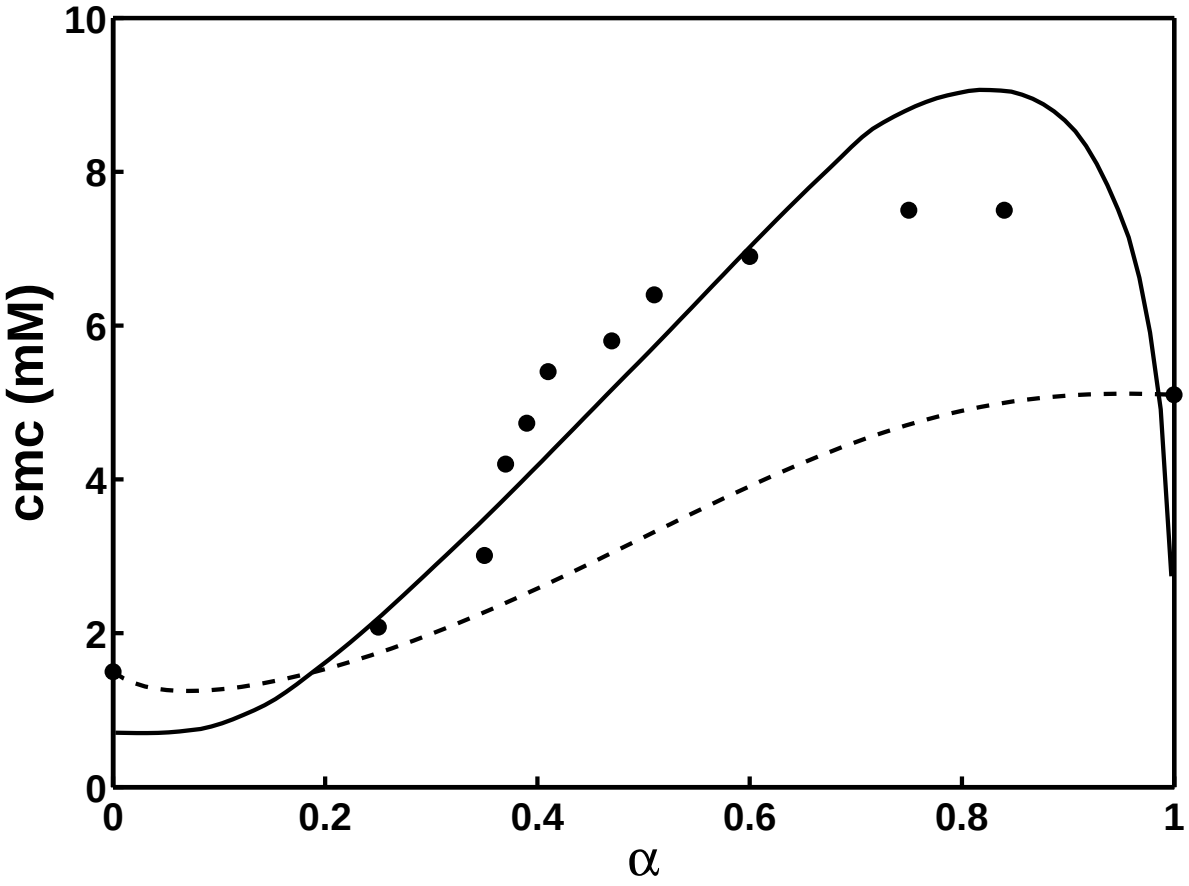

Figure 3-2: Comparison between the predicted (solid line) and the experimental (circles) cmc's of C_{12}DAO at 25°C, without added salt, as a function of the micelle composition, α. The experimental cmc's were measured by Imaishi et al.[157] The dashed line shows the results of a nonlinear regression of the experimental cmc data using regular solution theory (RST).

of RST correspond to the dashed line. Note that the experimental cmc's increase between $\alpha \approx 0.2$ and $\alpha \approx 0.8$, followed by a sharp decrease between $\alpha \approx 0.8$ and $\alpha = 1$. The predictions of the molecular-thermodynamic theory reproduce this experimental behavior in both a qualitative and a quantitative manner. However, RST fails to capture the maximum in the cmc that is observed at $\alpha \approx 0.8$. The origin of the observed experimental cmc behavior, and the reason for the failure of RST, can be understood by examining the behavior of g_{elec} as a function of α. At intermediate micelle compositions, g_{elec} increases sharply with α because the charging contribution associated with the cationic form of C_{12}DAO is much larger than the capacitor contribution associated with the dipolar form of C_{12}DAO (see eq B.15). However, g_{elec} of a charged micelle is also very sensitive to the ionic strength of the solution, as reflected in the inverse Debye-Hückel screening length, κ (see eq B.18 and the discussion that follows it). Larger values of α correspond to the addition of greater amounts of acid to the solution. As α approaches 1, the ionic strength of the solution steadily increases due to the addition of this acid. The increase in ionic strength leads to a net decrease in g_{elec} as α increases from 0.8 to 1. Furthermore, RST fails to capture the experimental cmc behavior because the dependence of g_{elec} on α is not well approximated by the quadratic functional form that is obtained when using a single, constant β_{RST} parameter.

3.4.4. Prediction of Micelle Sizes

An additional advantage of the molecular-thermodynamic approach is its ability to predict micelle shapes and sizes. To validate this predictive capability, we compared predicted and experimental weight-average micelle aggregation numbers, $\langle n \rangle_{\text{w}}$, as a function of α for C_{12}DAO in a 0.1 M NaCl aqueous solution (Figure 3-3) and in a 0.2 M NaCl aqueous solution (Figure 3-4), both at 25°C.

The experimental $\langle n \rangle_{\text{w}}$ values (circles) were measured by Kaimoto et al. using light scattering (for $0 < \alpha < 1$) and fluorescence (at $\alpha = 0$ and $\alpha = 1$), with a reported experimental uncertainty of 10%.[158] The light scattering measurements and predictions were carried out at a surfactant concentration of approximately 14 mM.

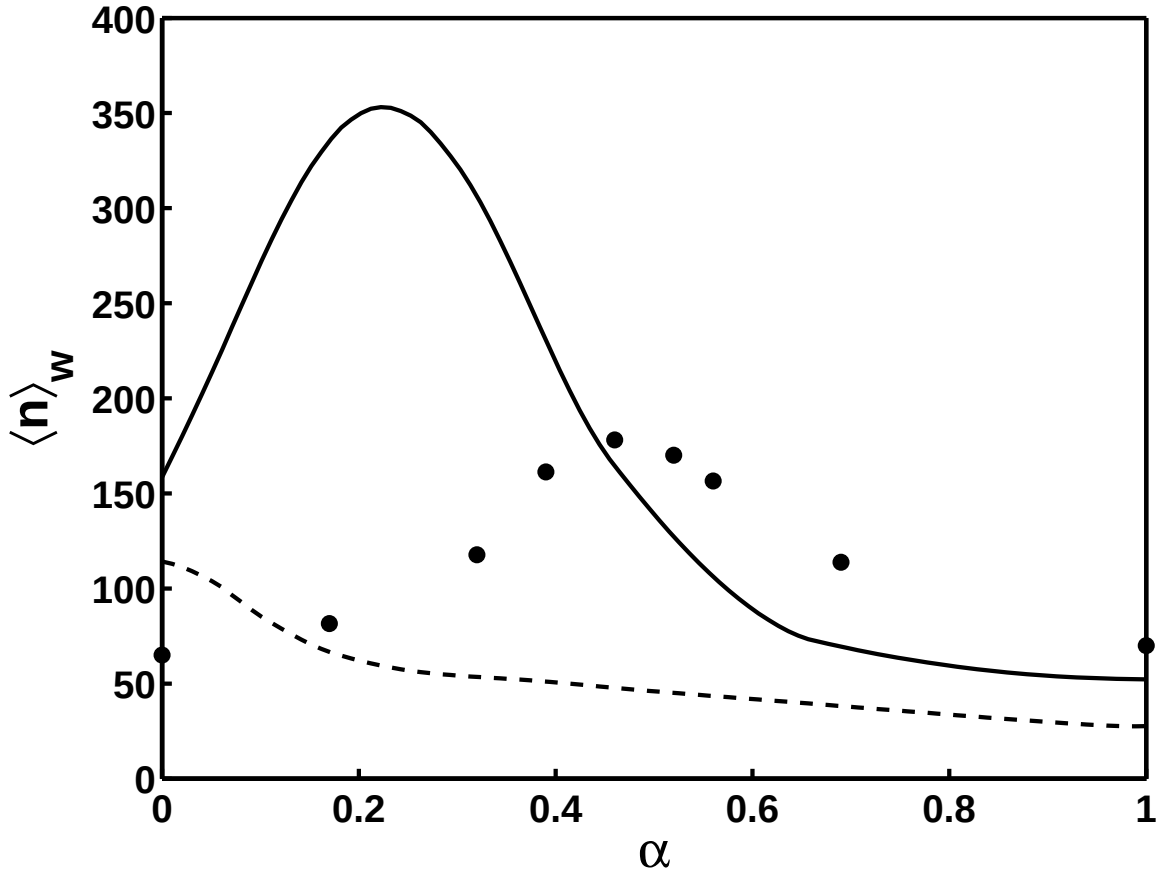

Figure 3-3: Comparison between the predicted (lines) and the experimental (circles) weight-average micelle aggregation number, $\langle n \rangle_{\mathrm{w}}$, of a micellar solution containing $\sim$14 mM C_{12}DAO and 0.1 M NaCl at 25°C as a function of the micelle composition, α. Theoretical predictions that account for counterion binding correspond to the solid line, and theoretical predictions that do not account for counterion binding correspond to the dashed line. The experimental $\langle n \rangle_{\mathrm{w}}$'s were measured by Kaimoto et al.[158]

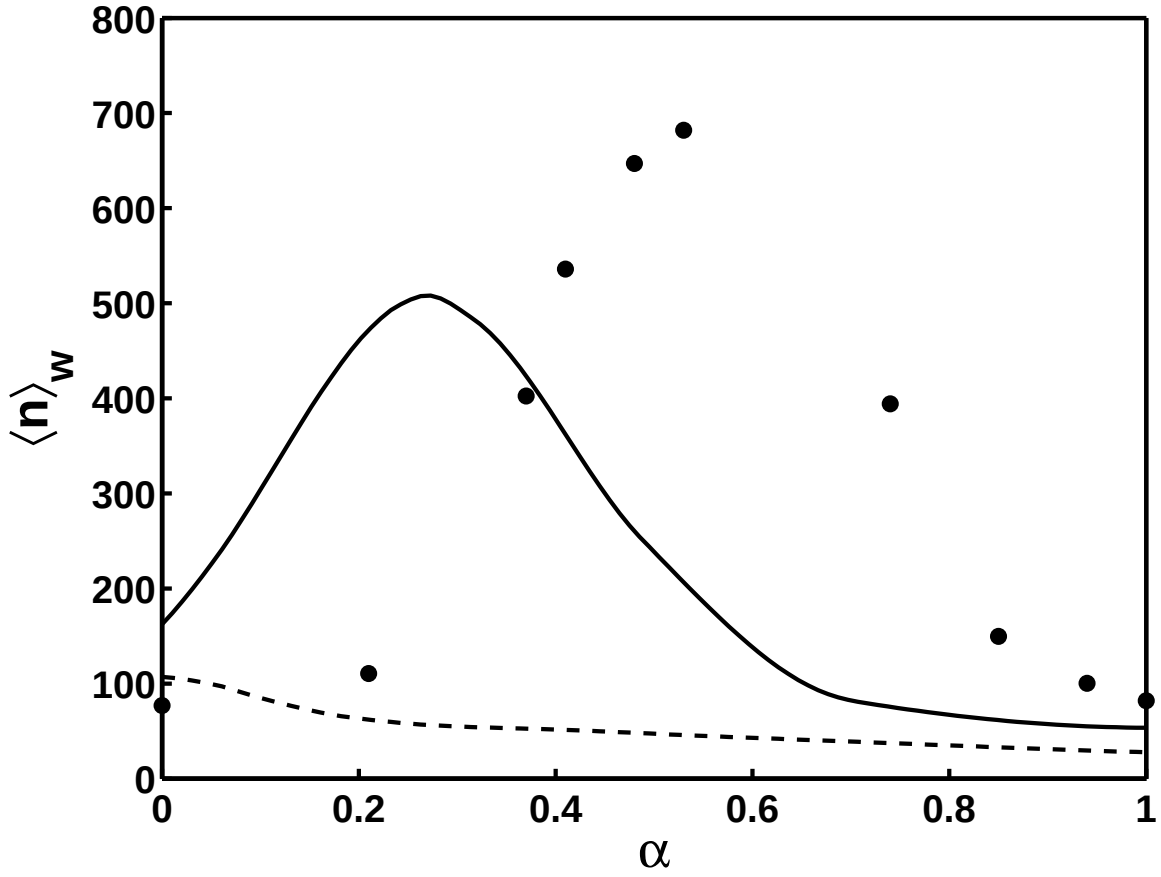

Figure 3-4: Comparison between the predicted (lines) and the experimental (circles) weight-average micelle aggregation number, $\langle n \rangle_{\mathrm{w}}$, of a micellar solution containing $\sim$14 mM C_{12}DAO and 0.2 M NaCl at 25°C as a function of the micelle composition, α. Theoretical predictions that account for counterion binding correspond to the solid line, and theoretical predictions that do not account for counterion binding correspond to the dashed line. The experimental $\langle n \rangle_{\mathrm{w}}$'s were measured by Kaimoto et al.[158]

The fluorescence measurements were carried out at the cmc. Note, however, that the aggregation numbers at the cmc should be nearly identical to those obtained at a surfactant concentration of 14 mM, since the micelle size was found to be quite insensitive to the surfactant concentration at $\alpha = 0$ and at $\alpha = 1$. The solid lines correspond to the predictions made using the molecular-thermodynamic theory presented in section 3.2. Since counterion binding was found to be important to obtain accurate micelle size predictions for ionic surfactant systems containing multivalent ions,[43] as well as for mixtures of ionic and nonionic surfactants,[138] in Figures 3-3 and 3-4, we also present predictions using the molecular-thermodynamic theory implemented without counterion binding (dashed lines).

The predicted optimal micelle shape is cylindrical at all compositions when counterion binding is accounted for. When $\langle n \rangle_w$ is much greater than the aggregation number of spherical micelles (approximately 50), eq 3.15 holds. Given this exponential dependence of the predicted weight-average micelle aggregation number, $\langle n \rangle_w$, on $\Delta\mu$, we consider our $\langle n \rangle_w$ predictions with counterion binding accounted for (the solid lines in Figures 3-3 and 3-4) to be in reasonable quantitative agreement with the experimental $\langle n \rangle_w$ values. Perhaps more importantly, both the experimental $\langle n \rangle_w$ data and the theoretical $\langle n \rangle_w$ predictions with counterion binding accounted for (the solid lines in Figures 3-3 and 3-4) show two important qualitative characteristics: (1) at $\alpha \approx 0$ and at $\alpha \approx 1$, the $\langle n \rangle_w$ values depend weakly on salt concentration, and (2) at an intermediate α value, $\langle n \rangle_w$ reaches a maximum, whose value increases with increasing salt concentration. On the other hand, the $\langle n \rangle_w$ predictions without counterion binding accounted for (the dashed lines in Figures 3-3 and 3-4) are practically independent of salt concentration, and $\langle n \rangle_w$ decreases monotonically as α increases. These results suggest that electrostatic effects do play a key role in correctly capturing the qualitative behavior of micelle growth in the C_{12}DAO system. Recall that micelle growth depends on the difference in g_m for spherical and cylindrical micelles, as captured in $\Delta\mu$ (see eqs 3.13 and 3.15). In the theory implemented without counterion binding, $\Delta\mu$ decreases monotonically with α, which yields the predicted monotonic decrease in $\langle n \rangle_w$ with increasing α (the dashed lines

in Figures 3-3 and 3-4). When counterion binding is included in the theory, $\Delta\mu$ initially increases at low α but then begins to decrease at $\alpha > 0.25$. Essentially, counterion binding preferentially decreases g_{m} for cylindrical micelles relative to spherical micelles. On the other hand, once $\alpha \gtrsim 0.25$, the electrostatic benefits associated with counterion binding for cylindrical micelles (relative to spherical micelles) become less pronounced, leading to a predicted maximum in $\langle n \rangle_{\mathrm{w}}$ at $\alpha \approx 0.25$, as shown in Figures 3-3 and 3-4.

Maeda has suggested that the experimentally observed maximum in $\langle n \rangle_{\mathrm{w}}$ at $\alpha \approx 0.5$ may be due to the formation of hydrogen bonds between protonated-deprotonated and protonated-protonated surfactant pairs at the micelle interface.[51] However, our theory suggests an electrostatic explanation: The theory clearly predicts a maximum value of $\langle n \rangle_{\mathrm{w}}$ due to the behavior of g_{elec}, where the location of this maximum could shift closer to $\alpha = 0.5$ if g_{elec} were further increased in the case of dipolar surfactants. For example, if the dielectric constant in the head-shell region of the micelle is decreased, then the location of the maximum in $\langle n \rangle_{\mathrm{w}}$ would shift to higher α values. Such a change would also serve to: (1) decrease the aggregation numbers at $\alpha \approx 0$, which are currently overestimated by the theory (see Figures 3-3 and 3-4), and (2) increase the cmc at $\alpha \approx 0$, which is currently underestimated by the theory (see Figure 3-1). However, the aggregation numbers in the presence of 0.2 M added NaCl would then be underestimated to an even greater extent than is observed in Figure 3-4.

Aggregation number predictions may also be improved by developing a more refined model for finite cylindrical micelles. Experimental evidence suggests that spherical micelles of C_iDAO surfactants coexist with cylindrical micelles of C_iDAO surfactants.[159,160] Although the current model can predict the coexistence of spherical and cylindrical micelles, it also predicts the formation of intermediate sized micelles that are not observed in the experimental micelle size distribution. More refined models for micelle shapes[83,118–120] utilize an additional free-energy penalty associated with the junction that connects the hemispherical endcaps to the cylindrical body of a rod-like micelle. An empirical correction for this phenomenon could readily be

incorporated into the theory, if better quantitative agreement is desired and if the relevant data are available for estimating the necessary input parameters.

3.4.5. Prediction of the Titration Behavior

3.4.5.1. Prediction of the Salt Dependence of the ΔpK

In Figure 3-5, we first consider how the ΔpK varies with the concentration of added NaCl for solutions of 50 mM C_{12}DAO at 24°C. The experimental titration data were measured by Zhang et al.[161] The predicted ΔpK values as a function of α correspond to the various lines in Figure 3-5(a). The experimental ΔpK values correspond to the various symbols in Figure 3-5(b), where the various lines are shown to guide the eye. (Note that the predicted and the experimental values are plotted separately for visual clarity.)

Although the predicted ΔpK values are consistently lower than the experimental values (by 0.5 to 1 unit), the curves are qualitatively similar. At the two highest salt concentrations examined (1 M and 0.2 M), both the predicted and the experimental ΔpK values decrease approximately linearly with α. According to eq 3.25, this trend implies that $\partial g_{\text{elec}}/\partial\alpha$ is approximately linear in α, and therefore, that g_{elec} has a nearly quadratic dependence on α. However, at the lowest salt concentrations (0.04 M and 0.01 M), the ΔpK values deviate more from linearity. In particular, at low α values, the ΔpK varies more rapidly, and at high α, the ΔpK values begin to plateau. Furthermore, at 0.01 M NaCl, the ΔpK is predicted to increase with α for $\alpha > 0.9$. This effect can be understood by examining how the ionic strength depends on α: At low α values (that is, when the surfactant is predominantly in its dipolar state), the concentration of added acid is small, and the ionic strength is determined primarily by the concentration of added salt. At high α values (that is, when the surfactant is predominantly in its ionic form), the concentration of added acid becomes comparable to, or greater than, the concentration of added salt, leading to a significant increase in the ionic strength. Increasing the surfactant (and the micelle) charge tends to increase g_{elec} and $\partial g_{\text{elec}}/\partial\alpha$, while increasing the ionic strength tends to decrease g_{elec}

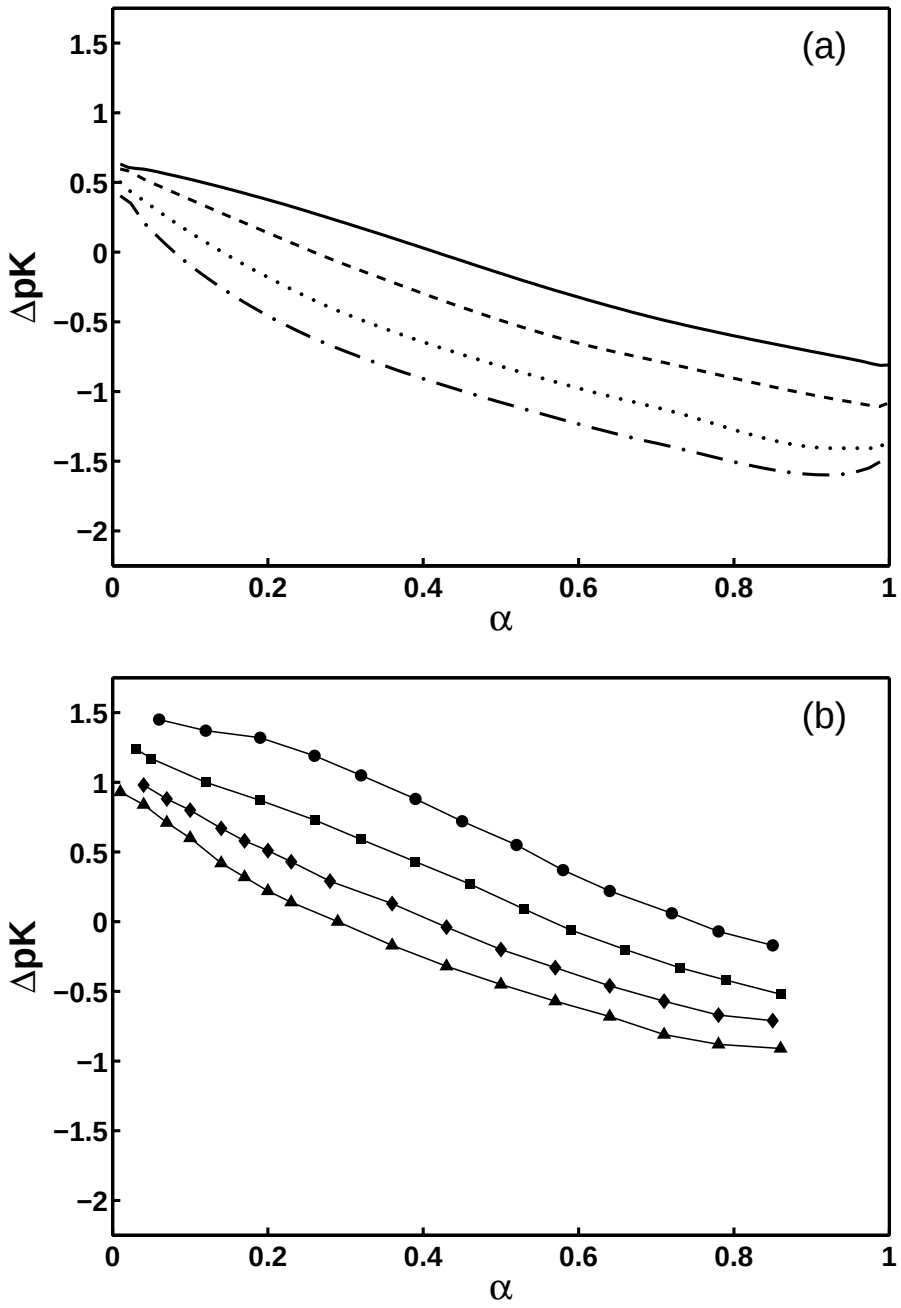

Figure 3-5: Comparison between the predicted and the experimental ΔpK's of 50 mM C_{12}DAO solutions at NaCl concentrations of 1.0 M, 0.2 M, 0.04 M, and 0.01 M at 24°C as a function of the micelle composition, α. The experimental titration data were measured by Zhang et al.[161] The predicted ΔpK's as a function of α correspond to the various lines in Figure 3-5(a). The experimental data correspond to the various symbols in Figure 3-5(b), where the various lines are shown to guide the eye. The concentrations of NaCl examined are 1.0 M (solid line and circles), 0.2 M (dashed line and squares), 0.04 M (dotted line and diamonds), and 0.01 M (dash-dotted line and triangles).

and $\partial g_{\text{elec}}/\partial\alpha$. The net result is a nonlinear variation of $\partial g_{\text{elec}}/\partial\alpha$ and $\Delta\text{p}K$ (see eq 3.25) with α at low salt concentrations.

Furthermore, as Figures 3-5(a) and 3-5(b) reveal, higher salt concentrations yield higher $\Delta\text{p}K$ values at any value of α. This trend results because increasing the salt concentration provides additional electrostatic screening, thus reducing g_{elec} and $\partial g_{\text{elec}}/\partial\alpha$. Equation 3.25 indicates that a decrease in $\partial g_{\text{elec}}/\partial\alpha$ leads to an increase in the $\Delta\text{p}K$.

Interestingly, at low α values, both the predicted and the experimental $\Delta\text{p}K$ values can be positive, indicating a composition range in which $\text{p}K_{\text{m}} > \text{p}K_1$. Other researchers have suggested that $\text{p}K_{\text{m}}|_{\alpha=0}$ can only be greater than $\text{p}K_1$ if there are non-electrostatic interactions.[51,64] In fact, Maeda has tentatively used $\Delta\text{p}K|_{\alpha=0}$ as an estimate of the free energy associated with hydrogen bond formation. However, our results indicate that at least part of this difference is associated with g_{elec}.

According to eq 3.25, $\Delta\text{p}K > 0$ implies that $\partial g_{\text{elec}}/\partial\alpha$ is negative. Therefore, our model leads to $\Delta\text{p}K|_{\alpha=0} > 0$ because $\partial g_{\text{elec}}/\partial\alpha|_{\alpha=0} < 0$, which implies that g_{elec} actually *decreases* as α increases when $\alpha \approx 0$. Therefore, our results show that electrostatic interactions, as embodied in g_{elec}, can in fact result in $\Delta\text{p}K|_{\alpha=0} > 0$. Nevertheless, it is important to recognize that non-electrostatic interactions play an indirect role, because the various contributions to g_{elec} are evaluated at the optimal micelle conditions, $\left\{\alpha^*, \hat{\beta}_{\text{C}}^*, l_{\text{c}}^*, S^*\right\}$, which are determined by fully minimizing g_{m} (see section 3.3).

Moreover, $\Delta\text{p}K = 0$ (or, equivalently, $\text{p}K_{\text{m}} = \text{p}K_1$) implies that $\partial g_{\text{elec}}/\partial\alpha = 0$ (see eq 3.25), which occurs when g_{elec} is minimized with respect to α. Experimentally, the values of α at which $\Delta\text{p}K = 0$ increase from approximately 0.25 to 0.75 as the salt concentration increases from 0.04 M to 1 M (see Figure 3-5(b)). The predicted values of α at which $\Delta\text{p}K = 0$, which increase from approximately 0.1 to 0.4 as the salt concentration increases from 0.04 M to 1 M (see Figure 3-5(a)), are smaller than the respective experimental values. This discrepancy may arise if our model underestimates g_{elec} for dipolar micelles (formed at the low α values), which would lead to $\partial g_{\text{elec}}/\partial\alpha$ being insufficiently negative at low α values. In addition, the predicted

results could be improved by incorporating hydrogen bonding into the theory, if an appropriate model for such a complex directional interaction can be developed (see section 3.4.1).

3.4.5.2. Prediction of the Effect of the Surfactant Tail Length on the ΔpK

The ΔpK of alkyldimethylamine oxide surfactants is known to vary with surfactant tail length.[51] In section 3.4.5.1, we also observed greater nonlinearity in the variation of ΔpK at lower salt concentrations. To examine both of these effects more fully, in Figure 3-6, we consider how the ΔpK varies with surfactant tail length in solutions without added salt.

The predicted (various lines) and the experimental (various symbols) ΔpK values as a function of α are shown in Figures 3-6(a) and 3-6(b), respectively, for solutions of C_iDAO (i = 12, 14, and 16). (Note that the predicted and the experimental values are plotted separately for visual clarity.) The experimental titration data were measured by Imaishi et al. for C_{12}DAO,[157] and by Abe et al. for C_{14}DAO and for C_{16}DAO.[162]

Although the predicted ΔpK values are quantitatively lower than the experimental values, the qualitative behavior is well captured by the theory. Irrespective of tail length, both the predicted and the experimental ΔpK values decrease rapidly with α at low α values and then begin to plateau. At high α values, the ΔpK values actually begin to increase, which is due to an increase in the solution ionic strength (similar to the results for the cmc with no added salt presented in section 3.4.3). At these conditions, g_{elec} changes due to the competition between increasing ionic strength and increasing micelle charge.

The theory also reproduces the qualitative trend that, at intermediate α values ($0.1 \lesssim \alpha \lesssim 0.8$), the shortest tail has the largest ΔpK, but at both $\alpha \approx 0$ and $\alpha \approx 1$, the ΔpK is nearly independent of surfactant tail length. To understand the change in ΔpK with surfactant tail length, we must also consider the effect of the surfactant tail length on g_{elec} and $\partial g_{\text{elec}}/\partial\alpha$. The primary effect is through changes in the ionic strength. Since there is no added salt, the ionic strength is determined

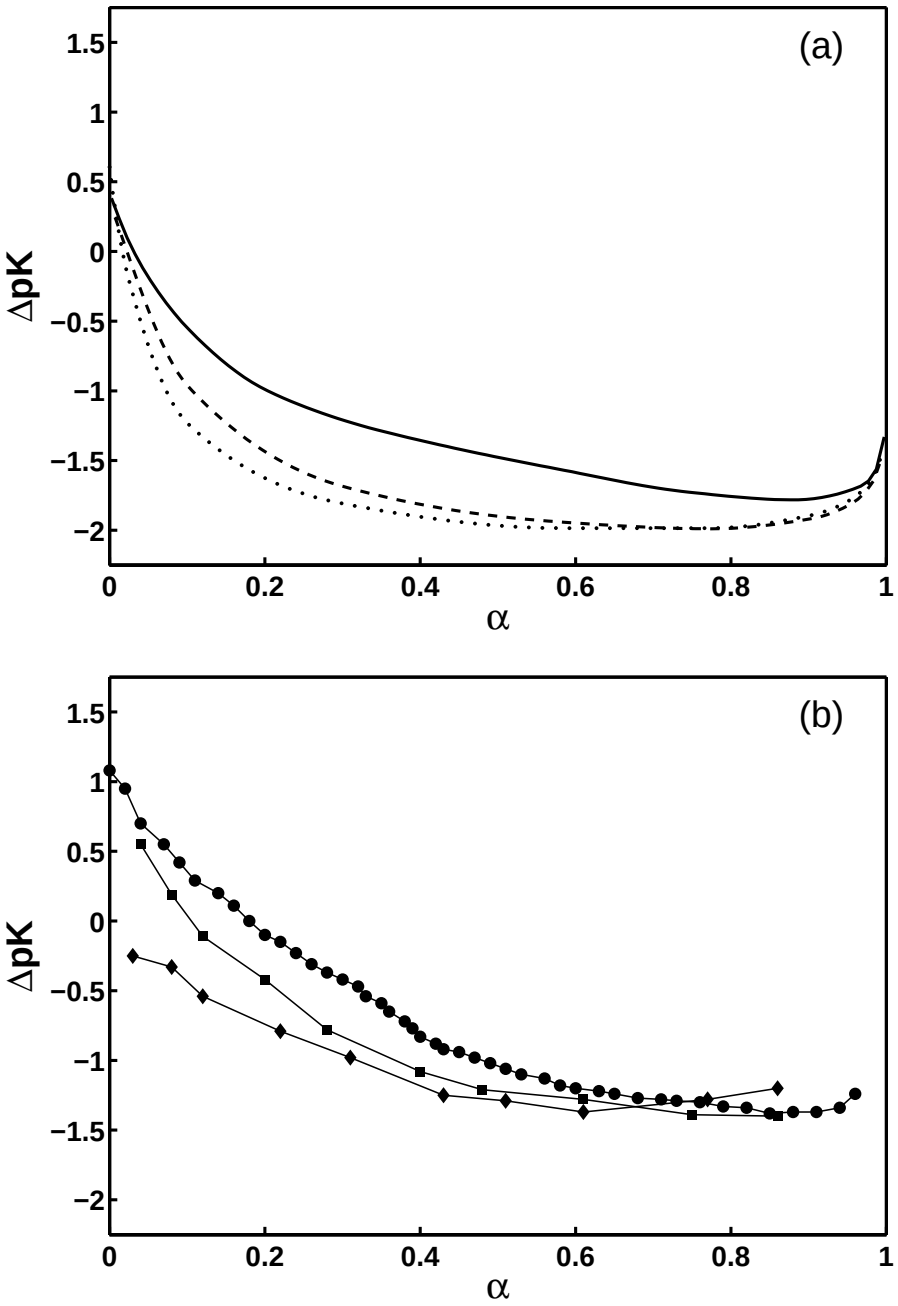

Figure 3-6: Comparison between the predicted and the experimental ΔpK's of solutions of C_iDAO ($i = 12$, 14, and 16), with no added salt, at various temperatures, as a function of the micelle composition, α. The predicted values correspond to the various lines in Figure 3-6(a). The experimental values correspond to the various symbols in Figure 3-6(b), where the various lines are shown to guide the eye. The surfactant concentrations and solution temperatures are 30 mM and 25°C for $C_{12}DAO$ (solid line and circles), 12 mM and 25°C for $C_{14}DAO$ (dashed line and squares), and 11 mM and 45°C for $C_{16}DAO$ (dotted line and diamonds). The experimental titrations were measured by Imaishi et al. for $C_{12}DAO$,[157] and by Abe et al. for $C_{14}DAO$ and for $C_{16}DAO$.[162]

by the surfactant monomers and by any added acid (or base). Since the surfactant monomer concentration is reasonably well approximated by the cmc, the longer the surfactant tail, the lower its monomer concentration and ionic strength will be. The lower ionic strength for the longer tails leads to larger values of g_{elec} and $\partial g_{\text{elec}}/\partial\alpha$, and therefore to smaller values of $\Delta\text{p}K$.

3.5. Conclusions

The theory presented in this chapter represents the first molecular-thermodynamic description of pH-dependent micellization. The theory can be used to predict various useful micellar properties of aqueous solutions of a single pH-sensitive surfactant type, along with any added acid, base, or salt. The theory yielded results that are qualitatively similar to the experimental data for the various solutions of alkyldimethylamine oxide surfactants considered. A very interesting feature of these surfactants is a self-synergy that is manifested as a minimum in the cmc and as a maximum in the average micelle aggregation number. Although hydrogen bonding has been proposed as a component of this synergy, we have demonstrated that electrostatics can also account for much of the observed self-synergy. In addition, we have shown that counterion binding must be included explicitly in the electrostatic description in order to account properly for the observed extrema in the cmc and in the average micelle aggregation number. The predicted cmc and $\langle n\rangle_{\text{w}}$ extrema occur at lower α values than is observed experimentally, perhaps due to an underestimation of g_{elec} for predominantly dipolar micelles (at $\alpha \approx 0$) or due to the neglect of hydrogen-bonding interactions.

The predicted cmc's agree reasonably well with the experimental values. In particular, the cmc behavior of C_{12}DAO with no added salt was accurately modeled by our theory, while regular solution theory provided a very poor description of this system. We also examined micellar titration data through the dependence of the $\Delta\text{p}K$ on α. Furthermore, we demonstrated that in the case of alkyldimethylamine oxide surfactants, the $\Delta\text{p}K$ is related to the derivative

of g_{elec} with respect to α. The predicted $\Delta \text{p}K$ values are consistently smaller than the experimental values, due to an underestimation of synergy. However, our theory correctly predicts the observed experimental trends with both salt concentration and surfactant tail length. One possible approach to better model the synergy of alkyldimethylamine oxide surfactants would be to combine a molecular-thermodynamic theory with a molecular simulation of the specific effect of the directional hydrogen-bonding interactions. To this end, Monte Carlo simulations which incorporate hydrogen bonds have been performed for C_{12}DAO.[147] Furthermore, such a hybrid molecular-thermodynamic/molecular-simulation approach has already been utilized to study the effect of an organic salt (sodium salicylate) on the micellization behavior of a cationic surfactant (cetyltrimethylammonium bromide).[163] Alternatively, improved quantitative predictions could have been obtained by "fitting" the physical inputs of the theory or by adding other empirical corrections. However, this would entail a departure from our molecular approach, and consequently we have not pursued it here.

Next, in Chapter 4, we develop a (*non-molecular*) theory based on regular solution theory that can be used to analyze mixtures of pH-sensitive and conventional surfactants. Following that, in Chapter 5, we lay the theoretical foundation for a *molecular* theory to model these mixtures by first extending the theory developed in Chapter 2 to ternary surfactant mixtures and to mixtures of commercial surfactants. Finally, in Chapter 6, we present a *molecular* theory to model mixtures of both pH-sensitive and conventional surfactants.

Chapter 4

Titration of Mixed Micelles Containing a pH-Sensitive Surfactant and Conventional Surfactants: A Regular Solution Theory Modeling Approach

4.1. Introduction

Hydrogen-ion titration has been used as a method to determine the composition, surface charge, and electrostatic surface potential of surfactant micelles.[47,49,50,70,148,150,164–181] In some cases, the surfactant itself is pH-sensitive, as in the case of alkyldimethylamine oxides.[47,49,50,148,150,164,165,167–169] In other cases, a pH-sensitive probe molecule (such as a fatty acid or a dye) is incorporated into the micelle.[70,170–181] Titration then allows the determination of the average degree of protonation of the pH-sensitive species. When the pH-sensitive species is only present in monomeric form (that is, it is not incorporated into micelles), the average degree of protonation of the monomers (x_1) is governed by the Henderson-Hasselbalch

equation:[51,141]

$$\mathrm{p}K_1 = \mathrm{pH} + \log \frac{x_1}{1 - x_1} \tag{4.1}$$

where $\mathrm{p}K_1$ denotes the equilibrium deprotonation constant of the pH-sensitive species in monomeric form. Note that eq 4.1 assumes that the solution is ideal, or that any nonidealities have been incorporated into the $\mathrm{p}K_1$.

When the pH-sensitive species is incorporated into micelles, the protonation equilibrium is affected by the change in the local environment. The protonation equilibrium can then be characterized by a micellar equilibrium deprotonation parameter ($\mathrm{p}K_\mathrm{m}$), defined analogously:

$$\mathrm{p}K_\mathrm{m} = \mathrm{pH} + \log \frac{x_\mathrm{mic}}{1 - x_\mathrm{mic}} \tag{4.2}$$

where x_mic is the protonated fraction of pH-sensitive species in the micelles.[51] Note that while the $\mathrm{p}K_1$ is a thermodynamic constant, the $\mathrm{p}K_\mathrm{m}$ is generally a function of x_mic, since the micellar environment can change substantially as x_mic changes. Perhaps for this reason, the introduction of the $\mathrm{p}K_\mathrm{m}$ has been criticized as being unnecessary and inappropriate.[49] Although a suitable model for micellization should allow x_mic to be directly related to the solution pH, the $\mathrm{p}K_\mathrm{m}$ is useful as a simple way to understand how the micellar nonidealities affect the protonation of a micellized pH-sensitive species. The $\mathrm{p}K_\mathrm{m}$ may also be a more familiar and practical concept for experimentalists and formulators who are accustomed to thinking about pH equilibrium in terms of deprotonation constants. For example, the $\mathrm{p}K_\mathrm{m}$ of micelles composed of the pH-sensitive surfactant dodecyldimethylamine oxide (C_{12}DAO) varies nearly linearly with x_mic at many solutions conditions,[169] while a plot of x_mic vs. pH is highly nonlinear. This linear behavior is easier to model empirically and suggests that a fundamental connection exists between x_mic and the $\mathrm{p}K_\mathrm{m}$.

The pH-sensitivity of several surfactants and solubilizates have been studied in the literature, including amine oxide surfactants in single surfactant systems[49,50,148,150,164,169] and in mixed surfactant systems,[69,166,182–187] as well as various other surfactants.[47,66,165,167,168] Common pH-sensitive molecules that

are used as solubilizates to probe the micelle local environment include fatty acids,[70,179] fluorescent dyes,[170,171,173–176,178] and drugs.[172,180,181] Because the local micellar environment affects the protonation equilibrium, the pK_{m} of surfactants, fatty acids, or drugs solubilized in micelles depends strongly on the charge characteristics of the surfactant serving as the solubilizer and on the salt concentration.[70,166,171,172,174–176,178,180,181]

Relatively few models have been developed to quantify hydrogen-ion titration in micellar systems.[26,64,67,147] Mille used a lattice theory that includes nearest-neighbor interactions to obtain an analytical expression for the pK_{m}, but found that charge-charge interactions alone were insufficient to capture the observed experimental behavior.[64] da Silva et al. modeled the titration of fatty acids solubilized in cationic, anionic, and nonionic micelles using Monte Carlo simulations and Poisson-Boltzmann calculations of electrostatic effects.[70] Maeda used a general thermodynamic analysis of micellar titration to relate the pK_{m} to the activity coefficients of the protonated and the deprotonated micellized surfactants.[67] If the activity coefficients can be modeled using regular solution theory (RST), Maeda observed that the pK_{m} varies linearly with x_{mic}, with a slope that is proportional to the RST interaction parameter, β. However, Maeda's model does not predict the intercept of the pK_{m} vs. x_{mic} curve. In other words, the model cannot be used to predict x_{mic} (and the micelle surface charge) as a function of pH, unless one or more pK_{m} values are independently known.

Regular solution theory was originally used to model micellization in binary surfactant mixtures,[35] and has also been extended to model multicomponent surfactant mixtures.[37] Although RST has been successfully applied to many mixtures of conventional surfactants,[71] the implications of using RST for the analysis of micellar titration have not been fully explored. With this in mind, in this chapter, we develop a theoretical description based on RST to quantify hydrogen-ion titration of mixed micelles containing a single pH-sensitive surfactant and any number of conventional (pH-insensitive) surfactants. Our description is similar to that of Maeda,[67] but differs from it in two important ways. First, we predict the intercept of the pK_{m} vs. x_{mic}

curve, in addition to the slope, by relating the pK_{m} to the pK_1. Second, we develop a more general theory applicable to a pH-sensitive surfactant mixed with an arbitrary number of surfactant components. This theory may be more useful for practical applications, which typically involve a large number of surfactant species resulting from polydisperse surfactant feedstocks or from the intentional mixing of surfactants. We validate the theory with titration data from the literature, as well as with our own experimental mixed micelle titration data. To our knowledge, the mixed micelle titration data reported here represent the first systematic study of the composition dependence of the pK_{m} of a pH-sensitive surfactant in mixed micelles.

4.2. Materials and Experimental Methods

The pH-sensitive surfactant C_{12}DAO (lot no. 436579/1 31402) and the cationic surfactant dodecyltrimethylammonium bromide (C_{12}TAB) (lot no. 63H05) were obtained from Sigma-Aldrich (St. Louis, MO). The nonionic surfactant dodecyl octa(ethylene oxide) ($C_{12}E_8$) (lot 9054) was obtained from Nikko Chemicals (Tokyo, Japan). The salt sodium chloride (NaCl) (lot 7544) was obtained from Mallinckrodt Chemicals (Paris, KY). Hydrochloric acid (HCl) (0.1 *N* lot no. X25515 and 0.5 *N* lot no. X10505) and sodium hydroxide (NaOH) (0.1 *N* lot no. X38505 and 0.5 *N* lot no. X27503) solutions were obtained from J.T. Baker (Phillipsburg, NJ). All these materials were used as received.

All the solutions were prepared using deionized water that was further purified using a Milli-Q ion exchange system from Millipore (Billerica, MA). All the glassware was cleaned by washing in a 50:50 ethanol:1 *N* NaOH bath, washing in a 1 *N* nitric acid bath, rinsing thoroughly with Milli-Q water, rinsing copiously with Milli-Q water, and then drying in an oven for at least 24 hours.

All the solutions were prepared on a mass basis using Milli-Q water. Final solutions of surfactant and salt were prepared using stock solutions of a single surfactant and 0.1 *M* NaCl. The final solutions had a total surfactant concentration of approximately 0.050 *M*. This surfactant concentration was selected so that the

concentration of micellized C_{12}DAO was much higher than the C_{12}DAO monomer concentration, thereby allowing us to neglect the contribution of the surfactant monomers during the titrations. (The upper limit of the C_{12}DAO monomer concentration was estimated to be 0.001 M, based on the cmc values reported in the literature.[51]) Each solution contained a surfactant mixture of C_{12}DAO/C_{12}TAB or C_{12}DAO/$C_{12}E_8$, with the amount of C_{12}DAO varying from 10% to 100%.

Titrations were conducted using a model PHB-45 pH-meter from Omega Engineering (Stamford, CT). Above a pH of approximately 6, dissolved carbon dioxide can lead to significant concentrations of carbonate and bicarbonate. Therefore, titrations above a pH of 5 were carried out under a nitrogen atmosphere in order to minimize any possible interference resulting from the atmospheric carbon dioxide. A "blank" titration was conducted by adding acid or base to a 0.1 M NaCl solution containing no surfactant (see below). Surfactant solutions were then titrated by adding acid or base.

In order to obtain the average degree of protonation of C_{12}DAO, a modification to the procedure used by Kakehashi et al.[148] was utilized. The method essentially assumes that for a given pH, the amount of free hydrogen ions in the solution can be deduced from the blank titration. Any additional hydrogen ions that are added to the solution (in our case, from HCl) are therefore assumed to react with C_{12}DAO to form the protonated form of the surfactant (C_{12}DAOH$^+$). Specifically, at each pH, we calculate the number of moles of C_{12}DAOH$^+$ in the solution using the following equation:

$$\langle x \rangle \, N_{\mathrm{surf}} = m_{\mathrm{H_2O}} \left[C^{(\mathrm{surf})}_{\mathrm{acid-base}} - C^{(\mathrm{blank})}_{\mathrm{acid-base}} \right] \tag{4.3}$$

where $\langle x \rangle$ is the average degree of protonation of all the C_{12}DAO molecules (both monomeric and in micelles), N_{surf} is the number of moles of C_{12}DAO in the solution, $m_{\mathrm{H_2O}}$ is the total mass of water in the solution, $C^{(\mathrm{surf})}_{\mathrm{acid-base}}$ is the concentration of acid minus base ($C_{\mathrm{HCl}} - C_{\mathrm{NaOH}}$) for the C_{12}DAO solution, and $C^{(\mathrm{blank})}_{\mathrm{acid-base}}$ is the amount of acid minus base of a solution containing no surfactant (a "blank" solution) at the same pH. Since the titrations were performed at a surfactant concentration well above the

cmc, $\langle x \rangle$ is approximately equal to x_{mic} (that is, the monomers contribute negligibly to $\langle x \rangle$). Note that C_{HCl} is the molal concentration of HCl added to the solution, and C_{NaOH} is the molal concentration of NaOH added to the solution. Therefore, $C^{(\mathrm{surf})}_{\mathrm{acid-base}}$ represents the amount of acid (or base) required to bring a solution of C_{12}DAO to a given pH, and $C^{(\mathrm{blank})}_{\mathrm{acid-base}}$ represents the amount of acid (or base) required to bring a "blank" solution (containing no surfactant) to the same pH. The difference $\left[C^{(\mathrm{surf})}_{\mathrm{acid-base}} - C^{(\mathrm{blank})}_{\mathrm{acid-base}}\right]$ corresponds to the concentration of hydrogen ions that have reacted with C_{12}DAO to form C_{12}DAOH$^+$. Although eq 4.3 can in principle be written using any concentration units, molal units are particularly convenient since they do not require any density or volume measurements.

Note that knowledge of N_{surf} is required in order to evaluate $\langle x \rangle$ using eq 4.3. One approach involves calculating N_{surf} directly from the weight of C_{12}DAO added to the solution, if the purity of the surfactant is accurately known. Kakehashi et al.[148] used another approach in which the solutions were fully titrated to the endpoints $\langle x \rangle = 0$ and $\langle x \rangle = 1$. However, because of the uncertainties associated with titration at the endpoints (see Section 4.4.1), we estimated N_{surf} using a linear regression technique that makes use of the behavior of eq 4.3 at low pH. We believe that our approach is less error prone since it utilizes multiple experimental data points to determine N_{surf}. Specifically, we carried out a linear regression analysis of the experimentally obtained data (the right-hand side of eq 4.3) as a function of $10^{-\mathrm{pH}}$, using titration data obtained over a range of pH values of approximately 2.5 to 4. The intercept of this regression line corresponds to the limiting value as $10^{-\mathrm{pH}} \rightarrow 0$ (or as the pH $\rightarrow -\infty$), which corresponds to eq 4.3 evaluated at $\langle x \rangle = 1$. Explicitly taking this limit shows that the intercept corresponds to N_{surf}:

$$\mathrm{Intercept} = \lim_{\mathrm{pH} \rightarrow -\infty} \langle x \rangle \, N_{\mathrm{surf}} = \langle x \rangle \, N_{\mathrm{surf}}|_{\langle x \rangle = 1} = N_{\mathrm{surf}} \tag{4.4}$$

4.3. Theory

4.3.1. Notation

The deprotonated form of the pH-sensitive surfactant is denoted as S. The protonated form is denoted as HS, which reflects the protonation reaction $H^+ + S \rightarrow HS^+$. The various conventional surfactants are denoted as components 1 to n_{surf}. The mole fraction of component i (i =1 to n_{surf}, HS, and S) in the micelle is denoted as α_i (referred to hereafter as the micelle composition of component i). Note that only $n_{surf} + 1$ compositions are independent, since the micelle composition must sum to unity, that is:

$$\alpha_{HS} + \alpha_S + \sum_{i=1}^{n_{surf}} \alpha_i = 1 \tag{4.5}$$

Similarly, the monomer composition, α_{1i} (i =1 to n_{surf}, HS, and S), are subject to the constraint:

$$\alpha_{1HS} + \alpha_{1S} + \sum_{i=1}^{n_{surf}} \alpha_{1i} = 1 \tag{4.6}$$

Recall that the fraction of the monomeric pH-sensitive surfactant in the protonated state, $x_1 = \alpha_{1HS}/(\alpha_{1HS} + \alpha_{1S})$, is related to the the pK_1 and to the solution pH via the Henderson-Hasselbalch equation (see eq 4.1). Similarly, the degree of protonation of the pH-sensitive surfactant in the micelles,

$$x_{mic} = \frac{\alpha_{HS}}{\alpha_{HS} + \alpha_S} \tag{4.7}$$

is related to the pK_m and to the solution pH by eq 4.2, which can also be written in terms of the micelle composition as:

$$pK_m = pH + \log \frac{\alpha_{HS}}{\alpha_S} \tag{4.8}$$

Note that even when very little pH-sensitive surfactant is present in the micelles (that is, when $\alpha_{HS} + \alpha_S \approx 0$), x_{mic} always varies between 0 and 1.

Combining eqs 4.1, 4.2, and 4.8, we find that the difference in the micellar and

the monomeric pK_a, ΔpK, is given by:

$$\Delta \mathrm{p}K = \mathrm{p}K_m - \mathrm{p}K_1 = \log \frac{\alpha_{HS}}{\alpha_S} - \log \frac{\alpha_{1HS}}{\alpha_{1S}} = \log \frac{x_{mic}}{1 - x_{mic}} - \log \frac{x_1}{1 - x_1} \tag{4.9}$$

Although the pK_m is useful to directly relate x_{mic} to the solution pH, the ΔpK is more useful to compare the titration behavior of the micellized surfactant to that of the monomeric surfactant.

4.3.2. Implications of the RST to Analyze Micellar Titrations

The key equations that result from utilizing the RST to analyze micellar titrations are summarized below (see Appendix D for a complete derivation). The ΔpK of a pH-sensitive surfactant in a mixed micelle is given by:

$$\Delta \mathrm{p}K = \log \left(\frac{\mathrm{cmc}_S}{\mathrm{cmc}_{HS}} \right) + (\log e) \left(\beta_{S,HS} \Delta\alpha + \sum_{j=1}^{n_{surf}} \Delta\beta_j \alpha_j \right) \tag{4.10}$$

where

$$\Delta\alpha \equiv \alpha_{HS} - \alpha_S \tag{4.11}$$

$$\alpha_{conv} \equiv \sum_{j=1}^{n_{surf}} \alpha_j = 1 - \alpha_{HS} - \alpha_S \tag{4.12}$$

$$\Delta\beta_j \equiv \beta_{S,j} - \beta_{HS,j} \tag{4.13}$$

In the case of a micelle containing a pH-sensitive surfactant and no conventional surfactant ($\alpha_{conv} = 0$), eq 4.10 simplifies to:

$$\begin{aligned} \Delta \mathrm{p}K &= \log \left(\frac{\mathrm{cmc}_S}{\mathrm{cmc}_{HS}} \right) + (\log e)\, \beta_{S,HS} \Delta\alpha \\ &= \log \left(\frac{\mathrm{cmc}_S}{\mathrm{cmc}_{HS}} \right) + (\log e)\, \beta_{S,HS}\, (2\alpha_{HS} - 1) \end{aligned} \tag{4.14}$$

where $\alpha_{HS} + \alpha_S = 1$ (when $\alpha_{conv} = 0$) has been used to relate $\Delta\alpha$ to α_{HS} (see eq 4.11). Some of the implications of eqs 4.10 and 4.14 are examined below in sections 4.3.2.1 and 4.3.2.2.

4.3.2.1. Single pH-Sensitive Surfactant Systems

Let us first examine the implications of eq 4.14 for micelles consisting entirely of a pH-sensitive surfactant. This analysis will prove helpful to understand the experimental observations in section 4.4.2. As indicated in section 4.3.1, knowing ΔpK is equivalent to knowing x_{mic} as a function of x_1 or of the pH. In addition, ΔpK and x_{mic} may be used to estimate other micelle properties, such as the electrostatic potential at the surface of a micelle and the average charge of a surfactant in the micelle.

A positive value of ΔpK indicates that the protonation equilibrium in the micelle has shifted toward the protonated state, relative to the equilibrium of the surfactant monomers. On the other hand, a negative value of ΔpK indicates that the protonation equilibrium in the micelle has shifted toward the deprotonated state. In practical terms, a positive ΔpK implies that less acid needs be added to obtain a high degree of protonation in the micelle (corresponding to a more positive micelle surface charge density), while a negative ΔpK implies that less base needs to be added to obtain a low degree of protonation (corresponding to a more negative micelle surface charge density).

Equation 4.14 indicates that ΔpK (and, therefore, the pH dependence of the micelle surface charge density) varies linearly with $\Delta\alpha$. In general, the ΔpK also depends on $\beta_{S,HS}$. However, at the half-protonated state ($\alpha_{HS} = \alpha_S$), which corresponds to $\Delta\alpha = 0$ (see eq 4.11), the ΔpK, which we denote as $\Delta pK_{1/2}$, only depends on the ratio of the cmc's of the deprotonated and the protonated species:

$$\Delta pK_{1/2} \equiv \Delta pK|_{\Delta\alpha=0} = \log\left(\frac{cmc_S}{cmc_{HS}}\right) \tag{4.15}$$

If these two cmc's are approximately equal ($cmc_S \approx cmc_{HS}$), as is the case for C_{12}DAO

(see section 4.4.2), it follows that $\Delta \mathrm{p}K_{1/2} \approx 0$. In that case, the micelles and the monomers will be half-ionized at approximately the same pH. If $\mathrm{cmc_S} > \mathrm{cmc_{HS}}$, it follows that $\Delta \mathrm{p}K_{1/2} > 0$, and in that case, the micelles will be half-protonated at a higher pH than the monomers. Conversely, if $\mathrm{cmc_S} < \mathrm{cmc_{HS}}$, it follows that $\Delta \mathrm{p}K_{1/2} < 0$, and in that case, the micelles will be half-protonated at a lower pH than the monomers. The validity of these $\Delta \mathrm{p}K_{1/2}$ predictions will be examined in section 4.4.2.

Since the β parameters which appear in the RST are known to vary with salt concentration,[150] or with surfactant tail length (see section 4.4.2), it is also useful to consider the effect of $\beta_{\mathrm{S,HS}}$ (see eq 4.13) on $\Delta \mathrm{p}K$. Typically, the interactions between most surfactant pairs are either ideal or synergistic (that is, $\beta_{ij} \leq 0$),[71] with a notable exception being hydrocarbon-fluorocarbon surfactant mixtures.[188] In addition, ideal interactions (that is, $\beta_{ij} = 0$) are typically limited to mixtures of nonionic surfactants. The two forms of a pH-sensitive surfactant are usually ionic and nonionic (or ionic and zwitterionic). Therefore, we also expect some degree of synergy between the two forms of the pH-sensitive surfactant (that is, $\beta_{\mathrm{S,HS}} < 0$). A negative value for $\beta_{\mathrm{S,HS}}$ indicates a negative slope of $\Delta \mathrm{p}K$ vs. $\Delta\alpha$ (or $\Delta \mathrm{p}K$ vs. α_{HS}), which indicates that it becomes increasingly more difficult to protonate the micelles as $\Delta\alpha$ increases (or, equivalently, as $\alpha_{\mathrm{HS}} \to 1$).

The $\mathrm{p}K_{\mathrm{m}}$ has also been assumed to be related to the electrostatic potential at the micelle surface (ψ_0) as follows[67] (see also Chapter 3):

$$\mathrm{p}K_{\mathrm{m}} = \mathrm{p}K_{\mathrm{m}}^{0} + (\log e)\,\frac{e_0\psi_0}{k_{\mathrm{B}}T} \tag{4.16}$$

where $\mathrm{p}K_{\mathrm{m}}^{0}$ is the $\mathrm{p}K_{\mathrm{m}}$ of a neutral micelle (for which $\psi_0 = 0$), e_0 is the charge of a proton, k_{B} is the Boltzmann constant, and T is the absolute temperature. In the case of micelles composed of amine oxide surfactants, the neutral species is the deprotonated form of the surfactant, and therefore, $\mathrm{p}K_{\mathrm{m}}^{0}$ corresponds to the $\mathrm{p}K_{\mathrm{m}}$ at $\alpha_{\mathrm{HS}} = 0$ (and, therefore, $\Delta\alpha = -1$, see eq 4.11). For amine oxide surfactants, it has been observed that $\mathrm{p}K_{\mathrm{m}}^{0} > \mathrm{p}K_1$.[67] This implies that obtaining deprotonated

amine oxide micelles is more difficult (that is, it requires a higher solution pH) than obtaining deprotonated amine oxide monomers. This difference has been explained in terms of hydrogen bonding between the protonated and the deprotonated surfactant molecules. However, an alternative explanation can be proposed in the context of the RST. For alkyldimethylamine oxide surfactants, $\mathrm{cmc_S} \approx \mathrm{cmc_{HS}}$ and $\beta_{\mathrm{S,HS}} < 0$, and as a result, $\mathrm{p}K_{\mathrm{m}}^{0} \approx \mathrm{p}K_1 - (\log e)\,\beta_{\mathrm{S,HS}}$ (see eq 4.14). Therefore, it follows that $\mathrm{p}K_{\mathrm{m}}^{0} > \mathrm{p}K_1$ because of the synergy ($\beta_{\mathrm{S,HS}} < 0$) between the protonated and the deprotonated forms of the pH-sensitive surfactant.

4.3.2.2. Mixtures of a pH-Sensitive Surfactant and Conventional Surfactants

Since commercial surfactants and practical formulations typically consist of many surfactant components, the impact on micellar titrations of mixing a pH-sensitive surfactant with conventional surfactants has practical significance. In this section, we examine such systems and present a way to simplify the modeling of multicomponent surfactant mixtures. As stated in section 4.3.1, knowing the $\Delta\mathrm{p}K$ is equivalent to knowing x_{mic} (and, therefore, the micelle surface charge density). The analysis presented here will also be helpful in interpreting the experimental data presented in section 4.4.3.

In the case of multicomponent surfactant mixtures, eq 4.10 indicates that $\Delta\mathrm{p}K$ varies linearly with both $\Delta\alpha$ and α_j. Note that eq 4.10 also suggests that all the conventional surfactant components can be modeled using the total composition of the conventional surfactants (α_{conv}) and a *single "effective" interaction parameter difference*, $\Delta\beta_{\mathrm{conv}}$, defined as:

$$\Delta\beta_{\mathrm{conv}} \equiv \frac{\sum_{j=1}^{n_{\mathrm{surf}}} \Delta\beta_j\alpha_j}{\sum_{j=1}^{n_{\mathrm{surf}}} \alpha_j} = \frac{\sum_{j=1}^{n_{\mathrm{surf}}} \Delta\beta_j\alpha_j}{\alpha_{\mathrm{conv}}} \tag{4.17}$$

Equation 4.17 indicates that $\Delta\beta_{\mathrm{conv}}$ is a composition-weighted average of the $\Delta\beta_j$ parameters of the conventional surfactants. Therefore, we restrict further discussion of multicomponent surfactant mixtures to the case of a pH-sensitive surfactant mixed

with one (effective) conventional surfactant, for which $\Delta \mathrm{p}K$ is given by:

$$\begin{aligned} \Delta \mathrm{p}K &= \log\left(\frac{\mathrm{cmc_S}}{\mathrm{cmc_{HS}}}\right) + (\log e)\left(\beta_{\mathrm{S,HS}}\Delta\alpha + \Delta\beta_{\mathrm{conv}}\alpha_{\mathrm{conv}}\right) \\ &= \log\left(\frac{\mathrm{cmc_S}}{\mathrm{cmc_{HS}}}\right) + (\log e)\,\beta_{\mathrm{S,HS}}\left(\alpha_{\mathrm{HS}} - \alpha_{\mathrm{S}}\right) + (\log e)\,\Delta\beta_{\mathrm{conv}}\alpha_{\mathrm{conv}} \end{aligned} \quad (4.18)$$

It is also useful to rewrite eq 4.18 in terms of x_{mic} and α_{conv} by combining eqs 4.7, 4.12, and 4.18:

$$\Delta \mathrm{p}K = \log\left(\frac{\mathrm{cmc_S}}{\mathrm{cmc_{HS}}}\right) + (\log e)\,\beta_{\mathrm{S,HS}}\left(1 - \alpha_{\mathrm{conv}}\right)\left(2x_{\mathrm{mic}} - 1\right) + (\log e)\,\Delta\beta_{\mathrm{conv}}\alpha_{\mathrm{conv}} \quad (4.19)$$

One useful feature of eq 4.19 is that x_{mic} (the protonated fraction of the pH-sensitive surfactant in the micelles) always varies from 0 to 1, independently of α_{conv} (the total composition of conventional surfactant in the micelles). On the other hand, the upper and lower bounds of $\Delta\alpha$ (the composition difference between the protonated and the deprotonated forms of the pH-sensitive surfactant in the micelles) depend on the fraction of the conventional surfactant in the micelle (α_{conv}). For a given pair of pH-sensitive and conventional surfactants, both $\beta_{\mathrm{S,HS}}$ and $\Delta\beta_{\mathrm{conv}}$ are essentially fixed, while x_{mic} and α_{conv} can be varied experimentally via the solution pH and the surfactant mixing ratio, respectively.

Let us next examine the case where the effective surfactant interacts equally well with the protonated and with the deprotonated forms of the pH-sensitive surfactant (that is, $\Delta\beta_{\mathrm{conv}} = 0$), which yields the following expression for $\Delta \mathrm{p}K$ (see eq 4.19):

$$\Delta \mathrm{p}K|_{\Delta\beta_{\mathrm{conv}}=0} = \log\left(\frac{\mathrm{cmc_S}}{\mathrm{cmc_{HS}}}\right) + (\log e)\,\beta_{\mathrm{S,HS}}\left(1 - \alpha_{\mathrm{conv}}\right)\left(2x_{\mathrm{mic}} - 1\right) \quad (4.20)$$

Equation 4.20 indicates that adding a conventional surfactant (that is, increasing α_{conv}) only serves to decrease the slope of $\Delta \mathrm{p}K$ vs. x_{mic}. In other words, even though $\Delta\beta_{\mathrm{conv}} = 0$, the addition of a conventional surfactant "dilutes" the interaction between the protonated and the deprotonated forms of the pH-sensitive surfactant that drives the shift in the $\Delta \mathrm{p}K$.

Next, we examine the limit $\alpha_{\text{conv}} \to 1$, which corresponds to infinite dilution of the pH-sensitive surfactant. (Note that this limit is particularly relevant to interpret experimental data using a pH-sensitive probe, since the experimental conditions correspond to using a minimal amount of probe to minimize perturbation of the micellar environment.) In this limit, eq 4.19 reduces to:

$$\Delta \mathrm{p}K = \log\left(\frac{\mathrm{cmc_S}}{\mathrm{cmc_{HS}}}\right) + (\log e)\,\Delta\beta_{\text{conv}} \tag{4.21}$$

indicating that $\Delta \mathrm{p}K$ no longer varies with x_{mic}. Instead, the $\Delta \mathrm{p}K$ is a constant that depends only on $\mathrm{cmc_S}$, $\mathrm{cmc_{HS}}$, and $\Delta\beta_{\text{conv}}$. The cmc's are essentially fixed by specifying the pH-sensitive surfactant. However, eq 4.21 indicates that $\Delta \mathrm{p}K$ of a pH-sensitive surfactant is sensitive to the micellar environment through its dependence on the parameter $\Delta\beta_{\text{conv}}$. If the conventional surfactant interacts more strongly with the protonated form of the pH-sensitive surfactant (that is, if $\Delta\beta_{\text{conv}} > 0$), then the $\Delta \mathrm{p}K$ will increase, indicating that it is "easier" to protonate the pH-sensitive species in the micellar environment. On the other hand, if the additional surfactant interacts more strongly with the deprotonated form of the pH-sensitive surfactant (that is, if $\Delta\beta_{\text{conv}} < 0$), then the $\Delta \mathrm{p}K$ will decrease, indicating that it is "harder" to protonate the pH-sensitive species in the micellar environment.

As an illustration, the above analysis can be utilized to analyze qualitatively the experimental titration data of da Silva et al.,[70] who measured the $\Delta \mathrm{p}K$ of a lauric acid probe in micelles composed of sodium dodecyl sulfate (SDS), $\mathrm{C_{12}E_8}$, or dodecyltrimethylammonium chloride ($\mathrm{C_{12}TAC}$). The respective $\Delta \mathrm{p}K$ values for solutions containing approximately 10 wt% surfactant (the total surfactant concentration) and $\alpha_{\text{conv}} \approx 0.98$ were found to be 2.4, 1.9, and 0.6. These $\Delta \mathrm{p}K$ values indicate that SDS has the highest $\Delta\beta$ and the strongest preference for the protonated, nonionic lauric acid, while $\mathrm{C_{12}TAC}$ has the lowest $\Delta\beta$ and the strongest preference for the deprotonated laurate anion (see eq 4.21).

Finally, in the general case when both α_{conv} and $\Delta\beta_{\text{conv}}$ are non-zero (see eq 4.19), it follows that the $\Delta \mathrm{p}K$ is a linear combination of three effects: (1) a

constant term determined by $\mathrm{cmc_S}$ and $\mathrm{cmc_{HS}}$, (2) a contribution whose magnitude decreases with α_{conv}, arising from the interactions between the protonated and the deprotonated forms of the pH-sensitive surfactant through $\beta_{\mathrm{S,HS}}$, and (3) a contribution whose magnitude increases with α_{conv}, arising from the preferential interaction of the conventional surfactant with the protonated or the deprotonated forms of the pH-sensitive surfactant through $\Delta\beta_{\mathrm{conv}}$.

4.4. Analysis of the Experimental Titration of Micelles Containing a pH-Sensitive Surfactant

In this section, the experimentally measured $\Delta\mathrm{p}K$ values will be compared to those predicted by the RST description (see eq 4.19). In section 4.4.1, we discuss the experimental uncertainty in $\Delta\mathrm{p}K$ as a function of x_{mic}, including how to appropriately account for that uncertainty during the regression analysis of $\Delta\mathrm{p}K$ vs. x_{mic}. In section 4.4.2, we examine systems containing two surfactant components (that is, only the pH-sensitive surfactant), by regressing the experimental $\Delta\mathrm{p}K$ vs. x_{mic} data (see eq 4.14). The key results of these regressions are summarized in Table 4.1. In section 4.4.3, we examine systems containing a pH-sensitive surfactant mixed with another conventional surfactant. The key results of these regressions are summarized in Table 4.2.

4.4.1. Uncertainty in the Analysis of the Experimental Micellar Titration Data

An examination of micellar titrations in the literature reveals that very little discussion has been devoted to the topic of the related experimental uncertainties. Therefore, we wish to highlight here an interesting aspect that may not be immediately apparent. Specifically, one can obtain a relationship between the uncertainty in the $\mathrm{p}K_{\mathrm{m}}$ and the uncertainties in the pH and in x_{mic} by taking the

total derivative of eq 4.2:

$$\mathrm{d}\left(\mathrm{p}K_\mathrm{m}\right) = \mathrm{d}\left(\mathrm{pH}\right) + \left(\log e\right)\left(\frac{1}{x_\mathrm{mic}} + \frac{1}{1 - x_\mathrm{mic}}\right)\mathrm{d}x_\mathrm{mic} \tag{4.22}$$

In Figure 4-1, we show the results of the experimental titration of dodecyldimethylamine oxide (C_{12}DAO) micelles (see section 4.2), in which the error bars were calculated using uncertainties of 0.05 units for the pH and 0.02 units for x_mic (typical uncertainties for the titration experiments described in section 4.2). Although it is an oversimplification to treat the uncertainty in x_mic as being independent of the specific value of x_mic, this nevertheless provides a reasonable approximation to quickly estimate the uncertainty in the pK_m measurements. Figure 4-1 shows that the uncertainties at the intermediate x_mic values ($0.2 < x_\mathrm{mic} < 0.8$) are approximately 0.06 units. In this case, eq 4.22 indicates that the uncertainty is primarily due to the uncertainty in the pH. However, as x_mic approaches 0 or 1, the uncertainty in x_mic dominates $\mathrm{d}\left(\mathrm{p}K_\mathrm{m}\right)$. For example, when $x_\mathrm{mic} = 0.02$ or $x_\mathrm{mic} = 0.98$, the corresponding uncertainty in the pK_m increases to approximately 0.5 units. In fact, eq 4.22 may also explain why Kakehashi et al.[148] noted that measuring the pK_m's of alkyldimethylamine oxide micelles requires more care in the limit $x_\mathrm{mic} \to 0$, and why Maeda reported that the pK_m measurements were less reliable for $x_\mathrm{mic} > 0.8$.[67]

With the above discussions in mind, one approach to utilizing the experimental micellar titration data would be to exclude pK_m measurements whose uncertainties are greater than some threshold value. However, we have chosen instead to utilize a weighted regression (linear, unbiased, minimum-variance estimation) where the weights are the squares of the uncertainties estimated using eq 4.22.[189] This approach has the advantage of using all the experimental micellar titration data while limiting the effect of pK_m measurements having a greater uncertainty.

4.4.2. Single pH-Sensitive Surfactant Systems

In this section, we examine single pH-sensitive surfactants possessing different pH-sensitive heads and different alkyl tails. In addition to testing the validity of

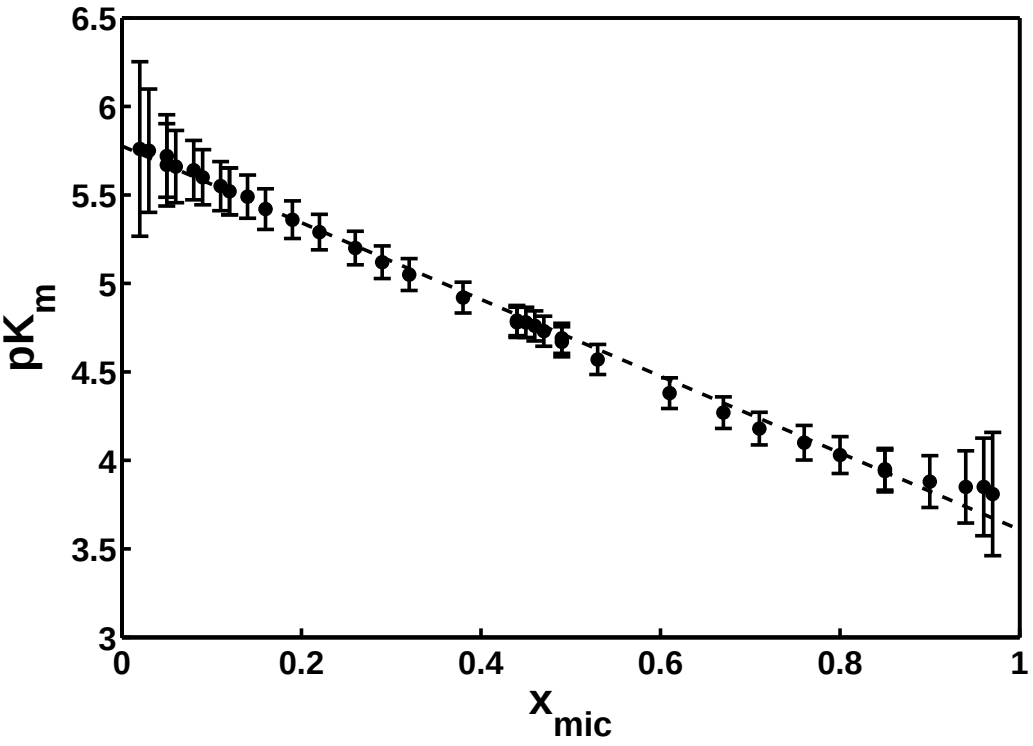

Figure 4-1: Error analysis of the pK_{m} as a function of x_{mic} for C_{12}DAO micelles, showing error bars. The experimental values (measured by us) correspond to the circles with the error bars, and the model fit corresponds to the dashed line.

the RST, we attempt to gain insight by examining the effect of varying the head or tail of the pH-sensitive surfactant on the value of $\beta_{S,HS}$. In section 4.4.2.1, we examine alkyldimethylamine oxide surfactants of various tail lengths. In section 4.4.2.2, we examine several dodecyl-tailed surfactants with different heads.

4.4.2.1. Effect of the Surfactant Tail Length

The titration behavior of alkyldimethylamine oxide surfactants (C_iDAO, where i denotes the number of carbon atoms in the tail) has been studied extensively in the literature. As we reported recently[190] (see also Chapter 3), the variation of the pK_m of C_{12}DAO as a function of α_{HS} shows distinctly non-linear behavior at low concentrations of added salt (below about 0.05 M for NaCl), because the electrostatic interactions between micellized ionic surfactants are not modeled well by the RST. Therefore, we limit our analysis using RST to micellar solutions containing added NaCl at concentrations of 0.1 M or greater. In particular, Figure 4-2 shows the ΔpK of C_iDAO (i = 10, 12, and 14) in 0.1 M NaCl solutions as a function of α_{HS}. The titration data for C_{10}DAO, C_{12}DAO, and C_{14}DAO were measured by Kakehashi et al.,[148] Maeda et al.,[169] and Maeda et al.,[150] respectively. The slope and intercept of the experimental data (ΔpK vs. α_{HS}), determined by linear regression, were used to calculate $\beta_{S,HS}$ and $\Delta pK_{1/2}$ (see eqs 4.14 and 4.15). The results are presented in Table 4.1, along with the experimental pK_1, cmc, β values, and any available uncertainties, as reported by the authors. The uncertainties of the theoretical $\beta_{S,HS}$ and $\Delta pK_{1/2}$ values correspond to a 95% confidence interval.

If the RST is valid, then eq 4.14 indicates that ΔpK should vary linearly with α_{HS}. The predicted linear behavior with α_{HS} fits the data for each tail length very well, as indicated by the R^2 values in Table 4.1, which are greater than 0.99. The interaction parameter $\beta_{S,HS}$ becomes more negative with increasing tail length, varying from –2.15 for C_{10} to –3.06 for C_{14}, indicating an increasing extent of synergy between the protonated and the deprotonated forms of the pH-sensitive surfactants. The $\beta_{S,HS}$ values for C_{10}DAO and C_{12}DAO also correspond reasonably well to the β values deduced from the cmc values obtained using surface tension measurements (denoted

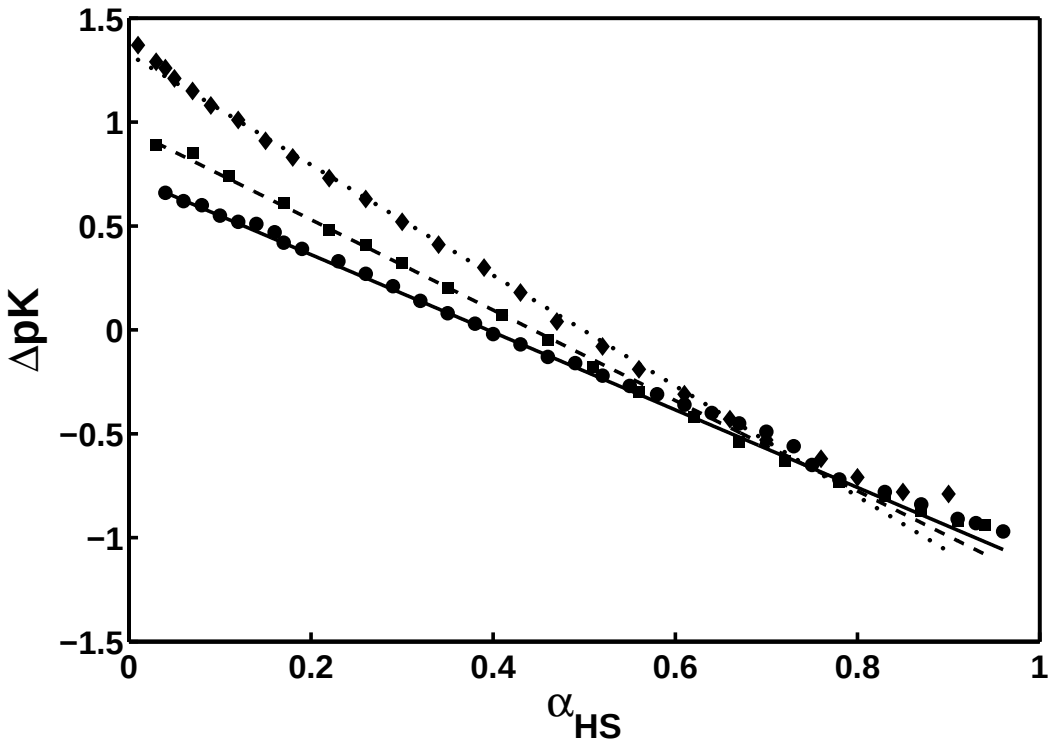

Figure 4-2: Comparison of the RST predictions (various lines) and the experimental (various symbols) of $\Delta \mathrm{p}K$ as a function of α_{HS} for $\mathrm{C}_i\mathrm{DAO}$ (i = 10, 12, and 14) in 0.1 M NaCl solutions at 25°C. The titration data for C_{10}DAO (solid line and circles), C_{12}DAO (dashed line and squares), and C_{14}DAO (dotted line and diamonds) were measured by Kakehashi et al.,[148] Maeda and Tsunoda et al.,[169] and Maeda and Kanakubo et al.,[150] respectively.

Table 4.1: RST analysis of the micellar experimental titration data for single pH-sensitive surfactant systems.

	Experimental						Regression		
Surfactant	pK_1	cmc_S (mM)	cmc_{HS} (mM)	β_{cmc} (k_BT)	$\log(\frac{cmc_S}{cmc_{HS}})$	ref	$\beta_{S,HS}$ (k_BT)	$\Delta pK_{1/2}$	R^2
C_{10}DAO	4.9±0.1	16.5±0.2	21.0±0.2	–1.9*	–0.10±0.02	148	–2.15±0.04	–0.198±0.005	0.997
C_{12}DAO	4.9±0.2	1.57	2.01	–2.1*	–0.11	67, 169	–2.51±0.06	–0.12±0.01	0.995
C_{14}DAO	4.9	0.18	0.20	-1.4 ± 0.2* -3.3 ± 0.1**	–0.05	150	–3.06±0.08	0.00±0.01	0.993
C_{12}DHEAO	4.9±0.1	0.81±0.01	1.76±0.02	–1.1*	–0.34±0.02	148	–2.5±0.4	–0.72±0.06	0.960
$C_{12}C_6$Bet	4.37	5.8	4.2	–1.2**	0.14	140	–1.30±0.07	0.13±0.01	0.995

*Estimated from cmc's determined using surface tension measurements.
**Estimated from monomer concentrations determined at a surfactant concentration of approximately 10 times the cmc (see the text for details).

as β_{cmc} in Table 4.1). However, the β_{cmc} value for C_{14}DAO is only -1.4 ± 0.2,[150] which is significantly less negative that the $\beta_{\mathrm{S,HS}}$ value of -3.06 ± 0.08 obtained using the linear regression. However, in ref 150, the authors also report a β value of -3.3 ± 0.1 from an analysis of the C_{14}DAO monomer concentrations in a 20 mM surfactant solution, obtained by applying a form of the Gibbs-Duhem equation to the experimental micellar titration data.[150] In addition, in ref 150, the authors suggest that the β parameter may vary significantly with surfactant concentration in the case of C_{14}DAO, which may be due to the C_{14}DAO micelles exhibiting a greater tendency to form long, cylindrical micelles, as compared to the micelles of C_{12}DAO and C_{10}DAO.

The validity of the RST can also be tested by comparing the value of $\Delta\mathrm{p}K_{1/2}$, the $\Delta\mathrm{p}K$ at the half-protonated state, which is predicted to depend only on the cmc's of the protonated and the deprotonated forms of the pH-sensitive surfactant (see eq 4.15). In Table 4.1, we list the experimentally measured cmc's and the logarithm of their ratio (referred to as the log-cmc-ratio for brevity), as well as the regressed value of $\Delta\mathrm{p}K_{1/2}$. Although the corresponding $\Delta\mathrm{p}K_{1/2}$ value (-0.12 ± 0.01) agrees well with the experimental log-cmc-ratio of C_{12}DAO (-0.11), there is a slight discrepancy for the other tail lengths. The $\Delta\mathrm{p}K_{1/2}$ of C_{10}DAO is more negative, and the $\Delta\mathrm{p}K_{1/2}$ of C_{14}DAO is less negative, than their corresponding log-cmc-ratio. However, both the log-cmc-ratio and the $\Delta\mathrm{p}K_{1/2}$ of C_{14}DAO are the least negative of the surfactants considered, corresponding to the cmc of the zwitterionic (deprotonated) form of C_{14}DAO being similar to the cmc of the cationic (protonated) form.

Since the RST is primarily an empirical model, the discrepancy between the model and the experimental data cannot be uniquely attributed to any single factor. Although experimental uncertainties were not reported for all the data presented, the available uncertainties suggest that the potential experimental uncertainties are not sufficient to explain the discrepancy with the RST. Instead, we conjecture that the most likely cause of the discrepancy is the failure of the pseudophase approximation. One consequence of this approximation is the assumption that the monomer concentration is exactly equivalent to the cmc. This assumption may be

particularly poor for C_{14}DAO, as indicated by the two markedly different values reported for the β parameter (see Table 4.1).[150] Furthermore, the pseudophase approximation ignores the effect of micelle shape and size. However, it is well known that micelles of both C_{12}DAO[158] and C_{14}DAO[150,191,192] exhibit varying degrees of growth with increasing surfactant concentration. If the titration behavior of spherical micelles differs from that of cylindrical micelles (as suggested by Maeda[51]), then cmc's and the β values obtained at the cmc (when the micelles are smaller) may not adequately describe the interactions and the micellar titration behavior well above the cmc (when the micelles are larger). In summary, the RST description explains very well the observed linearity of the experimental ΔpK vs. α_{HS} curves for alkyldimethylamine oxide surfactants, although the extracted parameters (β and $\Delta pK_{1/2}$) may not always correspond accurately to those estimated using experimental cmc measurements.

4.4.2.2. Effect of the Surfactant Head

The specific chemistry of the surfactant head is expected to affect the titration behavior of pH-sensitive surfactants. In this section, we compare two other dodecyl-tailed surfactants with C_{12}DAO. One of the surfactants, *N*,*N*-bis(2-hydroxyethyl)dodecylamine oxide (C_{12}DHEAO) has a bulkier head than that of the dimethylamine oxide surfactant. The other surfactant, α-(dodecyldimethylammonio)-ω-hexanoate ($C_{12}C_6$Bet), is an example of a carboxybetaine, in which the pH-sensitive moiety is a carboxylate group. The experimental titration data for C_{12}DHEAO and for $C_{12}C_6$Bet were obtained by Kakehashi et al.[148] and by Laughlin,[47] respectively. As shown in Figure 4-3, the experimental ΔpK data as a function of α_{HS} for these three surfactants are markedly different.

Although the amine oxide moieties of C_{12}DAO and C_{12}DHEAO are chemically similar, as reflected in their identical pK_1 values of 4.9 (see Table 4.1), their micellar titration behavior is extremely different. Perhaps most importantly, the experimental ΔpK vs. α_{HS} curve for C_{12}DHEAO (the square symbols in Figure 4-3) exhibits the greatest deviation from linearity. Although the R^2 value (0.960, see Table 4.1) of

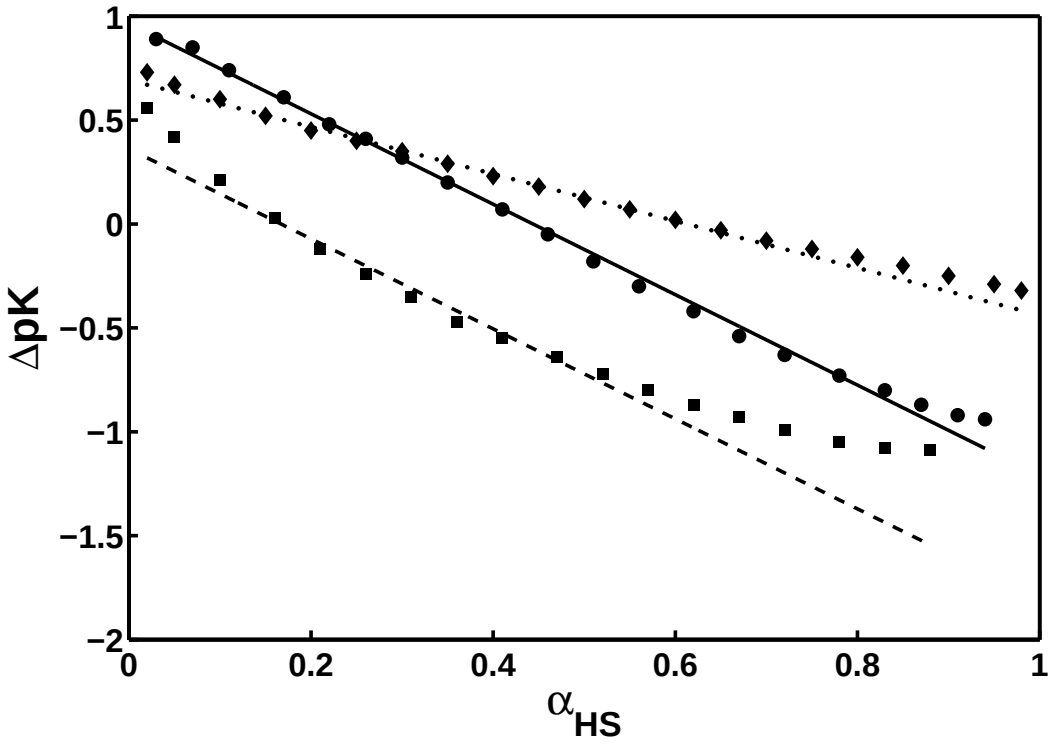

Figure 4-3: Comparison of the RST predictions (various lines) and the experimental (various symbols) of $\Delta \mathrm{p}K$ as a function of α_{HS} for C_{12}DAO, C_{12}DHEAO, and $C_{12}C_6$Bet in 0.1 M NaCl solutions at 25°C. The titration data for C_{12}DAO (solid line and circles), C_{12}DHEAO (dashed line and squares), and $C_{12}C_6$Bet (dotted line and diamonds) were measured by Maeda and Tsunoda et al.,[169] Kakehashi et al.,[148] and Laughlin,[47] respectively.

the fit is still quite high, the linear fit to eq 4.14 (the dashed line in Figure 4-3) shows a systematic deviation at both $\alpha_{HS} \approx 0$ and $\alpha_{HS} \approx 1$, suggesting that the interactions between the protonated and the deprotonated forms of C_{12}DHEAO are not well modeled by the quadratic form assumed in the RST. Although the interaction parameter obtained using cmc measurements shows less synergy for C_{12}DHEAO (–1.1, see Table 4.1) than for C_{12}DAO (–1.9), the β parameters extracted from the ΔpK data are quite similar: -2.5 ± 0.4 and -2.51 ± 0.06 for C_{12}DHEAO and C_{12}DAO, respectively. This discrepancy may be due to the differing behaviors of the cmc and the monomer concentration as a function of α_{HS}. For example, although the cmc ratio of $C_{12}DHEAOH^+/C_{12}$DHEAO is 2.2, the corresponding ratio of the monomer concentrations is estimated to be 3.6.[148] Similarly, the value of $\Delta pK_{1/2}$ for C_{12}DHEAO (–0.72) is more negative than the experimental log-cmc-ratio (–0.34, see eq 4.15). However, the ranking of the $\Delta pK_{1/2}$ of C_{12}DHEAO as being the most negative for the three surfactants considered in Figure 4-3 is consistent with the ranking of the log-cmc-ratios of the surfactants considered.

$C_{12}C_6$Bet also exhibits a rather different ΔpK behavior (the dotted line and the diamonds in Figure 4-3). Specifically, with a regressed $\beta_{S,HS}$ value of –1.30, titration of $C_{12}C_6$Bet micelles shows the least synergy (the least negative $\beta_{S,HS}$ value) of the surfactants considered. However, this result is consistent with the interaction parameter obtained using the cmc data ($\beta_{cmc} = -1.2$), obtained by titration.[47] $C_{12}C_6$Bet is also the only surfactant for which $\Delta pK_{1/2}$ is positive, which is consistent with the reported cmc of the deprotonated species (5.8 mM) being higher than the reported cmc of the deprotonated species (4.2 mM). In fact, the $\Delta pK_{1/2}$ and the log-cmc-ratio are equal, within the 95% confidence interval. The positive $\Delta pK_{1/2}$ value may arise because of the long spacer of five methylene groups that exist between the positively charged ammonium group and the pH-sensitive carboxylate/carboxylic acid group. In the protonated state, the spacer may not be fully solvated since the carboxylic acid group is not ionized, resulting in an additional hydrophobic contribution and a lower corresponding cmc. On the other hand, in the deprotonated state, the carboxylate group carries a negative charge that may increase solvation of

the spacer and decrease its hydrophobic interaction with the micelle core.

The functionality of the surfactant head clearly has a strong influence on the experimental micellar titration behavior, as embodied in the ΔpK. The RST description fits well the ΔpK data for $C_{12}DAO$ and for $C_{12}C_6Bet$. The regressed parameters ($\beta_{S,HS}$ and $\Delta pK_{1/2}$) also correlate well with the cmc data for these surfactants. However, the surfactant $C_{12}DHEAO$ displays unusual titration behavior that deviates somewhat from the RST predictions. However, even for this system, the $\Delta pK_{1/2}$ correlates well with the log-cmc-ratio.

4.4.3. Mixed Surfactant Systems

In this section, we discuss the titration of mixed micelles that contain a pH-sensitive surfactant and a conventional surfactant. In particular, the experimental titrations described in section 4.2 are regressed using eq 4.19. The two systems considered contain the same pH-sensitive surfactant, $C_{12}DAO$. The conventional surfactant is either cationic, dodecyltrimethylammonium bromide ($C_{12}TAB$), or nonionic, dodecyl octa(ethylene oxide) ($C_{12}E_8$). Note that no anionic surfactants were considered because the protonated, cationic $C_{12}DAO$ interacts very strongly with anionic surfactants, leading to the formation of precipitates.[187]

All the solutions considered contained 50 mM of total surfactant and 0.1 M NaCl. Five different $C_{12}DAO/C_{12}TAB$ mixtures were examined, with $C_{12}TAB$ compositions (α_{conv}) of 0, 0.24, 0.50, 0.76, or 0.90. Five different $C_{12}DAO/C_{12}E_8$ mixtures were examined, with $C_{12}E_8$ compositions of 0, 0.29, 0.50, 0.75, or 0.90. However, for visual clarity, the resulting ΔpK data are plotted only for α_{conv} of 0, 0.50, and 0.90 (see Figures 4-4 and 4-5 for $C_{12}DAO/C_{12}TAB$ and $C_{12}DAO/C_{12}E_8$, respectively). Table 4.2 summarizes the results of the weighted-regression analysis (with the reported uncertainties denoting the 95% confidence interval). As shown by the R^2 values close to one (0.980 for $C_{12}DAO/C_{12}TAB$ and 0.949 for $C_{12}DAO/C_{12}E_8$), the RST description provides a good fit for both sets of ΔpK data.

For each surfactant pair, a single regression of the entire set of titration data resulted in three parameters (see eq 4.19): $\beta_{S,HS}$, $\Delta\beta_{conv}$, and the $\Delta pK_{1/2}$. Alternately,

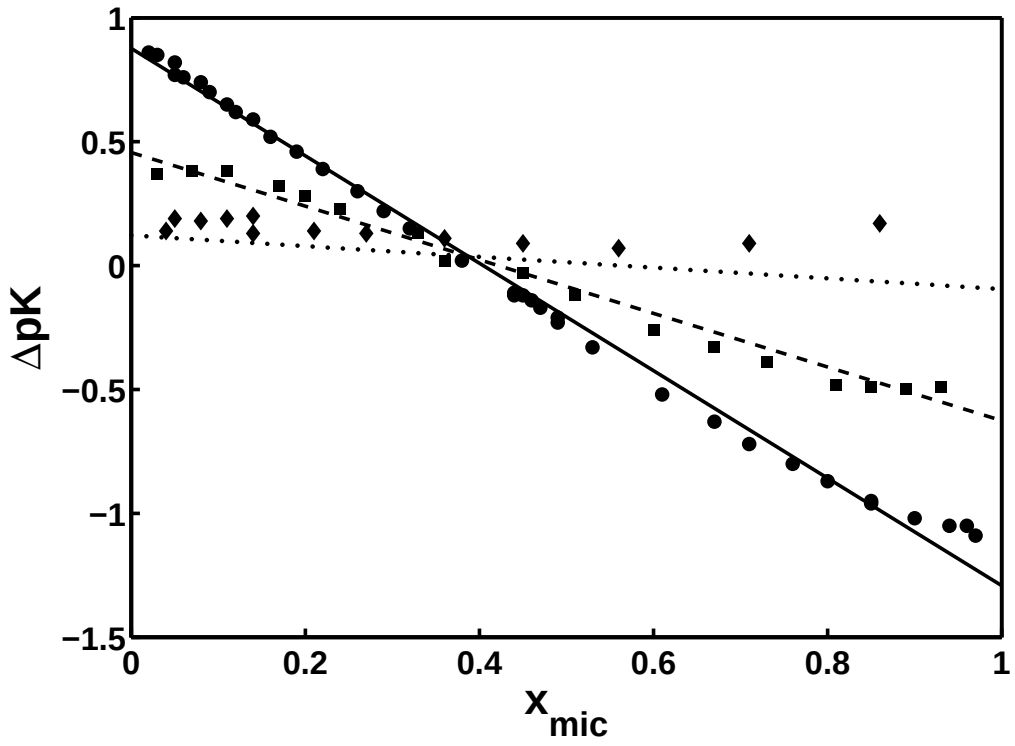

Figure 4-4: Comparison of the RST predictions (various lines) and the experimental (various symbols) $\Delta \mathrm{p}K$ as a function of x_{mic} for mixtures of C_{12}DAO/C_{12}TAB with C_{12}TAB compositions of 0 (solid line and circles), 0.50 (dashed line and squares), and 0.90 (dotted line and diamonds).

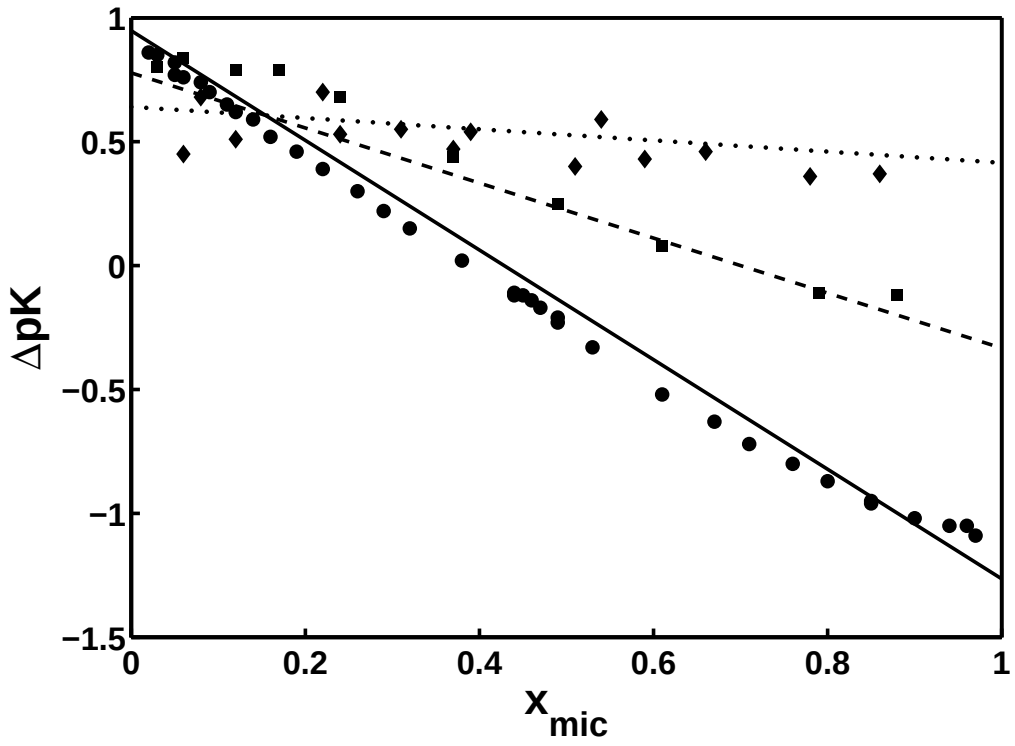

Figure 4-5: Comparison of the RST predictions (various lines) and the experimental (various symbols) $\Delta \mathrm{p}K$ as a function of x_{mic} for mixtures of $C_{12}DAO/C_{12}E_8$ with $C_{12}E_8$ compositions of 0 (solid line and circles), 0.50 (dashed line and squares), and 0.90 (dotted line and diamonds).

Table 4.2: RST analysis of the experimental micellar titration data for mixtures of a pH-sensitive and a conventional surfactant.

	Regression			
Surfactant Pair	$\beta_{S,HS}$	$\Delta\beta$	$\Delta pK_{1/2}$	R^2
$C_{12}DAO/C_{12}TAB$	–2.50±0.08	0.57±0.10	–0.21±0.02	0.980
$C_{12}DAO/C_{12}E_8$	–2.55±0.13	1.76±0.16	–0.16±0.04	0.949

the parameters $\beta_{S,HS}$ and the $\Delta pK_{1/2}$ may be obtained from a separate regression of the titration data from $C_{12}DAO$ micelles. However, we have included all three parameters in the regression in order to test the robustness of the model. For example, the parameter $\beta_{S,HS}$ of pure $C_{12}DAO$ (–2.51±0.06, see Table 4.1) is equal (within the confidence intervals) to the $\beta_{S,HS}$ parameters of both $C_{12}DAO/C_{12}TAB$ (–2.50±0.08) and of $C_{12}DAO/C_{12}E_8$ (–2.55±0.13), see Table 4.2. Likewise, the $\Delta pK_{1/2}$ of pure $C_{12}DAO$ (–0.12±0.01 in Table 4.1) is equal (within the confidence intervals) to the $\Delta pK_{1/2}$ of the $C_{12}DAO/C_{12}E_8$ system (–0.16±0.04 in Table 4.2). Although the $\Delta pK_{1/2}$ of the $C_{12}DAO/C_{12}TAB$ system (–0.21±0.02 in Table 4.2) is sufficiently negative to be considered statistically different from the value obtained for pure $C_{12}DAO$ (–2.15±0.04 in Table 4.1), it is still within the confidence interval of the value obtained for $C_{12}DAO/C_{12}E_8$ (–0.16±0.04 in Table 4.2). The fact that $\beta_{S,HS}$ and the $\Delta pK_{1/2}$ are relatively independent of the method of analysis used clearly demonstrates that the RST regression analysis is quite robust.

The parameter $\Delta\beta_{conv}$ indicates any preference that the conventional surfactant has for one of the forms of the pH-sensitive surfactant. In the case of $C_{12}DAO/C_{12}TAB$, $\Delta\beta_{conv} = 0.57\pm0.10$ indicates that $C_{12}TAB$ interacts slightly more favorably with the protonated, cationic form that with the deprotonated, zwitterionic form of $C_{12}DAO$. This surprising result is inconsistent with a simple electrostatic interaction (which should lead to more synergy with the deprotonated species), and it cannot be explained by hydrogen bonds, since $C_{12}TAB$ has no strong hydrogen bond donors or acceptors. Therefore, we propose that the observed $\Delta\beta_{conv}$ value is due to

the specific interactions of the bromide ions with the micelle. Since this proposal is related to the micelle structure, it will be discussed in further detail in section 6.5.3.2 in the context of a molecular-thermodynamic theory for micellar titration. $C_{12}E_8$ shows an even stronger preference ($\Delta\beta_{\text{conv}} = 1.76 \pm 0.16$) for the protonated, cationic form than for the deprotonated, zwitterionic form of C_{12}DAO. However, this preference is unsurprising, since $C_{12}E_8$ can significantly reduce electrostatic interactions when mixed with the protonated, cationic form of C_{12}DAO, and it can also serve as both a donor and an acceptor of hydrogen bonds, which suggests that $\beta_{\text{HS},C_{12}E_8} < 0$. Furthermore, $C_{12}E_8$ may interact nearly ideally ($\beta_{\text{S},C_{12}E_8} \approx 0$) with the deprotonated, dipolar form of C_{12}DAO. Therefore, both electrostatics and hydrogen bonding could lead to the larger, positive $\Delta\beta$ value observed in the C_{12}DAO/$C_{12}E_8$ system (see eq 4.13).

4.5. Conclusions

We have developed a theoretical description to quantify the titration behavior of pH-sensitive micelles based on the pseudophase approximation and the RST. The RST-based description can be used for systems containing any number of conventional surfactants and either a pH-sensitive surfactant or a pH-sensitive probe molecule. Several limiting behaviors of the theory were discussed. The theory was first validated using experimental micellar titration data of single pH-sensitive surfactant systems (obtained from the literature), and subsequently, of mixtures consisting of a pH-sensitive and a conventional surfactant (measured by us). For single pH-sensitive surfactant systems, the differences between various pH-sensitive surfactants were rationalized in terms of their differing cmc's and β interaction parameters. For mixtures containing a conventional surfactant, we also extracted an interaction parameter difference ($\Delta\beta_{\text{conv}}$). Once these parameters are estimated, the $\Delta\text{p}K$ can be estimated at any micelle composition. This information can then be used to determine what solution pH is required to obtain a particular micelle composition or micelle surface charge density.

One notable limitation of the pseudophase approach is a lack of detailed information about the micelle structure, for example, about the shape, size, and the degree of counterion binding. To overcome this limitation, a molecular-thermodynamic approach was recently developed to model micellization of a single, pH-sensitive surfactant[190] (see also Chapter 3). Before this approach is extended to solutions that also contain both pH-sensitive and conventional surfactants, in Chapter 5, we present a theoretical framework to model micelles composed of three or more surfactant species.

Chapter 5

Molecular-Thermodynamic Theory of Micellization of Ternary and Multicomponent Surfactant Mixtures

5.1. Introduction

Surfactants used in practical applications typically consist of complex surfactant mixtures. Typical formulations of both powdered[29] and liquid[30,31] detergents contain two or more classes of surfactants, each of which may be polydisperse. Surfactant mixtures can result from polydispersity in the hydrocarbon raw materials used, and from the reaction kinetics associated with the synthesis step, such as the Poisson distribution of head lengths in the case of alkyl poly(ethylene oxide) nonionic surfactants. More importantly, perhaps, surfactant mixtures are frequently used because they enable improved performance for various applications. For example, the use of multicomponent mixtures of anionic surfactants, or of mixtures of anionic and nonionic surfactants, reduces precipitation in hard water.[28] A survey of recent patents for liquid detergents[193] also reveals that complex surfactant mixtures continue to play an important role in improved detergent formulations.

In spite of the practical relevance of multicomponent surfactant mixtures, most

recent studies of mixed surfactant systems are limited to binary surfactant mixtures (see, for example, ref 194). Recently, Ashwari and Smith[16] utilized statistical analysis and experimental design principles to optimize realistic surfactant formulations. However, such an approach is empirical in nature and does not utilize any knowledge of the underlying physical principles that govern surfactant self-assembly. To our knowledge, the only models that have been developed explicitly to describe the micellization of three or more surfactants utilize the pseudophase approximation and model interactions in the micelle pseudophase using either (1) ideal mixing[34] or, more commonly, (2) regular solution theory (RST).[37] In order to predict the critical micelle concentration (cmc) of a surfactant mixture, RST requires knowledge of the single-component cmc's and additional parameters that characterize the pairwise interactions of the micellized surfactants (often referred to as the β parameters). Empirically determining these parameters for multicomponent surfactant mixtures requires extensive cmc measurements.[38] Nevertheless, the completely empirical RST approach has been applied to several ternary surfactant mixtures.[37,184,195–199] A more predictive approach has also been utilized, in which the β parameters,[45] or both the single-surfactant cmc's and the β parameters,[38,46] are predicted using molecular-thermodynamic theories of single[39] and binary[4,40,41] surfactant systems.

The molecular-thermodynamic (MT) approach overcomes many of the inherent limitations of RST. Like RST, the MT approach enables the prediction of the cmc and the monomer concentration, as well as of the monomer and the micelle compositions. However, unlike RST, the MT approach can also predict the shape and size of micelles, because it does not rely on the pseudophase approximation, where micelles are assumed to be infinitely large. Furthermore, the MT approach is completely predictive at the molecular level, in that it requires solely knowledge of the molecular structures of the surfactants involved and of the solution conditions (such as the total surfactant concentration, the temperature, and the type and concentration of any added salt). The MT approach has also been extended recently to model the effects of monovalent and multivalent counterion binding in single[42,43] and binary surfactant mixtures[138] (see also Chapter 2), and the micellization of pH-sensitive surfactants[190]

(see also Chapter 3).

However, to date, no MT theory has been developed to model mixtures of three or more surfactants. In this chapter, we develop such a theory and compare predicted micellization properties of ternary surfactant mixtures, as well as of a multicomponent commercial surfactant, to available experimental data and to empirical calculations carried out using RST or the ideal-mixing approximation. The new theory is a natural generalization of a theory developed in Chapter 6 to model mixtures of pH-sensitive and conventional surfactants, which are ternary surfactant mixtures of the conventional surfactant and the protonated and deprotonated forms of the pH-sensitive surfactant. Since the primary goal of this thesis is to model the micellization behavior of pH-sensitive surfactants, the validation of the theory for conventional surfactants presented in this chapter is limited in its scope. Nevertheless, the new theory presented here may serve as a useful modeling tool for future research in the area of micellization of multicomponent surfactant mixtures.

The remainder of this chapter is organized as follows. In section 5.2, the thermodynamic and the molecular components of the theory are described. The prediction of various micellar solution properties in the context of the MT theory is discussed in section 5.3. In section 5.4, the theory is utilized to gain physical insight into the micellization behavior of ternary surfactant mixtures. The predictions are also compared to available experimental data for several ternary surfactant mixtures and for a multicomponent commercial surfactant. Finally, concluding remarks are presented in section 5.5.

5.2. Theory

The MT theory is developed here for an arbitrary number of surfactants, including any combination of ionic, nonionic, or zwitterionic surfactants. The basic thermodynamic framework is based on a theory developed initially by our group to model the micellization of a single nonionic surfactant,[39] and later extended to model the micellization of binary mixtures of nonionic surfactants[40,41] (the reader is also referred

to ref 36 for a comprehensive review of other available theories of micellization). Electrostatic interactions are modeled using a formalism first applied to model binary surfactant mixtures containing charged surfactants.[4] Explicit counterion binding was incorporated recently into the theory in order to more accurately model ionic surfactants.[42,43] The theoretical framework presented below incorporates all of these advances, and is essentially a further generalization of a recently developed theoretical description of counterion binding to mixed micelles composed of ionic/nonionic or ionic/zwitterionic binary surfactant mixtures[138] (see also Chapter 2).

In section 5.2.1, we first present the thermodynamic framework to model the micellar equilibrium. In section 5.2.2, we briefly discuss the molecular model used to compute the free energy of micellization.

5.2.1. Thermodynamic Framework

The thermodynamic framework is developed for an arbitrary number of surfactant components, which we denote as n_{surf}. Since multiple counterions may also be present in the aqueous solution, the number of counterions is denoted as n_{ion}. We begin by writing an expression for the thermodynamic equilibrium of a micelle consisting of n surfactant molecules, where $n\alpha_i$ are of type i ($i = 1$ to n_{surf}), and of $n\hat{\beta}_j$ bound counterions of type j ($j = 1$ to n_{ion}). Note that $\{\alpha_i\}$ denotes the composition of the surfactants of type i in the micelle (which we subsequently refer to as the *micelle composition*), and $\{\hat{\beta}_j\}$ denotes the numbers of bound counterions of type j per surfactant molecule in the micelle. The more traditional degree of counterion binding of ion j, denoted by β_j, and defined as the number of bound counterions of type j per ionic surfactant in the micelle, is then related to $\hat{\beta}_j$ as follows[138] (see also Chapter 2):

$$\beta_j \;=\; \hat{\beta}_j / \left|z_{\text{mic}}\right| \tag{5.1}$$

where $z_{\text{mic}} = \sum_i z_i \alpha_i$ is the average valence of a surfactant in the micelle.

Using this notation, we obtain the following expression characterizing the condition of thermodynamic equilibrium between the micelles, the surfactant

monomers, and the free counterions[138] (see also Chapter 2):

$$X_{n\{\alpha_i,\hat{\beta}_j\}} = \frac{1}{e}\left(\prod_i X_{1i}^{n\alpha_i}\right)\left(\prod_j X_{1j}^{n\hat{\beta}_j}\right)\exp\left[-\frac{n}{k_{\mathrm{B}}T}g_{\mathrm{mic}}\left(S, l_{\mathrm{c}}, \{\alpha_i\}, \{\hat{\beta}_j\}\right)\right] \tag{5.2}$$

where X_{1i} denotes the mole fraction of surfactant species i in monomeric form, X_{1j} denotes the mole fraction of free (unbound) ions of type j, $X_{n\{\alpha_i,\hat{\beta}_j\}}$ denotes the mole fraction of micelles of type $n\{\alpha_i, \hat{\beta}_j\}$, k_{B} is the Boltzmann constant, T is the absolute temperature, and g_{mic} is the free energy of micellization. The quantity g_{mic} represents the free-energy gain per surfactant molecule associated with forming a micelle (an $n\{\alpha_i, \hat{\beta}_j\}$-mer) from $n\alpha_i$ surfactant monomers of type i and $n\hat{\beta}_j$ counterions of type j. Note that g_{mic} is a function of the following micelle characteristics: the shape factor (S), the core minor radius (l_{c}), the micelle composition ($\{\alpha_i\}$), and the degrees of counterion binding ($\{\hat{\beta}_j\}$). The shape factor S is 3 for spherical micelles, 2 for cylindrical micelles, and 1 for planar or discoidal micelles.[39] Note that l_{c} refers to the radius of the hydrophobic core of spherical or cylindrical micelles, or to the half-width of the hydrophobic core of planar or discoidal micelles.[39]

The micelle equilibrium can also be written in terms of the total concentration of the surfactant monomers, $X_1 = \sum_i X_{1i}$, as follows[138] (see also Chapter 2):

$$X_{n\{\alpha_i,\hat{\beta}_j\}} = \frac{1}{e}X_1^n \exp\left[-\frac{n}{k_{\mathrm{B}}T}g_{\mathrm{m}}\right] \tag{5.3}$$

where g_{m} is the modified free energy of micellization, defined as[4,42,138] (see also Chapter 2):

$$g_{\mathrm{m}} = g_{\mathrm{mic}} - k_{\mathrm{B}}T\left[\sum_i \alpha_i \ln \alpha_{1i} + \sum_j \hat{\beta}_j \ln X_{1j}\right] \tag{5.4}$$

Note that $\alpha_{1i} = X_{1i}/X_1$ is the fraction of the surfactant monomers of type i (referred to hereafter as the *monomer composition*).

Each species is also subject to a mass balance that equates its total mole fraction to its mole fraction in the bulk solution plus its mole fraction in the micelles. Following the methodology described in Chapter 2 and in ref 138, the mass balances are given

by the following two equations:

$$\alpha_i^{\text{total}} X_{\text{S}}^{\text{total}} = \alpha_{1i} X_1 + \sum_{S,n,l_c,\{\alpha_i,\hat{\beta}_j\}} n\alpha_i X_{n\{\alpha_i,\hat{\beta}_j\}} + E_{\text{dl},i} \tag{5.5}$$

$$X_j^{\text{total}} = X_{1j} + \sum_{S,n,l_c,\{\alpha_i,\hat{\beta}_j\}} n\hat{\beta}_j X_{n\{\alpha_i,\hat{\beta}_j\}} + E_{\text{dl},j} \tag{5.6}$$

where α_i^{total} is the overall composition of surfactant i, $X_{\text{S}}^{\text{total}}$ is the total concentration of surfactant, the summations in eqs 5.5 and 5.6 account for micelles of different types (that is, having different values of S, n, l_c, $\{\alpha_i\}$, and $\{\hat{\beta}_j\}$), and $E_{\text{dl},i}$ and $E_{\text{dl},j}$ are terms accounting for the depletion, or the enhancement, of the surfactant monomers and the ions, respectively, in the diffuse layer (dl), relative to their concentrations in the bulk solution (see Appendix A for details).

In summary, the experimentally known quantities (α_i^{total}, $X_{\text{S}}^{\text{total}}$, and X_j^{total}) are used, along with eqs 5.3, 5.5, and 5.6, to solve for the solution conditions ($\{\alpha_{1i}\}$, X_1, $\{X_{1j}\}$, and $X_{n\{\alpha_i,\hat{\beta}_j\}}$). Note that eq 5.3 depends also on g_{m}, whose calculation requires a model for the free energy of micellization, g_{mic}, which we describe next in section 5.2.2.

5.2.2. Molecular Model for the Free Energy of Micellization

The g_{mic} model for multicomponent surfactant micelles is a generalization of the g_{mic} model developed for binary surfactant mixtures with counterion binding[138] (see also Chapter 2). In this section, we briefly summarize the various contributions to the generalized g_{mic} model without presenting specific equations (note that the key equations of the g_{mic} model are provided in Appendix E, which may be useful in helping the reader to more clearly rationalize the results presented in section 5.4).

The free energy of micellization, g_{mic}, is modeled as the sum of six contributions[138] (see also Chapter 2):

$$g_{\text{mic}} = g_{\text{tr}} + g_{\text{int}} + g_{\text{pack}} + g_{\text{st}} + g_{\text{elec}} + g_{\text{ent}} \tag{5.7}$$

The first three contributions are associated with the formation of the micelle core: The transfer contribution, g_{tr}, accounts for the transfer of the surfactant hydrophobic tails from an aqueous to an oil-like environment (see eq E.1). The interfacial contribution, g_{int}, accounts for the free-energy penalty associated with the formation of an interface between the oil-like micelle core and the surrounding aqueous environment (see eq E.2). The packing contribution, g_{pack}, accounts for the additional entropic constraints associated with anchoring one end of each surfactant hydrophobic tail at the micelle core-water interface (see eq E.3). The fourth and fifth contributions are associated with the formation of the micelle interfacial region: The steric contribution, g_{st}, accounts for the steric interactions between the surfactant hydrophilic heads and the bound counterions in the micelle interfacial region (see eq E.4). The electrostatic contribution, g_{elec}, accounts for the electrostatic interactions at the micelle interface that operate in the case of ionic surfactants and bound counterions, and of zwitterionic surfactants (see eqs E.6-E.10). The last contribution, g_{ent}, accounts for the entropy of mixing the various components in a micelle (see eq E.5).

5.3. Determination of Useful Micellar Solution Properties

To determine various useful micellar solution properties, we simultaneously solve the mass balances (eqs 5.5 and 5.6) along with the equilibrium condition for micelle formation (eq 5.3). In these mass balances, the summations are in general over the mole fractions of micelles of every possible shape (S), aggregation number (n), core minor radius (l_{c}), composition ($\{\alpha_i\}$), and degrees of counterion binding ($\{\hat{\beta}_j\}$). Explicitly carrying out these summations would be computationally challenging, but fortunately, it is not necessary. Indeed, as shown previously[4,42,138] (see also Chapter 2), these summations can be approximated reasonably well by summations over the micelle aggregation number, n, where the optimal micelle shape (S^*), optimal core minor radius (l_{c}^*), optimal composition ($\{\alpha_i^*\}$), and optimal degrees of counterion

binding ($\{\hat{\beta}_j^*\}$) are determined by minimizing g_m (see eq 5.4) for a given aggregation number, n, with respect to S, l_c, $\{\alpha_i\}$, and $\{\hat{\beta}_j\}$, respectively. The resulting optimal value of g_m is denoted as g_m^*. This approximation then allows the calculation of additional micellar solution properties of interest, in particular, of the cmc. Since we will also be examining the maximum micelle radius (see section 5.4.1), we also present a theoretical derivation of the maximum micelle radius in section 5.3.2.

5.3.1. Calculating the Critical Micelle Concentration and Average Micelle Aggregation Numbers

The cmc is defined (in mole fraction units) as $\exp(g_m^*/k_BT)$, where g_m^* is the optimal modified free energy of micellization of the preferred micelle shape (having optimal values S^*, l_c^*, $\{\alpha_i^*\}$, and $\{\hat{\beta}_j^*\}$) at the given solution conditions.[39] Note that this definition still requires self-consistently solving the mass balances (eqs. 5.5 and 5.6), where the total concentration of surfactant is equal to the cmc. Because the cmc is defined in terms of the total surfactant concentration, the monomer concentration at the cmc is always slightly less than the cmc, since some of the surfactant will be present in micelles. Perhaps more importantly, the theory also allows the prediction of the monomer concentration at any surfactant concentration. As will be shown in section 5.4.3, in multicomponent surfactant mixtures, the monomer concentration can vary significantly with the surfactant concentration, due to changes in g_m^* with surfactant concentration.

In practice, our model for g_m is only applicable to "regular" micelle shapes (spherical micelles, infinite cylindrical micelles, and infinite planar bilayers), primarily due to restrictions imposed on our models for g_{pack} and g_{elec}.[4,39,42] The surfactants considered in this chapter are anticipated to form spherical or cylindrical micelles, and therefore, we do not consider finite bilayer (discoidal) micelles. We estimate g_m for finite cylindrical micelles by interpolating between the g_m values corresponding to the regular micelle shapes. Specifically, the interpolation equation can be conveniently expressed in terms of the growth parameter, $\Delta\mu$, which models the difference between

g_{m} of a spherical micelle and g_{m} of an infinite cylindrical micelle, and is given by[41]

$$\Delta\mu = g^*_{\mathrm{m,sph}} - g^*_{\mathrm{m,cyl}} \tag{5.8}$$

where $g^*_{\mathrm{m,sph}}$ and $g^*_{\mathrm{m,cyl}}$ are the optimal modified free energies of micellization (see eq 5.4) for spheres and for infinite cylinders, respectively. The modified free energy of micellization of a finite cylindrical micelle of aggregation number n (where $n > n_{\mathrm{sph}}$), denoted as $g^*_{\mathrm{m}}(n)$, is then given by[41]

$$g^*_{\mathrm{m}}(n) = g^*_{\mathrm{m,cyl}} + \left(n^*_{\mathrm{sph}}/n\right)\Delta\mu \tag{5.9}$$

where n^*_{sph} is the aggregation number of an optimal spherical micelle. Note that if $\Delta\mu$ is negative, cylindrical micelles are unfavorable. Conversely, if $\Delta\mu$ is positive, finite cylindrical micelles will form. In the limit of extensive cylindrical micelle growth, the average aggregation numbers depend exponentially on $\Delta\mu$:[144]

$$\langle n\rangle_{\mathrm{n}} = n^*_{\mathrm{sph}} + \left[\exp\left(n^*_{\mathrm{sph}}\Delta\mu/k_{\mathrm{B}}T\right)X_{\mathrm{mic}}\right]^{1/2} \tag{5.10}$$

$$\langle n\rangle_{\mathrm{w}} = n^*_{\mathrm{sph}} + 2\left[\exp\left(n^*_{\mathrm{sph}}\Delta\mu/k_{\mathrm{B}}T\right)X_{\mathrm{mic}}\right]^{1/2} \tag{5.11}$$

where $\langle n\rangle_{\mathrm{n}}$ and $\langle n\rangle_{\mathrm{w}}$ are the number-average and the weight-average micelle aggregation numbers, respectively, and $X_{\mathrm{mic}} = X_{\mathrm{S}}^{\mathrm{total}} - X_1$ denotes the mole fraction of surfactant that is in micelles. If the optimal micelle shape is spherical, we approximate the micelle size distribution as being monodisperse, and therefore, $\langle n\rangle_{\mathrm{n}} = \langle n\rangle_{\mathrm{w}}$. Due to a lack of experimental data, aggregation number predictions will not be presented. However, eqs 5.10 and 5.11 will be used to rationalize the behavior of the micelle composition in a multicomponent surfactant mixture (see section 5.4.3).

5.3.2. Theoretical Model for the Maximum Micelle Radius

Although the general shape and size of a micelle can vary widely depending on the structure of the surfactant and on the solution conditions, there is an upper

limit to the micelle radius that should be considered in any theoretical description. For single-surfactant micelles, the maximum radius of a micelle, $r_{\max}$, is simply the length of the fully extended surfactant tail, because a larger radius would lead to the formation of a hole in the center of the micelle. In the case of mixed micelles, the maximum radius depends on the shape and on the composition of the mixed micelle, in which case, the assumption that $r_{\max}$ is equal to the length of the longest surfactant tail may overestimate the value of $r_{\max}$. For example, Szleifer et al. estimated $r_{\max}$ for a mixed micelle composed of a mixture of C_{11} and C_5 chains (where C_i denotes a hydrocarbon chain containing i carbon atoms).[103] These authors found that the mixed micelle must contain at least 15% of the C_{11} chains in the case of spherical micelles, or at least 33% of the C_{11} chains in the case of cylindrical micelles, in order for $r_{\max}$ to correspond to the length of a fully extended C_{11} chain.[103] In their calculation, $r_{\max}$ was estimated by considering what volume of the C_{11} chains is available to the central core of the micelle while being simultaneously unreachable by the C_5 chains.

The algebraic expression for $r_{\max}$ obtained by Szleifer et al.[103] is generalized below to micelles containing any number of surfactant tails. For simplicity, we first derive the result for ternary surfactant mixtures, and then present the general result for $n_{\text{surf}} > 3$. Consider a micelle composed of the three surfactant tails, denoted as tails 1, 2, and 3, with 1 being the shortest and 3 being the longest. The volume, fully extended length, and micelle composition of tail i are denoted as v_i, l_i, and α_i, respectively. Note that the derivation also assumes that all the tails have the same cross-sectional area (a_0) when fully extended, so that $v_i = a_0 l_i$ for all i. This assumption will be satisfied when all the tails are linear hydrocarbons, which is the case for all the surfactants considered in this chapter, or when all the tails are linear fluorocarbons. Although more general expressions can be derived for other surfactant mixtures, they are beyond the scope of this thesis.

The value of $r_{\max}$ of the micelle is the minimum of $\{r_{\max}^{(i)}\}$ ($i = 1$, 2, or 3), where the $r_{\max}^{(i)}$ values are determined by the following three conditions: (1) $r_{\max}^{(1)} > l_1$ and the inner core (defined below) contains the maximum possible volume of tails 2 and 3, (2) $r_{\max}^{(2)} > l_2$ and the inner core contains the maximum possible volume of tails 3,

or (3) $r_{\max}^{(3)} = l_3$. The inner-core volume for condition i (1 or 2) refers to the region in a micelle of radius $r_{\max}^{(i)}$ that extends from the center of the micelle to a radius of $r_{\max}^{(i)} - l_i$, that is, to the region that is inaccessible to the tails of type i. The specific algebraic constraints corresponding to $r_{\max}^{(1)}$ and $r_{\max}^{(2)}$ are obtained by equating the inner-core volume to the "available" tail volume. The "available" tail volume is an excess volume per surfactant defined as $\Delta v_i = v_i - v_1$ ($i = 2$ and 3) for condition (1), or as $\Delta v_3 = v_3 - v_2$ for condition (2). Specifically, the following relations are obtained:

$$C_S \left(r_{\max}^{(1)} - l_1\right)^S = n\alpha_2 (v_2 - v_1) + n\alpha_3 (v_3 - v_1) \tag{5.12}$$

$$C_S \left(r_{\max}^{(2)} - l_2\right)^S = n\alpha_3 (v_3 - v_2) \tag{5.13}$$

where n is the micelle aggregation number and S is the shape factor of the micelle (3 for spheres, 2 for cylinders, and 1 for bilayers). C_S is a prefactor used to calculate the micelle volume, corresponding to $4\pi/3$ for spheres, πL for cylinders (where L is the length of the cylinder), and $2A$ for bilayers (where A is the surface area of the bilayer leaflet). Also, note that $r_{\max}$ refers to the maximum half-width of a bilayer. The dependence on n can be removed from eqs 5.12 and 5.13 by dividing each equation by the volume of the micelle core, which is given by both $C_S \left(r_{max}^{(j)}\right)^S$ and $n \sum_i \alpha_i v_i$, resulting in the following two expressions:

$$\left(\frac{r_{\max}^{(1)} - l_1}{r_{\max}^{(1)}}\right)^S = \frac{\alpha_2 (v_2 - v_1) + \alpha_3 (v_3 - v_1)}{\sum_i \alpha_i v_i} \tag{5.14}$$

$$\left(\frac{r_{\max}^{(2)} - l_2}{r_{\max}^{(2)}}\right)^S = \frac{\alpha_3 (v_3 - v_2)}{\sum_i \alpha_i v_i} \tag{5.15}$$

Similarly, the maximum radius for a mixture containing t different surfactant tails (numbered 1 to t from shortest to longest) is the smallest of l_t and $\{r_{\max}^{(i)}\}$ ($i =$

1 to $(t-1)$), with $r_{\max}^{(i)}$ given by the following expression:

$$\left(\frac{r_{\max}^{(i)} - l_i}{r_{\max}^{(i)}}\right)^S = \frac{\sum_{k=i}^{t} \alpha_k \left(v_k - v_i\right)}{\sum_{k=1}^{t} \alpha_k v_k} \tag{5.16}$$

Note that eq 5.16 reduces to the result obtained by Szleifer et al.[103] when $t = 2$, and to eqs 5.14 and 5.15 when $t = 3$.

In section 5.4.1, predicted $r_{\max}$ values, using eqs 5.14 and 5.15, will be compared to the $r_{\max}$ values predicted using explicit g_{pack} calculations.

5.4. Results and Discussion

The majority of the available experimental data on the micellization of multicomponent surfactant mixtures is restricted to ternary surfactant mixtures, with particular emphasis on measured cmc's. As a result, the new theory presented in this chapter is validated primarily for ternary surfactant mixtures. With this in mind, in section 5.4.1, we examine theoretically the behavior of the maximum micelle radius, $r_{\max}$, of a sample ternary surfactant mixture. In section 5.4.2, we consider theoretically and experimentally the cmc's of several ternary surfactant mixtures. Finally, in section 5.4.3, we consider theoretically the cmc, the monomer concentration, and the monomer and the micelle compositions of a polydisperse ($n_{\text{surf}} > 3$) commercial surfactant.

5.4.1. Comparison of $r_{\max}$ Values Predicted Using Eqs 5.14 and 5.15 and Explicit g_{pack} Calculations

Since the free energy of micellization depends on the micelle radius, the radius of a mixed micelle is of theoretical importance. Furthermore, practical applications may also benefit from the ability to control the micelle radius. For example, detergent formulations containing larger micelles may be less irritating to the skin than formulations containing smaller micelles, because the larger micelles are more

readily hindered from penetrating into the skin.[32] Similarly, applications involving the solubilization of poorly water-soluble compounds is aqueous vehicles (such as the formulation of water-insoluble drugs using aqueous micellar solutions) may benefit from a better understanding of how to control the micelle radius, since a larger hydrophobic micelle core will enable an enhanced drug solubilization capacity.[200] The micelle radius is also directly related to other micelle characteristics of practical relevance, including the micelle surface charge density and the average micelle surface area per surfactant molecule.

Although the *optimal* micelle radius is typically predicted by minimizing g_{m} (see section 5.3), the *maximum* micelle radius is determined solely by the packing constraints (as modeled in g_{pack}). As a general rule, the micelle radius that minimizes g_{pack} is also strongly correlated to the maximum micelle radius. In particular, the optimal g_{pack} for bilayer micelles composed of linear hydrocarbons is typically attained when the bilayer thickness is approximately equal to half of the maximum bilayer thickness, while the optimal g_{pack} for cylindrical and spherical micelles is typically attained when the micelle radius is approximately equal to 70% and 90% of the maximum micelle radius, respectively (data not shown).

Theoretical expressions for the maximum micelle radius, r_{max}, as a function of the micelle composition were presented in section 5.3.2 (see eqs 5.14 and 5.15). In practice, it may be extremely difficult to form micelles with radii close to the theoretical r_{max} value, which may be reflected in the inability to solve the mean-field equations that determine g_{pack}. Therefore, the mean-field model of g_{pack} may yield a more reasonable estimate of the physically realizable maximum micelle radius. Below, the maximum micelle radius predicted using eqs 5.14 and 5.15 ($r_{\mathrm{max}}^{(\mathrm{theory})}$) is compared to the maximum micelle radius predicted from the mean-field g_{pack} calculations ($r_{\mathrm{max}}^{(\mathrm{g_{pack}})}$) for a representative mixture of three surfactant tails, specifically, of C_7, C_{11}, and C_{15} tails. Note that odd-numbered tail lengths were selected since most of the surfactants considered in this chapter are modeled as containing an odd number of carbon atoms in their hydrophobic tails (see section 2.3.1 in Chapter 2). The specific tail lengths selected span the lengths of surfactant tails considered in this chapter, while ensuring

a relatively large length difference between each tail. Note that the fully extended tail lengths of the C_7, C_{11}, and C_{15} tails are approximately 10.4 Å, 15.4 Å, and 20.5 Å, respectively.[1]

In Figure 5-1, we show contour plots of $r_{\max}$ as a function of the micelle composition, with the various colors denoting the $r_{\max}$ values, as indicated in the color-bar scales. The left-hand side plots on each figure correspond to $r_{\max}^{(\text{theory})}$, and the right-hand side plots to $r_{\max}^{(g_{\text{pack}})}$. The top plots correspond to bilayer micelles, the middle plots to cylindrical micelles, and the bottom plots to spherical micelles. Note that the contour lines for $r_{\max}^{(g_{\text{pack}})}$ are not smooth due to the discretization done in the g_{pack} calculations. A more refined discretization was used for the bilayer calculations, because these data were less smooth. Specifically, the bilayer half-widths were discretized into 0.25 Å increments, while the radii of the cylindrical and the spherical micelles were discretized into 0.5 Å increments. In addition, the ternary composition space was discretized into composition intervals of 0.03 for the bilayers, and of 0.09 for the cylinders and the spheres.

As can be seen, in the case of bilayer micelles, $r_{\max}^{(g_{\text{pack}})} \approx r_{\max}^{(\text{theory})}$, within the noise introduced by the discretization. The contour lines are nearly vertical, indicating that $r_{\max}$ is almost unchanged if two C_{11} tails are replaced with a C_7 and a C_{15} tail. This invariance arises because: (1) eqs 5.14 and 5.15 indicate that the maximum half-width of a bilayer is equal to the composition average of the fully extended tail lengths of the surfactants ($\sum \alpha_i l_i$), and (2) the fully extended length of a C_{11} tail is exactly halfway between those of a C_7 and a C_{15} tail ($l_{11} = \frac{1}{2} l_7 + \frac{1}{2} l_{15}$).

In the case of cylindrical micelles, a slight discrepancy is observed, in that $r_{\max}^{(\text{theory})}$ is slightly larger than $r_{\max}^{(g_{\text{pack}})}$ at most compositions. For example, the large dark-red region in the $r_{\max}^{(\text{theory})}$ plot (where $r_{\max}^{(\text{theory})} \approx 20.5\,\text{Å}$) corresponds to a light-red region in the $r_{\max}^{(g_{\text{pack}})}$ plot (where $r_{\max}^{(g_{\text{pack}})} \approx 20.0\,\text{Å}$). However, the qualitative behavior of $r_{\max}^{(\text{theory})}$ and $r_{\max}^{(g_{\text{pack}})}$ is very similar. In particular, the red regions discussed above cover very similar composition ranges. These regions correspond to compositions for which $r_{\max}$ is approximately equal to l_{15}. To attain this $r_{\max}$, the minimum amount of C_{15} tails required decreases from approximately 35% (when no C_{11} tails are present)

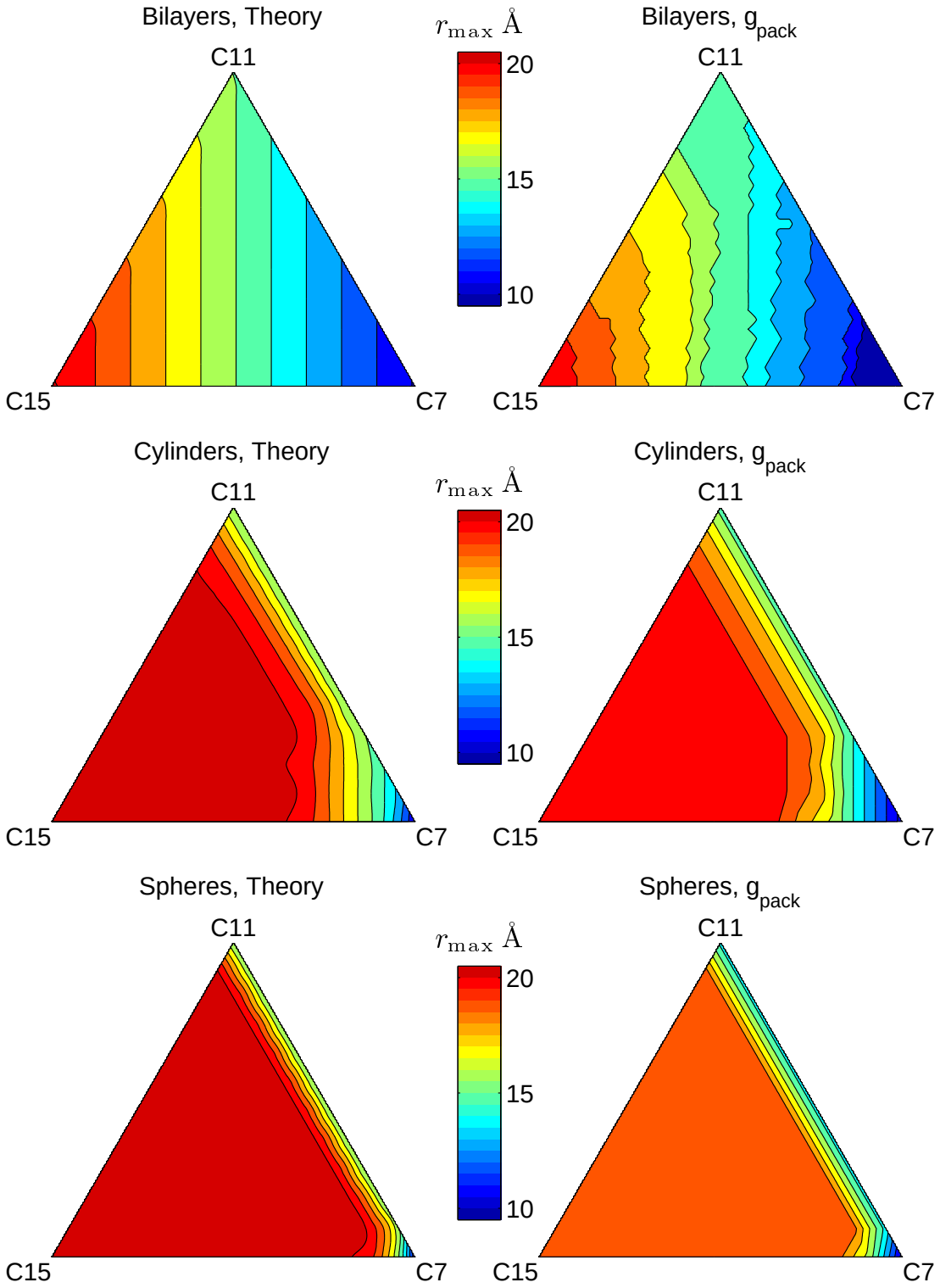

Figure 5-1: Comparison of $r_{\max}^{(\text{theory})}$ (left-hand side plots) and $r_{\max}^{(\text{g}_{\text{pack}})}$ (right-hand side plots) of micelles containing C_7, C_{11}, and C_{15} tails. The top plots correspond to bilayer micelles, the middle plots to cylindrical micelles, and the bottom plots to spherical micelles. The various colors shown correspond to the particular values of the maximum radii, as indicated in the color-bar scales.

to approximately 20% (when the micelle contains more than approximately 30% of the C_{11} tails).

Spherical micelles also show qualitative agreement between $r_{max}^{(g_{pack})}$ and $r_{max}^{(theory)}$. However, there is a larger difference in the absolute values, as illustrated by the large dark-red region in the $r_{max}^{(theory)}$ plot (where $r_{max}^{(theory)} \approx 20.5\,\text{Å}$) corresponding to the orange region in the $r_{max}^{(g_{pack})}$ plot (where $r_{max}^{(g_{pack})} \approx 19.0\,\text{Å}$). This discrepancy may be due to inadequate sampling during the g_{pack} calculations: although fewer long surfactant chains are needed in the case of large spherical micelles, the small micelle compositions and the small core volumes also require greater sampling to accurately solve the mean-field equations. In contrast to cylindrical micelles, very few C_{15} tails are required for r_{max} to correspond to the C_{15} limit: as indicated by the borders of the regions discussed above, the minimum amount of C_{15} tails required decreases from approximately 15% (when no C_{11} tails are present) to 10% (when the micelle contains more than approximately 10% of the C_{11} tails). A practical consequence of this finding is that even small fractions of long-tailed surfactants can potentially lead to large changes in micelle radii.

5.4.2. Prediction of cmc's of Ternary Surfactant Mixtures

5.4.2.1. The cmc's of a Homologous Series of Cationic Surfactants

In this section, predicted cmc's are compared to experimental cmc's for equimolar mixtures of ternary combinations of alkyl trimethylammonium bromide (C_iTAB) surfactants with tail lengths of i = 8, 10, 12, 14, and 16. The cmc's were determined experimentally by Murphy and Taggart at 30°C using surface tension and conductivity measurements.[201] Before considering the ternary surfactant mixtures, the theory was first validated in the case of the single cationic surfactants. In Figure 5-2, cmc's predicted using the MT theory (black bars) are compared to the experimental cmc's (white bars). Note that no experimental uncertainties were reported for these measurements, although a typical value is 5%. As can be seen, the predicted cmc's agree well with the experimental cmc's: the predictions for the

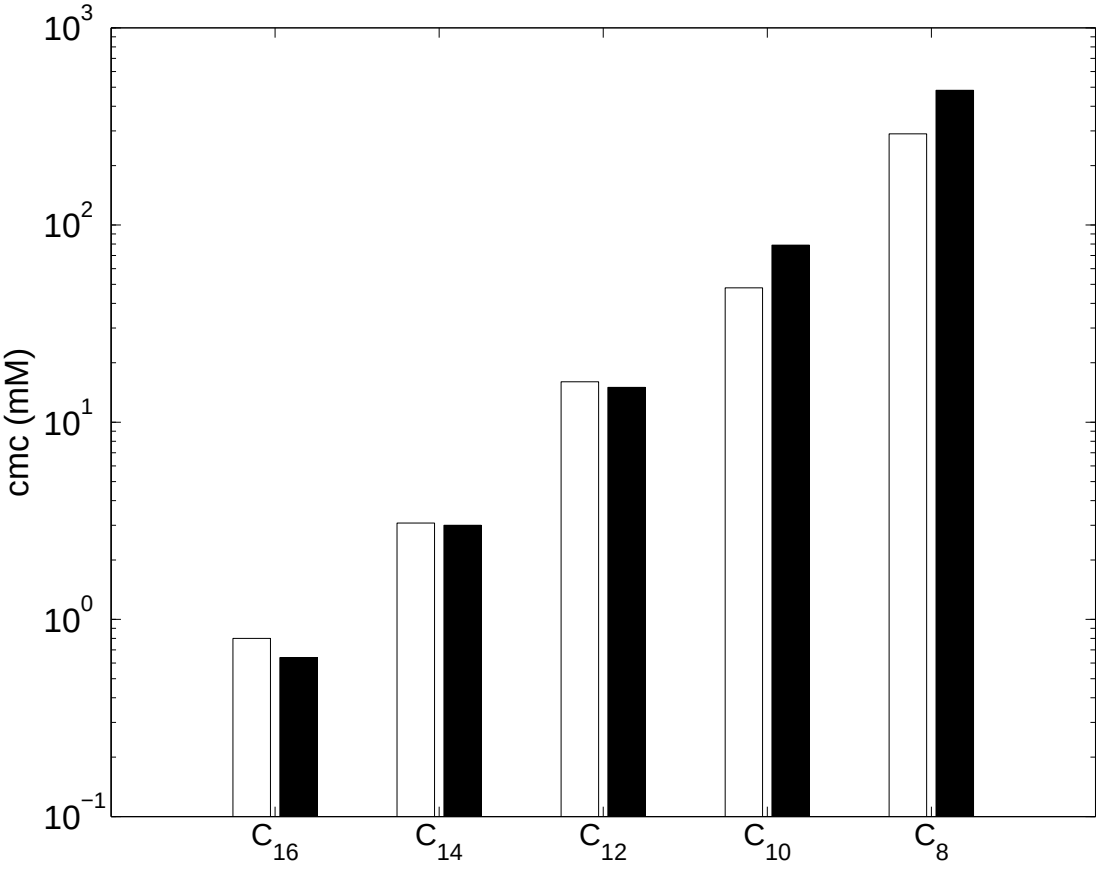

Figure 5-2: The cmc's of C_iTAB homologues (i = 8, 10, 12, 14, and 16) at 30°C. Predicted cmc's using the MT theory (black bars) are compared to the experimental cmc's (white bars) reported by Murphy and Taggart.[201]

C_{12}, C_{14}, and C_{16} homologues are within 20% of the experimental values, and the predictions for the C_8 and C_{10} homologues are within 70% of the experimental values.

Predicted and experimental cmc's were next compared for representative equimolar ternary surfactant mixtures. In Figure 5-3, the average experimental cmc's correspond to the white bars, with the error bars denoting standard deviations of cmc's measured using surface tension and conductivity. The grey bars correspond to the predictions of Murphy and Taggart using RST and experimental cmc data obtained for single-surfactant and binary-surfactant systems. The black bars correspond to the cmc's predicted using the MT theory. Good agreement is observed between the theoretical and the experimental cmc's, an agreement which is comparable to that obtained using the empirical RST. The predicted cmc's for ternary mixtures containing C_8 and C_{10} tails are slightly overpredicted, primarily because the cmc's of the short-tails C_iTAB homologues are also overpredicted (see Figure 5-2).

Although the data are not shown, we also examined cmc predictions using other cmc definitions (for example, the concentration at which 5% of the surfactant is in micelles). Interestingly, although the various cmc definitions yielded very similar results for single-surfactant systems, a more significant difference was observed between cmc definitions in the case of ternary surfactant mixtures. This cmc definitions vary more significantly in surfactant mixtures because the transition from monomers to micelles is not as sharp in the mixed surfactant system case as it is in the single surfactant system case. Perhaps the most important practical consequence is that the monomer concentration can increase steadily above the cmc for mixed surfactant systems. This effect will be explored more fully in section 5.4.3.

5.4.2.2. The cmc's of a Cationic/Anionic/Nonionic Ternary Surfactant Mixture

Although some synergy is observed in the cationic ternary surfactant mixtures examined in section 5.4.2.1, much greater synergy is observed in the case of mixtures containing ionic/nonionic and cationic/anionic surfactant pairs. With this in mind,

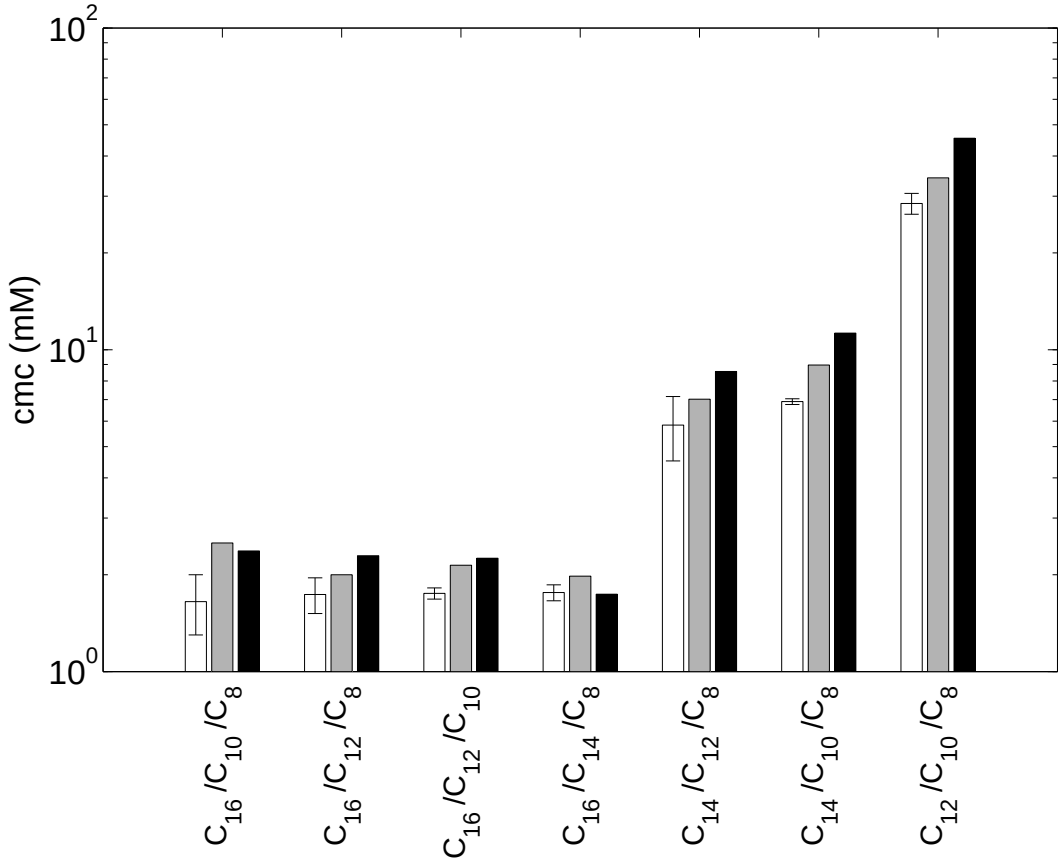

Figure 5-3: The cmc's of representative equimolar ternary mixtures of C_iTAB homologues (i = 8, 10, 12, 14, and 16). Predicted cmc's using the MT theory (black bars) and RST (grey bars) are compared to the experimental cmc's (white bars) reported by Murphy and Taggart.[201] The error bars correspond to the standard deviations of cmc's measured using two different experimental methods (surface tension and conductivity).

Table 5.1: Compositions of ternary mixtures of $NaC_{10}S$, $C_{10}TAB$, and C_8E_4 studied by Holland and Rubingh.[37]

	Component Composition		
Mixture	$NaC_{10}S$	$C_{10}TAB$	C_8E_4
A	0.224	0.207	0.569
B	0.360	0.334	0.306
C	0.628	0.194	0.178
D	0.216	0.601	0.183

in this section, we examine a cationic/anionic/nonionic ternary surfactant mixture, where each surfactant pair interacts strongly with each other. The specific cationic, anionic, and nonionic surfactants are $C_{10}TAB$, sodium decyl sulfate ($NaC_{10}S$), and octyl tetra(ethylene oxide) (C_8E_4), respectively. The experimental cmc's were determined by Holland and Rubingh using surface tension measurements for solutions containing 0.05 M NaBr (at 23°C).[37] The predicted and the experimental cmc's of single-surfactant and ternary-surfactant mixtures are compared in Figure 5-4. The compositions of the ternary surfactant mixtures studied (denoted as mixtures A, B, C, and D in Figure 5-4) are listed in Table 5.1.

As was observed in section 5.4.2.1, the predicted cmc's of the surfactants with C_8 and C_{10} tails are generally larger than their experimental values. Nevertheless, the predicted cmc's are within 40% of the experimental cmc's, except for the predicted cmc of $NaC_{10}S$, which is within a factor of 2 of the experimental cmc.

Figure 5-4 illustrates that the cmc's of the ternary surfactant mixtures studied are all very similar (1.3 to 1.9 mM), and significantly lower than any of the single-surfactant cmc's. Note that there is a relatively large uncertainty in reading the ternary cmc data from ref 37 (as indicated by the error bars in Figure 5-4), because these cmc's fall very close to the x-axis of the linear plot in which the data are presented. Therefore, it is difficult to discriminate between the various ternary surfactant mixtures. Having said that, Mixture A, which is rich in the nonionic C_8E_4

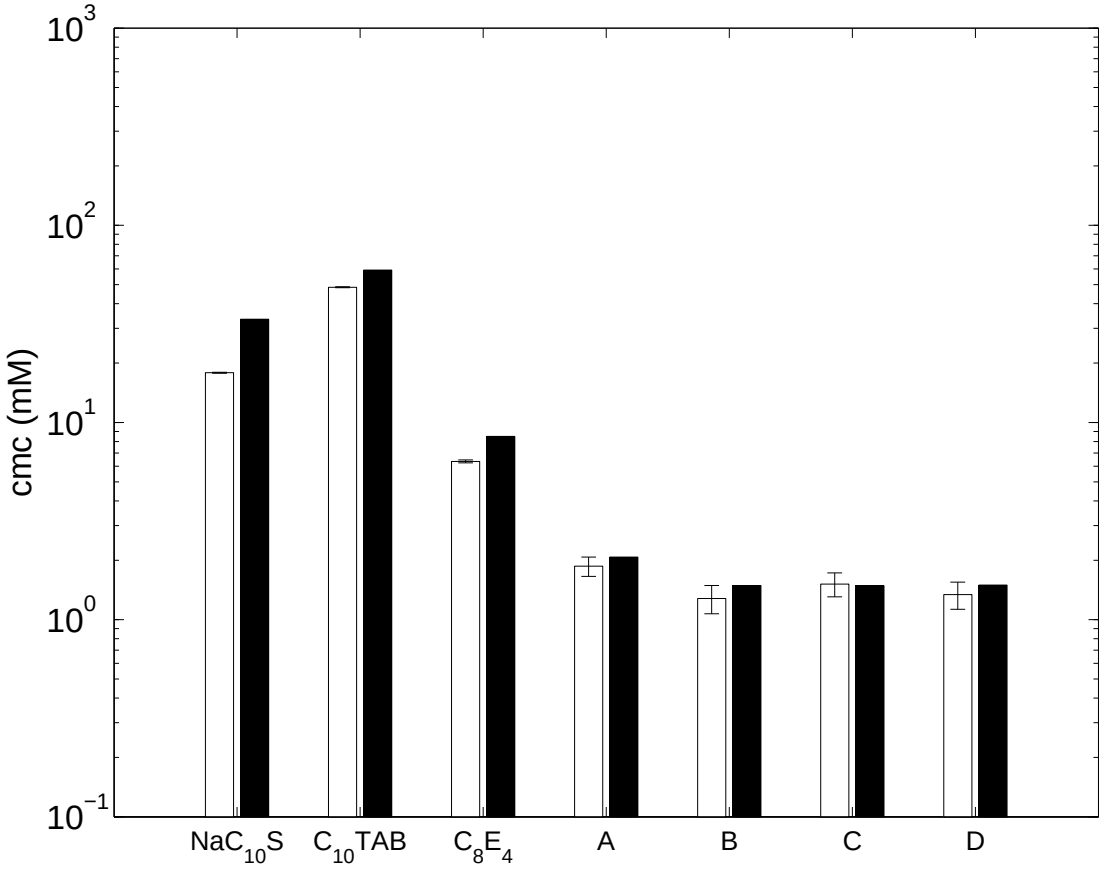

Figure 5-4: The cmc's of single components and ternary mixtures of the anionic surfactant $NaC_{10}S$, the cationic surfactant $C_{10}TAB$, and the nonionic surfactant C_8E_4 for solutions containing 0.05 *M* NaBr (at 23°C). The cmc's predicted using the MT theory are shown as black bars. The compositions of the ternary surfactant mixtures examined, denoted as A, B, C, and D, are listed in Table 5.1 The experimental cmc's (white bars) were reported by Holland and Rubingh.[37] The error bars on the experimental cmc data are the estimated uncertainties due to reading the cmc data from the figures in ref 37. The uncertainties of the single-surfactant cmc's are comparable to the thickness of the lines used to draw the white bars.

(see Table 5.1), appears to have a slightly larger experimental cmc, a trend that is clearly reproduced in the theoretical predictions. Both predicted and experimental cmc's are practically equal for the remaining three ternary surfactant mixtures, which represent a nearly equimolar system (Mixture B), an anionic-rich ternary mixture (Mixture C), and a cationic-rich ternary mixture (Mixture C).

In summary, the MT approach yields both qualitative and quantitative predictions of the cmc's of ternary surfactant mixtures with varying degrees of synergy. The cmc predictions are comparable to, and sometimes better than, those obtained in the context of RST. Note that the application of RST to ternary surfactant mixtures requires a minimum of six cmc measurements, including the measurement of three single-component cmc's and three cmc's of the corresponding binary surfactant mixtures (which are utilized to calculate the three β parameters). Therefore, the MT approach represents a significant improvement over RST, since determining the necessary RST parameters in the case of ternary surfactant mixtures requires significant experimental effort.

5.4.3. Prediction of Various Micellization Properties of a Commercial Nonionic Surfactant

A predictive micellization theory applicable to commercial surfactants could reduce the time and effort associated with trial-and-error formulation. More empirical modeling approaches, like RST, require experimental knowledge of single-surfactant and binary-surfactant cmc's, which may be very difficult, if not impossible, to obtain in the case of complex surfactant mixtures, where the individual surfactant components cannot be readily separated. In this section, we validate the MT theory by applying it to a commercial nonionic surfactant, Genapol UD-079, which is a polydisperse ethoxylated alcohol (C_iE_j) with an undecyl tail ($i = 11$) and a Poisson distribution of head lengths, with an average head length of 7 ethoxy units ($\langle j \rangle = 7$). This commercial surfactant was modeled with the MT theory as a *mixture of 16 individual surfactant components* ($C_{11}E_0$ through $C_{11}E_{15}$), accounting for 99.8% of

the population of a complete Poisson distribution. The predicted cmc of 0.28 mM agrees remarkably well with the experimental cmc of 0.28 mM (with a reported error of 5%), determined from surface tension measurements by Reif et al.[38] Additional micellization properties of Genapol UD-079 are discussed in detail below in Sections 5.4.3.1 and 5.4.3.2.

5.4.3.1. Prediction of the Monomer and the Micelle Concentrations

In Figure 5-5, the predicted monomer concentration (solid line) and the micelle concentration (dashed line) are shown as a function of the total surfactant concentration, $X_{\mathrm{S}}^{\mathrm{total}}$. The concentration range examined was selected to span at least one order of magnitude below the cmc and two orders of magnitude above the cmc. Note that above the predicted cmc (indicated by the arrow in Figure 5-5), the monomer concentration continues to increase, albeit at a significantly slower rate than below the cmc. In particular, at $X_{\mathrm{S}}^{\mathrm{total}} = 100$ mM, the predicted monomer concentration is nearly four times larger than the cmc. If the surfactants present in the mixture have different tail lengths, the variation in the monomer concentration will be even greater. This behavior is similar to what was observed in solutions of polydisperse nonylphenol ethoxylates, in which the monomer concentration was measured by ultrafiltration.[202] It is noteworthy that single-component solutions of nonionic surfactants exhibit much less variation in their monomer concentration above the cmc.[203–205] The significant variation of the monomer concentration above the cmc in commercial (mixed) surfactant systems occurs because both the monomer and the micelle compositions change as the total surfactant concentration changes. These composition changes, in turn, lead to changes in the modified free energy of micellization, g_{m}, and consequently, to changes in the monomer concentration, which is approximately equal to $\exp(g_{\mathrm{m}}/k_{\mathrm{B}}T)$ above the cmc.

5.4.3.2. Prediction of the Monomer and the Micelle Compositions

The monomer and the micelle compositions are of both fundamental and practical importance. Indeed, the monomer composition affects properties that are governed

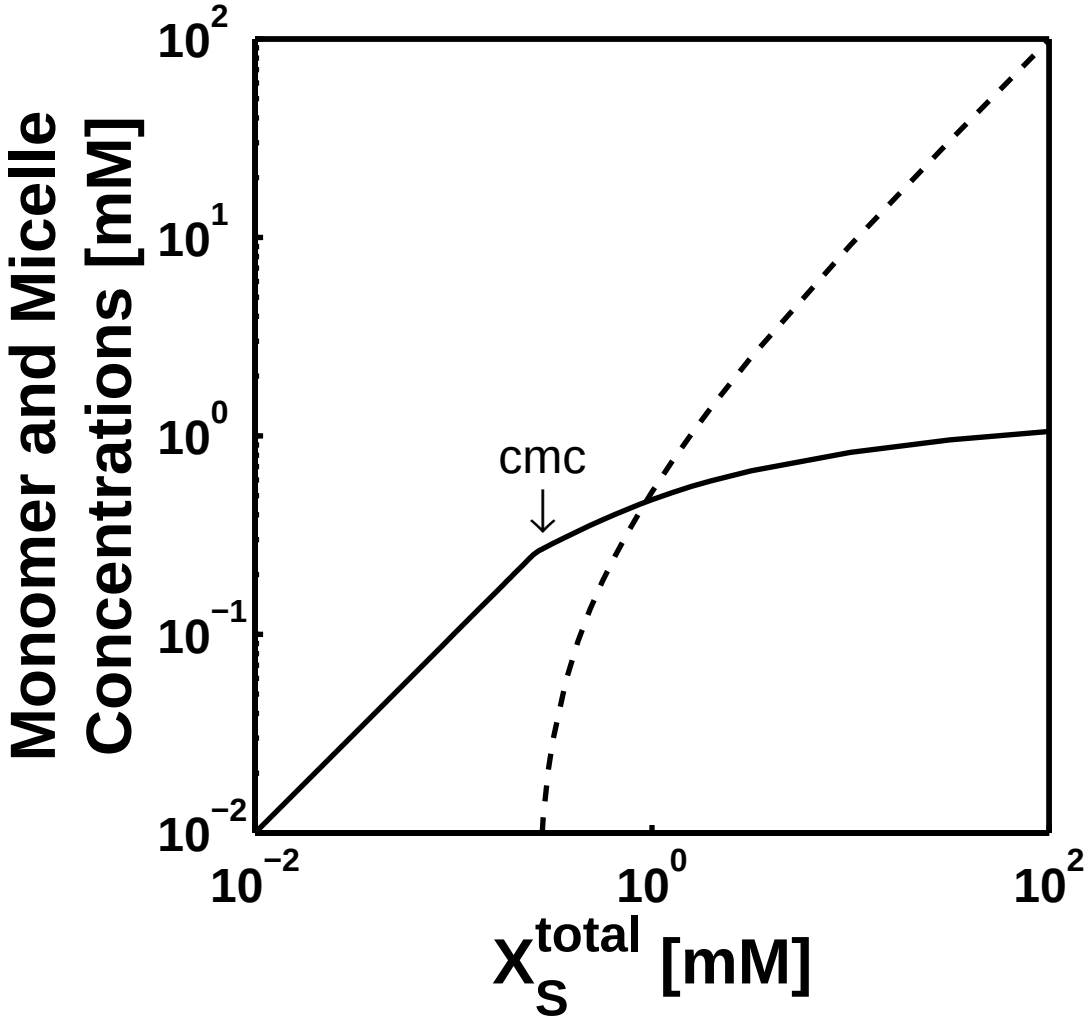

Figure 5-5: Predicted monomer concentration (solid line) and micelle concentration (dashed line) as a function of the total surfactant concentration (X_S^{total}) of the commercial surfactant Genapol UD-079. The cmc predicted by the MT theory is denoted by the arrow.

primarily by the activity of the surfactant monomers, such as the surface tension.[206] The micelle composition is intimately connected to the monomer composition and to every free-energy contribution to g_{m}. To better understand the behavior of the monomer and the micelle compositions, we have examined their behavior for the commercial nonionic surfactant Genapol UD-079.

Nonionic surfactants are often assumed to interact ideally in mixed micelles.[34,202] Therefore, we have compared the predicted monomer composition α_1 (see Figure 5-6) and the micelle composition α_{mic} (see Figure 5-7), both utilizing the MT theory (various lines) and assuming ideal mixing[34] (various symbols). Note that the ideal mixing calculations required input of the pure-component cmc's, which were predicted using the MT theory.

For visual clarity, only the compositions of four representative surfactant components are considered in each figure. In Figure 5-6, the MT predictions of the monomer composition of $C_{11}E_j$ (j = 5, 7, 8, and 11) correspond closely to those assuming ideal mixing, as indicated by the similarity of the various lines and the various symbols. Interestingly, the monomer composition of $C_{11}E_5$ (and of all the $C_{11}E_j$ surfactants with $j < 7$, data not shown) decreases monotonically with increasing surfactant concentration beyond the cmc (see Figure 5-6(a)). At the other extreme, the monomer composition of $C_{11}E_{11}$ (and of all the $C_{11}E_j$ surfactants with $j > 10$, data not shown) increases monotonically beyond the cmc (see Figure 5-6(b)). The surfactants $C_{11}E_7$ and $C_{11}E_8$ (and of all the $C_{11}E_j$ surfactants with $7 \leq j \leq 10$, data not shown) display a maximum in the monomer composition at some intermediate surfactant concentration beyond the cmc (see Figures 5-6(a) and (b)).

To understand this behavior, it is useful to examine the micelle composition and to realize that the mass balance constraints (see eq 5.5) require that $\alpha_i^{\mathrm{total}}$ must lie between α_{1i} and $\alpha_{\mathrm{mic}i}$. Therefore, if the mixed micelles are enriched in component i (that is, if $\alpha_{\mathrm{mic}i} > \alpha_i^{\mathrm{total}}$), then the monomers will be depleted in component i (that is, $\alpha_{1i} < \alpha_i^{\mathrm{total}}$), and vice versa.

In contrast to the relatively straightforward behavior exhibited by the predicted

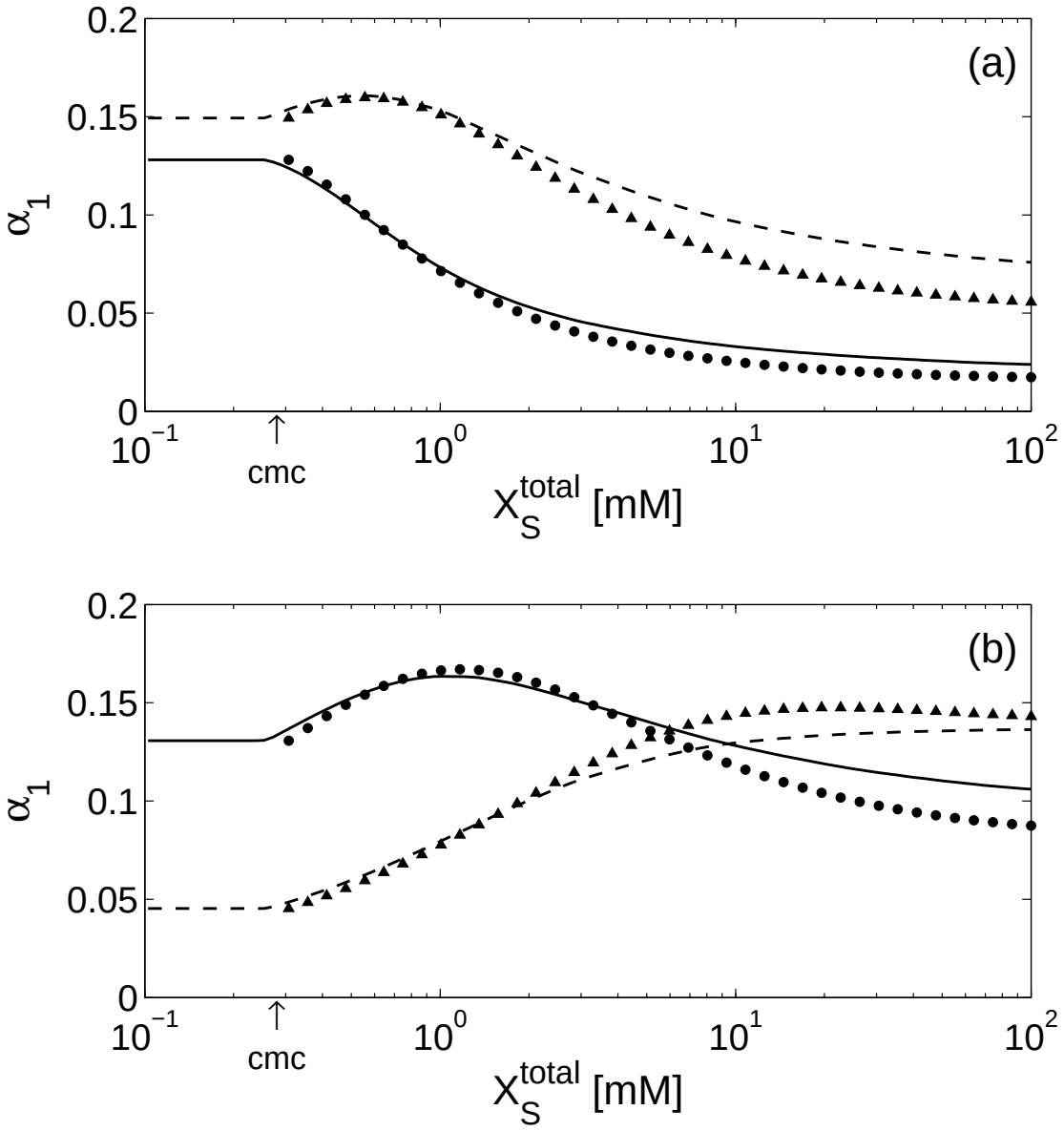

Figure 5-6: Predicted monomer composition (α_1) as a function of the total surfactant concentration (X_S^{total}) for representative components ($C_{11}E_j$, $j = 5$, 7, 8, and 11) of the commercial surfactant Genapol UD-079. The various lines correspond to the MT predictions. The various symbols correspond to compositions calculated assuming ideal mixing. The monomer composition of $C_{11}E_5$ (solid line and circles) and of $C_{11}E_7$ (dashed line and triangles) is shown in (a). The monomer composition of $C_{11}E_8$ (solid line and circles) and of $C_{11}E_{11}$ (dashed line and triangles) is shown in (b). The cmc predicted by the MT theory is denoted by the arrows on (a) and (b).

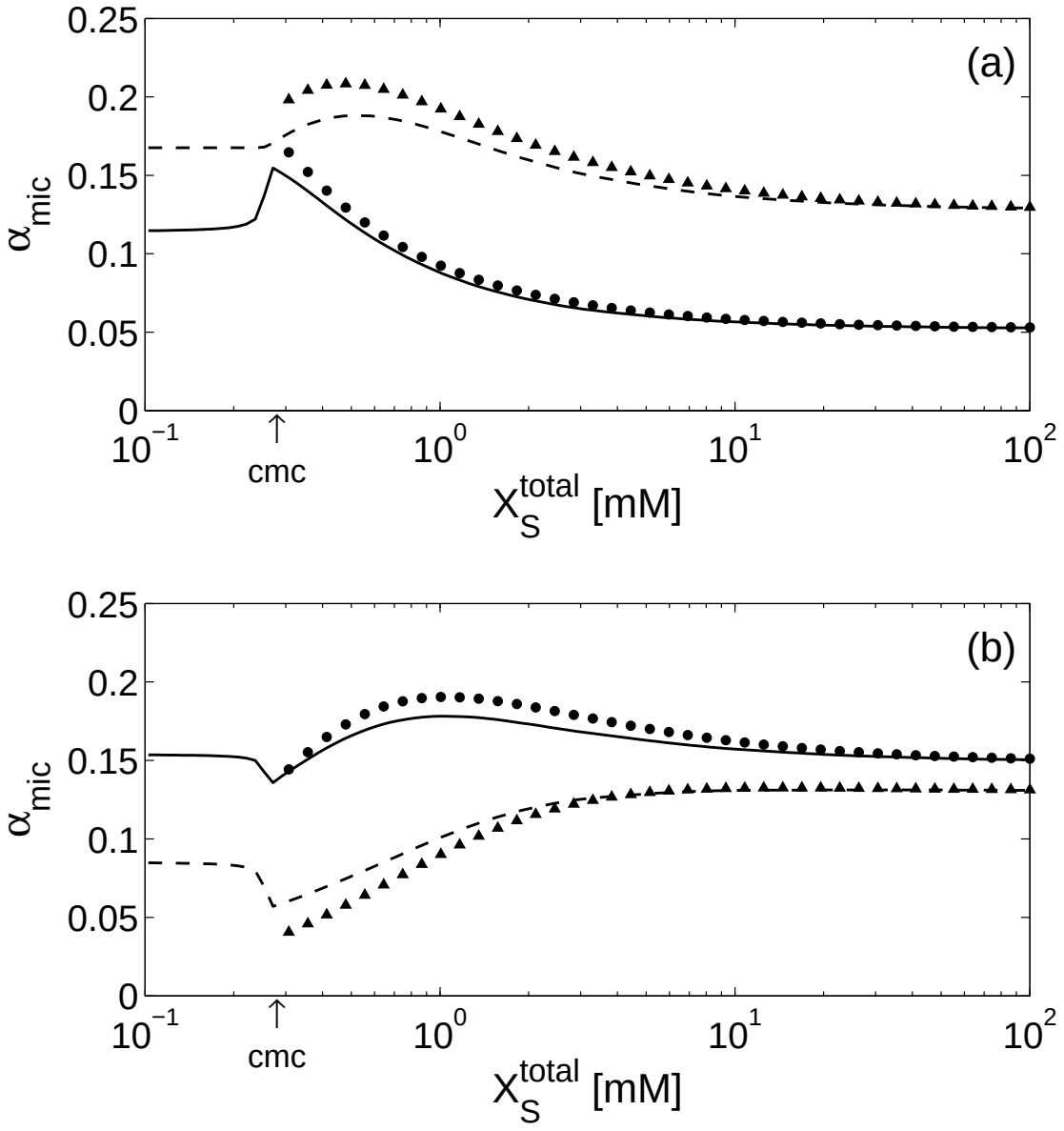

Figure 5-7: Predicted micelle composition ($\alpha_{\rm mic}$) as a function of the total surfactant concentration ($X_{\rm S}^{\rm total}$) for representative components ($C_{11}E_j$, $j = 3$, 5, 6, and 8) of the commercial surfactant Genapol UD-079. The various lines correspond to the MT predictions. The various symbols correspond to compositions calculated assuming ideal mixing. The micelle composition of $C_{11}E_3$ (solid line and circles) and of $C_{11}E_5$ (dashed line and triangles) is shown in (a). The micelle composition of $C_{11}E_6$ (solid line and circles) and of $C_{11}E_8$ (dashed line and triangles) are shown in (b). The cmc predicted by the MT theory is denoted by the arrows on (a) and (b).

monomer composition in Figure 5-6, the predicted micelle composition shown in Figure 5-7 exhibit surprisingly complex behavior near the cmc that deviates significantly from ideality. One important difference is that the MT theory allows the prediction of the micelle composition both above and below the cmc, while the ideal mixing model, which utilizes the pseudophase approximation, assumes that no micelles form below the cmc (therefore, no symbols appear below the cmc in Figure 5-7). Furthermore, as the surfactant concentration approaches and exceeds the cmc, the MT theory predicts that the micelle composition vary very rapidly, as indicated by the observed cusps in Figure 5-7. On the other hand, the ideal mixing model does not capture the complexity near the cmc that is predicted by the MT theory.

Since the only molecular difference between the various surfactant components of Genapol UD-079 is the size of the ethoxy head (reflected in the head cross-sectional area as a_{h}), this complex behavior must result from the effect of a_{h} on g_{mic}. Since the only contribution to g_{mic} that depends explicitly on a_{h} is g_{st} (see eq E.4 in Appendix E), the complex changes in the monomer and the micelle compositions are fundamentally related to the steric interactions, which favor the incorporation into micelles of the surfactant component with the smallest a_{h} value. On the other hand, entropic effects (captured in g_{ent}, see eq E.5 in Appendix E, and in the term $k_{\mathrm{B}}T\sum_i \alpha_i \ln \alpha_{1i}$ in eq 5.4) lead to the incorporation into the micelle of the other surfactant components.

Before proceeding to rationalize the predicted complex behavior near the cmc shown in Figure 5-7, let us examine the behavior above above the cmc in terms of the competition between steric end entropic effects discussed above. Based on steric effects, one would expect the micelles to be enriched, and the monomers to be depleted, in the smaller $\mathrm{C_{11}E}_j$ surfactants (that is, those having small j's). However, as the concentration of micelles increases, the micelle compositions of these surfactants must decrease and approach the overall solution composition in order to satisfy the mass balance (see eq 5.5), as shown by the asymptotic limits ($X_{\mathrm{S}}^{\mathrm{total}} \to 100\,\mathrm{m}M$) of α_{mic} in Figure 5-7. In turn, changes in the monomer composition (α_{1i}) are coupled

to changes in the micelle composition, since g_m depends on α_{1i} (see eq 5.4 and section 5.3). In fact, Figure 5-7 shows that, above the cmc, the micelle composition of the smaller $C_{11}E_j$ surfactants ($j < 5$) decreases monotonically with surfactant concentration, while the micelle composition of the larger $C_{11}E_j$ surfactants ($j > 7$) increases monotonically with surfactant concentration. Interestingly, both the MT theory and the calculations based on ideal mixing predict that the intermediate sized $C_{11}E_j$ surfactants ($5 \leq j \leq 7$) have a maximum composition at some intermediate surfactant concentration. Essentially, the maximum occurs only for surfactants of intermediate size for which the steric interactions and the entropic contribution are precisely balanced: the smaller surfactants ($j < 5$) favor the steric interactions too strongly to exhibit a maximum, while the larger surfactants ($j > 7$) favor the entropy too strongly to exhibit a maximum.

Although the competition of steric and entropic effects is sufficient to explain the behavior of the micelle (and the monomer) compositions above the cmc, one also needs to consider the micelle shape to explain the predicted behavior of the micelle composition near the cmc. In particular, steric and entropic effects are not sufficient to explain the predicted initial rise in α_{mic} of the smaller surfactants ($j < 5$, see Figure 5-7(a)) and the initial fall in α_{mic} of the larger surfactants ($j > 5$, see Figure 5-7(b)). In Figure 5-8, the compositions of spherical micelles (α_{sph}, solid lines), of infinite cylindrical micelles (α_{cyl}, dashed lines), and of the number-average micelle composition (α_{mic}, dotted line) are plotted for representative surfactant components of Genapol UD-079 ($C_{11}E_j$, $j = 2$, 5, and 7) as a function of the total surfactant concentration. Since the number-average micelle size is always between those of the spherical and the infinite cylindrical micelles, α_{mic} for $C_{11}E_2$, $C_{11}E_5$, and $C_{11}E_7$ lies between α_{sph} and α_{cyl} at all the surfactant concentrations examined.

Unlike α_{mic}, the predicted behaviors of α_{sph} and α_{cyl} are consistent with the competition between steric and entropic effects *at all the* X_S^{total} *values considered.* Specifically, α_{sph} and α_{cyl} of $C_{11}E_2$ decreases monotonically (see Figure 5-8(a)), while α_{sph} and α_{cyl} of $C_{11}E_7$ increase monotonically (see Figure 5-8(c)). On the other hand, there are three regimes of α_{mic} behavior: (1) below the cmc (marked by the arrow on

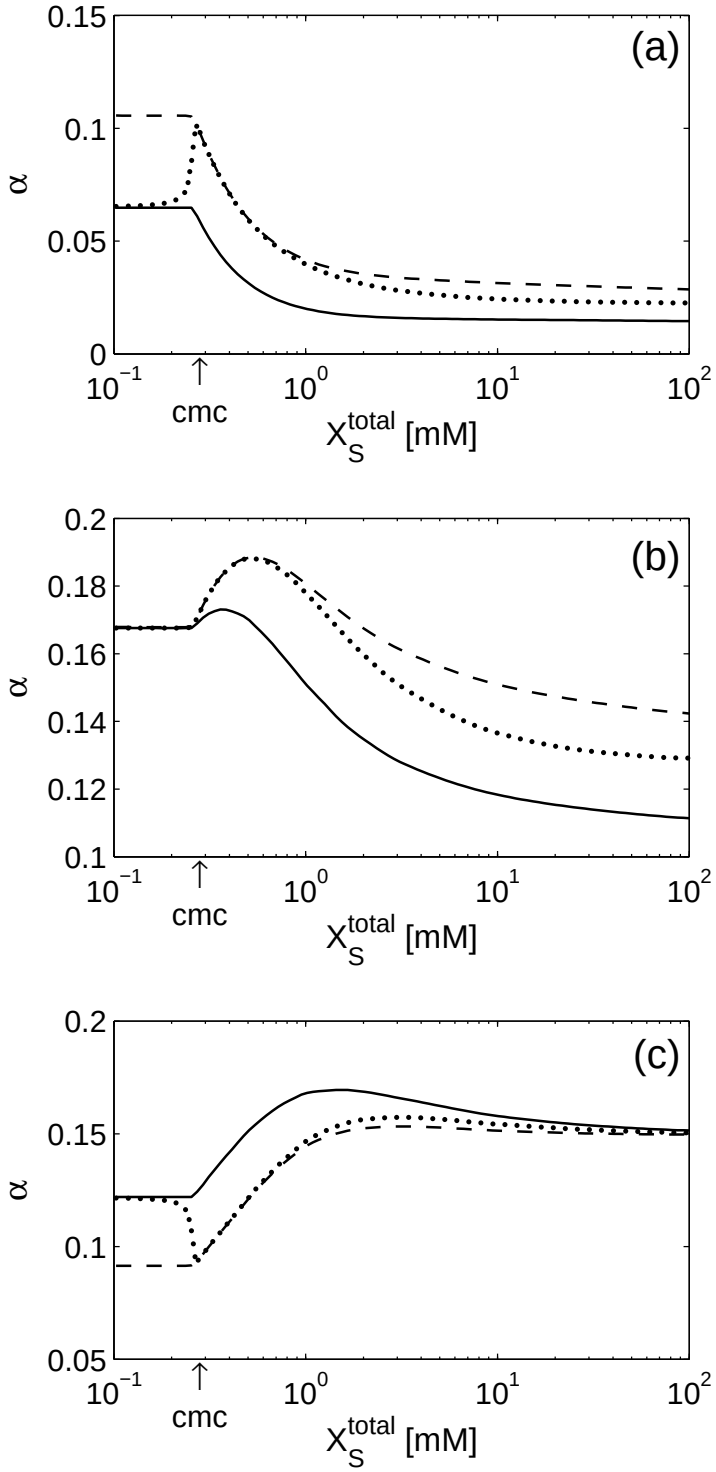

Figure 5-8: Predicted compositions (α) of spherical micelles ($\alpha = \alpha_{sph}$, solid line), of infinite cylindrical micelles ($\alpha = \alpha_{cyl}$, dashed line), and of the number-average micelle composition ($\alpha = \alpha_{mic}$, dotted line) as a function of the total surfactant concentration, X_S^{total}, of the $C_{11}E_2$ (a), $C_{11}E_5$ (b), and $C_{11}E_7$ (c) components of the commercial surfactant Genapol UD-079. The cmc predicted by the MT theory is denoted by the arrows.

the x-axis of each figure), the micelles are nearly spherical and $\alpha_{\text{mic}} \approx \alpha_{\text{sph}}$, (2) just below the cmc, cylindrical micelles form, and α_{mic} rapidly approaches α_{cyl}, and (3) above the cmc, α_{mic} approaches α_{sph} (indicating that the cylindrical micelles decrease in size, as explained below), until α_{mic} lies approximately halfway between α_{cyl} and α_{sph}. This predicted complex behavior arises because the growth of cylindrical micelles depends on two quantities (see eqs 5.10 and 5.11): the difference between g_{m} of spherical and infinite cylindrical micelles ($\Delta\mu$), and the total amount of surfactant in micelles (X_{mic}). Although X_{mic} *increases* monotonically with the total surfactant concentration, $\Delta\mu$ *decreases* monotonically (data not shown). The competition between these two effects leads to a maximum in the micelle size near the cmc, an interesting phenomenon that is not typically observed in single-surfactant systems, because $\Delta\mu$ does not vary significantly. Clearly, any phenomena that depends on micelle shape, such as the complex behavior shown in Figures 5-7 and 5-8, cannot be predicted by RST, where micelle shape is not accounted for.

In summary, the predicted variation in the monomer and the micelle compositions with the total surfactant concentration in solutions of Genapol UD-079 are due to the competition between steric and entropic effects. However, the specific predicted behaviors of α_1 and α_{mic} are complex because of changes in micelle shape near the cmc. In systems containing ionic surfactants, an even more complex behavior may result because of the existence of the electrostatic interactions (captured in g_{elec}). The results presented in Figures 5-7 and 5-8 suggest that it would be valuable to gather experimental data on the micelle aggregation numbers of Genapol UD-079 near and slightly above the cmc to verify that the behaviors of α_1 and α_{mic} predicted by the MT theory are indeed observed. Unfortunately, these measurements are beyond the scope of this thesis. The predicted variations in the micelle composition with the surfactant concentration shown in Figures 5-7 and 5-8 may be relevant in practical applications such as micellar-enhanced catalysis[207, 208] and micellar-based separations processes,[209, 210] which are strongly affected by the micelle composition when surfactant mixtures are used.

5.5. Conclusions

The theory presented in this chapter represents the first MT description of micellization for mixtures of three or more surfactant components. Several micellization properties of both fundamental and practical interest were examined. Specifically, the maximum micelle radius, which has practical significance for such varied applications as reducing surfactant-induced skin irritation and enhancing the solubilization of poorly water-soluble materials in aqueous media, was predicted for a mixed micelle consisting of ternary surfactant tails. The cmc's for ternary surfactant mixtures and for a commercial surfactant (Genapol UD-079) predicted using the MT theory were comparable to, and often better than, the cmc's calculated using the empirical RST approach. It is noteworthy that the ability to predict cmc's of multicomponent surfactant mixtures may facilitate the screening of surfactant formulations, since the cmc can often be correlated to practical performance characteristics, such as the amount of soil removed or the number of plates washed using a given amount of surfactant.[4] Furthermore, the MT theory was used to predict the behavior of the monomer and the micelle compositions of Genapol UD-079, which contains approximately 16 surfactant components. A complex behavior was predicted, which cannot be modeled utilizing the pseudophase approximation in the context of ideal mixing. Furthermore, the molecular basis of the MT theory allowed the predicted behavior to be rationalized in terms of steric and entropic effects. The ability to understand and predict the monomer and the micelle compositions may prove useful in predicting such practical properties as the surface tension of a micellar solution[211] and the micelle surface charge.[4]

Although the MT theory allows the prediction of a broad range of micellization properties, experimental studies of multicomponent surfactant mixtures have typically focused solely on cmc measurements. Experimental micelle aggregation numbers of multicomponent surfactant mixtures could provide particularly interesting data with which to test the MT theory presented in this chapter. The results presented in this chapter validate the MT theory as a useful tool for predicting and understanding

micellization properties of multicomponent surfactant mixtures. The theory can also be implemented in the area of surfactant formulation, in order to reduce time-consuming experiments and to gain physical insight. In the next chapter, the MT theory is further extended by incorporating pH-effects to model mixtures of conventional and pH-sensitive surfactants.

Chapter 6

Molecular-Thermodynamic Theory of Micellization of Mixtures of pH-Sensitive and Conventional Surfactants

6.1. Introduction

As indicated in Chapter 5, typical detergent formulations[29–31] consist of two or more types of surfactants. The major surfactant component is usually a conventional, pH-insensitive surfactant, typically anionic but sometimes nonionic. Small amounts of amphoteric (that is, pH-sensitive) surfactants are often added because of their performance boosting properties. In fact, the unique properties of amphoteric surfactants (for example, solubility over large pH ranges, low potential for skin or eye irritation, good foaming characteristics) has led to their use in a wide variety of products, including personal care formulations, disinfectants, detergents, and anti-corrosion coatings.[48] Furthermore, pH-sensitive surfactants are becoming increasingly important in novel applications, including controlled drug release, targeted gene delivery, and the fabrication of nanoscale materials for optics,

electronics, and sensors.[6,8–13,52–60]

In addition, pH-sensitive molecules, including surfactants, dyes, and drugs, have been used to probe micelles and, in particular, to infer the electrostatic potential at the micelle surface (ψ_0).[70,170–181] Probe molecules are utilized by solubilizing them in micelles, and using hydrogen ion titration to determine the equilibrium deprotonation parameter of the probe in the micelle ($\mathrm{p}K_\mathrm{m}$). The $\mathrm{p}K_\mathrm{m}$ is assumed to vary with ψ_0 according to the following equation[67] (see also Chapters 3 and 4):

$$\mathrm{p}K_\mathrm{m} = \mathrm{p}K_\mathrm{m}^0 + (\log e)\,\frac{e_0\psi_0}{k_\mathrm{B}T} \tag{6.1}$$

where $\mathrm{p}K_\mathrm{m}^0$ is the probe $\mathrm{p}K_\mathrm{m}$ in a neutral micelle (at $\psi_0 = 0$), e_0 is the charge of a proton, k_B is the Boltzmann constant, and T is the absolute temperature. The $\mathrm{p}K_\mathrm{m}^0$ is typically determined by titrating the probe solubilized in a nonionic micelle, since the $\mathrm{p}K_\mathrm{m}^0$ can differ significantly from the deprotonation constant of the probe in bulk aqueous solutions.[70,171,172,174–177]

In spite of the practical and technological relevance of mixtures containing pH-sensitive surfactants, to our knowledge, very little attention has been devoted to the theoretical modeling of these surfactants. The $\mathrm{p}K_\mathrm{m}$ of a fatty acid in nonionic, cationic, or anionic micelles was recently predicted theoretically by da Silva et al. using Poisson-Boltzmann calculations and Monte Carlo simulations.[70] However, these authors limited their studies to dilute concentrations of lauric acid, with approximately one lauric acid molecule per micelle. Zimmerman and Schnaare utilized regular solution theory (RST) and the pseudophase approximation to predict the pH-dependence of the critical micelle concentration (cmc) of mixtures of tetradecyldimethylamine oxide and hexadecyldimethyl betaine.[69] Although RST provided reasonable estimates of the cmc, a significant experimental effort was required to obtain the three β parameters (see Chapter 5).

With the above in mind, we have developed a molecular-thermodynamic (MT) theory to overcome the shortcomings of the limited theoretical studies that are currently available to model surfactant mixtures containing pH-sensitive surfactants.

The MT approach is fully predictive, in that it does not require any experimental data on the micellization properties of the surfactants of interest. Instead, the MT theory models the micellization process molecularly, and requires solely knowledge of the molecular structures of the surfactants, as well as of the solution conditions, including the temperature, the total surfactant concentration, and the type and concentration of additives (salt, acid, and/or base). The pH-dependent behavior of the micelles is captured by modeling the equilibrium of the surfactant monomers, and requires knowledge of the deprotonation constant of the pH-sensitive surfactant monomers (pK_1).

The remainder of this chapter is organized as follows. The materials and methods are briefly described in section 6.2. In section 6.3, the thermodynamic and the molecular components of the theory are described. The prediction of various micellar solution properties in the context of the MT theory is discussed in section 6.4. In section 6.5, the theoretical predictions are compared to available experimental data for several mixtures containing pH-sensitive surfactants. Finally, concluding remarks are presented in section 6.6.

6.2. Materials and Experimental Methods

Micellar titrations were conducted using the experimental procedure and materials described in Chapter 4. The titrations were conducted on 51 mM solutions of binary mixtures of the pH-sensitive surfactant dodecyldimethylamine oxide (C_{12}DAO) (lot no. 436579/1 31402), obtained from Sigma-Aldrich (St. Louis, MO), and the anionic surfactant sodium dodecyl sulfate (SDS) (lot no. 7718 X07624), obtained from Mallinckrodt Chemicals (Paris, KY). Note that the 51 mM surfactant concentration was selected in order for the concentration of the micellized C_{12}DAO surfactant to be much higher than the concentration of the C_{12}DAO surfactant monomers, thereby allowing us to neglect the contribution of the C_{12}DAO surfactant monomers during the titrations. Sodium chloride (NaCl) was added at a concentration of 0.1 M to maintain the ionic strength of the solution constant. Smirnova et al. reported that

the dissolution temperature of the C_{12}DAO/SDS solutions reaches a maximum of approximately 48°C at equimolar compositions and low pH.[187] Consequently, all the titrations were conducted at a temperature of 50°C to avoid precipitation. Three different mixtures were examined, having C_{12}DAO compositions of 1.00, 0.90, and 0.75. Solutions containing both C_{12}DAO and SDS became turbid when more than approximately 25% of C_{12}DAO was in the protonated state. (Note that Smirnova et al. also reported that some C_{12}DAO/SDS solutions were not transparent below pH 5.5.[187]) As a result, solutions having lower C_{12}DAO compositions were not examined. Although the exact nature of these solutions is unknown, they are probably not isotropic micellar solutions, which are usually transparent. (Some possible phases that could be forming include vesicles, ordered cylindrical phases, or lamellae.) Since the theory developed in this chapter is only applicable in the case of isotropic micellar solutions, experimental titration data are only reported for the conditions at which the micellar solution was transparent.

6.3. Theory

Solutions containing a pH-sensitive surfactant and a conventional surfactant are essentially ternary surfactant mixtures, since the pH-sensitive surfactant consists of both its protonated and deprotonated forms. Therefore, the MT theory presented in this chapter combines the theoretical framework developed for pH-sensitive surfactants in ref 190 and in Chapter 3 with the theoretical framework developed for ternary and multicomponent surfactant mixtures in Chapter 5. The experimental data used to validate the theory (see section 6.5) is limited to mixtures of a pH-sensitive surfactant and a single conventional surfactant. Nevertheless, the theory is developed below for the more general case of a mixture of a *single* pH-sensitive surfactant mixed with *any number* of conventional surfactants.

6.3.1. Notation

The deprotonated and protonated forms of the pH-sensitive surfactant are denoted as S and HS, respectively, reflecting the reaction $H^+ + S \rightarrow HS^+$. The total number of conventional surfactants is denoted as n_{surf}. The subscript i is used to refer generally to any of these $(n_{\text{surf}} + 2)$ pH-sensitive and conventional surfactant species. Note that using this notation allows many of the thermodynamic conditions to be written in exactly the same form as in the case of the multicomponent surfactant solutions discussed in Chapter 5. The solution may also contain any number of counterions, which may result from the addition of ionic surfactants, acid, base, or salt. The total number of counterions is denoted as n_{ion}, and the individual ions are denoted by the subscript j, which varies from 1 to n_{ion}.

A micelle is described in terms of several characteristics. The number of surfactants molecules in a micelle (or the aggregation number) is denoted as n. The micelle composition, denoting the mole fractions of the various surfactant types in the micelle, are α_{HS}, α_{S}, and α_i for the protonated surfactant, the deprotonated surfactant, and the conventional surfactant i, respectively. Counterions are explicitly allowed to bind to the micelle. The number of counterions j bound to the micelle is $n\hat{\beta}_j$, where $\hat{\beta}_j$ is referred to as the degree of counterion binding. The core minor radius of the micelle is denoted as l_{c}. The shape of the micelle is captured through the shape factor, S, which is 1 for planar bilayers, 2 for cylindrical micelles, and 3 for spherical micelles. The mole fraction of micelles sharing the same characteristics is denoted as $X_{n\{\alpha_i,\hat{\beta}_j\}}$. Note that S and l_{c} are not explicitly included in the subscript to simplify the notation. The total concentration of micelles of any type is denoted as X_{mic}.

The bulk solution contains free surfactant monomers, with the total monomer concentration denoted as X_1. The monomer composition is denoted as $\alpha_{1\text{HS}}$, $\alpha_{1\text{S}}$, and α_{1i} for the protonated surfactant monomers, the deprotonated surfactant monomers, and the conventional surfactant monomers i, respectively. The bulk solution also contains free ions j, whose concentration is denoted as X_{1j}. The bulk concentrations

of H^+ and OH^- are denoted as X_{1H} and X_{1OH}, respectively.

The experimentally controlled concentrations are the *total* concentrations of the various species. The total concentration of surfactant is denoted as X_{surf}^{total}, and the composition of the added surfactant is denoted as α_{HS}^{total}, α_{S}^{total}, and α_{i}^{total} for the protonated surfactant, the deprotonated surfactant, and the conventional surfactant i, respectively. The total concentration of ion j, which may result from the added surfactant, acid, base, or salt, is denoted as X_{j}^{total}. Finally, the total concentrations of H^+ and OH^- (added to the solution from acid and protonated surfactant, and base, respectively) are denoted as X_{H}^{total} and X_{OH}^{total}.

6.3.2. Thermodynamic Framework

Using the notation presented in section 6.3.1, the condition governing the thermodynamic equilibrium between the micelles, the surfactant monomers, and the free counterions is identical to that given in Chapter 5:

$$X_{n\{\alpha_i,\hat{\beta}_j\}} = \frac{1}{e}\left(\prod_i X_{1i}^{n\alpha_i}\right)\left(\prod_j X_{1j}^{n\hat{\beta}_j}\right)\exp\left[-\frac{n}{k_B T}g_{mic}\left(S, l_c, \{\alpha_i\}, \{\hat{\beta}_j\}\right)\right] \tag{6.2}$$

To facilitate the calculations, eq 6.2 can be expressed in terms of the total monomer concentration, X_1, as follows (see Chapter 5):

$$X_{n\{\alpha_i,\hat{\beta}_j\}} = \frac{1}{e}X_1^n \exp\left[-\frac{n}{k_B T}g_m\right] \tag{6.3}$$

where g_m is the modified free energy of micellization, defined as

$$g_m = g_{mic} - k_B T\left[\sum_i \alpha_i \ln \alpha_{1i} + \sum_j \hat{\beta}_j \ln X_{1j}\right] \tag{6.4}$$

Note that eqs 6.2-6.4 are identical in form to eqs 5.2-5.4, which were developed for mixtures of conventional surfactants. However, the subscript i in eqs 6.2-6.4 now denotes the n_{surf} conventional surfactants *and* the protonated and deprotonated forms of the pH-sensitive surfactant. In addition, the monomer composition of the

pH-sensitive surfactant (α_{1S} and α_{1HS}) is subject to the pH-equilibrium constraint, which can be written in terms of the Henderson-Hasselbalch equation[51,141] (see also Chapter 4):

$$\mathrm{pK}_1 = \mathrm{pH} - \log \frac{X_{1S}}{X_{1HS}} = \mathrm{pH} + \log \frac{\alpha_{1HS}}{\alpha_{1S}} \tag{6.5}$$

Each species is also subject to a mass balance constraint. For the conventional surfactants, the mass balance is identical to that given in eq 5.5 in Chapter 5:

$$\alpha_i^{\mathrm{total}} X_{\mathrm{surf}}^{\mathrm{total}} = \alpha_{1i} X_1 + \sum_{S,n,l_c,\{\alpha_i,\hat{\beta}_j\}} n\alpha_i X_{n\{\alpha_i,\hat{\beta}_j\}} + E_{\mathrm{dl},i} \tag{6.6}$$

where i denotes solely the conventional surfactant components (1 to n_{surf}), and $E_{\mathrm{dl},i}$ is a correction due to the enhancement, or the depletion, of surfactant i in the diffuse double layer (see Appendix F). In the case of the pH-sensitive surfactant, the appropriate mass balance is for the total concentration of both the protonated and the deprotonated forms (see Chapter 3):

$$\left(\alpha_{\mathrm{HS}}^{\mathrm{total}} + \alpha_{\mathrm{S}}^{\mathrm{total}}\right) X_{\mathrm{surf}}^{\mathrm{total}} = \left(\alpha_{1\mathrm{HS}} + \alpha_{1\mathrm{S}}\right) X_1 + \sum_{S,n,l_c,\{\alpha_i,\hat{\beta}_j\}} n\left(\alpha_{\mathrm{HS}} + \alpha_{\mathrm{S}}\right) X_{n\{\alpha_i,\hat{\beta}_j\}} + E_{\mathrm{dl,S}} \tag{6.7}$$

where $E_{\mathrm{dl,S}}$ is a correction due to the enhancement, or the depletion, of the pH-sensitive surfactant in the diffuse double layer (see Appendix F). Note that although eq 6.7 is similar to eq 5.5, which was developed for a pH-sensitive surfactant, eq 5.5 does not depend on the monomer or the micelle compositions.

The mass balance for ion j is identical to that in eq 5.6 in Chapter 5:

$$X_j^{\mathrm{total}} = X_{1j} + \sum_{S,n,l_c,\{\alpha_i,\hat{\beta}_j\}} n\hat{\beta}_j X_{n\{\alpha_i,\hat{\beta}_j\}} + E_{\mathrm{dl},j} \tag{6.8}$$

where $E_{\mathrm{dl},j}$ is a correction due to the enhancement, or the depletion, of ion j in the diffuse double layer (see Appendix F). Similar mass balances can be obtained for the ions H^+ and OH^- present in the solution. However, as discussed in ref 190 and in

Chapter 3, the following combined mass balance is more useful:

$$\left(X_{\mathrm{H}}^{\mathrm{total}} - X_{\mathrm{OH}}^{\mathrm{total}}\right) = (X_{1\mathrm{H}} - X_{1\mathrm{OH}}) + \alpha_{1\mathrm{HS}} X_1 + \sum_{S,n,l_c,\{\alpha_i,\hat{\beta}_j\}} n\alpha_{\mathrm{HS}} X_{n\{\alpha_i,\hat{\beta}_j\}} + (E_{\mathrm{dl,H}} - E_{\mathrm{dl,OH}}) \tag{6.9}$$

where $E_{\mathrm{dl,H}}$ and $E_{\mathrm{dl,OH}}$ are corrections due to the enhancement, or the depletion, of the H^+ and the OH^- ions in the diffuse double layer (see Appendix F). Finally, $X_{1\mathrm{OH}}$ is determined utilizing the equilibrium constant for the dissociation of water (K_{w}, obtained from ref 113):

$$X_{1\mathrm{H}} X_{1\mathrm{OH}} = K_{\mathrm{w}} \tag{6.10}$$

As in Chapter 3, we have assumed that activity coefficient effects are negligible in deriving eqs 6.5 and 6.10, or alternatively, that they can be accounted for in terms of effective values of the equilibrium constants.

In summary, the experimentally controlled variables ($X_{\mathrm{surf}}^{\mathrm{total}}$, $\alpha_i^{\mathrm{total}}$, X_j^{total}, $X_{\mathrm{H}}^{\mathrm{total}}$, and $X_{\mathrm{OH}}^{\mathrm{total}}$) are related to the concentrations of species in the bulk (X_1, α_{1i}, X_j, X_{H}, and X_{OH}) and to the micelle concentration ($X_{n\{\alpha_i,\hat{\beta}_j\}}$) by simultaneously solving eqs 6.3–6.10. Note that a model is also required for g_{mic}, which we describe next.

6.3.3. Molecular Model for the Free Energy of Micellization

Because of our choice of notation, the equations describing the g_{mic} model for mixtures of pH-sensitive and conventional surfactants are identical to those obtained for multicomponent surfactant mixtures (see Appendix E). For completeness, the main physical contributions to the g_{mic} model are summarized briefly below.

The free energy of micellization, g_{mic}, is modeled as the sum of six contributions[138] (see also Chapter 2):

$$g_{\mathrm{mic}} = g_{\mathrm{tr}} + g_{\mathrm{int}} + g_{\mathrm{pack}} + g_{\mathrm{st}} + g_{\mathrm{elec}} + g_{\mathrm{ent}} \tag{6.11}$$

The first three contributions are associated with the formation of the micelle core: The

transfer contribution, $g_{\rm tr}$, accounts for the transfer of the surfactant hydrophobic tails from an aqueous to an oil-like environment (see eq E.1). The interfacial contribution, $g_{\rm int}$, accounts for the free-energy penalty associated with the formation of an interface between the oil-like micelle core and the surrounding aqueous environment (see eq E.2). The packing contribution, $g_{\rm pack}$, accounts for the additional entropic constraints associated with anchoring one end of each surfactant hydrophobic tail at the micelle core-water interface (see eq E.3). The fourth and fifth contributions are associated with the formation of the micelle interfacial region: The steric contribution, $g_{\rm st}$, accounts for the steric interactions between the surfactant hydrophilic heads and the bound counterions in the micelle interfacial region (see eq E.4). The electrostatic contribution, $g_{\rm elec}$, accounts for the electrostatic interactions at the micelle interface that operate in the case of ionic surfactants and bound counterions and of zwitterionic surfactants (see eqs E.6-E.10). The last contribution, $g_{\rm ent}$, accounts for the entropy of mixing the various components in a micelle (see eq E.5).

6.4. Determination of Useful Micellar Solution Properties

As discussed in Chapters 3 and 5, the optimal micelle characteristics are determined by minimizing $g_{\rm m}$ with respect to $\{\alpha_i\}$, $\{\hat{\beta}_j\}$, and $l_{\rm c}$. Denoting the minimum $g_{\rm m}$ as $g^*_{\rm m}$, the cmc is approximated as $\exp(g^*_{\rm m}/k_{\rm B}T)$. The minimization is performed explicitly for spherical and infinite cylindrical micelles, and the corresponding $g_{\rm m}$ of finite cylinders is determined by interpolation (see Chapters 2 and 3).

In the case of micelles containing pH-sensitive surfactants, an additional property of interest is the p$K_{\rm m}$, which is a micellar deprotonation parameter analogous to the pK_1 of the surfactant monomers. The p$K_{\rm m}$ is defined as

$$\mathrm{p}K_{\rm m} = \mathrm{pH} + \log\left(\frac{\alpha_{\rm HS}}{\alpha_{\rm S}}\right) = \mathrm{pH} + \log\left(\frac{x_{\rm HS}}{1-x_{\rm HS}}\right) \tag{6.12}$$

where $x_{\rm HS} = \alpha_{\rm HS}/(\alpha_{\rm HS}+\alpha_{\rm S})$ is the degree of protonation of the micellized pH-sensitive

surfactant. Note that defining the p$K_{\rm m}$ of mixed micelles in terms of $x_{\rm HS}$, which always varies from 0 to 1, is more convenient than using the micelle composition, since $(\alpha_{\rm HS} + \alpha_{\rm S})$ is generally less than unity.

6.5. Results and Discussion

The theory presented in section 6.3 is validated below using experimental data from the literature and titration data that we collected (see section 6.2 and Chapter 4) for systems containing a pH-sensitive surfactant and a conventional surfactant. In most cases, the pH-sensitive surfactant is C_{12}DAO. A longer chain homologue, tetradecyldimethylamine oxide (C_{14}DAO), is used to validate the cmc predictions, due to the availability of experimental (cmc) data.[69] Note that the pK_1 of the C_{12}DAO and the C_{14}DAO monomers is approximately 4.9, indicating that half of the surfactant monomers are protonated at a pH of 4.9 (see eq 6.5). The conventional surfactants considered include anionic, cationic, nonionic, and zwitterionic surfactants.

6.5.1. Prediction of the Solution pH and of the Degree of Counterion Binding

Since the pK_1 of C_{12}DAO is approximately 4.9, C_{12}DAO is typically assumed to be only in its deprotonated, zwitterionic state at neutral pH or higher (pH > 7). However, as we will show below, the presence of small amounts of protonated C_{12}DAO (denoted as $C_{12}DAOH^+$) can have a significant effect on the solution pH when there is no added acid. In particular, $C_{12}DAOH^+$ is expected to interact very strongly with anionic surfactants. Therefore, we examine solutions containing C_{12}DAO and the anionic surfactant SDS, which were studied by Imae and Kakitana.[183] The pH's of 80 mM solutions of C_{12}DAO/SDS and varying compositions of SDS ($\alpha_{\rm SDS}^{\rm total}$) were measured at 25°C. The predicted (various lines) and the experimental (various symbols) solution pH as a function of $\alpha_{\rm SDS}^{\rm total}$ are compared in Figure 6-1. The experiments were conducted either with no added salt (solid line and circles) or with 50 mM NaCl (dashed line and

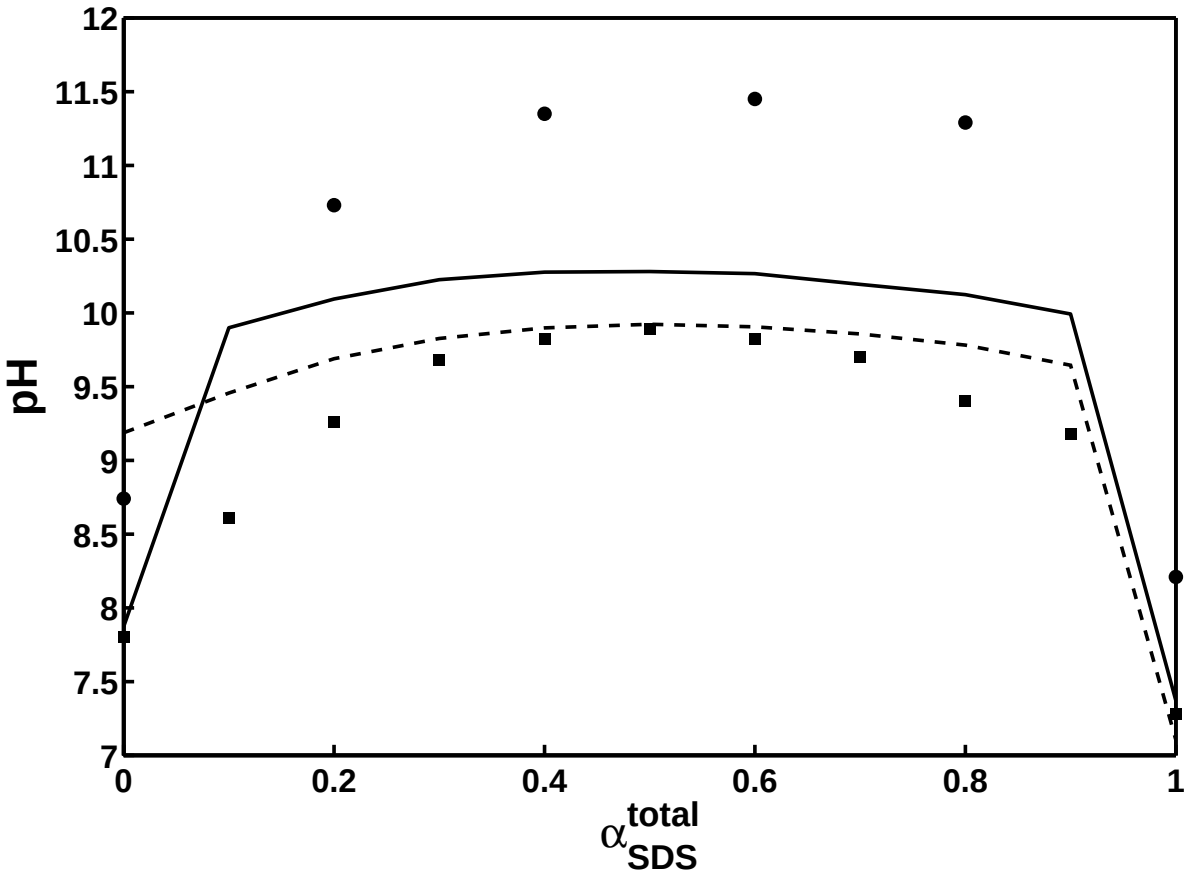

Figure 6-1: Comparison of the predicted (various lines) and the experimental[183] (various symbols) solution pH's in 80 mM solutions of C_{12}DAO/SDS as a function of SDS composition ($\alpha_{\rm SDS}^{\rm total}$) for solutions containing no salt (solid line and circles) and 50 mM NaCl (dashed line and squares).

squares). Note that the fraction of C_{12}DAO monomers that are protonated at these experimental conditions (see eq 6.5) is extremely small (less than 0.001 at a pH of 8, and less than 3×10^{-7} at a pH of 11.5). Since the vast majority of the pH-sensitive surfactant monomers are deprotonated at such conditions, one might assume that the $C_{12}DAOH^+$ could be neglected. However, since the system contains no strong acid or base and no buffer, the solution pH is very sensitive to the degree of protonation of the pH-sensitive surfactant. The presence of trace amounts of acid or base can also have a significant effect on the solution pH at such conditions. Therefore, we consider the predicted and the experimental pH values presented in Figure 6-1 to be in generally good agreement. We discuss the quantitative behavior in more detail below, along with one qualitative discrepancy.

Although the solutions considered contain no added acid or base, the solution pH varies considerably with α_{SDS}^{total} and with the salt concentration. The experimental points (circles and squares) in Figure 6-1 show that the solution pH increases steadily with α_{SDS}^{total} and eventually plateaus at $0.4 \lesssim \alpha_{SDS}^{total} \lesssim 0.6$, while the predicted solution pH plateaus over a much wider range of α_{SDS}^{total} values. The solution pH changes because the addition of SDS favors the formation and incorporation of $C_{12}DAOH^+$ into the micelles.

As the amount of $C_{12}DAOH^+$ in the micelles increases, the bulk concentration of H^+ ions must decrease in order to satisfy the H^+ and OH^- mass balances (see eq 6.9), which corresponds to an increase in the solution pH. In the case of no added salt, the experimental pH (the circles in Figure 6-1) is always higher than the predicted pH (the solid line in Figure 6-1), suggesting that the theory underestimates the total amount of protonated surfactant ($C_{12}DAOH^+$) in the micelles, due primarily to the electrostatic interactions. The electrostatic model (captured in g_{elec}) may be partially responsible. For example, if the ionic strength of the solution is overestimated, then g_{elec} will be too small, thereby reducing the driving force for the incorporation of $C_{12}DAOH^+$ into the micelles. This effect of increasing ionic strength on the solution pH is observed in both the predicted and the experimental data, since the solutions containing 50 mM NaCl have a lower pH than those with no added salt.

The one significant qualitative deviation between the predictions and the experiments is the solution pH at $\alpha_{\mathrm{SDS}}^{\mathrm{total}} = 0$. Specifically, the experimental solution pH decreases upon adding salt (see the points on the left-hand edge of Figure 6-1), while the predicted solution pH increases upon adding salt, corresponding to the region in Figure 6-1 where the dashed line lies above the solid line. The predicted results are consistent with a decrease in g_{elec} for the slightly cationic micelles that exist when no SDS is present, which leads to a larger amount of $C_{12}DAOH^+$ in the micelles at a given pH. Therefore, the solution pH is predicted to rise with salt concentration when there is no SDS. However, the experimental pH actually decreases slightly upon the addition of NaCl. This issue warrants further investigation to verify that the observed experimental trends without added SDS are reproducible. If the observed discrepancy is real, then it could point to limitations in the electrostatic model used or in our treatment of the diffuse layer (see Appendix F).

Imae and Kakitana also measured the degree of sodium (Na) binding to micelles ($\hat{\beta}_{\mathrm{Na}}$) using Na-selective electrodes.[183] The predicted and the experimental $\hat{\beta}_{\mathrm{Na}}$ values as a function of $\alpha_{\mathrm{SDS}}^{\mathrm{total}}$ are compared in Figure 6-2. Note that the predictions reproduce the qualitative behavior of $\hat{\beta}_{\mathrm{Na}}$, although the predictions are consistently lower than the experimental $\hat{\beta}_{\mathrm{Na}}$ values. This quantitative difference was observed previously (see ref 138 and Chapter 2), and was attributed to differences in which counterions are considered to be "bound" by the experimental technique used.

Smirnova et al.[187] also measured the pH of equimolar solutions of $C_{12}DAO$ and SDS. The experimental conditions used were 56 mM of surfactant, with $\alpha_{\mathrm{SDS}}^{\mathrm{total}} = 0.5$, no added salt, and a temperature of 50°C. The predicted and the experimentally measured solution pH values are compared in Figure 6-3. We have followed the authors' convention and reported the results as a function of $X_{\mathrm{H}}' \equiv X_{\mathrm{H}}^{\mathrm{total}}/(X_{\mathrm{H}}^{\mathrm{total}} + X_{\mathrm{C_{12}DAO}}^{\mathrm{total}})$. The experimental conditions at $X_{\mathrm{H}}' = 0$ (no added acid) are similar to those used by Imae and Kakitana at $\alpha_{\mathrm{SDS}}^{\mathrm{total}} = 0.5$ (see Figure 6-1). However, the reported pH values differ markedly (11.5 in Figure 6-1 and 8.5 in Figure 6-3). As mentioned earlier, when there is no added acid or base, the solution pH can be very sensitive to the presence of trace contaminants. In particular, the presence of dissolved CO_2

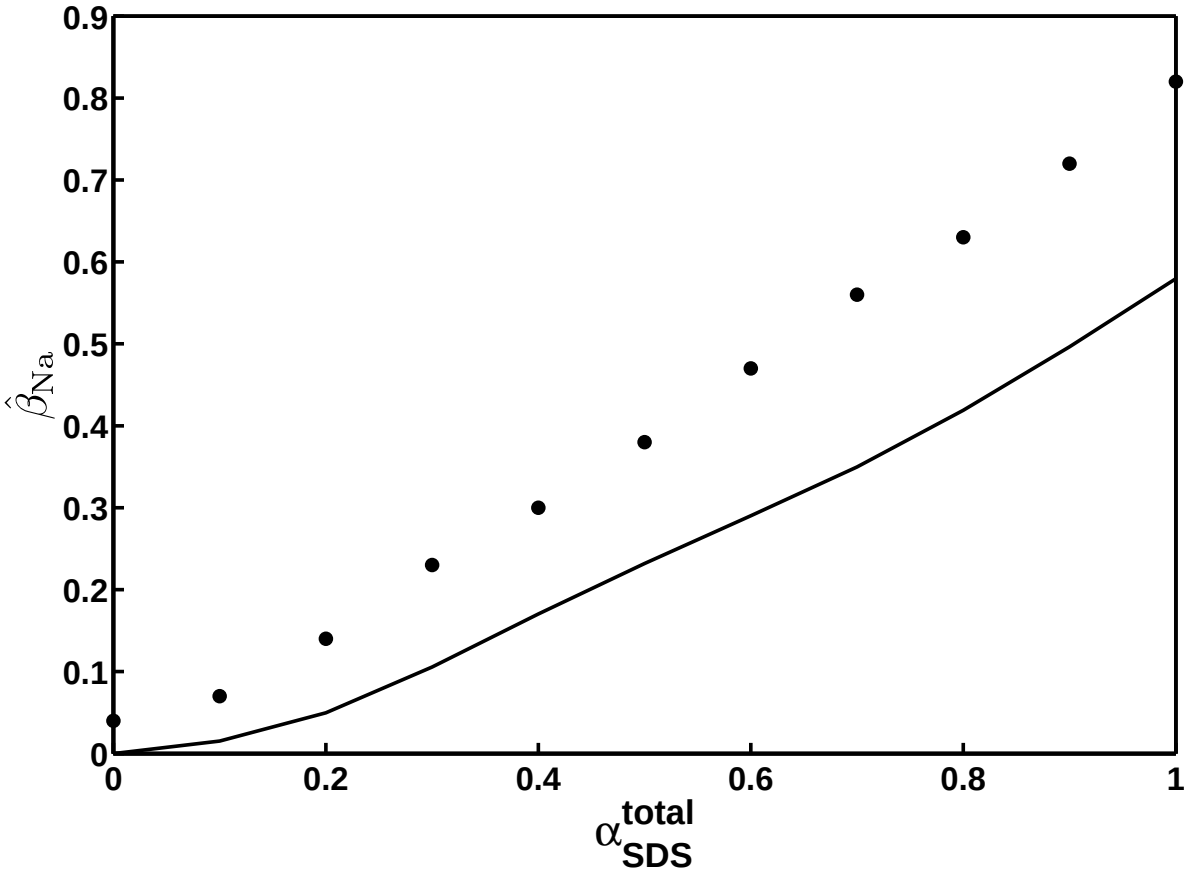

Figure 6-2: Comparison of the predicted (line) and experimental[183] (circles) degrees of sodium (Na) binding ($\hat{\beta}_{\mathrm{Na}}$) to C_{12}DAO/SDS micelles as a function of the SDS composition ($\alpha_{\mathrm{SDS}}^{\mathrm{total}}$).

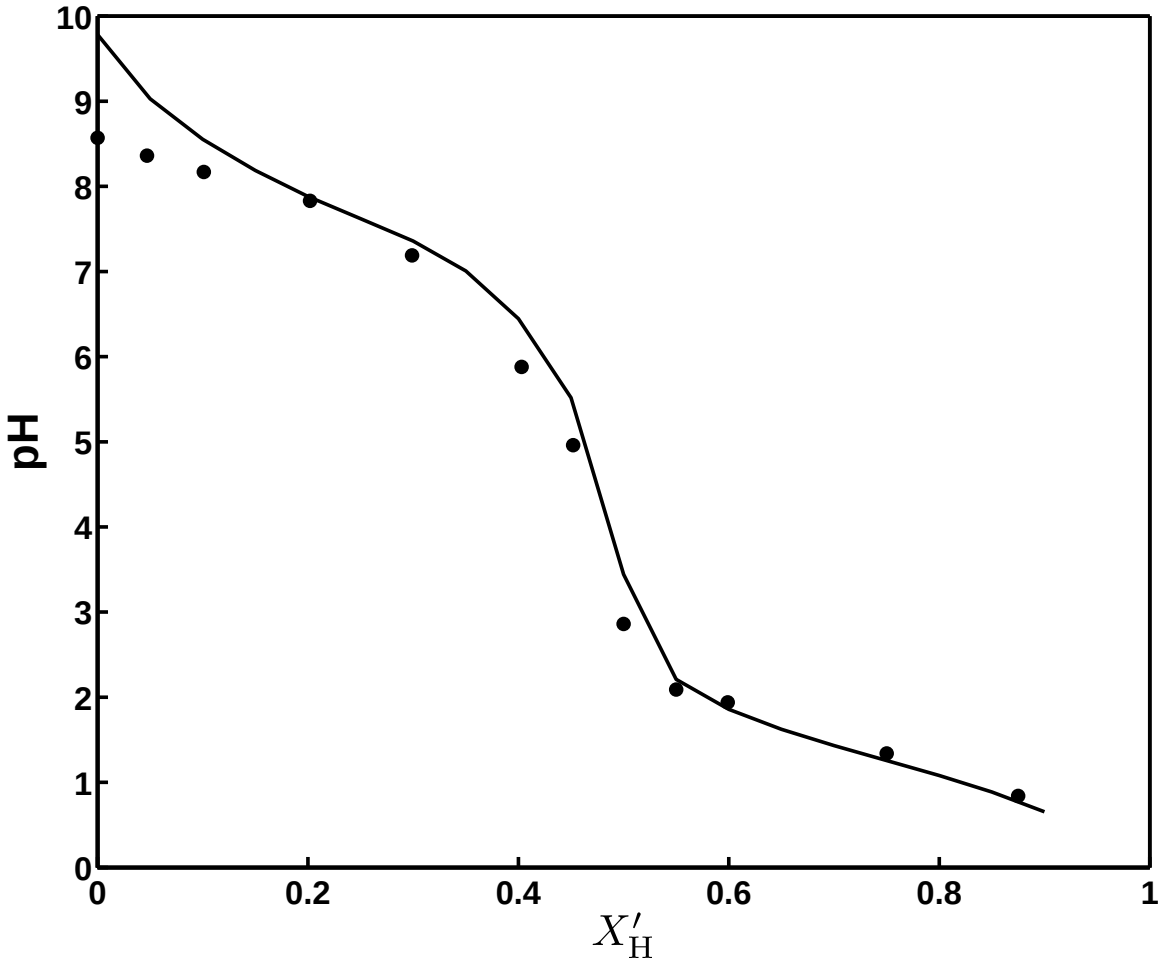

Figure 6-3: Comparison of the predicted (line) and the experimental[187] (circles) solution pH's in 56 mM equimolar mixtures of C_{12}DAO/SDS as a function the relative amount of added HCl (X'_{H}).

can significantly decrease the solution pH. Although Smirnova et al. report that they took special precautions to limit the absorption of CO_2, the significant discrepancy between their results and those of Imae and Kakitana suggests that one or both groups may not have removed all the contaminants from the solution. As a result, we consider the overprediction of solution pH at $X'_{\mathrm{H}} < 0.2$ to be within the experimental uncertainty at these conditions. At $X'_{\mathrm{H}} > 0.2$, the solution is much less sensitive to the presence of trace contaminants, and excellent agreement is observed between the predicted and the experimental pH values.

6.5.2. Prediction of the cmc of a pH-Sensitive Surfactant Mixture

Zimmerman and Schnaare[69] determined the cmc of various solutions of C_{14}DAO and the zwitterionic surfactant hexadecyldimethyl betaine (C_{16}Bet) at 30°C. The counterion concentration was maintained at 0.02 M through the addition of NaCl. Although C_{16}Bet is also a pH-sensitive surfactant, the authors argue that only the zwitterionic (deprotonated) form of C_{16}Bet needs to be accounted for at the pH conditions considered. To confirm that this approximation was reasonable, preliminary cmc calculations were done in which C_{16}Bet was modeled as a pH-sensitive surfactant with a pK_1 of 1.83.[69] These calculations indicated that the composition of protonated C_{16}Bet in the micelle is negligible (less than 0.015) when the solution pH is above 4 (data not shown). Since the minimum pH value considered below is 4.3, the neglect of the protonated C_{16}Bet constitutes a reasonable approximation. Treating C_{16}Bet as a conventional surfactant effectively results in a ternary surfactant mixture. Therefore, Zimmerman and Schnaare applied the multicomponent extension of regular solution theory (RST) in the context of the pseudophase model[37] to predict the cmc's of the ternary surfactant mixtures using cmc data obtained from binary surfactant mixtures. Note that the binary surfactant mixtures include: (1) protonated and deprotonated C_{14}DAO, (2) protonated C_{14}DAO and C_{16}Bet, and (3) deprotonated C_{14}DAO and C_{16}Bet.

Unfortunately, these authors appear to have implemented the Henderson-Hasselbalch equation (eq 6.5) incorrectly when calculating the composition of the protonated and the deprotonated C_{14}DAO monomers. In particular, the reported compositions of the protonated and the deprotonated C_{14}DAO are inconsistent with the reported pH values in Table 1 of ref 69. For example, the degree of protonation of C_{14}DAO is incorrectly reported to increase with pH. Therefore, we have assumed that the authors correctly reported the solution pH, since it is the quantity that they measured experimentally, and we have recalculated the compositions of the protonated and the deprotonated C_{14}DAO. In addition, we have recalculated the cmc's obtained using RST using the correct compositions. The cmc's in these mixtures are determined largely by the composition of the C_{16}Bet surfactant, since it has the longest tail. Consequently, most of the corrected cmc's differ from those reported by the authors by less than 1%, but two of the cmc's were modified by 20-30%. With the above in mind, we have utilized the corrected RST calculations in the comparisons which follow.

In Figure 6-4, experimental (white bars), RST calculated (grey bars), and MT predicted (black bars) cmc's are compared for the ternary surfactant mixtures examined. The pH and the corresponding compositions of these mixtures (denoted as mixtures A through G) are listed in Table 6.1. Both the RST and the MT predictions compare favorably to the experimental cmc's. Even though the RST approach makes use of some experimental cmc data, the MT predictions are better than those of the RST for mixtures A and D. In addition, both the MT and the RST predicted cmc's are within the experimental uncertainty for mixtures C and F, since these predicted cmc's fall within the error bars in Figure 6-4.

Mixtures B through F correspond to decreasing amounts of C_{16}Bet at a pH of 4.8. Since C_{16}Bet has a much lower cmc than either form of C_{14}DAO, it is not surprising that the MT and the RST predicted cmc's tend to increase with decreasing C_{16}Bet composition (that is, as we proceed from left to right from Mixture B to Mixture F in Figure 6-4). However, the experimental cmc's do not show such a trend, and both the RST and the MT theory show significant deviations from the experimental results for

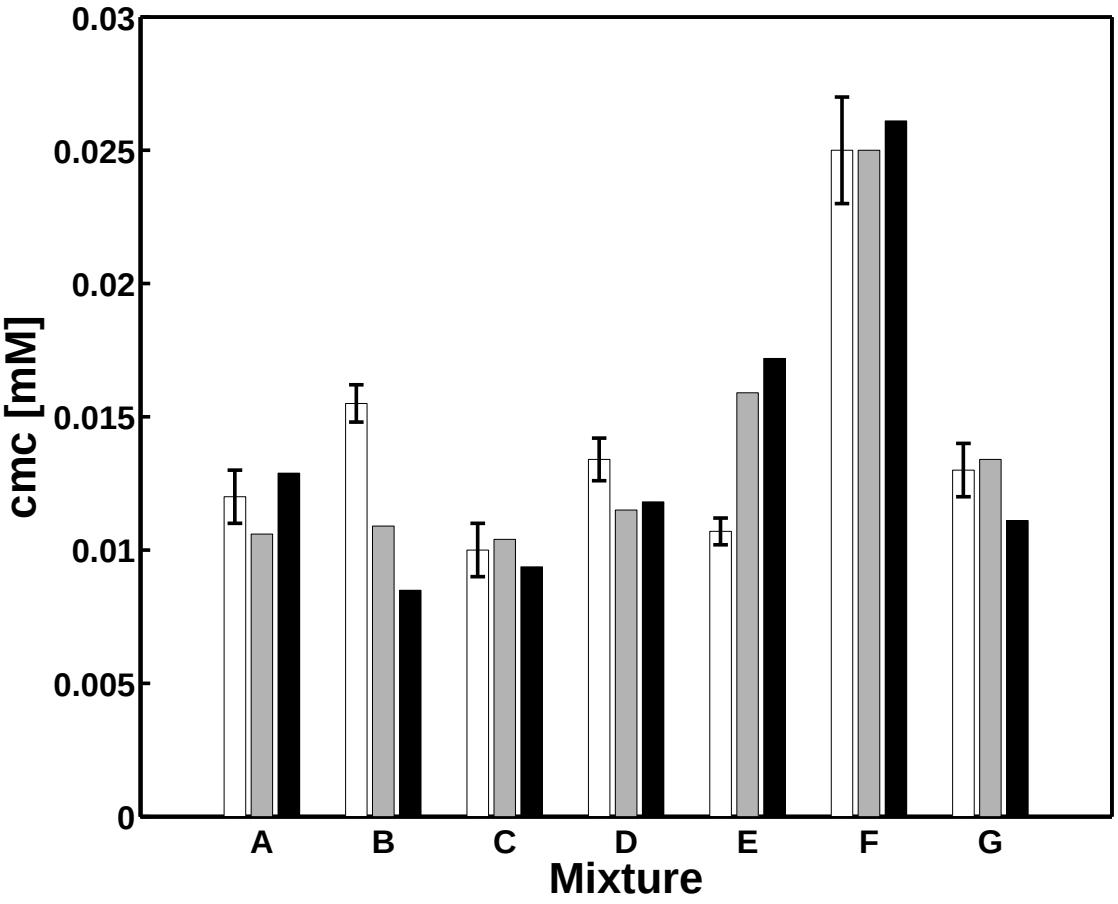

Figure 6-4: Comparison of experimental[69] (white bars), RST calculations (grey bars), and MT predictions (black bars) of the cmc's of mixtures of C_{14}DAO and C_{16}Bet. The compositions of the mixtures are listed in Table 6.1.

Table 6.1: Compositions of mixtures of C_{14}DAO and C_{16}Bet studied by Zimmerman and Schnaare.[69]

	Component composition			
Mixture	C_{16}Bet	C_{14}DAO	C_{14}DAOH$^+$	pH
A	0.50	0.10	0.40	4.3
B	0.90	0.04	0.06	4.8
C	0.75	0.11	0.14	4.8
D	0.50	0.22	0.28	4.8
E	0.25	0.33	0.42	4.8
F	0.10	0.40	0.50	4.8
G	0.50	0.36	0.14	5.3

mixtures B and E. These particular mixtures warrant further investigation to confirm that the observed experimental trend is reproducible. If the observed experimental trend is reproducible, this indicates that this system exhibits rather unique synergy that is not well modeled by either RST or the MT theory.

6.5.3. Prediction of the Micellar Titration Behavior

We next apply the MT theory to predict the titration behavior of micelles of C_{12}DAO and a conventional surfactant. Three conventional surfactants are examined: the nonionic surfactant dodecyl octa(ethylene oxide) ($C_{12}E_8$) and the cationic surfactant dodecyltrimethylammonium bromide (C_{12}TAB), which were also analyzed by an RST-based theory in Chapter 4, and the anionic surfactant SDS. The C_{12}DAO/SDS titrations are only reported up to 25% protonation of C_{12}DAO, since solutions with greater protonation became turbid. Because isotropic micellar phases are usually transparent, the turbidity suggests the formation of other phases (such as vesicles, ordered cylindrical phases, or lamellae) that are not modeled within the context of the MT theory.

Just as the pK_a is commonly used to characterize the pH equilibrium of a simple

acid, the pH equilibrium of micellized surfactant can be modeled in terms of the pK_m (see section 6.4). In Chapter 3, the predicted pK_m of C_{12}DAO was consistently lower than the experimental pK_m, a discrepancy that was tentatively attributed to hydrogen bonding and/or to additional electrostatic synergy. In this chapter, we are largely interested in the ability of the MT theory to capture the additional effect of the added conventional surfactant on the pK_m. Therefore, rather than comparing absolute pK_m values, which largely reflect the ability to model the self-interaction of C_{12}DAO, we compare relative pK_m values (ΔpK_m), which are defined as follows:

$$\Delta \mathrm{p}K_m = \mathrm{p}K_m - \mathrm{p}K_m(\alpha_{C_{12}DAO} \rightarrow 1) \tag{6.13}$$

where pK_m($\alpha_{C_{12}DAO} \rightarrow 1$) denotes the p$K_m$ in the limit of a micelle containing only deprotonated C_{12}DAO. The ΔpK_m should better reflect the ability of the MT theory to model the specific effect of the added conventional surfactant.

6.5.3.1. Mixtures of C_{12}DAO and the Nonionic Surfactant $C_{12}E_8$

In Figure 6-5, the predicted (lines) and the experimental ($\times$'s) ΔpK_m's are compared as a function of the protonated fraction of C_{12}DAO ($x_{C_{12}DAOH} \equiv \alpha_{C_{12}DAOH}/(\alpha_{C_{12}DAO} + \alpha_{C_{12}DAOH})$) for C_{12}DAO/$C_{12}E_8$ mixtures with $\alpha^{total}_{C_{12}E_8}$ =0.90 (Figure 6-5(a)), 0.75 (Figure 6-5(b)), 0.50 (Figure 6-5(c)), and 0.29 (Figure 6-5(d)). Excellent agreement is observed at $\alpha^{total}_{C_{12}E_8}$ = 0.90 , for which the ΔpK_m is slightly negative (0 to –0.5), indicating that it is slightly more difficult to incorporate $C_{12}DAOH^+$ into $C_{12}E_8$-rich micelles than into C_{12}DAO-rich micelles. The ΔpK_m shows only a weak dependence on $x_{C_{12}DAOH}$ when $\alpha^{total}_{C_{12}E_8}$ is high, as indicated by the small slopes of the curves in Figures 6-5(a) and (b). As $\alpha^{total}_{C_{12}E_8}$ decreases, the ΔpK_m curves have a more negative slope, which is accurately captured by the MT predictions. However, at $\alpha^{total}_{C_{12}E_8}$ =0.50 and 0.29, the MT theory underpredicts the ΔpK_m by approximately 0.5. The lower ΔpK_m values correspond to MT predictions "favoring" too much the deprotonated form of C_{12}DAO. One possible explanation that is consistent with the observations in pure C_{12}DAO micelles (see ref 190 and Chapter 3) is that the g_{elec} contribution to

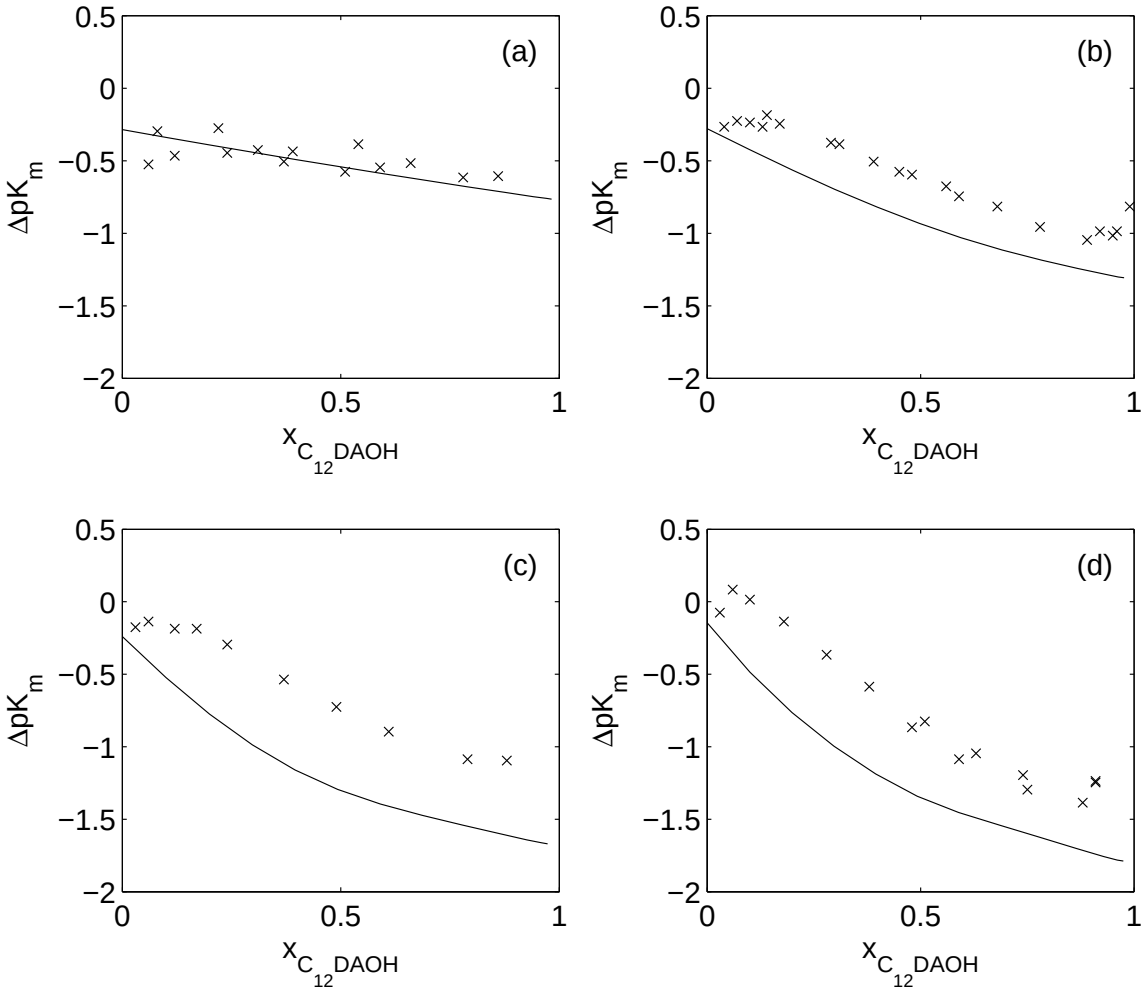

Figure 6-5: Comparison of the predicted (lines) and the experimental ($\times$'s) $\Delta \mathrm{p}K_\mathrm{m}$'s of $C_{12}DAO/C_{12}E_8$ micelles as a function of the degree of protonation of $C_{12}DAO$ ($x_{C_{12}DAOH}$). The composition of $C_{12}E_8$ ($\alpha^{\mathrm{total}}_{C_{12}E_8}$) is 0.90 (in (a)), 0.75 (in (b)), 0.50 (in (c)), and 0.29 (in (d)).

g_m may be too high for ionic surfactants and/or too low for zwitterionic surfactants.

As indicated in Chapter 3, the most important free-energy contribution for the determination of the pK_m is g_{elec}. Although the full MT theory is necessary to provide quantitative predictions, the observed behavior can be understood qualitatively by examining the effect of $\alpha_{C_{12}E_8}$ and $x_{C_{12}DAOH}$ on g_{elec}. As shown in Chapter 3, the pK_m decreases as g_{elec} increases. In particular, g_{elec} increases with the average valence of the micellized surfactant, $z_{mic} = x_{C_{12}DAOH}(1 - \alpha_{C_{12}E_8})$, as shown in eqs 22 and 2.22 in ref 138 and Chapter 2, respectively. Therefore, as $x_{C_{12}DAOH}$ increases, z_{mic} and g_{elec} increase, leading to a decrease in the pK_m. However, as $\alpha_{C_{12}E_8}$approaches unity, z_{mic} and g_{elec} only increase slightly with $x_{C_{12}DAOH}$, and the pK_m decreases only slightly as $x_{C_{12}DAOH}$ increases.

6.5.3.2. Mixtures of C_{12}DAO and the Cationic Surfactant C_{12}TAB

Extremely interesting titration behavior was found in mixtures of C_{12}DAO and C_{12}TAB. In Figure 6-6, the predicted (lines) and the experimental (×'s) ΔpK_m's are compared as a function of $x_{C_{12}DAOH}$ for mixtures with $\alpha^{total}_{C_{12}TAB} = 0.90$ (Figure 6-6(a)), 0.76 (Figure 6-6(b)), 0.50 (Figure 6-6(c)), and 0.24 (Figure 6-6(d)). Although the predicted ΔpK_m curves capture the slope of the experimental ΔpK_m curves reasonably well, the predicted ΔpK_m values are consistently too low by 1 to 1.5. The ΔpK_m values are all negative because the presence of the cationic C_{12}TAB increases g_{elec} and favors the micelle incorporating the zwitterionic C_{12}DAO rather than the cationic $C_{12}DAOH^+$. However, the experimental ΔpK_m data are much less negative than the predicted values. In fact, at $\alpha^{total}_{C_{12}TAB} = 0.90$, the experimental ΔpK_m is approximately –0.8 to –0.9, which is only slightly more negative than the value of –0.5 observed in the $C_{12}DAO/C_{12}E_8$ mixtures at $\alpha^{total}_{C_{12}E_8} = 0.90$. This indicates that the incorporation of $C_{12}DAOH^+$ into a highly-charged C_{12}TAB-rich micelle is only slightly more "difficult" (that is, it produces a slightly greater increase in g_m) than the incorporation of $C_{12}DAOH^+$ into a nearly neutral $C_{12}E_8$-rich micelle.

Although g_{elec} has been suggested as the source of the discrepancy in the $C_{12}DAO/C_{12}E_8$ system, the success of the MT theory for other predictions (see

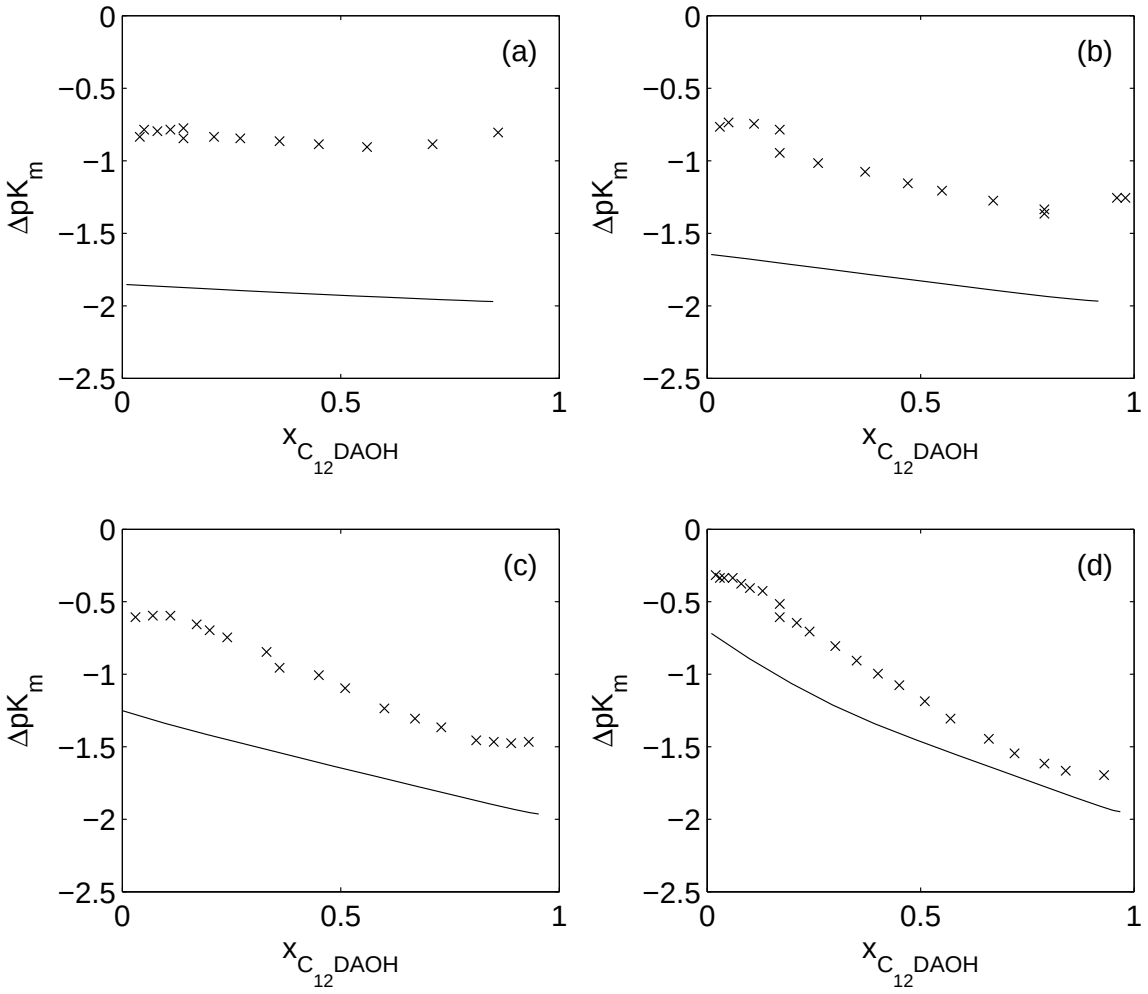

Figure 6-6: Comparison of the predicted (lines) and the experimental ($\times$'s) pK_{m}'s of C_{12}DAO/C_{12}TAB micelles as a function of the degree of protonation of C_{12}DAO ($x_{C_{12}\mathrm{DAOH}}$). The composition of C_{12}TAB ($\alpha^{\mathrm{total}}_{C_{12}\mathrm{TAB}}$) is 0.90 (in (a)), 0.76 (in (b)), 0.50 (in (c)), and 0.24 (in (d)).

Chapters 2, 3, and 5) suggests that g_{elec} is sufficiently accurate that it cannot be the only source of the discrepancy observed in the C_{12}DAO/C_{12}TAB system. Therefore, we conjecture that part of the discrepancy may arise from ion-specific interactions, and in particular, from the interactions of the bromide ions with the micelle. In fact, micelles of hexadecyltrimethylammonium are markedly more sensitive to bromide than to chloride, requiring only 0.1 M sodium bromide (NaBr) but 1.0 M NaCl to undergo a sphere-to-rod transition.[212,213] On the other hand, the pK_{m} of C_{12}DAO is lower in 0.06 M NaBr[49] than in 0.05 M NaCl,[169] suggesting that the bromide ions do not have any particular affinity for C_{12}DAOH$^+$. Instead, the bromide ions could have an indirect effect on the pK_{m}, for example, by favoring the formation of cylindrical micelles through their interactions with C_{12}TAB. Such an effect is consistent with experimental observations that the pK_{m} of C_{14}DAO cylindrical micelles is higher than the pK_{m} of spherical C_{12}DAO micelles.[51] Whether this effect is sufficient to explain the observed discrepancy between the predicted and the experimental ΔpK_{m} in the C_{12}DAO/C_{12}TAB system is presently unclear. Therefore, further experimental studies are warranted on C_{12}DAO/C_{12}TAB and related mixtures. For example, titrations should be conducted in mixtures of C_{12}DAO and the chloride analogue of C_{12}TAB. In addition, micellar titrations and light scattering studies at varying concentrations of NaCl and NaBr may help to identify the specific role of micelle shape on the pK_{m}.

6.5.3.3. Mixtures of C_{12}DAO and the Anionic Surfactant SDS

Finally, the predicted (lines) and the experimental ($\times$'s) ΔpK_{m} values are compared in Figure 6-7 for mixtures of C_{12}DAO and SDS. Due to the tendency of this system to become turbid, the only SDS compositions ($\alpha_{\text{SDS}}^{\text{total}}$) studied were 0.25 (Figure 6-7(a)) and 0.10 (Figure 6-7(b)), and the maximum $x_{\text{C}_{12}\text{DAOH}}$ value is 0.25. Because anionic SDS interacts more favorably with C_{12}DAOH$^+$ than with C_{12}DAO, the ΔpK_{m} values are positive at nearly all the conditions examined. Only after the amount of C_{12}DAOH$^+$ in the micelle exceeds the amount of SDS does ΔpK_{m} become negative. Due to the limited range of experimental conditions examined, such negative ΔpK_{m}

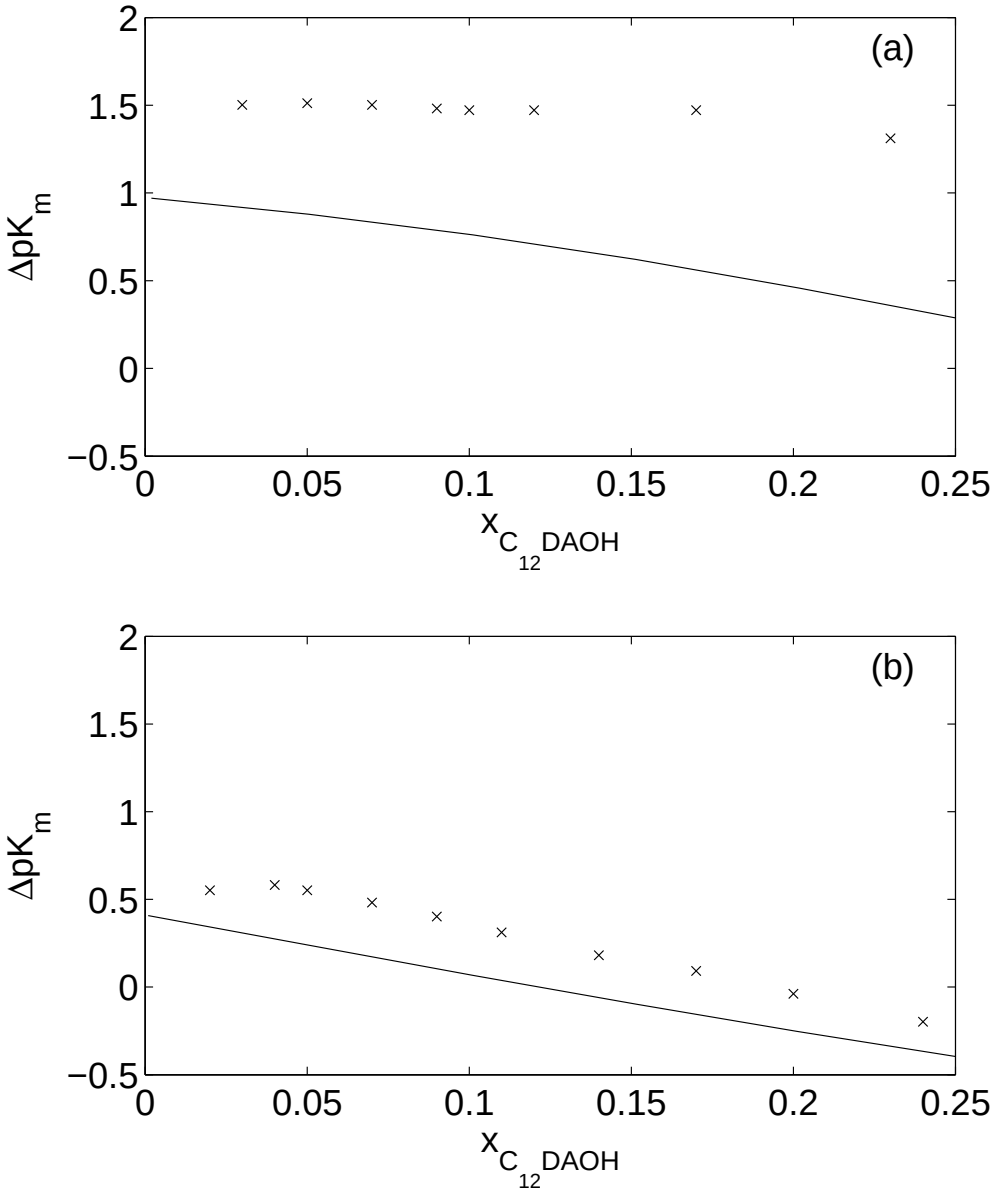

Figure 6-7: Comparison of the predicted (lines) and the experimental ($\times$'s) pK_{m}'s of C_{12}DAO/SDS micelles as a function of the degree of protonation of C_{12}DAO ($x_{C_{12}\mathrm{DAOH}}$). The composition of SDS ($\alpha_{\mathrm{SDS}}^{\mathrm{total}}$) is 0.25 (in (a)) and 0.10 (in (b)).

values are only observed for $\alpha_{\mathrm{SDS}}^{\mathrm{total}} = 0.1$ when $x_{\mathrm{C_{12}DAOH}}$ is greater than 0.15 (predicted) or 0.20 (experimental).

The predicted $\Delta \mathrm{p}K_{\mathrm{m}}$ values agree well with the experimental values for $\alpha_{\mathrm{SDS}}^{\mathrm{total}} = 0.1$. Although the $\Delta \mathrm{p}K_{\mathrm{m}}$ values are correctly predicted to be more positive for $\alpha_{\mathrm{SDS}}^{\mathrm{total}} = 0.25$, the predicted $\Delta \mathrm{p}K_{\mathrm{m}}$ values are 0.5 to 1.0 lower than the experimental $\Delta \mathrm{p}K_{\mathrm{m}}$ values. Perhaps more surprising, the experimental $\Delta \mathrm{p}K_{\mathrm{m}}$ values are nearly constant, except for the final data point at $x_{\mathrm{C_{12}DAOH}} = 0.23$, which is very close to the point where the solution became turbid. The $\Delta \mathrm{p}K_{\mathrm{m}}$ is only predicted to be independent of $x_{\mathrm{C_{12}DAOH}}$ in the limit $\alpha_{\mathrm{SDS}}^{\mathrm{total}} \to 1$. These results indicate that the MT theory underestimates the synergy between SDS and $\mathrm{C_{12}DAOH^+}$. Sources of additional synergy should be investigated further, including the formation of SDS/$\mathrm{C_{12}DAOH^+}$ ion pairs.

6.6. Conclusions

A molecular-thermodynamic (MT) theory was developed and validated for mixtures of pH-sensitive and conventional surfactants. The theory accurately predicted the pH of $\mathrm{C_{12}DAO}$/SDS solutions upon the addition of HCl, but only qualitatively captured the behavior of the solution pH without added acid. The MT theory explicitly accounts for counterion binding, and predictions of sodium binding in $\mathrm{C_{12}DAO}$/SDS mixtures compared favorably with the experimental values. Predicted cmc's of mixtures of $\mathrm{C_{14}DAO}$ and $\mathrm{C_{16}Bet}$ were comparable to, and sometimes better than, the cmc's determined using the empirical RST. Finally, $\mathrm{p}K_{\mathrm{m}}$ data were examined for mixtures of $\mathrm{C_{12}DAO}$ with $\mathrm{C_{12}E_8}$, $\mathrm{C_{12}TAB}$, and SDS. Although the $\mathrm{C_{12}DAO}$/$\mathrm{C_{12}E_8}$ mixtures were modeled reasonably well with the MT theory, both $\mathrm{C_{12}TAB}$ and SDS exhibited more favorable interactions with the protonated $\mathrm{C_{12}DAOH^+}$ than was predicted.

The MT theory may prove useful for understanding and designing surfactant mixtures of both fundamental and practical interest. In particular, the theory may assist in formulating commercial detergents, which typically utilize pH-sensitive surfactants as secondary components. Furthermore, the relationship between the $\mathrm{p}K_{\mathrm{m}}$

and the type and amount of conventional surfactant may lead to new or improved pH-responsive systems. These future research directions are explored in more detail in Chapter 7.

Chapter 7

Conclusions and Future Work

7.1. Thesis Summary

In this thesis, several models were developed to describe and quantify, at the molecular level, the micellization behavior of pH-sensitive and conventional surfactant mixtures. Two modeling approaches were utilized: (1) a molecular-thermodynamic[138,190] (MT) approach, and (2) an approach based on regular solution theory[35,37] (RST) in the context of the pseudophase approximation. The RST approach is conceptually simpler, and can often yield accurate predictions (since it incorporates experimental data). However, RST does not provide as much physical insight, and does not capture any details of the micelle structure. In contrast, the MT approach requires no experimental data, predicts micelle shape and size, and provides more physical insight.

In Chapter 2, a MT theory was developed to account for counterion binding to mixed micelles composed of ionic-nonionic and ionic-zwitterionic binary surfactant mixtures. The model successfully predicted the degree of counterion binding of monovalent and multivalent ions to mixed micelles as a function of the composition of the ionic surfactant in the micelle (α). Although the degree of counterion binding increased with α, the degree of counterion binding was negligible at low α, consistent with the existence of a critical value of α (or critical micelle surface charge density) for counterion binding. In addition, an inflection in the counterion

binding vs. α curve was correlated to a micelle shape transition. This inflection was rationalized in terms of the different behaviors of the degree of counterion binding for spherical and cylindrical micelles. The predicted degree of counterion binding was also compared to the apparent degree of counterion binding, inferred from the slope of the critical micelle concentration (cmc) vs. the salt concentration curve (the Corrin-Harkins slope).[130] The Corrin-Harkins slope was found to be a reasonable estimate of the degree of counterion binding only for micelles composed primarily of ionic surfactants. In addition, explicitly modeling counterion binding was found to improve the quantitative prediction of micelle aggregation numbers in mixtures of ionic and nonionic surfactants.

In Chapter 3, the MT theory presented in Chapter 2 was generalized to include pH effects in order to model the micellization of a pH-sensitive surfactant. To our knowledge, this theory is the first molecular theory to model pH-dependent micellization. The theory was validated by comparing the predictions to experimental data for alkyldimethylamine oxide surfactants (C_iDAO, where i denotes the length of the alkyl tail), which are cationic in the protonated state at low pH, zwitterionic in the deprotonated state at high pH, and mixtures of the two forms at an intermediate pH. Although the predictions were found to be qualitatively similar to the experimental data, some quantitative differences were observed. In particular, a minimum in the cmc and a maximum in the micelle aggregation number were predicted to occur at low α (that is, when the micelles are rich in the deprotonated, zwitterionic form of C_iDAO), while the experimentally observed extrema occurred at $\alpha \approx 0.50$. Consistent with observations in Chapter 2, the predicted micelle aggregation numbers of C_{12}DAO were substantially improved by explicitly modeling counterion binding. These extrema are due to self-synergy between the protonated and the deprotonated forms of C_iDAO, an effect which was previously attributed to the formation of surfactant-surfactant hydrogen bonds in the micelle.[51,146] Although hydrogen bonds were not explicitly included in the MT theory, the theory developed in Chapter 3 clearly demonstrates that electrostatic interactions can account for some of the observed self-synergy. Likewise, some of the discrepancy between the predicted and

the experimental properties may be due to limitations of the electrostatic model. In particular, the electrostatic penalty associated with incorporating zwitterionic surfactants into micelles could have been underestimated.

In addition, very good quantitative agreement was observed for the predicted cmc of C_{12}DAO in solutions containing no added salt. In fact, an observed maximum in the cmc was reproduced at $\alpha = 0.8$. This maximum could not be reproduced by the commonly used RST,[35,37] even though RST uses experimentally measured cmc's to fit the data. Furthermore, the MT theory allowed the cmc maximum to be rationalized in terms of electrostatic interactions between the micellized surfactants.

Micellar titration data were also examined in terms of the relative values of the micellar deprotonation equilibrium parameter (ΔpK). In the case of C_iDAO surfactants, the ΔpK was shown to be related to the derivative of the electrostatic contribution to the free energy of micellization (g_{elec}) with respect to α. Contrary to a previous electrostatic model of micellar titration,[64] the MT model of g_{elec} predicted $\Delta pK > 0$ in the limit of micelles composed entirely of the deprotonated C_iDAO, which is consistent with the experimental data.

In Chapter 4, a theory based on RST was developed to model the titration behavior of micelles containing a pH-sensitive surfactant and an arbitrary number of conventional surfactants. We also demonstrated that conventional surfactants can be equivalently modeled by a single effective surfactant, thus considerably simplifying the analysis of multicomponent surfactant mixtures. The theory predicts that the ΔpK depends on three quantities that characterize the surfactants and their interactions: (1) the ratio of the cmc's of the protonated and the deprotonated forms of the pH-sensitive surfactant, (2) the interaction between the deprotonated and the protonated forms of the pH-sensitive surfactant in the micelle, and (3) the preferential interaction of the conventional surfactant with the protonated, or with the deprotonated form, of the pH-sensitive surfactant in the micelle. The RST model was also validated using experimental titration data for single surfactant systems (obtained from the literature) and for binary surfactant mixtures (measured as part of this thesis). In addition, the experimental uncertainties in the experimental

titration data were examined, and a new method was proposed to account for these uncertainties by using a weighted regression analysis.

In Chapter 5, a MT theory was developed to model the micellization behavior of mixtures containing an arbitrary number of conventional surfactants. The maximum micelle radius, which depends on the packing contribution to the free energy of micellization, was examined theoretically for a ternary surfactant mixture. Due to the limited availability of experimental data, only predicted cmc's were compared to the experimental data. In this respect, good agreement was observed for the predicted cmc's, which were comparable to, and sometimes better than, the cmc's determined using RST.

Several difficulties are associated with the application of RST to a commercial surfactant containing a large number of components. Separating the individual surfactant components may be prohibitively difficult or expensive. Even if the individual surfactant components are available, the combinatorial growth of the number of β parameters with the number of surfactant components[38] translates into a prohibitively large number of cmc measurements. Therefore, the MT theory may be particularly advantageous for modeling commercial surfactants containing a large number of components. To this end, the MT theory was applied to a commercial nonionic surfactant (Genapol UD-079), which was modeled as a mixture of 16 surfactant components. The predicted cmc of Genapol UD-079 agreed remarkably well with the experimental cmc.

Other properties of aqueous solutions of Genapol UD-079 were examined theoretically. For example, the predicted monomer concentration was found to increase significantly above the cmc, consistent with experimental observations in other nonionic surfactant mixtures.[202] In addition, the predicted monomer and micelle compositions as a function of surfactant concentration were examined for representative surfactant components. Variations in the predicted micelle composition were rationalized in terms of the competition between steric and entropic effects. A transition in micelle shape was also predicted to affect the micelle composition near the cmc.

In Chapter 6, the MT theory for multicomponent surfactant mixtures developed in Chapter 5 was generalized to include pH effects. This theory allows the molecular-level prediction of the micellization behavior of mixtures of a pH-sensitive surfactant and an arbitrary number of conventional surfactants. Predicted values of the solution pH compared favorably to experimental data for solutions of the pH-sensitive surfactant C_{12}DAO and the anionic surfactant sodium dodecyl sulfate (SDS). The strong interactions between the protonated form of C_{12}DAO and the anionic SDS led to significant changes in the solution pH. In addition, the predicted pH-dependence of the cmc of various mixtures of two pH-sensitive surfactants compared favorably to the experimental data. The MT theory was also validated using titration data for varying compositions of mixed micelles containing C_{12}DAO. These data included the titration data presented in Chapter 4 for C_{12}DAO mixed with a cationic or with a nonionic surfactant. In addition, experimental data was presented for the titration of mixed micelles composed of C_{12}DAO and SDS. The MT theory accurately modeled the titration behavior of C_{12}DAO mixed with the nonionic surfactant. However, the experimental titration data for mixtures of C_{12}DAO and the cationic surfactant, or the anionic surfactant, suggest that the protonated form of C_{12}DAO experiences an additional favorable interaction with the ionic surfactants that is not captured by the MT theory, perhaps due to ion-specific interactions or ion-pair formation.

7.2. Future Research Directions

The research presented in this thesis has led to several interesting questions that have remained unanswered. With this in mind, some ideas for future research directions in the areas of counterion binding, multicomponent surfactant mixtures, and pH-sensitive surfactants are discussed below in sections 7.2.1, 7.2.2, and 7.2.3, respectively. In addition, some general ideas for possible future research on self-assembly are discussed in section 7.2.4.

7.2.1. Future Research Directions on Counterion Binding

The work on counterion binding presented in Chapter 2 suggests some interesting areas for future experimental and theoretical work. For example, we proposed that the degree of counterion binding predicted by the MT theory would correspond most closely to the experimental data obtained spectroscopically. In order to test this proposition, it would be useful to spectroscopically measure the degree of counterion binding in mixed micelles as a function of the micelle composition. In addition, as discussed in Appendices A and F, the approximations used to estimate the concentration of ions in the diffuse layer may not be quantitatively accurate at some experimentally relevant conditions. Therefore, it may be useful to combine the MT approach with a cell model like that developed by Gunnarsson et al.[82] Such a cell model would involve solving the Poisson-Boltzmann equation to determine the spatial distribution of ions around a micelle. The local concentration of ions can then be: (1) quantitatively correlated with the degree of counterion binding as measured by various experimental techniques, and (2) incorporated into more rigorous mass balances for the various ions present in the solution.

Counterion binding also plays an important role in micelle-enhanced catalysis. For example, micelles may enhance reaction rates for reactions involving materials possessing very different aqueous solubilities. In particular, a hydrophobic reactant can be solubilized in a micelle to increase its reaction rate with a hydrophilic moiety. Reactions with inorganic counterions may be particularly suitable for micelle-enhanced catalysis, since the local concentration of the counterions around a charged micelle will be much larger than the bulk concentration of the counterions. Since the micelles will generally contain both surfactants and solubilized reactants, the MT theory developed to model counterion binding to mixed micelles may be an appropriate starting point to model such systems.

The most commonly used approach to model micelle-enhanced catalysis is the pseudophase ion-exchange (PIE) model.[214–217] This approach utilizes the pseudophase approximation and generally assumes that the degree of counterion binding to micelles

is independent of the salt and the surfactant concentration. The MT approach can be used to relax both of these assumptions and to provide a quantitative estimate of the degree of counterion binding, which can then be used to calculate selectivity coefficients used in the analysis of the reaction kinetics. The MT theory may also offer advantages over more sophisticated alternatives to the PIE model. For example, cell models of micelle kinetics in which electrostatics are modeled with the Poisson-Boltzmann equation have utilized the micelle size as an adjustable parameter.[218,219] The MT theory offers a predictive alternative to both the PIE and the cell model approaches, offering the ability to predict how the degree of counterion binding and other micelle properties change with the solution conditions.

7.2.2. Future Research Directions on Multicomponent Surfactant Mixtures

The MT theory for multicomponent surfactant mixtures presented in Chapter 5 was only validated with experimental cmc's, due to the limited availability of literature data on other micellization properties. Therefore, one important direction for future research is to generate a larger set of experimental data on multicomponent surfactant mixtures. In particular, micelle aggregation numbers would be particularly useful to test the MT theory. For example, experimental studies of micelle aggregation numbers could be used to verify the MT prediction that the size of the micelles of Genapol UD-079 decreases with increasing surfactant concentration near the cmc. Unlike the commercial surfactant Genapol UD-079, for which all the surfactant components have the same hydrophobic tail, the commercial, nonionic surfactant Genapol 26-L-98, which exhibits polydispersity in the surfactant tails in addition to polydispersity in the degree of ethoxylation, would be an interesting subject for further theoretical and experimental studies. In addition, experimental cmc's of mixtures of Genapol 26-L-98 and the commercial cationic surfactant BTC-8358 have already been collected.[38] Conducting additional experiments to measure the micelle aggregation numbers of this ionic-nonionic commercial surfactant mixture would allow the multicomponent

MT theory to be further tested in the case of micelles possessing variable surface charge density. Since such a mixture is similar to the type of surfactant mixtures used in practical formulations, such studies could serve as a powerful validation of the MT theory for systems of industrial relevance.

Even at the level of cmc data, experimental studies of multicomponent surfactant mixtures have been largely limited to systems that can be modeled with relative success using RST. Although several studies have considered binary surfactant mixtures that are poorly modeled using RST (see ref 36 and references cited therein), analogous results have not yet been reported for ternary (or higher) multicomponent surfactant mixtures. These studies also indicate that the RST may be less accurate to model micelle compositions than to model cmc's. With this in mind, the MT theory could be used to screen ternary surfactant mixtures for experimental studies. Those mixtures for which the MT theory indicates that the micellization properties deviate the most from those predicted using RST can then be studied experimentally to determine their cmc's, micelle aggregation numbers, and micelle compositions. Such an approach may provide an efficient way to identify, for the first time, a ternary surfactant system that is not well characterized by the RST.

An additional direction for research on multicomponent surfactant mixtures would be the development of correlations with practical performance properties. For example, the behavior of the cmc was previously correlated to the cleaning ability of a mixture of anionic surfactants.[4] However, a recent study of multicomponent surfactant mixtures indicated that the optimal formulation depends on the particular performance criterion considered.[16] Some detergent formulations may be more appropriate for particular fabrics, or for particular stains (for example, dirt, grease, or oil). Although the authors in ref 16 identified some basic reasons why a particular surfactant may perform better in a particular application, a more fundamental analysis may be useful to optimize detergent formulations. For example, it may be useful to identify whether there is a correlation between cleaning ability, the surface charge of the fabric, and the micelle surface charge. Similarly, a recently developed MT theory of micellar solubilization[200] may be useful to correlate cleaning ability to

the solubilization capacity of a particular surfactant formulation.

7.2.3. Future Research Directions on pH-Sensitive Surfactants

In principle, the MT theory for pH-sensitive surfactants presented in Chapter 3 can be applied to any pH-sensitive surfactant for which suitable molecular parameters can be estimated. However, some pH-sensitive surfactants, such as fatty acids, do not micellize when they are either fully protonated or fully deprotonated. For such systems, it would be useful to couple the MT theory of micellization with the equilibrium constraints that govern solubility. This may be done following approaches that are similar to those used to combine precipitation and micellization thermodynamics for fatty acids[139] or for surfactant mixtures.[185,187] In particular, thermodynamic descriptions of solubility, such as solubility constants or solubility products, may be utilized with monomer concentrations predicted by the MT theory in order to determine whether precipitation will occur.

In addition, further research is needed to clarify the importance of hydrogen bonding to the micellized pH-sensitive surfactants. Fully atomistic molecular-dynamics (MD) simulations of micelles composed of pH-sensitive surfactants may provide the microstructural details needed to determine the effect of hydrogen bonding on micellization. If simulations of micellized surfactants confirm that hydrogen bonds form primarily between surfactant pairs rather than between surfactants and water, then further research must be conducted on how to best incorporate hydrogen bonding into the MT framework. To this end, the Monte Carlo approach used by Terada et al.[147] may provide a useful starting point. Specifically, these authors predicted the energetic contribution due to hydrogen bonds as a function of micelle composition. In theory, this energy profile could be fit using a polynomial, and then incorporated into the MT theory, similar to the approach currently used to incorporate the results of mean-field simulations of the packing of surfactant tails in the micelle core. In fact, the use of such hybrid approaches to model micellization will be further discussed in section 7.2.4. However, it is first necessary to address several issues. For example, although Maeda has suggested that the free energy associated with hydrogen bonding

may vary with the micelle shape,[51] the Monte Carlo simulations assumed a single value for the energy associated with the hydrogen bonds. Fully atomistic simulations may determine more quantitatively whether the hydrogen bond energetics are different for spherical and cylindrical micelles. In addition, the Monte Carlo simulations utilized a lattice model with a fixed micelle surface area per surfactant molecule. The MT approach allows this area to be determined through the minimization of the free energy of micellization. Therefore, additional simulations should be conducted to determine the sensitivity of the hydrogen bond energetics to the micelle surface area per surfactant molecule.

The titration results presented in Chapters 4 and 6 raised several interesting questions. For example, the protonated, cationic form of C_{12}DAO and the cationic surfactant dodecyltrimethylammonium bromide (C_{12}TAB) exhibited an unexpected high degree of synergy. In Chapter 6, we postulated that this synergy may be due to specific interactions of the bromide ions. Therefore, additional studies of mixtures of C_{12}DAO and either C_{12}TAB or the chloride analogue of C_{12}TAB (C_{12}TAC) could be conducted to test this hypothesis. In particular, micellar titrations should be conducted on C_{12}DAO/C_{12}TAC mixtures and compared to the micellar titrations of C_{12}DAO/C_{12}TAB. In addition, light scattering measurements should be conducted to determine the micelle aggregation numbers of mixtures of C_{12}DAO/C_{12}TAB and C_{12}DAO/C_{12}TAC. Finally, ion selective electrode measurements, or conductivity measurements, could be used to determine the degree of counterion binding to C_{12}DAO/C_{12}TAB and to C_{12}DAO/C_{12}TAC mixed micelles. Taken together, the results of these experiments could help clarify the role of the bromide or the chloride ions on the micellar titration behavior, including their indirect roles through changes in the micelle shape and size.

Similarly, the experimental titrations of C_{12}DAO and SDS exhibited an even greater degree of synergy than was predicted by the MT theory. Due to the tendency of this mixed surfactant system to precipitate, atomistic simulations may be a more convenient method to unravel the source of this synergy. For example, the simulations could identify whether ion pairs are formed. Simulations utilizing thermodynamic

integration could determine the free-energy change associated with replacing a deprotonated C_{12}DAO surfactant molecule in a micelle with a protonated C_{12}DAO surfactant molecule. Alternatively, simulations could be used to gain additional useful insight by studying the micellization of "artificial molecules" that could never be synthesized. For example, simulations of a surfactant that is identical to the anionic surfactant SDS, except that it would carry no net charge, could reveal the role of the electrostatic interactions. Likewise, the role of steric interactions could be studied by simulating SDS analogues that possess increasingly larger surfactant heads. Similarly, experimental studies could be conducted by replacing SDS with an anionic surfactant like sodium dodecyl poly(ethylene oxide) sulfate. Such a surfactant will likely experience weaker electrostatic interactions with C_{12}DAO, thereby reducing the tendency to precipitate or to form non-micellar phases. In fact, one such surfactant (sodium dodecyl di(ethylene oxide) sulfate) was used by Alargova et al.[73,74] to study multivalent counterion binding, presumably because SDS precipitates too readily in the presence of the multivalent ions.

The MT approach should also be extended to model more complex pH-sensitive molecules. In particular, the ability to model polyaromatic structures could prove useful for pharmaceutical applications. For example, the micellar solubilization of the pH-sensitive drug flurbiprofen was recently studied by Li and Zhao.[7] Although these authors successfully modeled the system, their model required the experimental determination of the partitioning of the protonated and the deprotonated forms of flurbiprofen between the bulk solution and the micelles. In principle, the partition coefficients could be predicted by using a suitable MT theory. In fact, a hybrid MD/MT approach was recently used to model the solubilization of ibuprofen,[220] although pH-effects were not explicitly considered. By coupling the hybrid MD/MT approach developed by Stephenson et al. with the model for pH-dependent mixed micellization developed in Chapter 6, the solubilization of pH-sensitive drugs like flurbiprofen could be modeled using a predictive, molecular theory. Such a MT theory could serve as a screening tool for the formulation of poorly water-soluble pharmaceuticals via aqueous micellar solubilization.

Although this thesis has focused on micellization, the adsorption behavior of pH-sensitive surfactants may be another interesting direction for future research. In fact, a MT theory has already been developed to model the surface tension of solutions containing ionic and zwitterionic surfactants.[211,221] This theory relates the surface tension of the solution to the monomer concentrations. In theory, the surface tension of solutions containing pH-sensitive surfactants could be predicted by combining this surface tension theory with the monomer concentrations predicted using the MT theory developed in Chapter 6. However, a few challenges need to be addressed first. The composition of solutions containing pH-sensitive surfactants is controlled by the addition of acid or base, which may effect the surface tension of the solution, as is observed upon the addition of inorganic salts. However, the surface tension theory has not yet been generalized to account for the effect of added salt. In addition, the surface tension theory requires as input a single experimentally measured surface tension for each surfactant component. In the case of a pH-sensitive surfactant, the relevant experimental quantities are the surface tensions of solutions containing only the protonated form of the pH-sensitive surfactant and only the deprotonated form of the pH-sensitive surfactant. However, the experimental availability of these "single-surfactant" solutions may require extreme values of pH, which could require significant addition of acid or base, and affect the surface tension measurements.

Finally, vesicles containing pH-sensitive surfactants provide a very promising vehicle for drug encapsulation and delivery.[6,8–13,52,53,55–60] A MT theory has already been developed by Yuet and Blankschtein to model the formation of vesicles.[222–224] Since this theory was developed for mixtures of cationic and anionic surfactants, it first needs to be generalized to mixtures of ionic-nonionic or ionic-zwitterionic surfactants. In addition, if hydrogen bonding is proven to be important for the micellization of pH-sensitive surfactants, it would also need to be incorporated into a description of pH-dependent vesiculation. Nevertheless, once these challenges are addressed, pH-dependence can be readily incorporated into a MT theory of vesiculation of pH-sensitive surfactants through the Henderson-Hasselbalch equation, as demonstrated in Chapters 3 and 6.

7.2.4. Future Research Directions on Self-Assembly

Recent experimental developments in macromolecular chemistry suggest some possible directions for future theoretical studies. In particular, theory lags behind experiment in the area of self-assembly and solubilization utilizing novel amphiphiles. Three amphiphiles worthy of future study are amphiphilic dendrimers, peptide–nucleic-acid amphiphiles (PNAA's), and colloidal-particle amphiphiles.

Dendrimers are highly branched polymers that show potential benefits as solubilization agents for drug encapsulation and release.[225,226] Amphiphilic dendrimers may self-assemble into micelle-like structures,[226–228] or they may be used as "unimolecular micelles" for solubilization purposes. The theories developed for surfactant self-assembly may serve as guidelines to model dendrimers. A "dendritic amphiphile" was recently synthesized that forms micelles and exhibits phase separation behavior.[228] In fact, this amphiphile is strikingly similar in its chemistry and micellar behavior to alkyl poly(ethylene oxide) surfactants, which have been successfully modeled using the MT approach.[40] Likewise, several other dendrimer amphiphiles have recently been observed to self-assemble into vesicles and micelles.[226,227] Therefore, dendritic amphiphiles may be the most natural starting point for the application of the MT approach to dendritic molecules. Small dendrimer amphiphiles with linear alkane tails may be modeled relatively easily by the current MT theory. However, larger dendritic amphiphiles may require more substantial changes to the MT theory. For such systems, it may be more useful to initially model their self-assembly with phenomenological or geometric approaches, similar to the early models developed by Tanford[1] and Israelachvili[3] for surfactant self-assembly.

Although individual dendrimer molecules are not supramolecular aggregates, their conformation in solution is governed by the same physical interactions that govern micelle self-assembly, including steric and electrostatic interactions. The encapsulation of drugs in dendrimers is conceptually similar to the solubilization of drugs in micelles. Therefore, the MT approach may be useful in modeling the pH-dependent solubilization and release of hydrophobic compounds, which has been

demonstrated experimentally for several dendrimer systems.[225] A typical strategy for pH-dependent release is to modulate the hydrophobicity of the interior of a dendrimer containing pH-sensitive functional groups, such as amines. At high pH, the interior amines will be uncharged and relatively hydrophobic, thus allowing the incorporation of hydrophobic drugs. At low pH, the interior amines become charged, thus creating a more hydrophilic environment that leads to the release of the encapsulated material. If a MT-type free-energy decomposition can be developed to model the solubilization of hydrophobic materials, it may be possible to predict the solubilization capacity of dendrimers, or to optimize the dendrimers for a particular application.

PNAA's are surfactant-like molecules composed of a hydrophobic moiety, amino acids, and hydrophilic nucleic acids.[229,230] Because PNAA's can bind complementary single-stranded or double-stranded DNA, they are promising tools for the separation and sensing of DNA. One particular challenge in the design of the PNAA chemistry is to develop the right balance of hydrophobic chain length and amino acid composition for the desired nucleic acid moiety.[229] Although the surfactant head for PNAA's is relatively large, the current MT approach may be useful for qualitative predictions of their cmc behavior. Subsequent modeling may need to focus on more accurately accounting for the interactions between the complex heads of these amphiphiles.

PNAA's that contain two hydrophobic tails have also been synthesized.[230] As expected based on geometric packing constraints,[3] these PNAA's are more readily incorporated into vesicles or liposomes. In this case, the existing MT theory of vesiculation may be useful to predict the vesicle properties. However, the existing MT theory will need to be generalized to model double-tailed surfactants.

Finally, colloidal particles have been demonstrated as a flexible material for controlled self-assembly, including the creation of liposome-like structures.[231–233] Colloidal particles can adsorb at interfaces and stabilize emulsions.[232] Colloidal particles adsorbed to droplets in an emulsion can be locked together by various methods,[233] creating a structure called a colloidosome, due to its similarity to a liposome. One potential challenge to modeling such systems is that they may not be equilibrium structures.[231] Nevertheless, the driving force for self-assembly can

be modeled utilizing principles common to surfactant science,[232] such as interfacial tensions and contact angles. Therefore, a coarse-grained or phenomenological approach may be the most useful starting point for modeling the self-assembly and the surface-activity of colloidal particles. In addition, colloidal particles may offer some advantages for experimental studies, including the availability of particles made from a wide range of materials with varying surface chemistries. Therefore, colloidal particles may allow more fine-grained control over physical interactions than is currently possible using traditional surfactants.

The modeling of such novel amphiphiles will undoubtedly present significant challenges. Fortunately, theoretical and computational advances bring new approaches to these tough problems. One promising approach that builds on the strength of the MT approach is the complementary use of MT theory and simulations.[163,220,234] Fully atomistic simulations provide microstructural details that are outside the scope of MT theories. However, such simulations are currently too computationally intensive to be used to model the entire micellization process. Consequently, practical simulations strategies must be developed. Future research directions could exploit various hybrid approaches.

For example, the MT theory may be used to simplify simulations, by treating only part of a micelle in fully atomistic detail. Such an approach was used by Mohanty et al. to model the effect of an organic counterion on micellization.[163] A multi-tiered approach could also be employed. For example, after identifying the hydrophobic "tail" and the hydrophilic "head" in a complex surfactant via MD simulations,[234] additional simulations could be subsequently utilized to estimate more accurately the steric interactions between the micellized surfactant heads. Alkyl poly(ethylene oxide) (C_iE_j) surfactants may be an interesting class of surfactants to study using this approach. By conducting simulations of C_iE_j micelles, one may be able to develop a better model for the head-head steric interactions than the hard-disk model currently used. Subsequently, this approach could be applied to amphiphiles with more complex heads, such as the dendritic amphiphiles or the PNAA's discussed above.

Lastly, recent developments in simulations offer the possibility of extending

simulation methodologies to longer time scales and larger systems. In particular, implicit solvent models are being developed so that only the surfactant molecules are simulated in molecular detail.[235] If such methods are further developed and validated, they may make simulation an even more useful tool for the study of micellization. Currently, the practical constraints imposed by atomistic simulation methods require the preassembly of micelles with a particular aggregation number. However, implicit solvent models offer the possibility of simulating systems over sufficiently long time scales that the spontaneous self-assembly of surfactants can be observed, thus allowing the determination of the optimal micelle size. Therefore, simulations utilizing implicit solvent models may be particularly useful for studying irregular micelle shapes, such as globular micelles, shapes that cannot be easily modeled using the MT approach.

7.3. Concluding Remarks

As stressed in Chapter 1, the central goal of this thesis was to develop molecular-level theories for the micellization of pH-sensitive surfactants. The development of these theories also led to the development of theories for the micellization of conventional surfactant mixtures. The availability of these theories may help close the gap between theory and the types of surfactant systems of interest for practical applications. Since many interesting questions still remain to be answered, we hope that this thesis will also stimulate and help guide future studies on micellization and self-assembly.

Appendix A

Diffuse-Layer Contribution to the Mole Balances

The distribution of ions in an aqueous solution is affected by the presence of charged micelles. In order to determine the bulk concentrations of the various ions, we have modified a recently introduced approximate model to calculate the ion mole balances which satisfies the requirement that the bulk solution remains electroneutral.[43] The original model essentially assumed that only counterions are affected by the charged micelles, and ignored the possible effect of the charged micelles on the other charged components in the solution. In our model, we account for the effect of the charged micelles on *all* the charged components present in the solution (including counterions, co-ions, and surfactant ions). Although our predictions of counterion binding presented in Section 2.5.1 are not affected significantly by this modification to the original model, for completeness, we present it in this appendix.

The modified model is derived by assuming that the diffuse ion clouds of the various micelles do not overlap, which is a reasonable approximation when the average intermicellar separation is larger than the characteristic Debye-Hückel screening length, κ^{-1}, an assumption that is valid for all the experimental systems considered in this paper. We imagine that the solution volume is divided into a region of volume V_{diff} that contains all the diffuse ion clouds around the charged micelles, and a volume V_{bulk} that contains the bulk solution. The boundary between the diffuse and the bulk

regions need not be explicitly defined, as we will later eliminate these variables from our equations.

In this appendix, we solve for $E_{\mathrm{dl},j}$, which represents the enhancement, or the depletion, of ions of type j in the diffuse layer (dl), relative to their mole fraction in the bulk, X_{1j}. We first explicitly solve Eq. 2.7 for $E_{\mathrm{dl},j}$ to obtain the following result:

$$E_{\mathrm{dl},j} = X_j - X_{1j} - \langle x_j n \rangle_n X_{\mathrm{mic}} \tag{A.1}$$

where X_j is the total mole fraction of ions of type j in the solution, x_j is the composition of ion j in the micelle (α if $j = \mathrm{A}$, $(1-\alpha)$ if $j = \mathrm{B}$, or $\hat{\beta}$ if $j = \mathrm{C}$), n is the micelle aggregation number, and $X_{\mathrm{mic}} = \sum X_{n\alpha\hat{\beta}}$ is the total mole fraction of micelles in the solution. Note that in Eq. A.1 we have taken the number average of the quantity $x_j n$, denoted by $\langle x_j n \rangle_n = \sum n x_j X_{n\alpha\hat{\beta}} / X_{\mathrm{mic}}$, since we treat α and $\hat{\beta}$ as functions of n. Next, we write the mole balance on a charged species j of valence z_j as follows:

$$N_j = C_j V_{\mathrm{bulk}} + C_j \int_{V_{\mathrm{diff}}} \exp\left(-\frac{z_j e \psi(r)}{k_{\mathrm{B}} T}\right) \mathrm{d}V + \langle x_j n \rangle_{\mathrm{n}} N_{\mathrm{mic}} \tag{A.2}$$

where N_j is the total number of ions of type j added to the solution, and the three terms on the right-hand side of Eq. A.2 represent the number of ions of type j located in the bulk, in the diffuse layer, and associated with the charged micelles, respectively. The amount of ions of type j in the bulk is given by the product of the bulk concentration C_j (molecules per unit volume) and the bulk volume V_{bulk} (see Eq. A.2). The amount of ions of type j in the diffuse layer is obtained by integrating the ion concentration over the diffuse volume V_{diff}, where the concentration of ions of type j at position r is given by $C_j \exp\left[-z_j e \psi(r)/k_{\mathrm{B}} T\right]$, where $\psi(r)$ is the electrostatic potential at position r (see Eq. A.2). Finally, the number of ions of type j associated with the charged micelles is given by the product of $\langle x_j n \rangle_n$, which represents the average number of ions of type j in a micelle, and the number of micelles in the solution N_{mic} (see Eq. A.2). Note that we only calculate the electrostatic potential for regular micelle shapes, and, therefore, we consider ψ to be a function of r only.

We next simplify the integral in Eq. A.2 by assuming that the electrostatic potential energy $z_j e\psi(r)$ is small relative to the thermal energy $k_B T$, which enables us to replace $\exp\left[-z_j e\psi(r)/k_B T\right]$ with $\left[1 - z_j e\psi(r)/k_B T\right]$. Although this approximation is not likely to be valid near the charged surface of a pure ionic micelle, it may be reasonable over much of the diffuse layer, where the electrostatic potential is smaller. In fact, this simplification yielded reasonable results even for the bulk concentration of a multivalent ion in an ionic micellar system.[43] Using this approximation, the simplified mole balance for ions of type j is given by:

$$N_j = C_j \left(V_{\text{bulk}} + V_{\text{diff}}\right) - z_j C_j \int_{V_{\text{diff}}} \left(\frac{e\psi(r)}{k_B T}\right) \mathrm{d}V + \langle x_j n \rangle_n N_{\text{mic}} \tag{A.3}$$

Next, we utilize the electroneutrality requirement to determine the value of the integral in Eq. A.3. Specifically, we write an expression modeling the electroneutrality of the entire solution:

$$\sum_j z_j N_j = \sum_j z_j \left[C_j \left(V_{\text{bulk}} + V_{\text{diff}}\right) - z_j C_j \int_{V_{\text{diff}}} \left(\frac{e\psi(r)}{k_B T}\right) \mathrm{d}V + \langle x_j n \rangle_j N_{\text{mic}}\right] = 0 \tag{A.4}$$

Expanding and simplifying the terms in Eq. A.4 yields:

$$\left(V_{\text{bulk}} + V_{\text{diff}}\right)\left(\sum_j z_j C_j\right) - \int_{V_{\text{diff}}} \left(\frac{e\psi(r)}{k_B T}\right) \mathrm{d}V \left(\sum_j z_j^2 C_j\right) + N_{\text{mic}} \left(\sum_j z_j \langle x_j n \rangle_n\right) = 0 \tag{A.5}$$

Because the bulk solution is electroneutral, the first summation in Eq. A.5 is zero. Essentially, the remaining equation states that the diffuse layer and the micelles must be electroneutral as a whole. Solving for the integral in Eq. A.5 yields:

$$\int_{V_{\text{diff}}} \left(\frac{e\psi(r)}{k_B T}\right) \mathrm{d}V = N_{\text{mic}} \frac{\left(\sum_j z_j \langle x_j n \rangle_n\right)}{\left(\sum_j z_j^2 C_j\right)}. \tag{A.6}$$

After combining Eqs. A.3 and A.6, we identify the diffuse layer contribution of the

ions of type j to the *concentration* balances, $\hat{E}_{\mathrm{dl},j}$, as follows:

$$\hat{E}_{\mathrm{dl},j} = -z_j C_j \left[\frac{z_{\mathrm{mic}} \left(N_{\mathrm{mic}}/V \right)}{2I} \right] \tag{A.7}$$

where V is the solution volume, $I = \frac{1}{2} \sum_j z_j^2 C_j$ is the solution ionic strength, and $z_{\mathrm{mic}} = \left(\sum_j z_j \left\langle x_j n \right\rangle_n \right)$ is the micelle valence. Converting each concentration to mole fraction units, we obtain $E_{\mathrm{dl},j}$, the diffuse layer contribution in *mole fraction units*:

$$E_{\mathrm{dl},j} = -z_j X_{1j} \left[\frac{z_{\mathrm{mic}} X_{\mathrm{mic}}}{2\mu} \right] \tag{A.8}$$

where X_{1j} and X_{mic} are the bulk mole fractions of ions of species j and of micelles, respectively, (the mole fraction equivalents of C_j and (N_{mic}/V), respectively, in Eq. A.7), and $\mu = \frac{1}{2} \left(\sum_j z_j^2 X_j \right)$ is the solution ionic strength in mole fraction units. Note that we can convert to mole fraction units using the reasonable approximation $X_j \approx C_j V / N_{\mathrm{w}}$, where N_{w} is the number of water molecules in the solution.

In the case of pH-sensitive surfactants, the appropriate surfactant mass balance is for the total amount of the protonated and the deprotonated surfactant species. In this case, $E_{\mathrm{dl,S}}$ denotes the enhancement, or depletion, of the total concentration of pH-sensitive surfactant, and is given by

$$E_{\mathrm{dl,S}} = -z_1 X_1 \left[\frac{z_{\mathrm{mic}} X_{\mathrm{mic}}}{2\mu} \right] \tag{A.9}$$

where $z_1 = \alpha_1 z_{\mathrm{HS}} + (1 - \alpha_1) z_{\mathrm{S}}$ is the average valence of the surfactant monomers. We must also consider the enhancement $E_{\mathrm{dl},j}$ of ions j =H^+ and OH^-. Using identical notation for the valence and monomer mole fraction, $E_{\mathrm{dl},j}$ is also given by eq A.8.

Note that the primary difference between this model and the previous one (see ref 43) is in the denominator of eq A.8. In the previous model, the denominator is a summation over *counterions only*, whereas in our model it is a summation over *all the ions*. This modification accounts for the fact that the diffuse layer neutralizes the charge of a micelle not only by increasing the local concentration of counterions but also by decreasing the local concentration of co-ions.

Appendix B

Key Equations of the g_{mic} Model for pH-Sensitive Surfactants

We summarize here the key equations of the g_{mic} model for pH-sensitive surfactants, as utilized in Chapter 3 (for complete details of the g_{mic} model, see Chapter 2 and ref 138). The transfer contribution is modeled as

$$g_{\mathrm{tr}} = \alpha g_{\mathrm{trHS}} + (1-\alpha)\, g_{\mathrm{trS}} \tag{B.1}$$

where α is the micelle composition and $g_{\mathrm{tr}i}$ is the transfer contribution of surfactant i (HS and S). Note that $g_{\mathrm{tr}i}$ depends on the number of carbon atoms in the surfactant hydrophobic tail, $n_{\mathrm{t}i}$, which is then correlated to experimental solubility data for linear alkanes in water.[1,41] If $n_{\mathrm{tHS}} = n_{\mathrm{tS}}$, then $g_{\mathrm{trHS}} = g_{\mathrm{trS}}$, and eq B.1 reduces to

$$g_{\mathrm{tr}} = g_{\mathrm{trS}} \tag{B.2}$$

The interfacial contribution is modeled as

$$g_{\mathrm{int}} = (a - a_0)\left[\alpha\sigma_{\mathrm{HS}} + (1-\alpha)\,\sigma_{\mathrm{S}}\right] \tag{B.3}$$

where a is the area per surfactant molecule at the micelle interface, a_0 is the interfacial area that is shielded by the chemical bond between the surfactant head and tail

(estimated to be 21 Å^2) , and σ_i is the interfacial tension of surfactant tail i (HS and S) against water. The curvature-corrected interfacial tension is estimated using experimental data for the interfacial tension of linear alkanes.[39] The interfacial tension also depends weakly on n_{ti}, but if $n_{\text{tHS}} = n_{\text{tS}}$, then $\sigma_{\text{HS}} = \sigma_{\text{S}}$, and eq B.3 reduces to

$$g_{\text{int}} = (a - a_0)\,\sigma_{\text{S}} \tag{B.4}$$

The packing contribution is modeled as

$$g_{\text{pack}} = \boldsymbol{l}\boldsymbol{C}_{S,n_{\text{tHS}},n_{\text{tS}}}\boldsymbol{\alpha}^{\text{T}} \tag{B.5}$$

where $\boldsymbol{l} = [\ 1 \quad l_{\text{c}} \quad l_{\text{c}}^2\ ]$ (where l_{c} is the micelle core minor radius), $\boldsymbol{\alpha} = [\ 1 \quad \alpha \quad \alpha^2 \quad \alpha^3\ ]$ (where α is the micelle composition), and $\boldsymbol{C}_{S,n_{\text{tHS}},n_{\text{tS}}}$ is a coefficient matrix that depends on the micelle shape parameter, S, and on the surfactant tail lengths, n_{tHS} and n_{tS}. The coefficient matrix $\boldsymbol{C}_{S,n_{\text{tHS}},n_{\text{tS}}}$ is determined by fitting[4,104] g_{pack} values that are calculated using a mean-field approach pioneered by Ben-Shaul, Szleifer, and Gelbart.[101–103] If $n_{\text{tHS}} = n_{\text{tS}}$, then the packing calculations are independent of α and eq B.5 reduces to

$$g_{\text{pack}} = \boldsymbol{l} \cdot \boldsymbol{c}_{S,n_{\text{tS}}} \tag{B.6}$$

where $\boldsymbol{c}_{S,n_{\text{tS}}}$ is a coefficient vector that depends on S and n_{tS}.

The steric contribution is modeled as

$$g_{\text{st}} = -k_{\text{B}}T\left(1 + \hat{\beta}_{\text{C}}\right)\ln\left[1 - \frac{\alpha a_{\text{hHS}} + (1-\alpha)\,a_{\text{hS}} + \hat{\beta}_{\text{C}}a_{\text{hC}}}{a}\right] \tag{B.7}$$

where $a_{\text{h}i}$ is the cross-sectional area of the head of surfactant i (i = HS and S) or the cross-sectional area of counterion i (i = C). If $a_{\text{hHS}} = a_{\text{hS}}$, then eq B.5 reduces to

$$g_{\text{st}} = -k_{\text{B}}T\left(1 + \hat{\beta}_{\text{C}}\right)\ln\left[1 - \frac{a_{\text{hS}} + \hat{\beta}_{\text{C}}a_{\text{hC}}}{a}\right] \tag{B.8}$$

The entropic contribution is modeled as

$$g_{\text{ent}} = k_{\text{B}}T\left[\alpha\ln\alpha + (1-\alpha)\ln(1-\alpha) + \hat{\beta}\ln\hat{\beta} - \left(1+\hat{\beta}\right)\ln\left(1+\hat{\beta}\right)\right] \tag{B.9}$$

The electrostatic contribution is modeled as

$$g_{\text{elec}} = g_{\text{disch}} + g_{\text{charge}} \tag{B.10}$$

where g_{disch} is the free-energy change associated with discharging ions in the bulk solution, and g_{charge} is the free-energy change associated with charging the ions at the micelle interface. The discharge contribution is given by

$$g_{\text{disch}} = \alpha g_{\text{dischHS}} + (1-\alpha)\, g_{\text{dischS}} + \hat{\beta}_{\text{C}} g_{\text{dischC}} \tag{B.11}$$

where $g_{\text{disch}i}$ is the discharge free energy of species i (HS, S, and C). For zwitterionic surfactants, the discharge contribution is given by

$$g_{\text{disch}i} = -\frac{d_{\text{sep}i}^2 e_0^2}{4\pi\epsilon_0\left(2\eta_{\text{w}}+1\right) r_{\text{h}i}^3} \tag{B.12}$$

where $d_{\text{sep}i}$ is the distance between the two charges in the zwitterionic surfactant head, e_0 is the charge of a proton, ϵ_0 is the dielectric permittivity of vacuum, η_{w} is the dielectric constant of bulk water, and $r_{\text{h}i}$ is the hydrated radius of the surfactant head (the same radius used to calculate $a_{\text{h}i}$). For ionic surfactants and counterions, the discharge contribution is given by

$$g_{\text{disch}i} = -\frac{z_i^2 e_0^2}{2\epsilon_{\text{b}} r_{\text{h}i}\left(1+\kappa r_{\text{h}i}\right)} \tag{B.13}$$

where z_i is the valence of component i, $\epsilon_{\text{b}} = 4\pi\epsilon_0\eta_{\text{w}}$, and $r_{\text{h}i}$ is the hydrated radius of the ionic surfactant head or the counterion. The inverse Debye-Hückel screening length is given by

$$\kappa = \left(8\pi e_0^2 I/\epsilon_{\text{b}} k_{\text{B}}T\right)^{1/2} \tag{B.14}$$

where $I = \left(\sum_i z_i^2 C_i\right)/2$ is the solution ionic strength. The summation in the definition of I is over *all* the ionic components, including co-ions, where C_i is the bulk concentration of component i.

The charging contribution in eq B.10 is given by

$$g_{\text{charge}} = g_{\text{cap}} + \int_0^{q_{\text{f}}} \psi_{\text{s}}(q)\ \mathrm{d}q \tag{B.15}$$

where g_{cap} is a capacitor contribution, $\psi_{\text{s}}(q)$ is the electrostatic potential at the Stern surface, determined as a function of q, the micelle charge per surfactant molecule, and q_{f} is the final micelle charge per surfactant molecule.

The capacitor contribution, g_{cap}, is given by

$$g_{\text{cap}} = \sum_i \frac{2\pi}{4\pi\epsilon_0\eta_{\text{int}}a_i}\left(\sum_{j=1}^{i} q_{j\text{f}}\right)^2 \mathcal{F}(S, d_i, R_i) \tag{B.16}$$

where the subscript i denotes a particular micelle surface on which charge groups are located, η_{int} denotes the dielectric constant in the micelle interfacial region (which we define as the region from the micelle core-water interface to the Stern surface), a_i denotes the area per surfactant molecule at surface i, R_i is the distance from the micelle center to surface i, and d_i is the distance between surface i and surface $(i+1)$. The final distance is calculated with respect to the position of the Stern surface. We chose η_{int} to be half the value in bulk water, η_{w}. The summation term in eq B.16 can be interpreted as the work of charging associated with forming a series of capacitors, which we refer to as g_{cap}. The function $\mathcal{F}$ captures the dependence of the capacitor's energy on its geometry, and is defined as follows:

$$\mathcal{F}(S, d_i, R_i) = \begin{cases} d_i, & \text{for } S = 1 \text{ (planar or discoidal micelles)} \\ R_i \ln\left(1 + d_i/R_i\right), & \text{for } S = 2 \text{ (cylindrical micelles)} \\ d_i/\left(1 + d_i/R_i\right), & \text{for } S = 3 \text{ (spherical micelles)} \end{cases} \tag{B.17}$$

We solve for $\psi_{\text{s}}(q)$ in eq B.15 using an approximate solution to the

Poisson-Boltzmann equation derived by Oshima, Healy, and White (OHW):[117]

$$s = 2\sinh(y_0/2) + \frac{2\,(S-1)}{x_0}\tanh(y_0/4) \tag{B.18}$$

where $s = (4\pi e_0/\epsilon_w k_B T\kappa)\sum_i q_{if}/a_s$ is the dimensionless surface charge density (a_s is the area per surfactant molecule at the Stern surface), $y_0 = e_0\psi_s/k_B T$ is the dimensionless surface potential, and $x_0 = \kappa R_{Stern}$ is the dimensionless location of the Stern surface. Complete details can be found in section 2.3 and ref 138.

The effect of salt on g_{elec} is captured through its effect on κ (see eq B.14). In particular, increasing the ionic strength (by increasing the salt concentration) increases κ, which in turn decreases the magnitude of g_{dischi} for ionic species (see eq B.13). Increasing κ also decreases both s and y_0 (or, equivalently, ψ_s, see eq B.18), and therefore decreases the integral term in g_{charge} (see eq B.15). Physically, increasing the salt concentration increases electrostatic screening, which decreases the magnitude of the ionic interactions (as reflected in g_{disch} and g_{charge}).

Appendix C

Evaluation of $\frac{\partial g_{\mathrm{m}}}{\partial \alpha}$

In this appendix, we show how to obtain the following identity, which is useful in relating $\Delta \mathrm{p} K_{\mathrm{m}}$ to g_{mic}:

$$\frac{1}{k_{\mathrm{B}}T}\frac{\partial g_{\mathrm{m}}}{\partial \alpha} = \frac{1}{k_{\mathrm{B}}T}\frac{\partial}{\partial \alpha}\left[g_{\mathrm{mic}} - g_{\mathrm{ent}}\right] + \ln\frac{\alpha}{1-\alpha} - \ln\frac{\alpha_1}{1-\alpha_1} \tag{C.1}$$

First, using the definitions of g_{m} and g_{mic} (eqs 3.4 and 3.12, respectively), we can express g_{m}as follows

$$g_{\mathrm{m}} = (g_{\mathrm{mic}} - g_{\mathrm{ent}}) + g_{\mathrm{ent}} - k_{\mathrm{B}}T\left[\alpha \ln \alpha_1 + (1-\alpha)\ln(1-\alpha_1) + \hat{\beta}_{\mathrm{C}} \ln X_{1\mathrm{C}}\right] \tag{C.2}$$

Next, we differentiate eq C.2 with respect to α to obtain

$$\frac{1}{k_{\mathrm{B}}T}\frac{\partial g_{\mathrm{m}}}{\partial \alpha} = \frac{1}{k_{\mathrm{B}}T}\frac{\partial}{\partial \alpha}\left[g_{\mathrm{mic}} - g_{\mathrm{ent}}\right] + \frac{1}{k_{\mathrm{B}}T}\frac{\partial g_{\mathrm{ent}}}{\partial \alpha} - \ln\frac{\alpha_1}{1-\alpha_1} \tag{C.3}$$

Subsequently, we differentiate g_{ent} with respect to α using the definition provided in Appendix B (eq B.9). This yields

$$\frac{1}{k_{\mathrm{B}}T}\frac{\partial g_{\mathrm{ent}}}{\partial \alpha} = \ln\frac{\alpha}{1-\alpha} \tag{C.4}$$

Finally, combining eqs C.3 and C.4 yields the desired result (eq C.1).

Appendix D

Derivation of eqs 4.10 and 4.14 in the Context of RST

In this appendix, we use the pseudophase approximation and the RST to relate the $\Delta \mathrm{p}K$ to the micellar interactions, as quantified by the pairwise interaction β parameters defined below. We begin with the following constraints that result from the pseudophase approximation:[35]

$$\alpha_{1\mathrm{HS}}\mathrm{cmc}_{\mathrm{mix}} = \alpha_{\mathrm{HS}} f_{\mathrm{HS}} \mathrm{cmc}_{\mathrm{HS}} \tag{D.1}$$

$$\alpha_{1\mathrm{S}}\mathrm{cmc}_{\mathrm{mix}} = \alpha_{\mathrm{S}} f_{\mathrm{S}} \mathrm{cmc}_{\mathrm{S}} \tag{D.2}$$

where $\mathrm{cmc}_{\mathrm{mix}}$ is the cmc of the surfactant mixture, $\mathrm{cmc}_{\mathrm{HS}}$ and $\mathrm{cmc}_{\mathrm{S}}$ are the cmc's of the protonated and the deprotonated forms of the pH-sensitive surfactant, respectively, and f_{HS} and f_{S} are the micellar activity coefficients of the protonated and the deprotonated forms of the pH-sensitive surfactant, respectively. Next, we divide eq D.1 by eq D.2 to obtain:

$$\frac{\alpha_{1\mathrm{HS}}}{\alpha_{1\mathrm{S}}} = \frac{\alpha_{\mathrm{HS}} f_{\mathrm{HS}} \mathrm{cmc}_{\mathrm{HS}}}{\alpha_{\mathrm{S}} f_{\mathrm{S}} \mathrm{cmc}_{\mathrm{S}}} \tag{D.3}$$

Taking the logarithm of eq D.3 yields:

$$\log\left(\frac{\alpha_{1\mathrm{HS}}}{\alpha_{1\mathrm{S}}}\right) = \log\left(\frac{\alpha_{\mathrm{HS}} f_{\mathrm{HS}} \mathrm{cmc}_{\mathrm{HS}}}{\alpha_{\mathrm{S}} f_{\mathrm{S}} \mathrm{cmc}_{\mathrm{S}}}\right) = \log\left(\frac{\alpha_{\mathrm{HS}}}{\alpha_{\mathrm{S}}}\right) + \log\left(\frac{\mathrm{cmc}_{\mathrm{HS}}}{\mathrm{cmc}_{\mathrm{S}}}\right) + \log f_{\mathrm{HS}} - \log f_{\mathrm{S}} \tag{D.4}$$

Equation D.4 can be rearranged to yield:

$$\log\left(\frac{\alpha_{\mathrm{HS}}}{\alpha_{\mathrm{S}}}\right) - \log\left(\frac{\alpha_{1\mathrm{HS}}}{\alpha_{1\mathrm{S}}}\right) = \log\left(\frac{\mathrm{cmc}_{\mathrm{S}}}{\mathrm{cmc}_{\mathrm{HS}}}\right) + \log f_{\mathrm{S}} - \log f_{\mathrm{HS}} \tag{D.5}$$

Combining eqs 4.9 and D.5 yields:

$$\Delta \mathrm{p}K = \log\left(\frac{\mathrm{cmc}_{\mathrm{S}}}{\mathrm{cmc}_{\mathrm{HS}}}\right) + \log f_{\mathrm{S}} - \log f_{\mathrm{HS}} = \log\left(\frac{\mathrm{cmc}_{\mathrm{S}}}{\mathrm{cmc}_{\mathrm{HS}}}\right) + (\log e)\left(\ln f_{\mathrm{S}} - \ln f_{\mathrm{HS}}\right) \tag{D.6}$$

According to the RST, the free energy of the micellar pseudophase composed of the protonated and the deprotonated forms of a pH-sensitive surfactant and n_{surf} conventional surfactants is given by:[236]

$$G_{\mathrm{mic}} = \sum_i N_i \left(\mu_i^{\circ} + k_{\mathrm{B}} T \ln \alpha_i\right) + \frac{1}{2} \sum_i \sum_{j \neq i} N_i N_j \beta_{ij} \tag{D.7}$$

where N_i is the number of moles of surfactant i (i =1 to n_{surf}, HS, and S), μ_i° is the standard-state chemical potential of surfactant i, k_{B} is the Boltzmann constant, T is the absolute temperature, and β_{ij} is the pairwise interaction energy in units of $k_{\mathrm{B}}T$ (referred to as the β parameter) between surfactant i and surfactant j in a mixed micelle. The activity coefficient of component i, f_i, can then be obtained by differentiating G_{mic} to obtain the chemical potential of surfactant i:

$$\mu_i \equiv \left(\frac{\partial G_{\mathrm{mic}}}{\partial N_i}\right)_{N_{j \neq i}} = \mu_i^{\circ} + k_{\mathrm{B}} T \ln f_i \alpha_i \tag{D.8}$$

The resulting expressions for f_{HS} and f_{S} are:[37]

$$\ln f_{\mathrm{S}} = \beta_{\mathrm{S,HS}}\alpha_{\mathrm{HS}}^2 + \sum_{j=1}^{n_{\mathrm{surf}}} \beta_{\mathrm{S},j}\alpha_j^2 + \sum_{j=1}^{n_{\mathrm{surf}}} \left(\beta_{\mathrm{S,HS}} + \beta_{\mathrm{S},j} - \beta_{\mathrm{HS},j}\right)\alpha_{\mathrm{HS}}\alpha_j + \sum_{j=1}^{n_{\mathrm{surf}}-1}\sum_{k=j+1}^{n_{\mathrm{surf}}} \left(\beta_{\mathrm{S},j} + \beta_{\mathrm{S},k} - \beta_{j,k}\right)\alpha_j\alpha_k \quad \text{(D.9)}$$

$$\ln f_{\mathrm{HS}} = \beta_{\mathrm{S,HS}}\alpha_{\mathrm{S}}^2 + \sum_{j=1}^{n_{\mathrm{surf}}} \beta_{\mathrm{HS},j}\alpha_j^2 + \sum_{j=1}^{n_{\mathrm{surf}}} \left(\beta_{\mathrm{S,HS}} + \beta_{\mathrm{HS},j} - \beta_{\mathrm{S},j}\right)\alpha_{\mathrm{S}}\alpha_j + \sum_{j=1}^{n_{\mathrm{surf}}-1}\sum_{k=j+1}^{n_{\mathrm{surf}}} \left(\beta_{\mathrm{HS},j} + \beta_{\mathrm{HS},k} - \beta_{j,k}\right)\alpha_j\alpha_k \quad \text{(D.10)}$$

Subtracting eq D.10 from eq D.9 yields:

$$\ln f_{\mathrm{S}} - \ln f_{\mathrm{HS}} = \beta_{\mathrm{S,HS}}\left(\alpha_{\mathrm{HS}}^2 - \alpha_{\mathrm{S}}^2\right) + \sum_{j=1}^{n_{\mathrm{surf}}} \left(\beta_{\mathrm{S},j} - \beta_{\mathrm{HS},j}\right)\alpha_j^2 + \sum_{j=1}^{n_{\mathrm{surf}}} \left[\beta_{\mathrm{S,HS}}\left(\alpha_{\mathrm{HS}} - \alpha_{\mathrm{S}}\right) + \beta_{\mathrm{S},j}\left(\alpha_{\mathrm{HS}} + \alpha_{\mathrm{S}}\right) - \beta_{\mathrm{HS},j}\left(\alpha_{\mathrm{HS}} + \alpha_{\mathrm{S}}\right)\right]\alpha_j + \sum_{j=1}^{n_{\mathrm{surf}}-1}\sum_{k=j+1}^{n_{\mathrm{surf}}} \left[\left(\beta_{\mathrm{S},j} - \beta_{\mathrm{HS},j}\right) + \left(\beta_{\mathrm{S},k} - \beta_{\mathrm{HS},k}\right)\right]\alpha_j\alpha_k \quad \text{(D.11)}$$

For convenience, we define the following variables:

$$\Delta\alpha \equiv \alpha_{\mathrm{HS}} - \alpha_{\mathrm{S}} \quad \text{(D.12)}$$

$$\alpha_{\mathrm{conv}} \equiv \sum_{j=1}^{n_{\mathrm{surf}}} \alpha_j = 1 - \alpha_{\mathrm{HS}} - \alpha_{\mathrm{S}} \quad \text{(D.13)}$$

$$\Delta\beta_j \equiv \beta_{\mathrm{S},j} - \beta_{\mathrm{HS},j} \quad \text{(D.14)}$$

Physically, $\Delta\alpha$ is the difference in the compositions of the protonated and the deprotonated forms of the pH-sensitive surfactant in the micelle, α_{conv} is the total composition of conventional surfactant in the micelle, and $\Delta\beta_j$ is a quantitative measure of how strongly the conventional component j interacts with the deprotonated surfactant (S), *relative to its interaction with the protonated surfactant*

(HS). Note that synergy corresponds to a negative β parameter, so that $\Delta\beta_j > 0$ implies that component j interacts more favorably (more synergistically) with the protonated form of the pH-sensitive surfactant, while $\Delta\beta_j < 0$ implies that component j interacts more favorably (more synergistically) with the deprotonated form of the pH-sensitive surfactant. Next, we rewrite eq D.11 using the definitions in eqs D.12, D.13, and D.14:

$$\begin{aligned} \ln f_{\mathrm{S}} - \ln f_{\mathrm{HS}} &= \beta_{\mathrm{S,HS}}\Delta\alpha\left(1-\alpha_{\mathrm{conv}}\right) + \sum_{j=1}^{n_{\mathrm{surf}}} \Delta\beta_j\alpha_j^2 + \\ &\sum_{j=1}^{n_{\mathrm{surf}}} \left[\beta_{\mathrm{S,HS}}\Delta\alpha + \Delta\beta_j\left(1-\alpha_{\mathrm{conv}}\right)\right]\alpha_j + \\ &\sum_{j=1}^{n_{\mathrm{surf}}-1}\sum_{k=j+1}^{n_{\mathrm{surf}}} \left[\Delta\beta_j + \Delta\beta_k\right]\alpha_j\alpha_k \end{aligned} \tag{D.15}$$

Collecting the various β terms yields:

$$\begin{aligned} \ln f_{\mathrm{S}} - \ln f_{\mathrm{HS}} &= \beta_{\mathrm{S,HS}}\left[\Delta\alpha\left(1-\alpha_{\mathrm{conv}}\right) + \Delta\alpha\sum_{j=1}^{n_{\mathrm{surf}}}\alpha_j\right] + \\ &\sum_{j=1}^{n_{\mathrm{surf}}} \Delta\beta_j\alpha_j^2 + \sum_{j=1}^{n_{\mathrm{surf}}} \Delta\beta_j\alpha_j\left(1-\alpha_{\mathrm{conv}}\right) + \\ &\sum_{j=1}^{n_{\mathrm{surf}}-1}\sum_{k=j+1}^{n_{\mathrm{surf}}} \left[\Delta\beta_j + \Delta\beta_k\right]\alpha_j\alpha_k \end{aligned} \tag{D.16}$$

Combining and simplifying the summations in eq D.16 yields:

$$\begin{aligned} \ln f_{\mathrm{S}} - \ln f_{\mathrm{HS}} &= \beta_{\mathrm{S,HS}}\Delta\alpha\left[\left(1-\alpha_{\mathrm{conv}}\right) + \sum_{j=1}^{n_{\mathrm{surf}}}\alpha_j\right] + \\ &\sum_{j=1}^{n_{\mathrm{surf}}} \Delta\beta_j\left[\alpha_j + \left(1-\alpha_{\mathrm{conv}}\right)\right]\alpha_j + \\ &\sum_{j=1}^{n_{\mathrm{surf}}-1}\sum_{k=j+1}^{n_{\mathrm{surf}}} \left[\Delta\beta_j + \Delta\beta_k\right]\alpha_j\alpha_k \end{aligned} \tag{D.17}$$

Recalling the definition of α_{conv} (see eq D.13), eq D.17 simplifies to

$$\begin{aligned} \ln f_{\text{S}} - \ln f_{\text{HS}} &= \beta_{\text{S,HS}}\Delta\alpha + \\ &\sum_{j=1}^{n_{\text{surf}}} \Delta\beta_j \left[\alpha_j + (1-\alpha_{\text{conv}})\right]\alpha_j + \\ &\sum_{j=1}^{n_{\text{surf}}-1}\sum_{k=j+1}^{n_{\text{surf}}} \left[\Delta\beta_j + \Delta\beta_k\right]\alpha_j\alpha_k \end{aligned} \tag{D.18}$$

The two $\Delta\beta$ terms in eq D.18 can be combined by separating the terms and reordering the double-summation as follows:

$$\begin{aligned} \sum_{j=1}^{n_{\text{surf}}-1}\sum_{k=j+1}^{n_{\text{surf}}} \left[\Delta\beta_j + \Delta\beta_k\right]\alpha_j\alpha_k &= \sum_{j=1}^{n_{\text{surf}}-1}\sum_{k=j+1}^{n_{\text{surf}}} \Delta\beta_j\alpha_j\alpha_k + \sum_{j=1}^{n_{\text{surf}}-1}\sum_{k=j+1}^{n_{\text{surf}}} \Delta\beta_k\alpha_j\alpha_k \\ &= \sum_{j=1}^{n_{\text{surf}}-1}\sum_{k=j+1}^{n_{\text{surf}}} \Delta\beta_j\alpha_j\alpha_k + \sum_{k=2}^{n_{\text{surf}}}\sum_{j=1}^{k-1} \Delta\beta_k\alpha_j\alpha_k \\ &= \sum_{j=1}^{n_{\text{surf}}}\sum_{\substack{k=1 \\ k\neq j}}^{n_{\text{surf}}} \Delta\beta_j\alpha_j\alpha_k \\ &= \sum_{j=1}^{n_{\text{surf}}} \Delta\beta_j\alpha_j \left[\sum_{\substack{k=1 \\ k\neq j}}^{n_{\text{surf}}} \alpha_k\right] \end{aligned} \tag{D.19}$$

Note that the first simplification in eq D.19 utilizes the identify $\sum_{j=1}^{n_{\text{surf}}-1}\sum_{k=j+1}^{n_{\text{surf}}} f(j,k) = \sum_{k=2}^{n_{\text{surf}}}\sum_{j=1}^{k-1} f(j,k)$, and the second simplification utilizes the identify $\sum_{k=j+1}^{n_{\text{surf}}} f(j,k) + \sum_{k=1}^{j-1} f(j,k) = \sum_{k=1,k\neq j}^{n_{\text{surf}}} f(j,k)$. Equations D.17 and D.19 are then combined to yield

$$\begin{aligned} \ln f_{\text{S}} - \ln f_{\text{HS}} &= \beta_{\text{S,HS}}\Delta\alpha + \sum_{j=1}^{n_{\text{surf}}} \Delta\beta_j \left[\alpha_j + (1-\alpha_{\text{conv}})\right]\alpha_j + \sum_{j=1}^{n_{\text{surf}}} \Delta\beta_j\alpha_j \sum_{\substack{k=1 \\ k\neq j}}^{n} \alpha_k \\ &= \beta_{\text{S,HS}}\Delta\alpha + \sum_{j=1}^{n_{\text{surf}}} \Delta\beta_j \left[\alpha_j + (1-\alpha_{\text{conv}}) + \sum_{\substack{k=1 \\ k\neq j}}^{n_{\text{surf}}} \alpha_k\right]\alpha_j \\ &= \beta_{\text{S,HS}}\Delta\alpha + \sum_{j=1}^{n_{\text{surf}}} \Delta\beta_j\alpha_j \left[(1-\alpha_{\text{conv}}) + \sum_{k=1}^{n_{\text{surf}}} \alpha_k\right] \end{aligned} \tag{D.20}$$

Recalling the definition of α_{conv} (eq D.13), eq D.20 simplifies to

$$\ln f_{\text{S}} - \ln f_{\text{HS}} = \beta_{\text{S,HS}}\Delta\alpha + \sum_{j=1}^{n_{\text{surf}}} \Delta\beta_j\alpha_j \tag{D.21}$$

Finally, using eq D.21 in eq D.6 yields:

$$\Delta\text{p}K = \log\left(\frac{\text{cmc}_{\text{S}}}{\text{cmc}_{\text{HS}}}\right) + (\log e)\left(\beta_{\text{S,HS}}\Delta\alpha + \sum_{j=1}^{n_{\text{surf}}} \Delta\beta_j\alpha_j\right) \tag{D.22}$$

which is eq 4.10 in the text. If the micelles contain only the pH-sensitive surfactant (that is, if $\alpha_j = 0$), then eq D.22 becomes

$$\begin{aligned} \Delta\text{p}K &= \log\left(\frac{\text{cmc}_{\text{S}}}{\text{cmc}_{\text{HS}}}\right) + (\log e)\,\beta_{\text{S,HS}}\Delta\alpha \\ &= \log\left(\frac{\text{cmc}_{\text{S}}}{\text{cmc}_{\text{HS}}}\right) + (\log e)\,\beta_{\text{S,HS}}\,(2\alpha_{\text{HS}} - 1) \end{aligned} \tag{D.23}$$

where we have also used the fact that, for systems that do not contain conventional surfactants, $\Delta\alpha = 2\alpha_{\text{HS}} - 1$, since $\alpha_{\text{HS}} + \alpha_{\text{S}} = 1$ and $\alpha_{\text{HS}} = x_{\text{mic}} = 1 - \alpha_{\text{S}}$ (see eqs 4.5 and 4.7). Equation D.23 is 4.14 in the text.

Appendix E

Generalization of the g_{mic} Model to Multicomponent Surfactant Mixtures

In this appendix, we summarize the key equations of the g_{mic} model discussed in section 5.2.2 (for complete details, see ref 138 and Chapter 2). The transfer contribution is modeled as

$$g_{\mathrm{tr}} = \sum_i \alpha_i g_{\mathrm{tr}i} \tag{E.1}$$

where α_i and $g_{\mathrm{tr}i}$ are the micelle composition and the transfer contribution, respectively, for surfactant i. Note that $g_{\mathrm{tr}i}$ depends on the number of carbon atoms in the hydrophobic tail of surfactant i, $n_{\mathrm{t}i}$, which can be correlated to experimental solubility data for linear alkanes in water.[1,41]

The interfacial contribution is modeled as

$$g_{\mathrm{int}} = (a - a_0) \sum_i \alpha_i \sigma_i \tag{E.2}$$

where a is the area per surfactant molecule at the micelle interface, a_0 is the interfacial area that is shielded by the chemical bond between the surfactant head and tail (estimated to be 21 $\mathrm{Å}^2$) , and σ_i is the interfacial tension of surfactant tail i against water. This curvature-corrected interfacial tension depends weakly on $n_{\mathrm{t}i}$ and is estimated using experimental data for the interfacial tension of linear alkanes against

water.[39]

The packing contribution has been extended to micelles containing three distinct surfactant tails. Since several surfactants may be modeled as having the same tail, the treatment of three distinct tails is sufficient for modeling many multicomponent surfactant mixtures of practical interest. The packing contribution depends on the total amount of each tail that is in the micelle. Denoting the three distinct tails as T_1, T_2, and T_3, we define composition variables for each of these tails, $\alpha_{\mathrm{T}1}$, $\alpha_{\mathrm{T}2}$, and $\alpha_{\mathrm{T}3}$. For example, $\alpha_{\mathrm{T}1}$ is the sum of the compositions of all surfactants with a T_1 tail.

For each ternary set of tails $\{T_1, T_2, T_3\}$, g_{pack} values are calculated using a mean-field approach pioneered by Ben-Shaul, Szleifer, and Gelbart.[101–103] Because these calculations are more computationally intensive than the other contributions to g_{mic}, the mean-field result is only calculated once for micelles of various shapes, S, minor core radii, l_{c}, and compositions, $\{\alpha_{\mathrm{T}i}\}$. For each micelle shape, g_{pack} is then fit to a polynomial function of the form[4, 104]

$$g_{\mathrm{pack}} = \sum_{p=0}^{3} \sum_{q=0}^{3} \sum_{r=0}^{4} C_{Spqr} \alpha_{\mathrm{T}1}^{p} \alpha_{\mathrm{T}2}^{q} l_{\mathrm{c}}^{r} \tag{E.3}$$

where $\{C_{Spqr}\}$ denotes the coefficients of the polynomial for micelles of shape S.

The steric contribution is modeled as

$$g_{\mathrm{st}} = -k_{\mathrm{B}}T \left(1 + \sum_j \hat{\beta}_j\right) \ln\left[1 - \frac{\sum_i \alpha_i a_{\mathrm{h}i} + \sum_j \hat{\beta}_j a_{\mathrm{h}j}}{a}\right] \tag{E.4}$$

where $a_{\mathrm{h}i}$ and $a_{\mathrm{h}j}$ are the cross-sectional areas of surfactant head i or counterion j, respectively.

The entropic contribution is modeled as

$$g_{\mathrm{ent}} = k_{\mathrm{B}}T \left[\sum_i \alpha \ln \alpha + \sum_j \hat{\beta}_j \ln \hat{\beta}_j - \left(1 + \sum_j \hat{\beta}_j\right) \ln\left(1 + \sum_j \hat{\beta}_j\right)\right] \tag{E.5}$$

The electrostatic contribution is modeled as

$$g_{\text{elec}} = g_{\text{disch}} + g_{\text{charge}} \tag{E.6}$$

where g_{disch} is the free-energy change associated with discharging ions in the bulk aqueous solution, and g_{charge} is the free-energy change associated with charging the ions at the micelle interface. The discharge contribution is given by

$$g_{\text{disch}} = \sum_i \alpha_i g_{\text{disch}i} + \sum_j \hat{\beta}_j g_{\text{disch}j} \tag{E.7}$$

where $g_{\text{disch}i}$ and $g_{\text{disch}j}$ are the discharge free energies of surfactant ions i and counterions j, respectively. For zwitterionic surfactants, the discharge contribution is given by

$$g_{\text{disch}i} = -\frac{d_{\text{sep}i}^2 e_0^2}{4\pi\epsilon_0 \left(2\eta_{\text{w}} + 1\right) r_{\text{h}i}^3} \tag{E.8}$$

where $d_{\text{sep}i}$ is the distance between the two charges in the head of zwitterionic surfactant i, e_0 is the charge of a proton, ϵ_0 is the dielectric permittivity of vacuum, η_{w} is the dielectric constant of bulk water, and $r_{\text{h}i}$ is the hydrated radius of the head of surfactant i (the same radius used to calculate $a_{\text{h}i}$). For ionic surfactants and counterions, the discharge contribution is given by

$$g_{\text{disch}i} = -\frac{z_i^2 e_0^2}{2\epsilon_{\text{b}} r_{\text{h}i} \left(1 + \kappa r_{\text{h}i}\right)} \tag{E.9}$$

where z_i is the valence of surfactant component or counterion i, $\epsilon_{\text{b}} = 4\pi\epsilon_0\eta_{\text{w}}$, and $r_{\text{h}i}$ is the hydrated radius of the ionic surfactant head i or counterion i. The inverse Debye-Hückel screening length is given by

$$\kappa = \left(8\pi e_0^2 I/\epsilon_{\text{b}} k_{\text{B}} T\right)^{1/2} \tag{E.10}$$

where $I = \left(\sum_i z_i^2 C_i\right)/2$ is the solution ionic strength. The summation in the definition of I is over *all* the ionic components, including co-ions, where C_i is the bulk concentration of component i.

The equations governing g_{charge} are identical to those presented in ref 138 and in Chapter 2. The only change required to calculate g_{charge} for multicomponent surfactant mixtures is to determine the average charge on the micelle surface by averaging over all the surfactant components and the bound counterions present in the mixed micelle.

Appendix F

Diffuse-Layer Contribution to the Mole Balances at High Micelle Concentrations and at Low Ionic Strengths

Several of the experimental conditions considered in Chapter 6 are at a micelle concentration that is much higher than the ionic strength of the solution, including the case of no added salt. Unfortunately, the model developed in Appendix A is inappropriate at such conditions, since it can lead to negative concentrations of the co-ions in the solution. Although the model for the diffuse-layer contribution developed previously[43] is somewhat less rigorous, it does not lead to negative co-ion concentrations (since this model essentially assumes that the distribution of the co-ions is unaffected by the presence of the micelles). Therefore, for the calculations in Chapter 6 only, we have used the diffuse-layer model developed in ref 43, which is summarized here for completeness. In practice, the diffuse-layer behavior lies somewhere between the extremes represented by these two models. Specifically, the model in ref 43 overestimates the enhancement of the counterions in the diffuse layer, while the model in Appendix A overestimates the depletion of the co-ions in

the diffuse layer. Until a better model of the diffuse layer is developed, the best choice of diffuse-layer models will largely depend on the experimental conditions: (1) at low micelle concentrations, either model is appropriate, as they both lead to negligible enhancements or depletions, (2) at high ionic strengths and high micelle concentrations, eq A.8 may be more appropriate, and (3) at low ionic strengths and high micelle concentrations, eq F.1 may be more appropriate.

The model for the diffuse-layer enhancement of the counterions from ref 43 is written in our notation as follows:

$$E_{\mathrm{dl},j} = -z_j X_{1j} \left[\frac{z_{\mathrm{mic}} X_{\mathrm{mic}}}{\mu} \right] \tag{F.1}$$

where X_{1j} and X_{mic} are the bulk mole fractions of ions of species j and of micelles, respectively, z_{mic} is the average charge per surfactant of a micelle, and μ is the solution ionic strength in mole fraction units. In this model, note that j only refers to the *counterion species*. For every other species k, there is no enhancement or depletion in the diffuse layer (that is, $E_{\mathrm{dl},k} = 0$). Also, in contrast to A.8, the denominator of eq F.1 is μ.

Perhaps, in the future, a more rigorous model for the diffuse layer can be developed. In particular, an improved model must avoid the linearization of the Boltzmann distribution of ion concentrations that is inherent in the development of both eqs A.8 and F.1. If such a model can be developed, it may allow more accurate predictions of the activities of ions in micellar solutions, particularly at high micelle concentrations.

Bibliography

[1] Tanford, C. *The Hydrophobic Effect: Formation of Micelles and Biological Membranes*, 2nd ed.; Wiley: New York, NY, 1991.

[2] Rosen, M. J. *Surfactants and Interfacial Phenomena*, 2nd ed.; Wiley: New York, NY, 1989.

[3] Israelachvili, J. N. *Intermolecular and Surface Forces*; Academic Press: London, 1991.

[4] Shiloach, A.; Blankschtein, D. *Langmuir* **1998,** *14,* 1618-1636.

[5] Myers, D. *Surfactant Science and Technology*, 3rd ed.; Wiley: Hoboken, NJ, 2006.

[6] Briscoe, P.; Caniggia, I.; Graves, A.; Benson, B.; Huang, L.; Tanswell, A. K.; Freeman, B. A. *Am. J. Physiology* **1995,** *268,* L374-L380.

[7] Li, P.; Zhao, L. *J. Pharm. Sci.* **2003,** *92,* 951-956.

[8] Liang, C.-W. *Use of biodegradable pH-sensitive surfactants in liposome mediated oligonucleotide delivery,* Thesis, U. of Florida, Gainesville, 1998.

[9] Liang, E.; Hughes, J. A. *J. Membrane Bio.* **1998,** *166,* 37-49.

[10] Liang, E.; Rosenblatt, M. N.; Ajmani, P. S.; Hughes, J. A. *Eur. J. Pharm. Sci.* **2000,** *11,* 199-205.

[11] Wang, S.; Bui, V.; Hughes, J. A.; King, M. A.; Meyer, E. M. *Neurochem. Intl.* **2000,** *37,* 1-6.

[12] Fielden, M. L.; Perrin, C.; Kremer, A.; Bergsma, M.; Stuart, M. C.; Camilleri, P.; Engberts, J. B. F. N. *Eur. J. Biochem.* **2001,** *268,* 1269-1279.

[13] Guo, X. *Ortho ester-based surfactants for pH-triggered release in drug and gene delivery,* Thesis, U. of California, San Francisco, 2001.

[14] Szostak, J. W.; Bartel, D. P.; Luisi, P. L. *Nature (London)* **2001,** *409,* 387-390.

[15] Matsui, H.; Holtman, C. *Nano Lett.* **2002,** *2,* 887-889.

[16] Ashrawi, S. S.; Smith, G. A. In *Handbook of Detergents, Part D: Formulation*; Showell, M. S., Ed.; Surfactant Science Series 128; Taylor & Francis: Boca Raton, FL, 2006; Chapter 2, pp 27–50.

[17] Larson, R. G.; Scriven, L. E.; Davis, H. T. *J. Chem. Phys.* **1985,** *83,* 2411-2420.

[18] Smit, B.; Hilbers, P. A. J.; Esselink, K.; Rupert, L. A. M.; van Os, N. M.; Schlijper, A. G. *Nature (London)* **1990,** *348,* 624-625.

[19] Smit, B.; Hilbers, P. A. J.; Esselink, K.; Rupert, L. A. M.; van Os, N. M.; Schlijper, A. G. *J. Phys. Chem.* **1991,** *95,* 6361-6368.

[20] Larson, R. G. *J. Chem. Phys.* **1992,** *96,* 7904-7918.

[21] Smit, B.; Esselink, K.; Hilbers, P. A. J.; van Os, N. M.; Rupert, L. A. M.; Szleifer, I. *Langmuir* **1993,** *9,* 9-11.

[22] Floriano, M. A.; Caponetti, E.; Panagiotopoulos, A. Z. *Langmuir* **1999,** *15,* 3143-3151.

[23] Care, C. M.; Dalby, T. *Europhys. Lett.* **1999,** *45,* 38-44.

[24] Rodríguez-Guadarrama, L. A.; Talsania, S. K.; Mohanty, K. K.; Rajagopalan, R. *Langmuir* **1999,** *15,* 437-446.

[25] Pool, R.; Bolhuis, P. G. *J. Phys. Chem. B* **2005,** *109,* 6650-6657.

[26] Maeda, H. *Colloids Surf. A: Physicochem. Eng. Aspects* **1996,** *109,* 263-271.

[27] Hill, R. M. In *Mixed Surfactant Systems*; Ogino, K.; Abe, M., Eds.; Surfactant Science Series 46; Marcel Dekker: New York, NY, 1992; Chapter 11, pp 317–336.

[28] Scamehorn, J. F.; Harwell, J. H. In *Mixed Surfactant Systems*, 2nd ed.; Abe, M.; Scamehorn, J. F., Eds.; Surfactant Science Series 124; Marcel Dekker: New York, 2005; Chapter 18, pp 601–656.

[29] Showell, M. S. In *Powdered Detergents*; Schowell, M. S., Ed.; Surfactant Science Series 71; Marcel Dekker: New York, 1998; Chapter 1, pp 1–19.

[30] Hargreaves, T. *Chemical Formulation: An Overview of Surfactant-based Preparations Used in Everyday Life*; Royal Soc. Chem.: Cambridge, UK, 2003.

[31] *Liquid Detergents*, 2nd ed.; Lai, K.-Y., Ed.; Surfactant Science Series 129; Taylor & Francis: Boca Raton, 2006.

[32] Moore, P. N.; Shiloach, A.; Puvvada, S.; Blankschtein, D. *J. Cosmetic Sci.* **2003,** *54,* 143-159.

[33] Moore, P. N.; Puvvada, S.; Blankschtein, D. *J. Cosmetic Sci.* **2003,** *54,* 29-46.

[34] Clint, J. H. *J. Chem. Soc., Faraday Trans. 1* **1975,** *71,* 1327-1334.

[35] Rubingh, D. N. In *Solution Chem. Surfactants*; Mittal, K. L., Ed.; Plenum: New York, NY, 1979; pp 337–354.

[36] Hines, J. D. *Current Opinion Colloid Interface Sci.* **2001,** *6,* 350-356, and references cited therein.

[37] Holland, P. M.; Rubingh, D. N. *J. Phys. Chem.* **1983,** *87,* 1984-1990.

[38] Reif, I.; Mulqueen, M.; Blankschtein, D. *Langmuir* **2001,** *17,* 5801-5812.

[39] Puvvada, S.; Blankschtein, D. *J. Chem. Phys.* **1990,** *92,* 3710-3724.

[40] Puvvada, S.; Blankschtein, D. *J. Phys. Chem.* **1992,** *96,* 5567-5579.

[41] Puvvada, S.; Blankschtein, D. *J. Phys. Chem.* **1992,** *96,* 5579-5592.

[42] Srinivasan, V.; Blankschtein, D. *Langmuir* **2003,** *19,* 9932-9945.

[43] Srinivasan, V.; Blankschtein, D. *Langmuir* **2003,** *19,* 9946-9961.

[44] Nagarajan, R. In *Mixed Surfactant Systems*; Holland, P. M.; Rubingh, D. N., Eds.; ACS Symposium Series 501; American Chemical Society: Washington, DC, 1992; Chapter 4, pp 54–95.

[45] Shiloach, A.; Blankschtein, D. *Langmuir* **1998,** *14,* 4105-4114.

[46] Coret, J.; Shiloach, A.; Berger, P.; Blankschtein, D. *J. Surfactants Detergents* **1999,** *2,* 51-58.

[47] Laughlin, R. G. *Langmuir* **1991,** *7,* 842-847.

[48] *Amphoteric Surfactants*, 2nd ed.; Lomax, E. G., Ed.; Surfactant Science Series 59; Marcel Dekker: New York, NY, 1996.

[49] Rathman, J. F.; Christian, S. D. *Langmuir* **1990,** *6,* 391-395.

[50] Zimmerman, J. A.; Schnaare, R. L. *Langmuir* **1999,** *15,* 384-390.

[51] Maeda, H.; Kakehashi, R. *Adv. Colloid Interface Sci.* **2000,** *88,* 275-293.

[52] Imae, T.; Trend, B. *Langmuir* **1991,** *7,* 643-646.

[53] Hafez, I. M.; Ansell, S.; Cullis, P. R. *Biophysical J.* **2000,** *79,* 1438-1446.

[54] Matsui, H.; Gologan, B. *J. Phys. Chem. B* **2000,** *104,* 3383-3386.

[55] Bergsma, M.; Fielden, M. L.; Engberts, J. B. F. N. *J. Colloid Interface Sci.* **2001,** *243,* 491-495.

[56] Kawasaki, H.; Souda, M.; Tanaka, S.; Nemoto, N.; Karlsson, G.; Almgren, M.; Maeda, H. *J. Phys. Chem. B* **2002,** *106,* 1524-1527.

[57] Johnsson, M.; Wagenaar, A.; Stuart, M. C. A.; Engberts, J. B. F. N. *Langmuir* **2003,** *19,* 4609-4618.

[58] Chen, F.-J.; Asokan, A.; Cho, M. J. *Biochim. Biophys. Acta* **2003,** *1611,* 140-150.

[59] Chung, M.-H.; Chung, Y.-C.; Chun, B. C. *Colloids Surf. B: Biointerfaces* **2003,** *29,* 75-80.

[60] Chung, M.-H.; Park, C.; Chun, B. C.; Chung, Y.-C. *Colloids Surf. B: Biointerfaces* **2004,** *34,* 179-184.

[61] Santoso, S. S.; Vauthey, S.; Zhang, S. *Current Opinion Colloid Interface Sci.* **2002,** *7,* 262-266.

[62] Luk, Y.-Y.; Abbott, N. L. *Current Opinion Colloid Interface Sci.* **2002,** *7,* 267-275.

[63] Löwik, D. W. P. M.; van Hest, J. C. M. *Chem. Soc. Rev.* **2004,** *33,* 234-245.

[64] Mille, M. *J. Colloid Interface Sci.* **1981,** *81,* 169-179.

[65] Maeda, H. *J. Phys. Chem.* **1988,** *92,* 4490-4498.

[66] Mille, M.; Vanderkooi, G. *J. Colloid Interface Sci.* **1977,** *61,* 475-484.

[67] Maeda, H. *J. Colloid Interface Sci.* **2003,** *263,* 277-287.

[68] Lair, V.; Bouguerra, S.; Turmine, M.; Letellier, P. *Langmuir* **2004,** *20,* 8490-8495.

[69] Zimmerman, J. A.; Schnaare, R. L. *J. Colloid Interface Sci.* **1999,** *220,* 75-80.

[70] da Silva, F. L. B.; Bogren, D.; Söderman, O.; Åkesson, T.; Jönsson, B. *J. Phys. Chem. B* **2002,** *106,* 3515-3522.

[71] Holland, P. M. In *Mixed Surfactant Systems*; Holland, P. M.; Rubingh, D. N., Eds.; ACS Symposium Series 501; American Chemical Society: Washington, DC, 1992; Chapter 2, pp 31–44.

[72] Porte, G.; Appell, J.; Poggi, Y. *J. Phys. Chem.* **1980,** *84,* 3105-3110.

[73] Alargova, R. G.; Ivanova, V. P.; Kralchevsky, P. A.; Mehreteab, A.; Broze, G. *Colloids Surf. A: Physicochem. Eng. Aspects* **1998,** *142,* 201-218.

[74] Alargova, R. G.; Danov, K. D.; Kralchevsky, P. A.; Broze, G.; Mehreteab, A. *Langmuir* **1998,** *14,* 4036-4049.

[75] Bucci, S.; Fagotti, C.; Degiorgio, V.; Piazza, R. *Langmuir* **1991,** *7,* 824-826.

[76] Lindman, B.; Lindblom, G.; Wennerstrom, H.; Gustavsson, H. In *Micellization, Solubilization, Microemulsions, [Proc. Int. Symp.],* Vol. 1; Mittal, K. L., Ed.; Plenum: New York, NY, 1977; pp 195–227.

[77] Thomas, J. K.; Grieser, F.; Wong, M. *Berichte der Bunsen-Gesellschaft* **1978,** *82,* 937-949.

[78] Romsted, L. S. In *Micellization, Solubilization, Microemulsions, [Proc. Int. Symp.]*, Vol. 2; Mittal, K. L., Ed.; Plenum: New York, NY, 1977; pp 509–530.

[79] Bell, G. M. *Trans. Faraday Soc.* **1964,** *60,* 1752-1759.

[80] Bell, G. M.; Dunning, A. J. *Trans. Faraday Soc.* **1970,** *66,* 500-508.

[81] Yoshida, N. *J. Chem. Phys.* **1978,** *69,* 4867-4871.

[82] Gunnarsson, G.; Jönsson, B.; Wennerström, H. *J. Phys. Chem.* **1980,** *84,* 3114-3121.

[83] Heindl, A.; Kohler, H.-H. *Langmuir* **1996,** *12,* 2464-2477.

[84] Stigter, D. *J. Phys. Chem.* **1964,** *68,* 3603-3611.

[85] Stigter, D. *J. Phys. Chem.* **1975,** *79,* 1008-1014.

[86] Stigter, D. *J. Phys. Chem.* **1975,** *79,* 1015-1022.

[87] Beunen, J. A.; Ruckenstein, E. *J. Colloid Interface Sci.* **1983,** *96,* 469-487.

[88] Ruckenstein, E.; Beunen, J. A. *Langmuir* **1988,** *4,* 77-90.

[89] Hall, D. G.; Price, T. J. *J. Chem. Soc., Faraday Trans. 1* **1984,** *80,* 1193-1199.

[90] Hall, D. G.; Meares, P.; Davidson, C.; Wyn-Jones, E.; Taylor, J. In *Mixed Surfactant Systems*; Holland, P. M.; Rubingh, D. N., Eds.; ACS Symposium Series 501; American Chemical Society: Washington, DC, 1992; Chapter 7, pp 128–141.

[91] Maeda, H. *J. Colloid Interface Sci.* **2003,** *258,* 390-395.

[92] Manabe, M.; Kaneko, M.; Miura, T.; Akiyama, C.; Kawamura, H.; Katsuura, H.; Shiomi, M. *Bull. Chem. Soc. Japan* **2002,** *75,* 1967-1972.

[93] Treiner, C.; Fromon, M.; Mannebach, M. H. *Langmuir* **1989,** *5,* 283-286.

[94] Rathman, J. F.; Scamehorn, J. F. *Langmuir* **1987,** *3,* 372-377.

[95] Treiner, C.; Khodja, A. A.; Fromon, M. *J. Colloid Interface Sci.* **1989,** *128,* 416-421.

[96] Treiner, C.; Mannebach, M. H. *Colloid Polym. Sci.* **1990,** *268,* 88-95.

[97] Rathman, J. F.; Scamehorn, J. F. *J. Phys. Chem.* **1984,** *88,* 5807-5816.

[98] ChemSW, Inc., Fairfield, CA "Molecular Modeling Pro, version 3.2", ;.

[99] Quinn, J. A. "A New Method for the Calculation of Hydrophilic Surface Area (HSA) from Structure", `http://www.norgwyn.com/hsa.zip`, 2003 Norgwyn Montgomery Software Inc., North Wales, PA.

[100] Carale, T. R.; Pham, Q. T.; Blankschtein, D. *Langmuir* **1994,** *10,* 109-121.

[101] Ben-Shaul, A.; Szleifer, I.; Gelbart, W. M. *J. Chem. Phys.* **1985,** *83,* 3597-3611.

[102] Szleifer, I.; Ben-Shaul, A.; Gelbart, W. M. *J. Chem. Phys.* **1985,** *83,* 3612-3620.

[103] Szleifer, I.; Ben-Shaul, A.; Gelbart, W. M. *J. Chem. Phys.* **1987,** *86,* 7094-7109.

[104] Naor, A.; Puvvada, S.; Blankschtein, D. *J. Phys. Chem.* **1992,** *96,* 7830-7832.

[105] Verwey, E. J. W.; Overbeek, J. T. G. *Theory of the Stability of Lyophobic Colloids*; Elsevier: New York, NY, 1948.

[106] Bockris, J. O.; Reddy, A. K. N. *Modern Electrochemistry*; Plenum Press: New York, NY, 1970; Vol. 1.

[107] Nagarajan, R.; Ruckenstein, E. *Langmuir* **1991,** *7,* 2934-2969.

[108] Jönsson, B.; Wennerström, H. *J. Colloid Interface Sci.* **1981,** *80,* 482-496.

[109] Evans, D. F.; Mitchell, D. J.; Ninham, B. W. *J. Phys. Chem.* **1984,** *88,* 6344-6348.

[110] Hayter, J. B. *Langmuir* **1992,** *8,* 2873-2876.

[111] Onsager, L. *J. Am. Chem. Soc.* **1936,** *58,* 1486-1493.

[112] Böttcher, C. J. F. In *Theory of Electric Polarization*, Vol. 1, 2nd ed.; Elsevier: New York, NY, 1973; pp 130–133.

[113] *CRC Handbook of Chemistry and Physics*, 84th ed.; Lide, D. R., Ed.; CRC Press: Boca Raton, FL, 2003.

[114] Hasted, J. B.; Ritson, D. M.; Collie, C. H. *J. Chem. Phys.* **1948,** *16,* 1-11.

[115] Shiloach, A.; Blankschtein, D. *Langmuir* **1997,** *13,* 3968-3981.

[116] Shiloach, A.; Blankschtein, D. *Langmuir* **1998,** *14,* 7166-7182.

[117] Ohshima, H.; Healy, T. W.; White, L. R. *J. Colloid Interface Sci.* **1982,** *90,* 17-26.

[118] Eriksson, J. C.; Ljunggren, S. *Langmuir* **1990,** *6,* 895-904.

[119] Bauer, A.; Woelki, S.; Kohler, H.-H. *J. Phys. Chem. B* **2004,** *108,* 2028-2037.

[120] May, S.; Ben-Shaul, A. *J. Phys. Chem. B* **2001,** *105,* 630-640.

[121] Blankschtein, D.; Thurston, G. M.; Benedek, G. B. *J. Chem. Phys.* **1986,** *85,* 7268-7288.

[122] Penfold, J.; Staples, E.; Thompson, L.; Tucker, I.; Hines, J.; Thomas, R. K.; Lu, J. R. *Langmuir* **1995,** *11,* 2496-2503.

[123] Reiss-Husson, F.; Luzzati, V. *J. Phys. Chem.* **1964,** *68,* 3504-3511.

[124] Soldi, V.; Keiper, J.; Romsted, L. S.; Cuccovia, I. M.; Chaimovich, H. *Langmuir* **2000,** *16,* 59-71.

[125] Keiper, J.; Romsted, L. S.; Yao, J.; Soldi, V. *Colloids Surf. A: Physicochem. Eng. Aspects* **2001,** *176,* 53-67.

[126] Akisada, H. *J. Colloid Interface Sci.* **2001,** *240,* 323-334.

[127] Manning, G. S. *J. Chem. Phys.* **1969,** *51,* 924-933.

[128] Patist, A.; Bhagwat, S. S.; Penfield, K. W.; Aikens, P.; Shah, D. O. *J. Surfactants Detergents* **2000,** *3,* 53-58.

[129] Bjerrum, N. *Kgl. Danske Videnskab. Selskab. Math.-fys. Medd.* **1926,** *7,* 1-48.

[130] Corrin, M. L.; Harkins, W. D. *J. Am. Chem. Soc.* **1947,** *69,* 683-688.

[131] Palepu, R.; Hall, D. G.; Wyn-Jones, E. *J. Chem. Soc., Faraday Trans.* **1990,** *86,* 1535-1538.

[132] Maeda, H. *J. Colloid Interface Sci.* **2001,** *241,* 18-25.

[133] Kameyama, K.; Muroya, A.; Takagi, T. *J. Colloid Interface Sci.* **1997,** *196,* 48-52.

[134] Balzer, D. In *Nonionic Surfactants: Alkyl Polyglucosides*, Vol. 91; Balzer, D.; Lüders, H., Eds.; Marcel Dekker: New York, NY, 2000; Chapter 5, p 105.

[135] Moisés de Oliveira, H. P.; Gehlen, M. H. *Langmuir* **2002,** *18,* 3792-3796.

[136] Warr, G. G.; Grieser, F. *J. Chem. Soc., Faraday Trans. 1* **1986,** *82,* 1813-1828.

[137] Maeda, H. *J. Colloid Interface Sci.* **1995,** *172,* 98-105.

[138] Goldsipe, A.; Blankschtein, D. *Langmuir* **2005,** *21,* 9850-9865.

[139] Lucassen, J. *J. Phys. Chem.* **1966,** *70,* 1824-1830.

[140] Weers, J. G.; Rathman, J. F.; Axe, F. U.; Crichlow, C. A.; Foland, L. D.; Scheuing, D. R.; Wiersema, R. J.; Zielske, A. G. *Langmuir* **1991,** *7,* 854-867.

[141] Stryer, L. *Biochemistry*, 3rd ed.; WH Freeman: New York, NY, 1988.

[142] Davies, C. W. *Ion Association*; Butterworths: Washington, DC, 1962.

[143] *Activity Coefficients in Electrolyte Solutions*; Pytkowicz, R. M., Ed.; CRC Press: Boca Raton, FL, 1979; Vol. 2.

[144] Missel, P. J.; Mazer, N. A.; Benedek, G. B.; Young, C. Y.; Carey, M. C. *J. Phys. Chem.* **1980,** *84,* 1044-1057.

[145] Marcus, R. A. *J. Chem. Phys.* **1955,** *23,* 1057-1068.

[146] Imae, T.; Ikeda, S. *J. Colloid Interface Sci.* **1986,** *113,* 449-455.

[147] Terada, Y.; Maeda, H.; Odagaki, T. *J. Phys. Chem. B* **1997,** *101,* 5784-5788.

[148] Kakehashi, R.; Yamamura, S.; Tokai, N.; Takeda, T.; Kaneda, K.; Yoshinaga, K.; Maeda, H. *J. Colloid Interface Sci.* **2001,** *243,* 233-240.

[149] Maeda, H.; Muroi, S.; Ishii, M.; Kakehashi, R.; Kaimoto, H.; Nakahara, T.; Motomura, K. *J. Colloid Interface Sci.* **1995,** *175,* 497-505.

[150] Maeda, H.; Kanakubo, Y.; Miyahara, M.; Kakehashi, R.; Garamus, V.; Pedersen, J. S. *J. Phys. Chem. B* **2000,** *104,* 6174-6180.

[151] Mukerjee, P.; Mysels, K. J. *Critical Micelle Concentrations of Aqueous Surfactant Systems*; U.S. National Bureau of Standards: Washington, DC, 1971.

[152] Srinivasan, V.; Blankschtein, D. *Langmuir* **2005,** *21,* 1647-1660.

[153] Bakshi, M. S.; Crisantino, R.; De Lisi, R.; Milioto, S. *J. Phys. Chem.* **1993,** *97,* 6914-6919.

[154] Desai, T. R.; Dixit, S. G. *J. Colloid Interface Sci.* **1996,** *177,* 471-477.

[155] Haque, M. E.; Das, A. R.; Rakshit, A. K.; Moulik, S. P. *Langmuir* **1996,** *12,* 4084-4089.

[156] Bharadwaj, S.; Ahluwalia, J. C. *J. Am. Oil Chem. Soc.* **1996,** *73,* 39-45.

[157] Imaishi, Y.; Kakehashi, R.; Nezu, T.; Maeda, H. *J. Colloid Interface Sci.* **1998,** *197,* 309-316.

[158] Kaimoto, H.; Shoho, K.; Sasaki, S.; Maeda, H. *J. Phys. Chem.* **1994,** *98,* 10243-10248.

[159] Imae, T.; Hayashi, N. *Langmuir* **1993,** *9,* 3385-3388.

[160] Majhi, P. R.; Dubin, P. L.; Feng, X.; Guo, X.; Leermakers, F. A. M.; Tribet, C. *J. Phys. Chem. B* **2004,** *108,* 5980-5988.

[161] Zhang, H.; Dubin, P. L.; Kaplan, J. I. *Langmuir* **1991,** *7,* 2103-2107.

[162] Abe, A.; Imae, T.; Shibuya, A.; Ikeda, S. *J. Surface Sci. Technol.* **1988,** *4,* 67-80.

[163] Mohanty, S.; Davis, H. T.; McCormick, A. V. *Langmuir* **2001,** *17,* 7160-7171.

[164] Tokiwa, F.; Ohki, K. *J. Phys. Chem.* **1966,** *70,* 3437-3441.

[165] Tokiwa, F.; Ohki, K. *J. Phys. Chem.* **1967,** *71,* 1824-1829.

[166] Tokiwa, F.; Ohki, K. *J. Colloid Interface Sci.* **1968,** *27,* 247-252.

[167] Corkill, J. M.; Gemmell, K. W.; Goodman, J. F.; Walker, T. *Trans. Faraday Soc.* **1970,** *66,* 1817-1824.

[168] Yalkowsky, S. H.; Zografi, G. *J. Colloid Interface Sci.* **1970,** *34,* 525-533.

[169] Maeda, H.; Tsunoda, M.-a.; Ikeda, S. *J. Phys. Chem.* **1974,** *78,* 1086-1090.

[170] Mukerjee, P.; Banerjee, K. *J. Phys. Chem.* **1964,** *68,* 3567-3574.

[171] Fernández, M. S.; Fromherz, P. *J. Phys. Chem.* **1977,** *81,* 1755-1761.

[172] García-Soto, J.; Fernández, M. S. *Biochim. et Biophys. Acta Biomembr.* **1983,** *731,* 275-281.

[173] Drummond, C. J.; Warr, G. G.; Grieser, F.; Ninham, B. W.; Evans, D. F. *J. Phys. Chem.* **1985,** *89,* 2103-2109.

[174] Lovelock, B.; Grieser, F.; Healy, T. W. *J. Phys. Chem.* **1985,** *89,* 501-507.

[175] Drummond, C. J.; Grieser, F. *Photochemistry and Photobiology* **1987,** *45,* 19-34.

[176] Drummond, C. J.; Grieser, F.; Healy, T. W. *J. Phys. Chem.* **1988,** *92,* 2604-2613.

[177] Grieser, F.; Drummond, C. J. *J. Phys. Chem.* **1988,** *92,* 5580-5593.

[178] Cassidy, M. A.; Warr, G. G. *J. Phys. Chem.* **1996,** *100,* 3237-3240.

[179] Whiddon, C. R.; Bunton, C. A.; Söderman, O. *J. Phys. Chem. B* **2003,** *107,* 1001-1005.

[180] Chakraborty, H.; Banerjee, R.; Sarkar, M. *Biophys. Chem.* **2003,** *104,* 315-325.

[181] Chakraborty, H.; Sarkar, M. *J. Colloid Interface Sci.* **2005,** *292,* 265-270.

[182] Weers, J. G.; Rathman, J. F.; Scheuing, D. R. *Colloid Polym. Sci.* **1990,** *268,* 832-846.

[183] Imae, T.; Kakitani, M. *Colloid Polym. Sci.* **1996,** *274,* 1170-1175.

[184] Hofmann, S.; Hoffmann, H. *J. Phys. Chem. B* **1998,** *102,* 5614-5624.

[185] Smirnova, N.; Vlasov, A. *Fluid Phase Equilib.* **1999,** *158-160,* 511-522.

[186] Goloub, T. P.; Pugh, R. J.; Zhmud, B. V. *J. Colloid Interface Sci.* **2000,** *229,* 72-81.

[187] Smirnova, N. A.; Murch, B.; Pukinsky, I. B.; Churjusova, T. G.; Alexeeva, M. V.; Vlasov, A. Y.; Mokrushina, L. V. *Langmuir* **2002,** *18,* 3446-3453.

[188] Almgren, M.; Wang, K.; Asakawa, T. *Langmuir* **1997,** *13,* 4535-4544.

[189] Mandel, J. *The Statistical Analysis of Experimental Data*; Dover: New York, 1964.

[190] Goldsipe, A.; Blankschtein, D. *Langmuir* **2006,** *22,* 3547-3559.

[191] Gorski, N.; Kalus, J. *J. Phys. Chem. B* **1997,** *101,* 4390-4393.

[192] Garamus, V. M.; Pedersen, J. S.; Kawasaki, H.; Maeda, H. *Langmuir* **2000,** *16,* 6431-6437.

[193] Gambogi, J.; Arvanitidou, E. S.; Lai, K.-Y. In *Liquid Detergents*, 2nd ed.; Lai, K.-Y., Ed.; Surfactant Science Series 129; Taylor & Francis: Boca Raton, 2006; Chapter 7, pp 171–238.

[194] *Mixed Surfactant Systems*, 2nd ed.; Abe, M.; Scamehorn, J. F., Eds.; Surfactant Science Series 124; Marcel Dekker: New York, 2005.

[195] Hines, J. D.; Thomas, R. K.; Garrett, P. R.; Rennie, G. K.; Penfold, J. *J. Phys. Chem. B* **1998,** *102,* 9708-9713.

[196] Ghosh, S.; Moulik, S. P. *J. Colloid Interface Sci.* **1998,** *208,* 357-366.

[197] Graciaa, A.; Ben Ghoulam, M.; Marion, G.; Lachaise, J. *J. Phys. Chem.* **1989,** *93,* 4167-4173.

[198] Das Burman, A.; Dey, T.; Mukherjee, B.; Das, A. R. *Langmuir* **2000,** *16,* 10020-10027.

[199] Ghosh, S. *J. Colloid Interface Sci.* **2001,** *244,* 128-138.

[200] Srinivasan, V. *Theoretical modeling of micellization and solubilization in ionic surfactant systems,* Thesis, Mass. Inst. of Tech., 2003.

[201] Murphy, A.; Taggart, G. *Colloids Surf. A: Physicochem. Eng. Aspects* **2002,** *205,* 237-248.

[202] Warr, G. G.; Grieser, F.; Healy, T. W. *J. Phys. Chem.* **1983,** *87,* 1220-1223.

[203] Funasaki, N.; Hada, S.; Neya, S. *J. Phys. Chem.* **1988,** *92,* 7112-7116.

[204] Funasaki, N.; Shim, H.-S.; Hadad, S. *J. Chem. Soc., Faraday Trans.* **1991,** *87,* 957-961.

[205] Ōkawauchi, M.; Shinozaki, M.; Ikawa, Y.; Tanaka, M. *J. Phys. Chem.* **1987,** *91,* 109-112.

[206] Nikas, Y. J.; Puvvada, S.; Blankschtein, D. *Langmuir* **1992,** *8,* 2680-2689.

[207] Rubingh, D. N.; Bauer, M. In *Mixed Surfactant Systems*; Holland, P. M.; Rubingh, D. N., Eds.; ACS Symposium Series 501; American Chemical Society: Washington, DC, 1992; Chapter 12, pp 210–226.

[208] Wright, S.; Bunton, C. A.; Holland, P. M. In *Mixed Surfactant Systems*; Holland, P. M.; Rubingh, D. N., Eds.; ACS Symposium Series 501; American Chemical Society: Washington, DC, 1992; Chapter 7, pp 227–233.

[209] Kamei, D. T. *Protein and viral partitioning in two-phase aqueous micellar systems,* Thesis, Mass. Inst. of Tech., 2001.

[210] Lam, H. N. H. *Electrostatic and affinity enhancements of protein partitioning in two-phase aqueous micellar systems,* Thesis, Mass. Inst. of Tech., 2005.

[211] Mulqueen, M.; Blankschtein, D. *Langmuir* **1999,** *15,* 8832-8848.

[212] Dorshow, R. B.; Bunton, C. A.; Nicoli, D. F. *J. Phys. Chem.* **1983,** *87,* 1409-1416.

[213] Imae, T.; Kamiya, R.; Ikeda, S. *J. Colloid Interface Sci.* **1985,** *108,* 215-225.

[214] Neves, M. d. F. S.; Zanette, D.; Quina, F.; Moretti, M. T.; Nome, F. *J. Phys. Chem.* **1989,** *93,* 1502-1505.

[215] Abuin, E.; Lissi, E. *J. Colloid Interface Sci.* **1991,** *143,* 97-102.

[216] Romsted, L. S.; Bunton, C. A.; Yao, J. *Current Opinion Colloid Interface Sci.* **1997,** *2,* 622-628.

[217] Bunton, C. A. *J. Molec. Liquids* **1997,** *72,* 231-249.

[218] Bunton, C. A.; Moffatt, J. R. *J. Phys. Chem.* **1985,** *89,* 4166-4169.

[219] Ortega, F.; Rodenas, E. *J. Phys. Chem.* **1987,** *91,* 837-840.

[220] Stephenson, B. C.; Rangel-Yagui, C. O.; Pessoa Jr., A.; Tavares, L. C.; Beers, K.; Blankschtein, D. *Langmuir* **2006,** *22,* 1514-1525.

[221] Mulqueen, M.; Blankschtein, D. *Langmuir* **2000,** *16,* 7640-7654.

[222] Yuet, P. K.; Blankschtein, D. *Langmuir* **1995,** *11,* 1925-1933.

[223] Yuet, P. K.; Blankschtein, D. *Langmuir* **1996,** *12,* 3802-3818.

[224] Yuet, P. K.; Blankschtein, D. *Langmuir* **1996,** *12,* 3819-3827.

[225] Ambade, A. V.; Savariar, E. N.; Thayumanavan, S. *Mol. Pharm.* **2005,** *2,* 264-272.

[226] Al-Jamal, K. T.; Ramaswamy, C.; Florence, A. T. *Adv. Drug Delivery Rev.* **2005,** *57,* 2238-2270.

[227] Al-Jamal, K. T.; Ramaswamy, C.; Singh, B.; Florence, A. T. *J. Drug Delivery Sic. Tech.* **2005,** *15,* 11-18.

[228] Aathimanikandan, S. V.; Savariar, E. N.; Thayumanavan, S. *J. Am. Chem. Soc.* **2005,** *127,* 14922-14929.

[229] Vernille, J. P.; Kovell, L. C.; Schneider, J. W. *Bioconjugate Chem.* **2004,** *15,* 1314-1321.

[230] Marques, B. F.; Schneider, J. W. *Langmuir* **2005,** *21,* 2488-2494.

[231] Whitesides, G. M.; Boncheva, M. *Proc. Natl. Acad. Sci. U. S. A.* **2002,** *99,* 4769-4774.

[232] Binks, B. P. *Current Opinion Colloid Interface Sci.* **2002,** *7,* 21-41.

[233] Dinsmore, A. D.; Hsu, M. F.; Nikolaides, M. G.; Marquez, M.; Bausch, A. R.; Weitz, D. A. *Science* **2002,** *298,* 1006-1009.

[234] Stephenson, B. C.; Beers, K.; Blankschtein, D. *Langmuir* **2006,** *22,* 1500-1513.

[235] Morisada, S.; Shinto, H.; Higashitani, K. *J. Phys. Chem. B* **2005,** *109,* 11762-11769.

[236] Prigogine, I.; Defay, R. *Chemical Thermodynamics*; Wiley: New York, NY, 1954.